ISSN 0869-6632

ИЗВЕСТИЯ ВЫСШИХ УЧЕБНЫХ ЗАВЕДЕНИЙ

# ПРИКЛАДНАЯ НЕЛИНЕЙНАЯ ДИНАМИКА

# APPLIED NONLINEAR DYNAMICS

3

2002

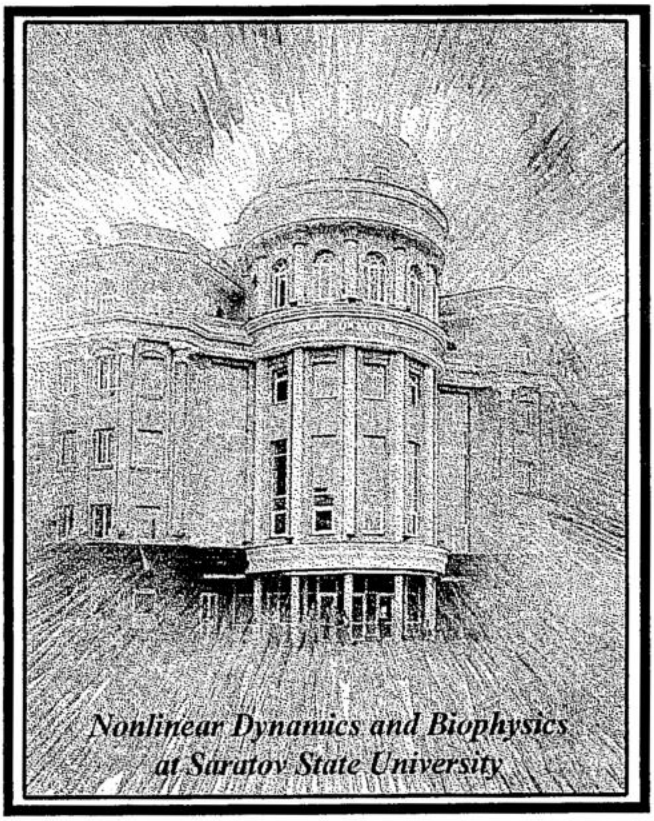

*Nonlinear Dynamics and Biophysics*
*at Saratov State University*

ИЗДАНИЕ САРАТОВСКОГО УНИВЕРСИТЕТА

We would like to present the special issue of the Journal «Applied Nonlinear Dynamics». This issue includes in general papers of leading researchers of the Scientific and Educational Center on Nonlinear Dynamics and Biophysics (REC-006) that was created in Saratov State University in June 2000 in the framework of the Joint Program of the Russian Ministry of Education and the US Civilian Research and Development Foundation «Basic Research and Higher Education».

The contents of the papers reflect the main research directions in the framework of the REC Research Program and enable to get an idea of the level of the presented results. Collecting the materials for this special issue we tried to choose those papers that can be considered both as certain reviews on the existing achievements and as original papers with recent new results that reflect the achievements of representatives of the School on Nonlinear Dynamics and Biophysics of Saratov State University.

*Editorial Board*

***Издание выпуска поддержано грантом***
***CRDF REC-006 СГУ Программы BRHE***

**МИНИСТЕРСТВО ОБРАЗОВАНИЯ РОССИЙСКОЙ ФЕДЕРАЦИИ**

Известия высших учебных заведений

**ПРИКЛАДНАЯ НЕЛИНЕЙНАЯ ДИНАМИКА**

***научно-технический журнал***

издается с 1993 года

Выходит 6 раз в год

Том 10, №3, 2002, Саратов

## СОДЕРЖАНИЕ

### ОБЗОРЫ АКТУАЛЬНЫХ ПРОБЛЕМ НЕЛИНЕЙНОЙ ДИНАМИКИ

*Четвериков А., Эбелинг В.* Нелинейные проблемы молекулярной физики . . . 3

### БИФУРКАЦИИ В ДИНАМИЧЕСКИХ СИСТЕМАХ РАЗЛИЧНОЙ ПРИРОДЫ

*Кузнецов С.П.* Разнообразие критических явлений, ассоциирующихся с квазипериодическим движением при соотношении частот, равном золотому среднему . . . 22

### НЕЛИНЕЙННЫЕ ВОЛНЫ. СОЛИТОНЫ

*Мельников Л.А., Конюхов А.И., Вешнева И.В., Дербов В.Л., Серов В.В.* Нелинейная динамика пространственных и временных структур в лазерах и атомной оптике: лазеры с керровской синхронизацией мод, зеемановский лазер, атомный конденсат Бозе-Эйнштейна . . . 40

### ДЕТЕРМИНИРОВАННЫЙ ХАОС

*Астахов В.В., Шабунин А.В., Стальмахов П.А.* Мультистабильность, синфазная и противофазная синхронизация в системах с бифуркациями удвоения периода . . . 63

*Кузнецов А.П., Тюрюкина Л.В., Савин А.В., Сатаев И.Р., Седова Ю.В., Милованов С.В.* Многопараметрическая картина перехода к хаосу . . 80

*Храмов А.Е., Короновский А.А., Ремпен И.С., Трубецков Д.И.* Исследование переходного хаоса в гиролампе со встречной волной, синхронизируемой внешним сигналом . . . 97

### АВТОВОЛНЫ. САМООРГАНИЗАЦИЯ

*Вадивасова Т.Е., Анищенко В.С., Стрелкова Г.И., Фомин А.И.* Кластерная и глобальная синхронизация в цепочке квазигармонических автогенераторов с шумом . . . 110

*Сосновцева О.В., Постнов Д.Э., Фомин А.И.* Образование индуцированных шумом пространственных структур в возбудимых средах . . . 125

### ПРИКЛАДНЫЕ ЗАДАЧИ НЕЛИНЕЙНОЙ ТЕОРИИ КОЛЕБАНИЙ И ВОЛН

*Безручко Б.П., Селезнев Е.П., Пономаренко В.И, Прохоров М.Д., Смирнов Д.А, Диканев Т.В., Сысоев И.В., Караваев А.С.* Специальные подходы при глобальной реконструкции уравнений по временным рядам . . . 137

*Усанов Д.А., Скрипаль А.В., Скрипаль А.В., Абрамов А.В., Клецов А.А.* Нелинейная динамика полупроводниковых СВЧ и оптических генераторов . . . 159

### НОВОЕ В ПРИКЛАДНОЙ ФИЗИКЕ

*Хлебцов Н.Г., Богатырев В.А., Дыкман Л.А., Краснов Я.М., Мельников А.Г.* Оптические свойства биоконъюгатов коллоидного золота . . . 172

*Зимняков Д.А., Свиридов А.П., Омельченко А.И., Трифонов В.А., Агафонов Д.Н., Захаров П.В., Кузнецова Л.В.* Спекл-диагностика релаксационных процессов в нестационарных рассеивающих системах . . . 188

### МЕТОДИЧЕСКИЕ ЗАМЕТКИ ПО НЕЛИНЕЙНОЙ ДИНАМИКЕ

*Дмитриев Б.С., Левин Ю.И., Шараевский Ю.П.* Физический эксперимент в университетском образовании. . . 205

*Publication of the issue is supported by Award*
*REC-006 of the CRDF Program BRHE*

**DEPARTMENT OF EDUCATION OF RUSSIAN FEDERATION**
Izvestiya VUZ
**APPLIED NONLINEAR DYNAMICS**
*scientific-technical journal*
published since 1993

Published 6 times a year Vol.10, № 3, 2002, Saratov

## CONTENTS

REVIEWS OF ACTUAL PROBLEMS OF NONLINEAR DYNAMICS

Nonlinear problems of molecular physics. *A. Chetverikov, W. Ebeling* . . . . . 3

BIFURCATIONS IN DYNAMICAL SYSTEMS

A variety of critical phenomena associated with the golden mean quasiperiodicity. *S.P. Kuznetsov* . . . . . 22

NONLINEAR WAVES. SOLITONS

Nonlinear dynamics of spatial and temporal patterns in lasers and atom optics: Kerr-lens mode-locked laser, Zeeman laser and Bose-Einstein atomic condensate. *L.A. Melnikov, A.I. Konukhov, I.V. Veshneva, V.L. Derbov, V.V. Serov* . . . . . 40

DETERMINISTIC CHAOS

Multistability, in-phase and anti-phase chaos synchronisation in period-doubling systems. *V. Astakhov, A. Shabunin, P. Stalmakhov* . . . . . 63
Multi-parameter picture of transition to chaos. *A.P. Kuznetsov, L.V. Turukina, A.V. Savin, I.R. Sataev, J.V. Sedova, S.V. Milovanov* . . . . . 80
Investigation of transient chaos in gyro-backward-wave-oscillator synchronized by the external signal. *A.E. Hramov, A.A. Koronovskii, I.S. Rempen, D.I. Trubetskov* . . . . . 97

AUTOWAVES. SELF-ORGANIZATION

Cluster and global synchronization in a quasi-harmonic self-oscillatory chain in the presence of noise. *T.E. Vadivasova, V.S. Anishchenko, G.I. Strelkova, and A.I. Fomin* . . . . . 110
Noise-induced spatial structures in excitable media. *O.V. Sosnovtseva, D.E. Postnov, A.I. Fomin* . . . . . 125

APPLIED PROBLEMS OF NONLINEAR OSCILLATION AND WAVE THEORY

Special approaches to global reconstruction of equations from time series. *B.P. Bezruchko, Ye.P. Seleznev, V.I. Ponomarenko, M.D. Prokhorov, D.A. Smirnov, T.V. Dikanev, I.V. Sysoev, A.S. Karavaev* . . . . . 137
Nonlinear dynamics of microwave and optical semiconductor oscillators. *D.A. Usanov, Al.V. Skripal, An.V. Skripal, A.V. Abramov, A.A. Kletsov* . . . 159

INNOVATIONS IN APPLIED PHYSICS

Optical properties of colloidal-gold bioconjugates. *N.G. Khlebtsov, V.A. Bogatyrev, L.A. Dykman, Ya.M. Krasnov, A.G. Melnikov* . . . . . 172
Speckle diagnostics of relaxation processes in non-stationary scattering systems. *D.A. Zimnyakov, A.P. Sviridov, A.I. Omel'chenko, V.A. Trifonov, D.N. Agafonov, P.V. Zakharov, L.V. Kuznetsova* . . . . . 188

METODICAL PAPERS ON NONLINEAR DYNAMICS

Physical experiment in university education. *B.S. Dmitriev, Yu.I. Levin, Yu.P. Sharaevsky* . . . . . 205

Review of actual problems of nonlinear dynamics

Izv. VUZ «AND», vol.10, № 3, 2002

# NONLINEAR PROBLEMS OF MOLECULAR PHYSICS

*A. Chetverikov, W. Ebeling*

A survey on investigations of some nonlinear problems of molecular physics carried out by molecular dynamics simulations is given. Among them there are problems of elementary excitations in fluids, the dynamics of chemical reactions in solutions, dynamical properties of dilute plasma, dynamic phenomena in phase transitions in mesoscopic systems, structural properties of chains of nonlinear oscillators. Several new results about the distribution of clusters and of a method of identification of clusters are presented.

## 1. Introduction

The paper reviews some recent results of investigations of modern nonlinear problems concerning molecular physics, physics of condensed matter, plasma physics and others. All of them use the same method of the study - computer simulation based on the molecular dynamics method (molecular dynamics simulation, MDS) [1-3]. The paper does not claim for complete coverage of all problems of mentioned fields of science, the selection is restricted mainly to subjects of the researches performed within a collaboration between groups in Berlin-Moscow-Saratov. The purpose of the survey is to give an insight into modern problems of studies of nonlinear phenomena, observed, for example, in elementary excitations, in phase transformations of matter, in chemical reactions, in plasma processes. The main subject is preceded by brief explanation of the basic principles of intermolecular interactions and the molecular dynamics simulation method.

## 2. Interaction of molecules and molecular dynamics simulations

Let us first consider a problem: what is the minimal number $N$ of particles of a substance necessary to explore its physical, chemical, thermodynamic etc. properties? On the first sight, billions and billions of molecules or atoms are required. However, there is a number of phenomena when ensembles of only a few thousand or even hundreds of particles exhibit almost the same properties as large volumes of a substance. Besides, study of processes in ensembles of rather small number of particles (clusters, mesoscopic systems (see, for example, [4])) and the observation of evolution of their properties with increasing number of a particles often yield a key to understanding of what happens in real volumes of substances - macroscopic systems. These observations allow to offer a

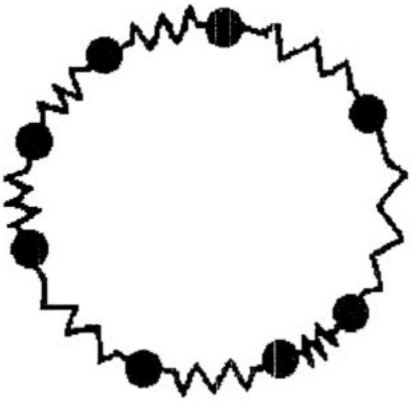

Fig. 1. A molecular system in a one-dimensional space with periodic boundary conditions

method of the theoretical analysis based on the direct numerical simulation of a motion of particles in rather small ensembles and calculation of different macrocharacteristics by means of statistical treatment [1-3].

The important feature of molecular dynamics simulations is the application of periodic boundary conditions in studies of macroscopic systems.The influence of boundary conditions (requirements on a surface) should be minimal. Let us first consider a molecular system consisting of $N$ particles in a one-dimensional (1D) space. In this case periodic boundary conditions are equivalent to placing the particles on a ring (Fig. 1). Let us discuss now the interaction of 2 particles at a distance $r$. If the average distance is $\sigma$ (which plays the role of the specific volume) the simplest interaction model is a linear spring described by the parabolic potential (Fig. 2)

$$V^p(r) = \tfrac{1}{2} m\omega_0^2 (r - \sigma)^2, \tag{1}$$

where standard notations are used. A standard model for a description of nonlinear interactions is the Toda model (Fig. 2)

$$V^T(r) = (a/b)[e^{-b(r-a)} - 1] + a(r - \sigma) \tag{2}$$

with constant parameters $a$ and $b$. In higher dimensions the process is supposed to take place in a parallepiped of sizes $L_x$, $L_y$, $L_z$ in 3D model or $L_x$, $L_y$ in 2D one, accordingly, and the space outside its limits is supposed to be filled with its precise copies immediately adjacent to each other (Fig. 3). Each particle has infinitely many copies in the space located on distances $L_x$, $L_y$, $L_z$ in the relevant directions. If a particle abandons the field considered in a numerical modeling by crossing any boundary of the parallepiped, its copy enters the field through an opposite boundary. In calculations of forces of particles interaction taking place in the vicinity of boundaries, the interaction with particles located outside of the field is taken into account if they are apart smaller

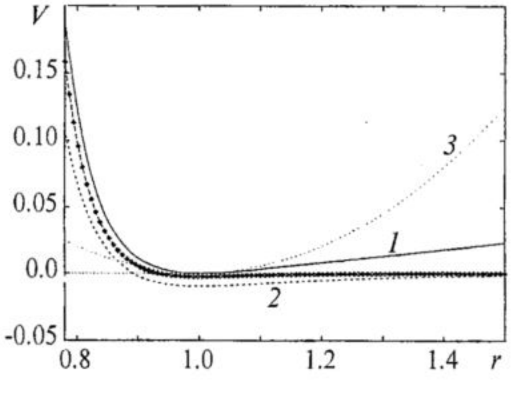

Fig. 2. Several models of the interaction potential $V(r)$: (1) - Toda potential, (2) - Lennard-Jones potential, (3) - harmonic oscillator potential and (•) - Morse potential

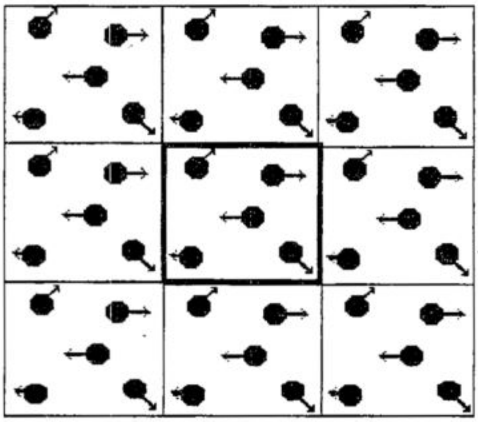

Fig. 3. A molecular system in a two-dimensional space with periodic boundary conditions

than some effective radius (see below). The periodic boundary conditions allow formally to assume $N \to \infty$ already for $N \sim 2^5$-$2^{10}$. In investigations of mesoscopic systems with limited number $N$ the interaction space is considered as unbounded.

The kind of a theoretical model for an analysis is determined by physical properties of an explored system, and the type of forces of intermolecular interaction is principal among them. In this paper we consider only simple models with classical dynamics. The force of interaction between any two molecules is supposed to be depended only on the their distance $r$. The interaction potential in various models may be different (Fig. 2), but the methods of its calculation are not a subject of the analysis of this article. The models in which interaction of molecules takes place due to Van der Waals forces are defined by the Lennard-Jones potential

$$V^{LJ}(r) = 4\varepsilon[(\sigma/r)^{12} - (\sigma/r)^{6}] \tag{3}$$

or its modification, more suitable for computer modeling, the finite-range Lennard-Jones potential

$$V^{FLG}(r) = A[(\sigma/r)^{n} - 1]\exp[(r/\sigma - {}^{3}\!/_{2})^{-1}] \quad \text{if} \quad r < ({}^{3}\!/_{2})\sigma,$$

$$V^{FLG}(r) = 0 \quad \text{if} \quad r \geq ({}^{3}\!/_{2})\sigma \tag{4}$$

are examined here (Fig. 2). Here $\varepsilon$ is a well depth in minimum of the potential well $V(r)$, and $V(r=\sigma)=0$. Also the models with particles interacting via conservative Morse forces described by the Morse potential

$$V^{M}(r) = (a/2b)(e^{-br} - 1)^{2} - (a/2b) \tag{5}$$

are considered. In the models we study here parameters $\varepsilon$, $\sigma$, and a mass of interacting particles also are used as units of the relevant quantities, which are figured as dimensionless in the models. Note, the nonlinear potentials are «short-range» and $V(r)$ is close to zero at $r \geq 1.5$. It allows to introduce an effective radius $r_{eff} \approx 1.5\sigma$ so interaction of particles located more than $r_{ij}$ from each other can be neglected. Therefore in calculations of, for example, complete potential energy of the system

$$U = \Sigma_{i<j=1}^{N} V(r_{ij}) \tag{6}$$

only those potentials of two-particle interactions, for which $r_{ij} < r_{eff}$, should be taken into account. Here $r_{ij}$ is a distance between particles number $i$ and number $j$.

An initial position of particles and sizes $L_x$, $L_y$, $L_z$ as yet depend on a type of a problem. If the system with random structure (gas, plasma) is studied, the sizes of the interaction space are chosen based on density at given number of particles $\rho = N/(L_x L_y L_z)$, and it is usually $L_x = L_y = L_z$. If the initial structure is a crystal lattice, for example, quantities $L_x$, $L_y$, $L_z$ must match each other, depending on the type of symmetry of a lattice. Let us discuss now the problem how thermodynamic equilibrium for the system can be realized. The velocity distribution of the particles ensemble in a study of processes which proceed should be Maxwellian so that the average kinetic energy of particles defines temperature and is uniformly distributed among all coordinates, and the velocity distribution function of particles is Gaussian. Additional requirements to the problem are also possible. For example, for processes in a crystal lattice the average potential energy and the kinetic one should be the same at small temperature. To satisfy these requirements in computer experiments, the calculations of the «equilibrium» performances of the system are preceded by modeling of a nonequilibrium stage (stage of «heating»), when the trajectory of a motion of each particle obeys a Langevin equation ($m=1$)

$$v_l = dr_l/dt, \quad dv_l/dt = -\partial U(r,t)/\partial r_l - \gamma v_l + (2D)^{1/2}\zeta_l(t). \tag{7}$$

$$\langle \zeta_i(t) \rangle = 0 \qquad \langle \zeta_i(t)\zeta_j(t_0) \rangle = \delta_{ij}\delta(t - t_0).$$

Here $i$ is equal to $x$, $y$, $z$ in 3D case, $v_{x,y,z}$ and $r_{x,y,z}$ are the velocities and coordinates of a particle, $\gamma$ is a friction coefficient, $D$ is a diffusion constant, $\zeta_i(t)$ is a random function modeling a white noise. In order to bring the system to thermodynamic equilibrium at temperature $T$, the Einstein relation

$$D = k_B g T \tag{8}$$

should be satisfied. Here $k_B$ is the Boltzman constant. After reaching the given temperature, external sources are «switched off» and modeling of an equilibrium stage starts. It is possible to estimate precision of calculations at this stage based on precision of satisfaction of a conservation law of a total energy of a system $E=T+U$, where $T$ is kinetic energy. In further, speaking about energies, we shall mean energy per one particle, if it is not stipulated other. Let us consider now specific applications of molecular dynamics simulations.

## 3. Elementary excitations in fluids

In fluids the typical dynamical phenomena are collective excitations in ensembles of particles. It is common to suppose that phonons and solitons are most important among them. Suitable model for investigation of their properties is the one-dimensional lattice (chain) of oscillators, in particular, of nonlinear Toda oscillators [5]. The Toda chain is chosen as one of basic models because many macroscopic characteristics can be calculated analytically due to unique properties of defined in section 1 Toda potential despite of the nonlinearity of the underlying processes [6]. In addition, such data can be served as a fine test instrument in computer simulations of processes in nonlinear chains.

In chains each particle interacts with two adjacent only, executing oscillations in a potential well formed due to interaction. The equation of motion (7) in combination with the Einstein relation (8) becomes

$$\begin{aligned}(d^2/dt^2)r_i = {} & [V'(r_{i+1}) - 2V'(r_i) + V'(r_{i-1})] + \\ & + \gamma^{1/2}[(2kT/m)^{1/2}\zeta_i(t) - \gamma^{1/2}(dr_i/dt)].\end{aligned} \tag{9}$$

At small oscillation amplitudes (small temperature) the potential is parabolic

$$V(r) = ab[(1/2)(r - \sigma)^2]. \tag{10}$$

In this case each particle executes simple harmonic motions, and the collective excitations of a chain are phonons. The frequencies and wave numbers of them obey the dispersion equation

$$\omega = 2\omega_0 \sin(k\sigma/2). \tag{11}$$

In the other limiting case, at high temperature, interaction of particles is mostly repelling, and the collective excitations are soliton-like. As a result the transformation of the thermodynamic properties of a lattice is observed in heating up. Most characteristics (the mean specific volume, the pressure, the specific internal energy, the mean potential energy et al.) can be calculated for an unlimited Toda chain analytically [5]. In particular, the specific heat per molecular at constant volume $c_V$ as the function of temperature is represented in a Fig. 4. It shows that $c_V$ varies from the value $k_B$, relevant to the ideal phonon gas, up to $0.5k_B$, relevant to the ideal soliton gas. There is the transition region near the temperature $T_{tr}$, defined by a relation $c_V(T_{tr})=0.75k_B$ ($c_V(T_{tr})$ is equal to average value of two limiting values), where a set of interesting properties initiated by interaction of nonlinear collective excitations is observed. Some of them are explored by a molecular dynamics simulations in ring chains with quite small number ($N$=10-20) of particles.

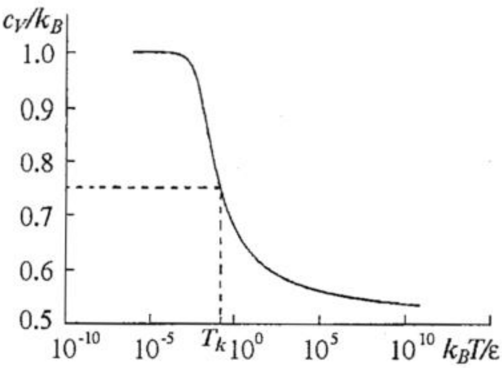

Fig. 4. Specific heat per molecular $c_V$ at constant lenth of the Toda chain. In the region around the transition temperature $T_{tr}$ (defined by $c_V(T_{tr})=(3/4)k_B$) we observe the most interesting physical effects due to the interaction between solitary waves. For chosen parameters $v=\sigma$ and $b=100/\sigma$, we obtain $T_{tr} \simeq 0.16\ \varepsilon$

If $N$ is even, $N/2$-1 of waves (phonons), running on the right, and the same, running on the left, are excited in the ring at small temperature. Also, the phonon with frequency equal to an upper frequency of a phonon band and «a zero phonon» with a frequency and a wave number close to zero, corresponding to very slow rotation of a ring as a whole, are excited. So the frequency distribution of non-zero phonons modes contains $N/2$ discrete peaks. When temperature increases and nonlinear effects are developed, the phonons begin to interact with each other, and then to transform to nonlinear (cnoidal) waves, also interacting with each other. The wave length of cnoidal waves on a ring is restricted by its length, and only at increasing number of particles they will differ ever less from solitons in a boundless chain.

The interaction of nonlinear excitations is most strong near to the transition temperature. In particular, it follows from the spectrum $(FF)_\omega$, defined as the Fourier transform of the time correlation function (ACF) of the force acting on a particle. The ACF is calculated from molecular dynamic simulations in order to identify thermally activated soliton-like excitations in the spectrum (Fig. 5). We can observe a noisy range of the spectrum near to a region containing frequencies of phonons, and also a broadband coloured noise of a $1/f$ type at low frequencies. The last implies a hierarchy of beatings where periods with more energetic compression pulses are more probable to appear at longer time intervals. Its appearance is associated also with diffusion processes in the system and testifies an opportunity of transformation of white noise of a surrounding medium to coloured noise.

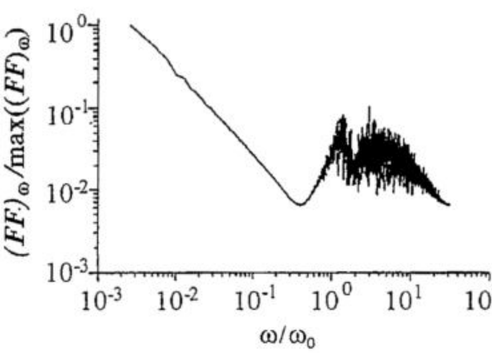

Fig. 5. Spectra $(FF)_\omega$ of single-particle forces $F$ in uniform rings of $N$=10 (solid) and $N$=20 (dashed) Toda oscillators with oscillation frequency $\omega_0$ and stiffness $b=100/\sigma$ in thermal equilibrium with a bath in the transition-temperature region ($k_BT=0.26\varepsilon$ corresponds to $c_V(T_{loc})=0.73k_B$). The friction parameter is $\gamma=10^{-3}\omega_0$. The spectra were obtained by Fourier transformation of the auto-correlation function. We observe broad peaks around the second-phonon frequencies as well as $1/f$ tails at the low end of the spectra

Some details of the process of interaction of nonlinear excitations are clarified by the analysis of a dynamic structure factor (DSF) of a chain [7]. It is defined as follows [8]

$$S(\omega,k) = 1/(2\pi N)\int_{-\infty}^{\infty} e^{i\omega t}\langle\rho(\mathbf{k},t)\rho(-\mathbf{k},0)\rangle dt\,.\quad(12)$$

Here **k** and $\omega$ are a wave vector and a frequency, $\rho$ is density of a particles ensemble, the angular brackets mean the operation of an average on a set of time series. DSF allows to judge time behaviour of spatial (collective) structures of specific scales, generated on a ring. Setting quantity $k$, defining a frequency composition $S(\omega,k)$ and estimating breadth of spectrum lines, it is possible to judge a stability of structures (nonlinear waves) and velocity of their motion on a ring. In particular, in a ring

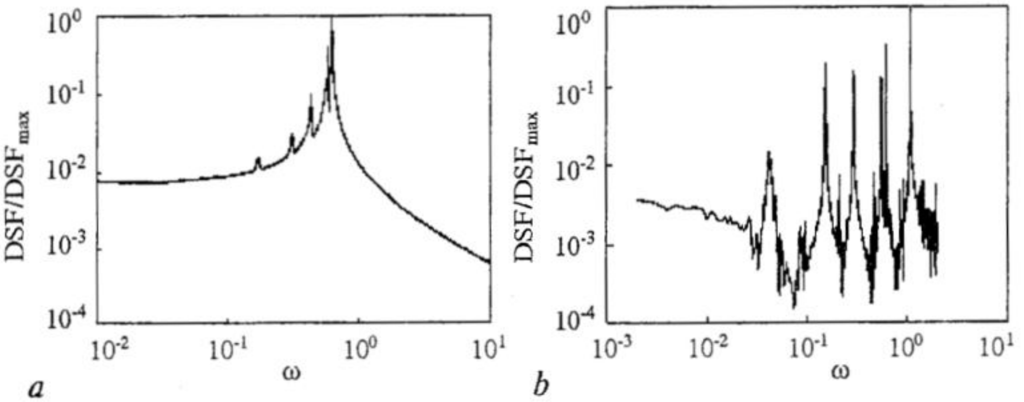

Fig. 6. The dynamic structure factor $S(\omega, k)$ /max $S(\omega, k)$ versus frequency ω for a Hamiltonian ring chain ($N$=10, $\gamma$=0) for the wave number $k=k_{01}=2\pi/N$: *a*) at low temperature, the particles interactions correspond to the cubic weak nonlinear (Fermi-Pasta-Ulam type) potential; *b*) in the transition-temperature region at $T=T_{tr}$.

with $N$=10 it is possible to observe transformation of dynamics when reaching a stationary temperature and «switching-off» of an external environment by calculating a dynamic structure factor at different temperatures using MMS [9, 10]. It has been seen (Fig. 6, *a*), that at small temperature, when the nonlinearity is week, $S(\omega)$ at a wave number corresponding to the resonant structure of the largest scale - to the first phonon-contains combination frequency components in addition to the first phonon frequency $\omega_1$. They arise due to interaction of five phonons with frequencies $\omega_i$, $i$=1,5 on quadratic nonlinearity and have frequencies $\omega_{cj}=\omega_{j+1}-\omega_j$, $j$=1,4. With increasing temperature the first phonon (and then others) transforms to a cnoidal wave with velocity more than velocity of a sound. In particular, at transition temperature it is approximately twice higher (Fig. 6, *b*). The nonlinear wave in this temperature range strongly interacts with other waves, but remains rather stable, as far as it is possible to judge from a spectrum $S(\omega)$, consisting of a small number of narrow discrete peaks. This tendency is specific under further temperature increase also, when the spectrum displaces to the right as a whole because of a velocity rise of nonlinear waves, and the region of combination waves is rared as the waves begin to resemble solitons more and more and their interactions weaken.

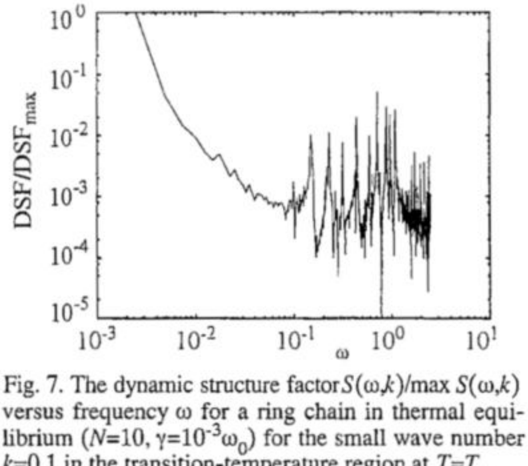

Fig. 7. The dynamic structure factor $S(\omega,k)$/max $S(\omega,k)$ versus frequency ω for a ring chain in thermal equilibrium ($N$=10, $\gamma=10^{-3}\omega_0$) for the small wave number $k$=0.1 in the transition-temperature region at $T=T_{tr}$

If the ring is not switched-off from external environment after reaching equilibrium temperature, the dynamic structure factor also indicates excitation of 1/*f* of noise at low frequencies for small values of a wave number *k* (Fig. 7). However it is necessary to note, that the details of processes corresponding to 1/*f* noise in the model described are still not clear and a more complete understanding of the matter calls for further study [5].

## 4. Dynamic structure factor of plasma

The problems of structure evolution arise, as a rule, in studies of phase transitions in gas-fluid, fluid-solid, gas-plasma and have many aspects. The distribution function, certainly, is not the unique characteristic of such states. In particular, the use of the dynamic structure factor mentioned above (8) is effective in researches of spatial structures and their time behaviour both in plasma and fluid. An important advantage of DSF is that it can be defined experimentally and it is associated with several regular characteristics which on many occasions can be determinated only as by means DSF. For example, having known DSF, one may find the plasma electric inductivity and dispersion, including the case of such density when it is very difficult to calculate these characteristics by other methods. Now let us discuss features of simulation of particles behaviour in plasma before we analyze results of DSF calculating.

Usually what is implied when one speaks about plasma, is the dense plasma. It is more similar to fluid than to gas by a number of properties. Really, Coulomb potential is more «long-range», than, for example, Lennard-Johnes potential, therefore in dense plasma each particle simultaneously interacts with several others particles, i.e. the interaction is collective. The definitions «isotropic», «homogeneous», «ideal» and so on are used for namely this kind of plasma. Its behaviour is oscillatory or wave, as a rule, and is studied within the framework of hydrodynamic or electrodynamic models. On the other hand, the density in dilute plasma is small and particles interact pairwise, as in gas. Therefore the dynamics can be investigated using models developed for studies of gas properties. However collective phenomena are exhibited more and more in dynamics of such plasma under increasing density (it can not be called dilute already). The application of MDS is most effective for study specifically these phenomena, evolution of their properties, changes in dynamics taking place when density grows. Moreover, there are situations, when MDS is the unique effective method of the analysis of behaviour of a plasma system.

Two stages can be identified in studies using MDS in the general case: the stage of determination of a potential share for each particular case of particles interaction and the stage of determination of the dynamics of the particles ensemble given by this interaction. First of them is not a subject of the present paper, we will not discuss that here. Note only, that a model of interaction of particles in plasma is developed as a rule based on concepts of a quantum mechanics. At the second stage the computer simulation of the particles interaction is carried out and the results obtained are used for determination of the different performances of a system. Usually a classical Coulomb potential is used for presentation of charged particles interaction in the theory. The point is that very high accelerations are developed when opposite-charged particles are coming together in the numerical model with the classical potential and calculations become illconditioned. As a matter of fact, the quantum phenomena come into force when particles close to each other at a distance exceeding that comparable an atomic scale, and they lead to a little bit other behaviour in compprison with «Coulomb» one. But the quantum models are very complicated and it is not efficiently to apply them to simulation of phenomena, in which «quantum» interactions take only a small part of a total duration of the process. That is why quasi-classical models are developed, in which the classical motion obeying the Coulomb potential force takes place, and only when particles are getting to close the specific shapes of a potential defined on the basis of quantum mechanics laws are applied [8]. We do not discuss details of those models, but the results obtained by a MDS in the frame of quasi-classical models, are very interesting.

In a Fig. 8 the data of calculation [8] of a certain coefficient $R(\mathbf{k},\omega)$, proportional $S(\mathbf{k},\omega)$, for plasma within the framework of a quasi-classical model developed in that work are represented. (The difference between R and S is not basic for our consideration, see the details in [8]). The cases of both moderate coupling ($\Gamma=1$), when the autocorrelation function (ACF) falls monotonically to zero, and strong coupling ($\Gamma=100$), when ACF shows oscillations with a frequency close to the plasma frequency $\omega_p$, have been explored. Here $\Gamma$ is the coupling strength parameter. The results are given as

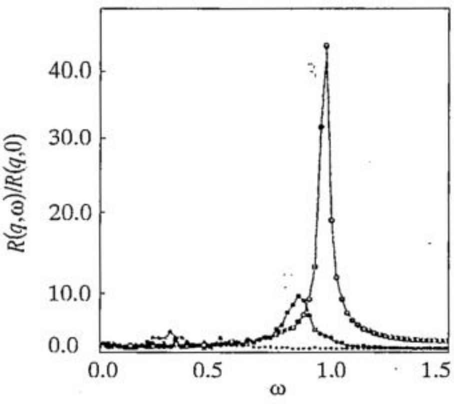

Fig. 8. The loss function $R(q,\omega)$ versus frequency $\omega/\omega_p$ for different wavevectors $q$ at $\Gamma=100$

dependencies $R$ as a function of dimentionless frequency $\omega$ for different wavevectors $q=ka$, where $a$ is a characteristic space scale of the system. As we see the peak at $\omega \simeq \omega_p$ (plasmon) is observed only for smallest $q$ value (defined by the size of simulation space). The effect is not unexpected, as just the particles clusters of size comparable with big enough scale, corresponding to small values $q$, have an sufficient effect on motion of a individual particle at small coupling. Therefore the plasmon does not manifest itself really at small coupling in this case. However with increasing $\Gamma$ (density) the plasmon peak rises although does not reach the same magnitude as at small $k$. The peak is close to $\omega_p$, but under change in a wave number it is shifted distinctly. It allows to determine the dispersion that may be both positive and negative. The peak is identified even in the region of the strong Landau attenuation, where it is impossible in fact to determine dispersion by ordinary technique.

## 5. Distribution function of clusters and phase transitions

The big number of problems of molecular dynamics is associated with investigations of properties of clusters. In molecular dynamics the term cluster is used for designation of an aggregation of particles located close enough to each other and bound by forces of an intermolecular interaction, in particular, of the Lennard-Jones or Morse type. For example, clusters are formed in rings of particles interacting via Morse forces if density of particles is small [11]. The clusters are stable enough, i.e. their lifetime is long so that events in which clusters take part could be detected by spectroscopic methods, for example [4]. What the stability of a cluster depends on? Let's consider, for example, conditions at which two particles (the neutral molecules) will form a cluster. Apparently, this couple will be stable if its summary kinetic energy is less than the potential energy - they are in a potential well and can not overcome the potential barrier in the absence of an external excitation. It is likely that the cluster will be stable if the total energy of the system is negative: $E=T+U<0$. Therefore, the clusters are produced in processes when kinetic energy of particles decreases. For example, if to open the cock of a vessel containing hot gaseous carbon, clusters will be formed in jet discharged owing to abrupt cooling of the gas. The proportion of clusters containing given number $n$ of particles (monomers, dimers etc.), is characterized by a distribution function $f(n)$ (cluster size distributions, CSD [12]). Experimentally found $f(n)$ for carbon, for example, under conditions mentioned above is given in Fig. 9 [13]. Note, the function characterizes a stationary, steady state. But there is a specific interest in evolution of clusters in processes of forming, dislocation, deformation, i.e. in the function $f(n,t)$. Let us now consider the procedure for theoretical calculation of the function, based on the geometric-energy approach.

For the configuration of the ensemble of particles obtained during MD-simulation at some instant «geometrical» clusters are determined first on the basis of the agreement that the particle is considered belonging to a certain cluster, if it is at a distance from any particle not exceeding the distance $R \approx 1.2\sigma$. The latter is taken as a characteristic size of a particle. Then, after each of particles has been identified as belonging to any cluster and

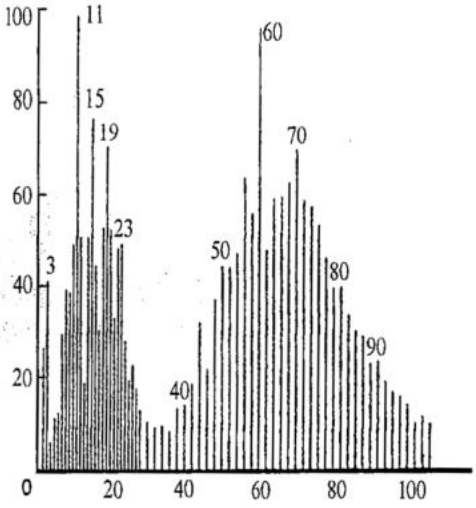

Fig. 9. Mass-spectrum of the carbon clusters [13], i.e. relative intensity as a function of a number of carbon atoms in the cluster

the number of clusters has been counted, the total energy of each cluster is calculated. If it is subzero, the cluster is regarded to be stable (though, of course, it can be abandoned by some particles later on). If it is not, the fastest of particles is «extracted» numerically from the cluster until the energy of the stayed aggregation does not become negative. If the number of the particles discarded is small (it is less, say, 10) it may be considered as a stable one, i.e. it is a safe assumption that it does not break down. But if the number of them is big, we deal with a non-stationary phase - the phase of shaping or active deformation of clusters.

As an example of calculation of CSD in MD-simulation we will consider a problem about «spreading» of a «drop» of a fluid (big cluster (Fig. 10)) owing to such change of surroundings, that the drop energy became close to zero at some instant. Because of that the particles with high kinetic energy turned out to be a part of the cluster, and then they start leaving it. There is every indication that the result will depend critically on friction in the system. In Fig. 11 the plots $f(n,t)$ for three cases of different values of a friction coefficient are represented. It is shown that at small friction the cluster in fact entirely collapses (Fig. 11, *a*) reaching fast the steady-state of big number of monomers, some dimers and insignificant number of clucters of big number of particles (Fig. 10). If the friction is appreciable (Fig. 11, *b*), the initial «big» cluster stays stable due to fast cooling (only some monomers and one-two clusters of a small number of particles break off). A steady state is established fast enough in this case also. And it is not a success to reach a steady state during carrying out of the computer experiment in the intermediate case (Fig. 11, *c*) - fragments of the cluster collapsed have not ceased to deform.

The phenomenon of transitions of matter from some phase to another one is associated also with the problems of clusters. A number of theoretical and experimental studies has been devoted to this problem having a great deal of aspects and items. Not

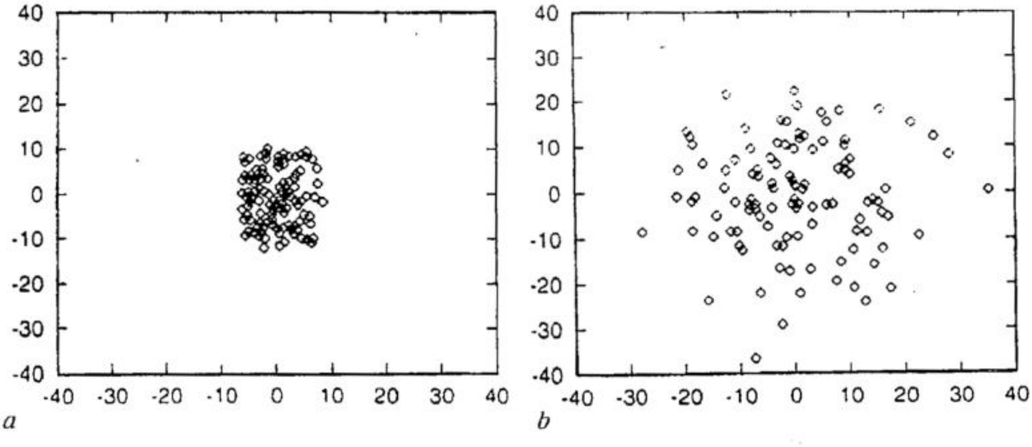

Fig. 10. Locations of interacting particles: *a*) at an initial moment («drop» of a fluid) and *b*) at stationary state at small friction

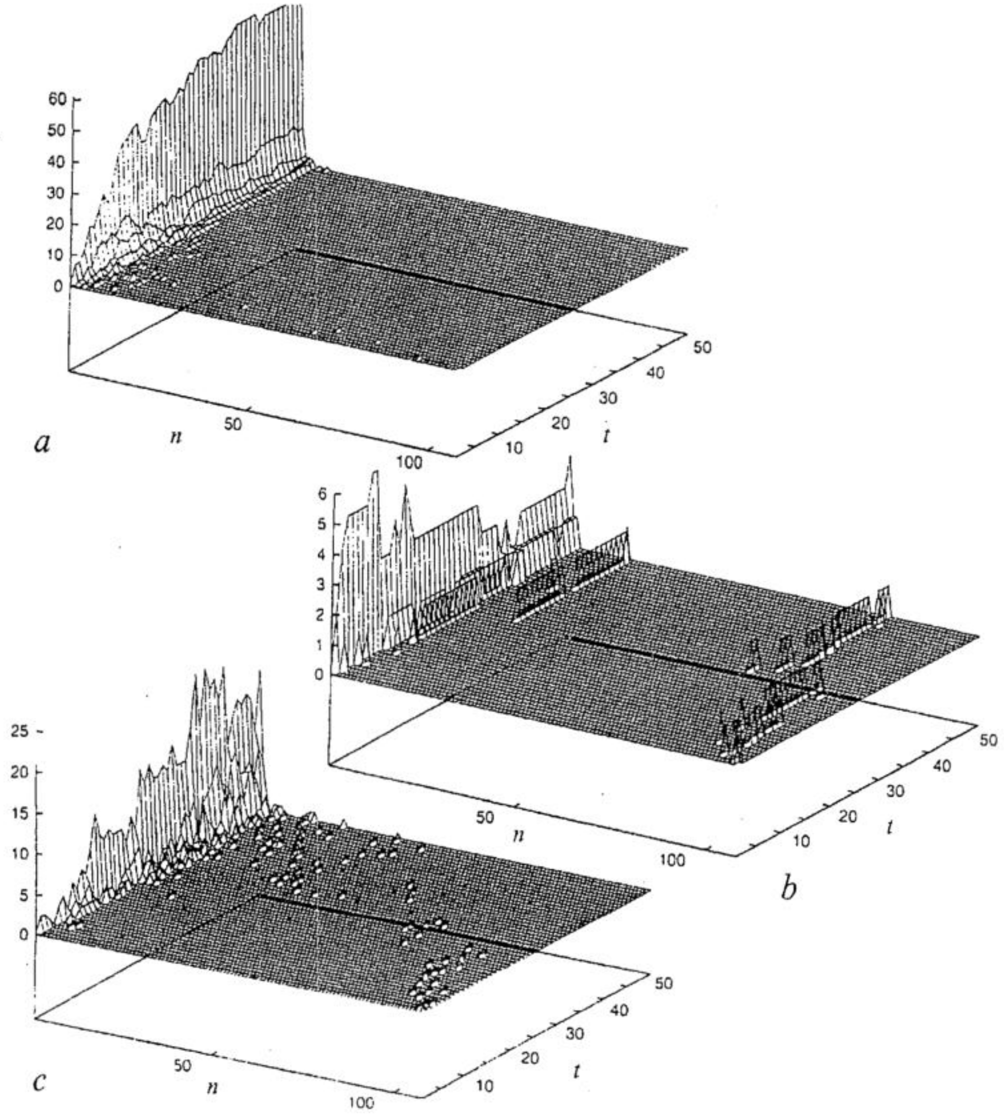

Fig. 11. Distribution function of clusters $f(n,t)$ for three cases of different values of a friction coefficient: *a*) small friction, *b*) appreciable friction, *c*) intermediate case

seeking to perform a complete overview and analysis of them, we will restrict ourselves to the discussion of only those of them, which are effectively explored by molecular dynamics simulation. In particular, this is a phenomenon that may be called as a problem about «fusion» of molecular clusters under heating. The difficulties of the analysis of phase transitions in real volumes of matter are accounted mainly by enormous number of particles taking part in the process and practical impossibility to analyze all created patterns of a uninterruptedly varying potential surface. However phase transitions of small enough (mesoscopic) objects - clusters - can be studied in detail. This problem is interesting by itself, as it appears, the phase transitions in clusters of a small particles number do not run as in extended volumes of matter. And on the other hand, increasing a number of particles, it is possible to trace evolution of properties in the transition from a «cluster» state of matter to a «volume» state. Note, mesoscopic systems take up an intermediate position between the macroscopic and microscopic of them. To investigate phase transitions in clusters the analysis of the shape of a potential surface established by

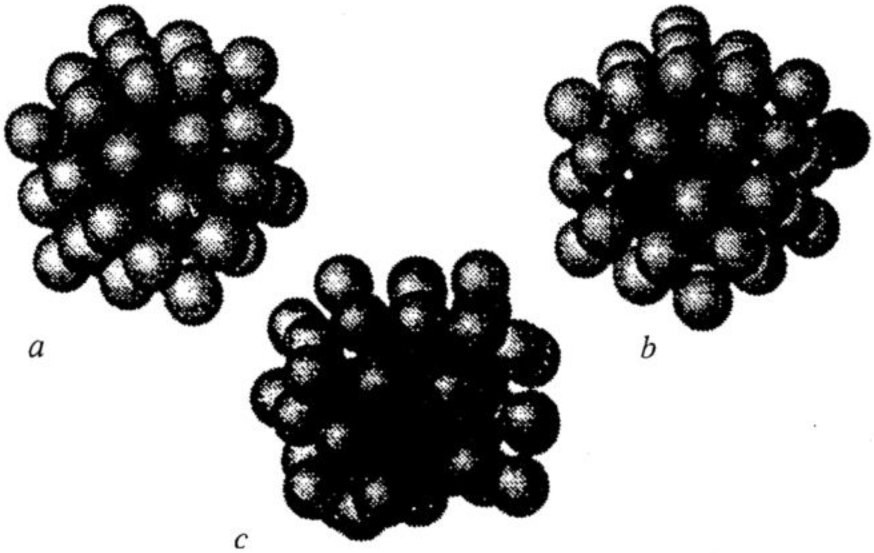

Fig. 12. Representative (quenched) structures of the coexisting phases in $Ar_{55}$: *a*) solid icosahedral, *b*) surface melted with one floater and *c*) homogeneously melted. The core atoms and the floaters are represented by dark spheres, the outer shell atoms by light one

cluster particles can be used as the very perspective approach [4]. The main item is the definition of location of local minimums of the potential and a depth of potential wells being in process of computer modeling by MD-method. The existence of a few phase states of a cluster may be regarded as the most interesting effect discovered recently. Three distinct phase states - microcrystalline (solid), homogeneously melted and solid kern with a melted shell - have been found by computer modeling [4] of isothermal dynamics of a three-dimensional cluster. At specific temperatures they can occur at the same time with a sense of such state is a little another, than in macroscopic systems. It has been revealed the certain, precisely distinguishable level of the potential energy corresponds to each phase. The simultaneous existence of several phases of a cluster means that it periodically goes from one state to another, and the residence time of each phase depends on a well depth and a width of transition between adjacent local minimums. In Fig. 12 the different states $Ar_{55}$ (*a* - solid icosahedron (micro-crystal), *b* - with a melted surface consis-ting one «floater», *c* - with a homogeneous melted surface) and in Fig. 13 a time dependence of energy of a cluster are shown at different temperatures. There is no doubt that in a temperature range between $T$=30$K$, corresponding to a microcrystal, and $T$=40$K$, corresponding to melted matter, the states are established when there is periodic «switching» from one phase to another. Having determined levels of energy of each phase and their residences, one can calculate by means of statistical processing the probability distribution functions for different quantities, a diffusion constant for each phase, the entropy etc. Purposeful searching of states with given properties and methods of control in them may be carried out with help of characteristics mentioned. The field of phase transitions of mesoscopic systems are under active study now and discoveries of many interesting properties of such systems may be anticipated in future.

## 6. Transition processes and reactions

The model presented above is not sufficient for explanation of processes in several important and interesting cases. Let us consider, in particular, the problem about reaction

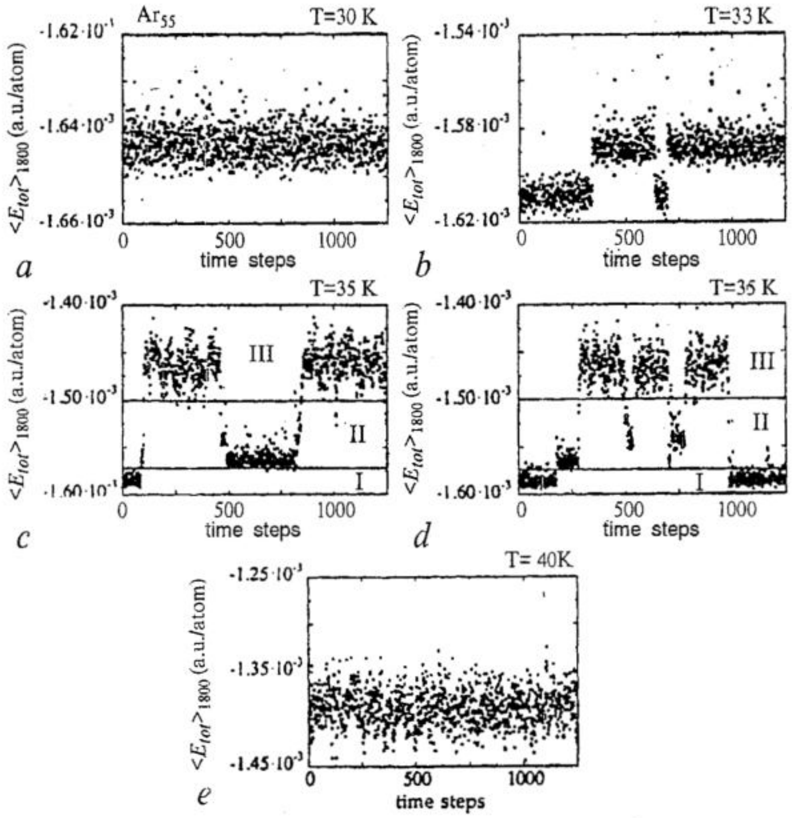

Fig. 13. The short-time averaged internal energy$\langle E_{tot}\rangle_{\tau}$ of $Ar_{55}$ for the temperatures $T$=30$K$ ($a$), 33$K$ ($b$), 35$K$ [($c$) and ($d$)], and 40$K$ (e). Each point represents an average over $\tau$=18000 time steps of $3\cdot 10^{-15}$ s each. The solid lines in ($d$) correspond to the energy limits used in the simulations to distinguish between energy regions of the different phases, I denoting the solid phase, II the surface-melted phase, and III the homogeneously melted phase ($e$)

rates at different temperatures. As it is known, the rate of many chemical reactions is defined by the Arrhenius law

$$K = K_0 \exp(-\Delta U / k_B T), \tag{13}$$

where $K_0$ is a reaction rate at $T\to\infty$, $\Delta U$ is the activation energy equal to a depth of a potential barrier, which should be overcome to split a bond, $k_B$ is the Boltzmann constant. Arrhenius behaviour was marked for the first time more than hundred years ago and has been under an experimental test in different kinds of reactions. In 1940 Kramers developed the theoretical model becoming in the further the prototype of a statistical reaction theory. The Kramers-theory of reaction rates is based on a Fokker-Planck equation for the reactive molecule or on the corresponding Langevin equation with white noise sources (see [14, 15]). One of implications of this theory is the Arrhenius law. However recently it was clarified, that the Arrhenius-law is not always fulfilled precisely. Besides, it was revealed, that some other experimental data do not always correspond to behaviours following from the Kramers-theory [14, 15]. The search for the reason has lead to a presumption that one of basic assumptions of the Kramers-theory about lack of correlation of elementary exposure acts to other particles is disturbed in mentioned above cases. Indeed, it was shown in [16, 17] that if a noise source in the Langevin equation is assumed to be colored, it results in consequences leading to Arrhenius behaviour violation, in particular. But what is the reason for occurrence of preferred scales in the source? It has been hypothesized that it takes place due to specific exhibition of nonlinear (and dispersive, to some degree) properties of systems of particles distributed in space [14]. We will leave the Arrhenius law for now and shall consider processes in solutions in more details.

As it is known, the solution is a mixture of particles of two sorts at least - a solvent and an impurity. The solvent concentration is much higher, for example, one molecule of the impurity is per 30 molecules of the solvent. It was found that the Arrhenius law is disturbed in such system if molecules of the solvent are «hard», and the others are «soft» [14]. It is implied that the interaction of «hard» molecules between themselves is much more restoring, than that of «hard» and «soft» molecules, and proceeds much faster. It has been supposed [14], that so-called local energy spots are formed in such system. They are located on soft particles and hard particles acquire the high potential energy. To verify this hypothesis the simple one-dimensional model of a solution in the form of a Toda chain has been considered [18]. As mentioned above, soliton-like local excitations of a density can exist in a homogeneous Toda chain (when the parameters $a$, $b$, $\sigma$ are identical for all sites of a chain, see (2)). In the general case they arise, as known, under a certain relation of nonlinear and dispersion properties of a system. In a nonlinear chain soliton-like structures are excited for specific values of nonlinear potential parameters specifying both nonlinear and dispersion properties. If in a chain the small part of molecules are «soft», the soliton-like excitations formed by hard molecules can «stick» at the soft sites during some time, transferring coherently appreciable amount of energy to them. Indeed, the times of the interaction of the soliton with the «hard» and «soft» molecules are as $\tau/\tau_0=b/b_0$, where the index 0 refers «soft» molecules. Moreover it is supposed, that the dynamics of «soft» molecules also obeys the potential of the same form (6), but with other parameter values. In particular, $b_0<<b$, so during relaxation the «soft» molecule can accumulate energy even more than that of one soliton. As a result the probability of overcoming of a potential barrier appreciably increases, and the reaction rate rises. It leads to a consequence that the fraction of high-energy soft molecules of the distribution as a function of the potential energy of the soft molecules increases, shifted to higher values and acquires longer tails. This conclusion is confirmed by the analytical calculations in [14]. But for systems with other kinds of a potential, furthermore for two-dimensional and three-dimensional systems, it is impossible to obtain the analytical results. That is why in [14] the molecular dynamics method has been used for calculation of the distribution functions.

The interaction of 32 particles, one of them was soft, was considered in 1D-, 2D- and 3D-models with the modified Lennard-Jones potential (4) which at $A=28$, $n=8$ well approximates the real Lennard-Jones potential, but is much more suitable for numerical calculations. It is shown in a Fig. 14, *a* that the maximum of the distribution function $f(U)$ for a 2D-case for soft molecules is really shifted to the range of high energy events relatively the maximum of the function for hard molecules and the fraction of high-energy molecules («a high-energy tail») is by an order of magnitude greater (fig. 14, *b*). Besides the average potential energy of soft molecules can be several times higher exceeding (fig. 15) average kinetic energy. (Note, at small temperatures, when interaction of molecules is in fact linear, these quantities are equal.) Results are the same for 1D- and 3D-models, and they do not change when the number particles is increasing. Taking into account this effect of formation of the energy spots, we shall return now to the Arrhenius law and consider specific systems, in which it is violated.

We shall consider the model of the dissociation of diatomic molecules [15]. The atoms in such molecule are bound by potential force arising from the Kramers bistable potential

$$V^{K}(x,y,z) = \varepsilon - x(x^4 - 2x^2) + \varepsilon_y y^2 + \varepsilon_z z^2 . \tag{14}$$

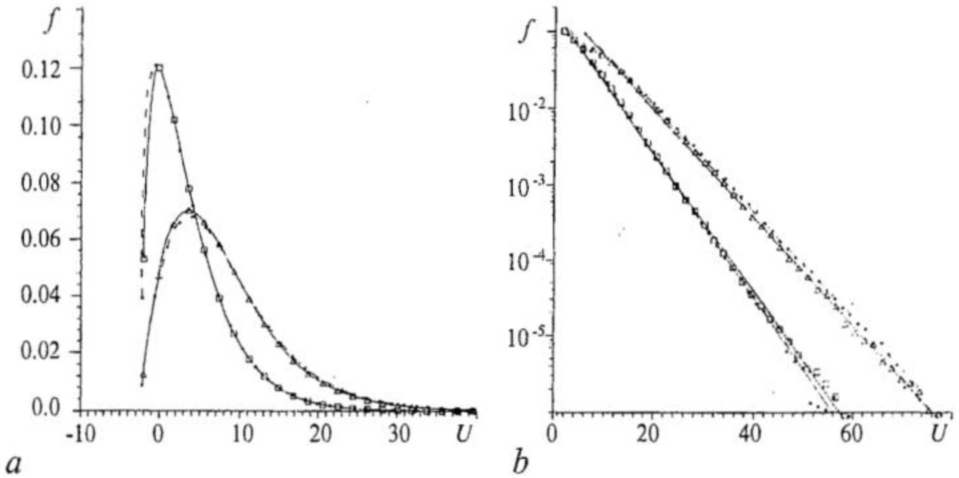

Fig. 14. The distribution function (*a*) and its tails (*b*) for $T$=7 and finite size potentials in the two-dimensional system ($N$=32: triangles = soft, squares = hard molecules; $N$=200: stars = soft, fat stars = hard molecules)

Two minima of the potential correspond to two possible configurations of such soft molecule (Fig. 16) The potential barrier must be overcome to reach dissociation. The energy for overcoming is accumulated by a molecule owing to interaction with surrounding hard molecules, and the interaction force is given by the Lennard-Jones potential. The interaction potential of hard molecules with hard molecules is the same, but with parameters providing much more shorter time of relaxation. The study has been carried out within the scope of 2D-model with 100 particles. Initial positions of particles correspond to minima of the potential function, and then the system reaches the given temperature during a stage of «heating». A short segment of the plot of the coordinate $x$ of the particle into a potential well of the diatomic molecule against time is shown in Fig. 17. The mean time $\tau$ of transition between two states connected with the reaction rate by a relation $\tau=1/K$ has been calculated (Fig. 18) based on the function $x(t)$ presented above. It is certain that $\ln\tau$ as a function of the quantity $\Delta U/T$, is not linear, as it should according to the Arrhenius law, but it is parabolic instead. Similar results have been obtained in the simulation of a reaction with participation of the diatomic molecule, in which bond of atoms occurs by the Morse potential reads in the form

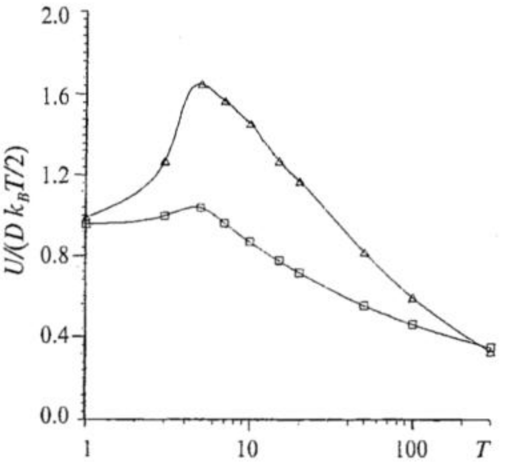

Fig. 15. The temperature dependence of the mean potential energy in $Dk_BT/2$ units for the two-dimensional case ($N$=32: triangles = soft, squares = hard molecules)

$$V_\mu(r) = \varepsilon[(\exp(-6(r-\sigma_L 2^{1/6})) - 1)^2 - 1]. \tag{15}$$

$\ln\tau$ as a function of $\Delta U/T$ at fixed $\Delta U$=50 proves to be not linear again, and at a

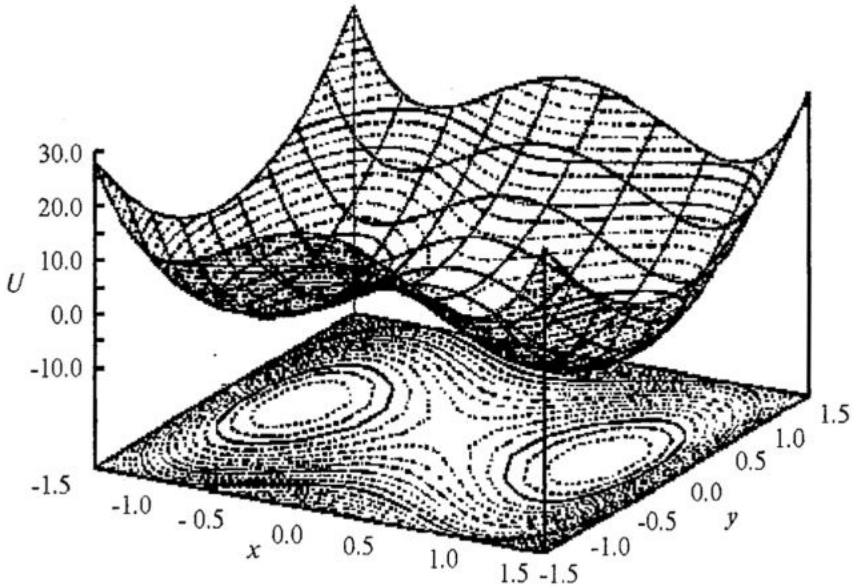

Fig. 16. The shape of a bistable 2D Kramers potential. The minima correspond to the stable states of the active molecule

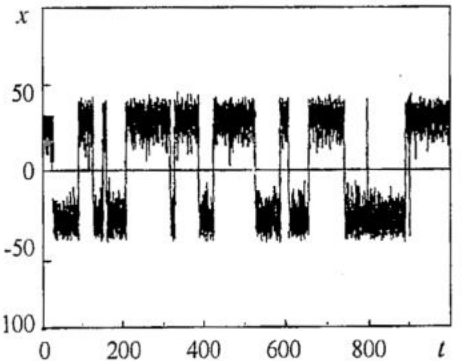

Fig. 17. Transitions between the 2 wells of the bistable Kramers potential caused by molecular collisions

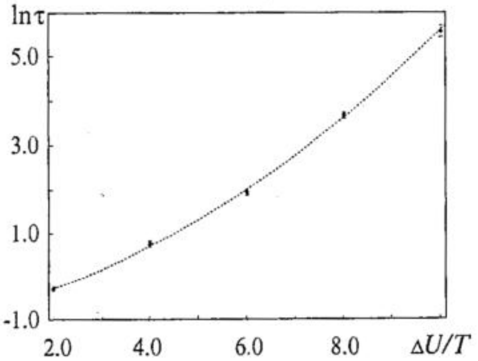

Fig. 18. The logarithm of the average time between transitions from one of the Kramers wells to the other one, as a function of the Arrhenius exponent ($\Delta U/T$)

fixed value $T$=7.5 it is almost linear, but with a slope 0.5 instead of 1, as it should be in agreement with the Arrhenius behaviour (Fig. 19). Thus, the effective temperature of the system is not in agreement with the actual, classically defined temperature of a solution, because of the noise excited in collisions of molecules, is not white and effective temperature depends on its spectrum. Currently it is impossible to

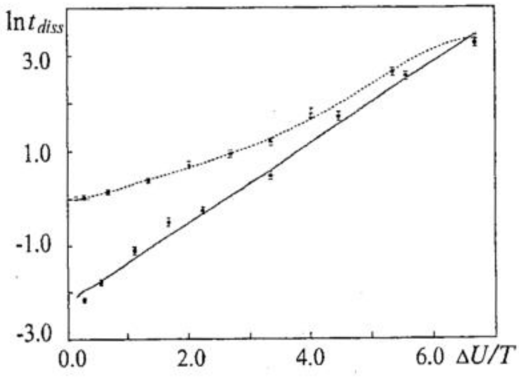

Fig. 19. The logarithm of the dissociation time for a Morse molecule as a function of the Arrhenius exponent. The full line corresponds to a fixed value of the potential barrier $\Delta U$=50 and the dashed line to fixed temperature $T$=7.5 and variable potential barriers. All energies and temperatures are given in the Argon-units used in [15] (i.e. $T$=1 corresponds to 119$K$)

finally conclude that phenomena considered are explained entirely by existence of local energy spots [15]. Nevertheless, this explanation is believed to be the most probable, and further researches in this lead are still in progress.

## 7. Nonequilibrium phenomena

There is an ample class of problems about various flows and instabilities in fluids. They are solved usually within the framework of hydrodynamic models. The results of many of them are well known (see, for example, [19]). In particular, it is known, that at low gradients of temperature and pressure the flow of a fluid is laminar, i.e., for example, the flow velocity is the same at all points of a jet. However this statement is valid only for spatial scales much more than characteristic sizes of molecules and a free length. The trajectories of a motion of molecules corresponding microscales remain chaotic. What is the way to structure unordered motion of individual molecules to collective motion of big ensembles? The molecular dynamics simulation allowing to calculate trajectories of molecules and then to carry out averaging complying with various scales plays an invaluable role in studies answering this question.

Let's consider for an example a motion of molecule of a fluid under conditions, at which the instability of Rayleigh-Benar is harnessed [20]. The results of simulation of motion of 5000 particles in a fluid layer in a rectangular vessel to be heated up from below are presented there. It is known [19] from the analysis of this system taking a hydrodynamic approach, that the type of collective motion of particles depends on a value of a non-equilibrium parameter - the Rayleigh number

$$R_\alpha = \alpha(T_L - T_U) l_x g / \nu D_\tau . \qquad (16)$$

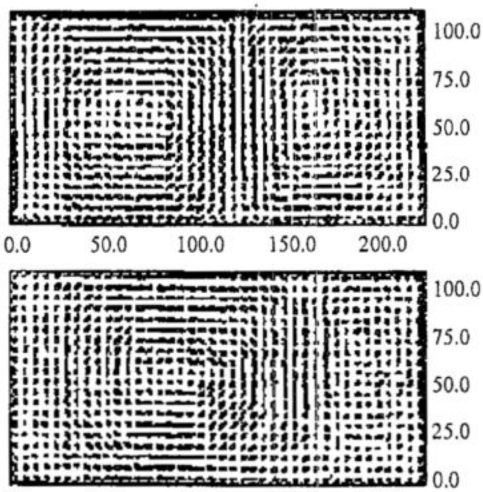

Fig. 20. Velocity field of molecular dynamics simulation with 5000 particles and aspect ratio = 2;( *a*) and (*b*) show transient states after 8000 and 10500 steps respectively; (*c*) displays the final state after 20000 steps (averaged over the last 10000 steps)

Here $\alpha$ is a thermal expansion coefficient, $\nu$ is kinematic viscosity, $D_\tau$ is a coefficient of thermal diffusion, $l_x$ is a width of a vessel, $T_U$, $T_L$ are temperatures on a top and a bottom, accordingly. As known, at small values of the Rayleigh number collective motion is laminar - this result confirms in [16] also. To obtain this a space averaging over small ensembles containing about 6 particles was carried out. The simulation field was divided into 800 «statistical» cells and an averaging was performed over all particles residing in of each cell at instant, and then a time averaging was carried out. The result was interpreted as a velocity of fluid at the centre of a cell. Increasing of the temperature gradient (the Rayleigh number) causes loss of stability of a homogeneous state and vortexes arise. Their «portrait» is represented in a Fig. 20. Vectors obtained by an average of velocities of all particles belonging to a given cell are shown in it by arrows. The vortexes are stationary inconvertible structures, and this deduction is well in accord with known «hydrodynamic» one. However authors noted, that an average over an ensemble of only 6 particles is crude enough. For example, plots of the velocity distributions obtained by MDS and in hydrodynamic approximation, differ in details, being the same qualitatively (Fig. 21). In this connection in [20] the chance to research effects of birth of small-scale vortexes and, in the long run, the turbulence, by MDS is estimated skeptically enough. The point is that a rising number of «cells» and the particles number in a «cell» for obtaining of data up to acceptable accuracy is required with growth of number of vortexes under the Rayleigh number increasing (i.e. under decreasing of characteristic scales). However, it seems likely that this problem will be overcome with computer efficiency increasing. At all events, it is early to put an end to further investigations.

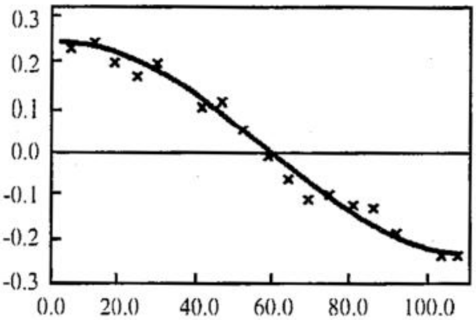

Fig. 21. Horizontal component of the velocity as a function of $z$, for a vertical slice located at $x=L_x/4$. The curve refers to the hydrodynamical calculation where as the crosses represent the molecular dynamics data averaged over the last 10000 steps. Both axes are scaled in system units

## 8. Conclusion

The molecular dynamics simulations (MDS) based on numerical solving of equations of motion for a small ensemble of particles, is effective for studies of properties of both a bulk state of matter (macroscopic systems) and states formed by clusters (mesoscopic systems). In both cases a main field of application of a method is in the systems which are nonequilibrium or are in a state of phase transitions «gas - fluid», «fluid - solid», «gas - plasma». For many problems MDS is the only research instrument. The models are used both with a classical nonlinear potential (Lennard-Johnes, Morse, Toda etc.), and semiclassical, in which individual events of particles interaction occur potentials determinated on the basis of quantum mechanical calculations. It is implemented effectively not only for three-dimensional models, but also for two-dimensional and in particular one-dimensional. It is possible in the last case to compare computer simulation data with analytic results. Among the problems related to properties of bulk states, problems concerning origin and evolution of structure transformation in ensembles of particles used in studies of properties of chemical reactions, dilute plasma, near-boundary fluids, processes of ionization etc., are assumed as most interesting. The development of technique of determination of quantitative characteristics of structure transformations (distribution functions, dynamical structure factor, probability distributions and others) is very important. In researches of mesoscopic systems the datas can be highlighted on availability of some phase states of clusters with a small number of particles and opportunity of simultaneous existence of them. It seams likely that studies of connection of properties of potential surfaces, created by cluster particles, with nonlinear dynamics of particles and collective cluster performances are highly promising. The examinations of transformation of the performances of mesoscopic systems under increasing of a particles number are interesting because they lay a bridge between mesoscopic and macroscopic systems.

Acknowledgements: The authors are grateful to A.A.Valuev for discussions. A.Chetverikov is grateful to Deutscher Akademischer Austausch-Dienst (DAAD) for the grants which made possible his participation in this work.

## References

1. *Allen M.P., Tildesley D.J.* Computer Simulations of Liquids // Clarendon Press, Oxford. 1990.

2. *Norman G.E., Podlipchuk V.Yu., Valuev A.A.* Molecular Dynamics Method: Theory and Applications // J.Moscow Phys. Soc. 1992. №2. P. 7.

3. *Norman G.E., Podlipchuk V.Yu., Valuev A.A.* Theory of Molecular Dynamics Method // Molecular Simulation. 1993. № 9. P. 417.

4. *Kunz R.E.* Dynamics of First Order Phase Transitions In Mesoscopic and Macroscopic Equilibrium and Nonequilibrium Systems. Thun. Frankfurt am Main. Deutsch. 1995.

5. *Jenssen M., Ebeling W.* Distribution functions and excitation spectra of Toda systems at intermediate temperatures // Physica D 141, 2000. P. 117.

6. *Toda M.* Theory of Nonlinear Lattices // Springer, Berlin. 1981.

7. *Croxton C.A.* Liquid state physics - A statistical mechanical introduction // Cambridge University Press, 1974.

8. *Ebeling W., Ortner J.* Quasiclassical Theory and Simulations of Strongly Coupled Plasmas // Physica Scripta. 1997. P. 1.

9. *Ebeling W., Chetverikov A., Jenssen* M. Statistical thermodynamics and nonlinear excitations of Toda systems // Ukr. J. Phys. 2000. Vol. 45, № 4-5. P. 479.

10. *Ebeling W., Chetverikov A.* Complex Dynamics on Nonlinear Excitations in Rings of Interacting Bronian Particles // Preprint Sfb555-9A-2000, Sonderforschungbereich 555 «Komplexe Nichtlineare Prozesse», Humboldt Univ., Berlin, 2000.

11. *Dunkel J., Ebeling W., Erdmann U.* Thermodynamics and Transport in Active Morse Chains// Eur.Phys.J, 2001 /in press/.

12. *Orgzall I., Lorenz B.* Grain and Cluster Structures in the Process of Nucleation and Growth // In: Nucleation-Clusters-Fractals. Proc. of the Workshop Serrahn (Dec.1990). Ed. by F. Schweitzer, H. Ulbricht. Rostock, 1991. P. 19.

13. *Rohlfing E.A., Cox D.M., Kaldor A.* // J. Chem. Phys. 1984. Vol. 81. P. 3322.

14. *Ebeling W., Podlipchuk V.Yu., Valuev A.A.* Molecular dynamics simulation of the activation of soft molecules solved in condensed media // Physica A. 1995. Vol. 217. P. 22.

15. *Ebeling W., Sapeshinsky M., Valuev A.* Microscopic Models and Simulations of Local Activation Processes // Int. J. Bifurcations and Chaos. 1998. Vol.8, № 5. P.755.

16. *Schimansky-Geier L., Zulicke L.* Effect of Harmonic Noise on Bistable Systems // Z.Phys. 1990. Vol. B79. P. 451.

17. *Hesse J.J., Schimansky-Geier L.* Inversion in Harmonic Noise Driven Bistable Oscillators // Z.Phys. 1991. Vol. B84. P. 467.

18. *Ebeling W., Jenssen M.* Trapping and fusion of solitons in a nonuniform Toda lattice // Physica D. 1988. Vol.32. P. 183.

19. *Landau L.D., Lifshits E.M.* Theoretical physics.V.6. Hydrodynamics. M.: Nauka, 1986.

20. *Mansour M.M., Puhl A., Mareschal M., Kestemont E.* Convective instability by molecular dynamics // In: Irreversible Processes and Selforganization. Proc. of the 4th Int. Conf. on Irreversible Processes and Selforganization. Ed. by W. Ebeling and H. Ulbricht Leipzig, BSB Teubner. 1989. P. 208.

*Saratov State University*
*Humboldt-Universisy*

*Received 30.10.2001*

УДК 519.876

# НЕЛИНЕЙНЫЕ ПРОБЛЕМЫ МОЛЕКУЛЯРНОЙ ФИЗИКИ

*А.П. Четвериков, В. Эбелинг*

Представлен обзор исследований некоторых проблем молекулярной физики, проведенных методом молекулярной динамики. Среди них проблемы элементарных возбуждений в жидкостях, динамика химических реакций в растворах, динамические свойства разреженной плазмы, динамические явления при фазовых переходах в мезоскопических системах, структурные свойства цепочек нелинейных осцилляторов. Обсуждаются также некоторые новые результаты исследований распределений кластеров и метод идентификации кластеров.

*Chetverikov Alexander* was born in 1953, graduated from the Faculty of Physics of Saratov State University in 1975, Candidate of Science in Physics and Mathematics since 1981, Doctor of Science in Physics and Mathematics since 1996. Now he is Professor of Chair of Electronics, Oscillations and Waves of Saratov State University. His research and teaching interests include nonlinear dynamics of distributed systems, microwave electronics, computer experiments. He is the author of more than 80 scientific publications.

*Ebeling Werner* was born in 1936, he studied physics at the University of Rostock and at Moscow State University, received his Diplom in Physics, his Doctor rer. nat and Doctor sc. nat at the Rostock University (1959, 1963, 1968). Now he is Professor of Chair of Statistical Physics and Nonlinear Dynamics of Humboldt University in Berlin. He is well known specialist in theoretical physics, one of the leading experts in statistical theory of electrolytes and plasmas and on the theory of selforganization and evolution of non-equilibrium systems. He is the author and editor of more than 20 books and great number of other scientific publications. Werner Ebeling is Honorary Professor of Saratov State University.

Bifurcations in dynamical systems

Izv. VUZ «AND», vol.10, № 3, 2002

# A VARIETY OF CRITICAL PHENOMENA ASSOCIATED WITH THE GOLDEN MEAN QUASIPERIODICITY

*S.P. Kuznetsov*

The paper presents several universality classes of critical behavior, which may occur at the onset of chaotic or strange nonchaotic attractors via quasiperiodicity. Parameter space arrangement and respective scaling properties are discussed and illustrated.

## 1. Introduction

Turbulence as a dynamical process in spatially extended systems attracts attention of researchers for a long time. An important aspect of the problem is the question: how does the spatio-temporal chaos originate from simple regular regimes as we vary one or more control parameters? As known, chaotic dynamics in multi-dimensional systems may arise via quasiperiodicity, in a course of subsequent birth of oscillatory components with incommensurate frequencies, followed by chaotization (see e.g., early works of Landau, Hopf, and Ruelle and Takens [1, 2, 3]). However, details of the transition from quasiperiodicity to chaos are subtle and complicated. Some of them may be revealed if we turn to a restricted problem: Suppose that the object can be decomposed to a master subsystem with quasiperiodic behavior, and a driven slave subsystem that demonstrates transition to chaos. Then, what are possible scenarios of the onset of chaos in the second subsystem? (This question also is of special interest in context of synchronization of systems with complex dynamics by periodic external force.)

One important advance on this way of reasoning was formulation of the concept of strange nonchaotic attractor (SNA) [4-6]. In the phase space SNA is an object of fractal geometrical structure, but without instability in respect to initial conditions. In quasiperiodically forced systems SNA are found to be very typical in an intermediate region between order and chaos.

One more essential idea consists in application of the renormalization group (RG) approach, proven to be very efficient for understanding dynamics in critical states at the chaos threshold (e.g. [7-13]). The critical behavior may be universal for a class of systems of distinct physical and mathematical nature. Hence, all relevant details for the critical dynamics may be revealed in one model, the simplest representative of the universality class. Originally, this approach has been developed by Feigenbaum for the period-doubling scenario of the onset of chaos [7, 8, 9], and latter for quasiperiodic transition to chaos by Feigenbaum-Kadanoff-Shenker and Ostlund et al. [10-12]. Afterwards, analogous treatment was applied to some cases of birth of SNA [14-16].

If a system we deal with possesses several control parameters, it is natural to introduce parameter space and speak about structure of this space in geometrical terms. It may contains some bifurcation surfaces, critical surfaces, separating domains of chaos and order, critical lines and points, where some special regularities of dynamical behavior at the onset of chaos occur. In Refs [13, 17, 18] such a picture is revealed and studied in some details for the period-doubling transitions to chaos.

In the present paper we review and discuss several types of critical behavior associated with the onset of chaotic or strange nonchaotic dynamics via quasiperiodicity in model systems. We consider two-frequency quasiperiodic motions with the golden-mean ratio of the basic frequencies, $w=(5^{1/2}-1)/2$. This irrational number is a traditional choice in many studies of quasiperiodicity. One reason is simplicity of the theoretical description. Another is a possibility to observe more subtle details of bifurcational structures in numerical and physical experiments than it would be possible for any other selection of the frequency ratio. In Sec.2 the procedure of RG analysis appropriate for the golden-mean quasiperiodicity is explained, and a two-dimensional generalization of approach of Feigenbaum-Kadanoff-Shenker [10] and Ostlund et al. [11, 12] is developed. In Sec.3 we discuss model systems including quasiperiodically driven logistic, circle, and fractional-linear maps. In Sec. 4 our generalized RG scheme is used to reproduce some results of classic analysis of quasiperiodic transition to chaos in the circle map [9-12]. In Sections 5, 6, and 7 we review three novel types of critical behavior discovered in a course of joint research program with the group of nonlinear dynamics and statistical physics from Potsdam University (A. Pikovsky, U. Feudel, E. Neumann) [15 ,16, 19]. For each type of criticality we illustrate scaling for the critical attractor associated with dynamics exactly at the critical point, and scaling of topography of the parameter plane near the criticality.

## 2. A two-dimensional generalization of the Feigenbaim-Kadanoff-Shenker equation

Let us consider quasiperiodic dynamics in some system with two basic frequencies, $\omega_1$ and $\omega_2$, and assume that two subsystems associated with these frequencies are coupled unidirectionally. To describe dynamics in terms of Poincaré map, we perform stroboscopic cross-section of the extended phase space by planes of constant time, separated by $T = 2\pi/\omega_2$. The first subsystem («master») is independent of the second one, and the associated dynamical variable is the phase $\varphi$ governed by equation $\varphi_{n+1}=\varphi_n+\omega_1 T$ (mod$2\pi$). For the second subsystem («slave») we assume that the dynamics is essentially one-dimensional: $x_{n+1}=F(x_n,\varphi_n)$. In respect to the second argument the function $F(x,\varphi)$ is $2\pi$–periodic. Instead of $\varphi$ we introduce a variable $u$ defined modulo 1:

$$x_{n+1} = f(x_n,u_n), \quad u_{n+1} = u_n + w \,(\mathrm{mod}1), \tag{1}$$

where $f(x,u)=F(x,2\pi u)$, $w=\omega_1 T/2\pi=\omega_1/\omega_2$. In the further study we fix $w=(5^{1/2}-1)/2$.

In general context of nonlinear dynamics, the basic idea of the RG analysis consists in the following. We start with an evolution operator of a system on a definite time interval and apply this operator several times to construct the evolution operator for larger interval. Then, we try to adjust parameters of the original system to make the new operator reducible to the old one by scale change of dynamical variables. This procedure is called the RG transformation. The adjusted parameters will define location of the critical point. The RG transformation may be applied again and again to obtain a sequence of the evolution operators for larger and larger time intervals. If the approach works, one possibility is that the produced operators become asymptotically identical, and we speak about a fixed point of the RG transformation. Another possibility is that they repeat each other after several steps of the RG transformation, and we speak about a periodic orbit, or a cycle of it. In any of these cases, the rescaled long-time evolution operators will be determined by structure of the RG transformation, rather than by concrete dynamical equations of the original dynamical system. This implies *universality*. On the other hand, repetition of the rescaled evolution operators at subsequent steps of the RG transformation means that the system manifests similar dynamics on different time scales. This implies *scaling*.

How can we apply this approach to critical phenomena associated with the golden-mean quasiperiodicity? As known, the convergent sequence of rationals for $w=(5^{1/2}-1)/2$ is defined as $F_{k-1}/F_k$, where $F_k$ are the Fibonacci numbers ($F_0=0$, $F_1=1$, $F_{k+1}=F_k+F_{k-1}$). This sequence delivers the best possible approximation for $w$, and the dynamics on a time interval $F_k$ is close to periodic. So, it is natural to consider a sequence of evolution operators over intervals of discrete time given by the Fibonacci numbers.

Let $f^{F_k}(x,u)$ and $f^{F_{k+1}}(x,u)$ designate transformation of $x$ after $F_k$ and $F_{k+1}$ iterations, respectively. To construct the next operator, for $F_{k+2}$ iterations, we start from $(x,u)$ and perform first $F_{k+1}$ iterations to arrive at $(f^{F_{k+1}}(x,u),\ u+F_{k+1}w)$, and then the rest $F_k$ iterations with the result

$$f^{F_{k+2}}(x,u) = f^{F_k}(f^{F_{k+1}}(x,u),\ u+wF_{k+1}). \tag{2}$$

To have a reasonable limit behavior of the evolution operators we change scales for $x$ and $u$ by some factors $\alpha$ and $\beta$ at each new step of the construction, and define the renormalized functions as

$$g_k(x,u) = \alpha^k f(x/\alpha^k,\ u/\beta^k). \tag{3}$$

Note that $wF_{k+1} = -(-w)^{k+1}(\mathrm{mod}1)$, so it is natural to set $\beta=-1/w=-1.618034....$ Rewriting (2) in terms of the renormalized functions we come to the functional equation [15, 16, 19]

$$g_{k+2}(x,u) = \alpha^2 g_k(\alpha^{-1} g_{k+1}(x/\alpha,\ -uw),\ w^2u + w). \tag{4}$$

In the present article we deal with several different solutions of this equation - fixed points or cycles in the functional space. The constant $\alpha$ is specific for each universality class; it is evaluated in a course of solution of the functional equation.

The next step of the RG analysis consists in the following. Let us suppose now that we deal with dynamics not precisely at the critical point, but in a vicinity of it in the parameter space. Then, a perturbation of the solution appears. Analyzing evolution of the perturbation we come to an eigenvalue problem. A number of relevant eigenvalues define a *codimension* of the critical situation. The relevant eigenvalues are those, which are larger than 1 in modulus, not associated with infinitesimal variable changes, and not violating the commutative properties of successively applied evolution operators (see e.g. [10-12, 15, 16, 19] for details). The codimension may be understood as a number of parameters, which must be adjusted to reach the criticality. For instance, in three-dimensional parameter space the codimension-one situations may occur at some surfaces, codimension-two situations at curves, and codimension-three at points.

To derive an explicit form of the linearized RG equation appropriate for a vicinity of a fixed point $g(x,u)$ we substitute $g_k(x,u)=g(x,u)+\varepsilon h_k(x,u)$, $\varepsilon<<1$ and account terms of the first order in $\varepsilon$ in Eq. (4). Then, setting $h_k(x)=\delta^k h(x)$ we arrive to the eigenvalue problem

$$\begin{aligned}\delta^2 h(x,u) = \alpha\delta g'(g(x/\alpha,\ -uw),\ w^2u+w)h(x/\alpha,\ -uw) +\\ + \alpha^2 h(\alpha^{-1} g(x/\alpha,\ -uw),\ w^2u + w).\end{aligned} \tag{5}$$

where the prime designates derivative of the function in respect to the first argument.

For each particular type of criticality, with specific $g(x,u)$ and $\alpha$, this equation can be solved numerically to obtain spectrum of relevant $\delta$.

## 2. Basic models

The simplest example, for which the developed RG scheme is applicable is the well known circle map [20, 21, 10-12, 9]

$$x_{n+1} = x_n + r - (K/2\pi)\sin 2\pi x_n\,(\mathrm{mod}1), \tag{6}$$

where $r$ and $K$ are two relevant control parameters. The function in the right-hand part is monotone in the subcritical domain $K<1$, and it has maxima and minima in the supercritical domain $K>1$. For critical value $K=1$ the function has cubic inflection points.

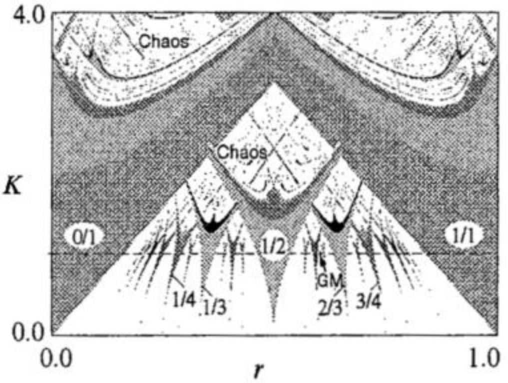

Fig.1. Chart of dynamical regimes on the parameter plane of the circle map. Numbers inside Arnold tongues indicate the respective rotation numbers

Fig. 1 shows chart of dynamical regimes on the parameter plane $(r,K)$. For $K<1$ one can observe periodic or quasiperiodic regimes associated with rational or irrational values of the rotation number defined as $\rho(r, K)=\lim_{n\to\infty}(x_n/n)$.

Periodic regimes are observed inside the Arnold tongues, and quasiperiodic motions are observed between them for $K<1$. Here one can find a curve of constant golden-mean rotation number: $\rho(r,K)=w$. This curve starts at $K=0$, $r=w$, and meets the critical line $K=1$ at the point

$$K_{GM} = 1, \quad r_{GM} = 0.60666106347... \tag{7}$$

we call *the GM critical point* (GM stands for the «golden mean»). It was discovered by Shenker [21] and afterwards studied in terms of RG analysis by Feigenbaum-Kadanoff-Shenker and by Ostlund et al. [10-12].

Further examples of types of critical behavior we discuss in the present article occur in quasiperiodically forced maps.

One model is the quasiperiodically driven logistic map [22-26, 15, 16]. A usual logistic map $x_{n+1}=\lambda-x_n^2$ is a basic model to study period-doubling transition to chaos. As it has the only relevant parameter $\lambda$, a natural generalization for presence of the external driving is to assume that this parameter is modulated with some frequency. In our study this frequency, measured in units of time discretization, is fixed: $w=(5^{1/2}-1)/2$. So, the model is

$$x_{n+1} = \lambda - x_n^2 + \varepsilon\cos 2\pi n w. \tag{8}$$

Fig. 2 shows a chart of dynamical regimes for this model on the parameter plane $(\varepsilon,\lambda)$.

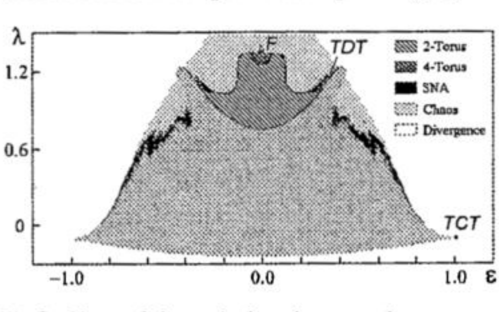

Fig.2. Chart of dynamical regimes on the parameter plane of quasiperiodically driven logistic map (8)

For $\varepsilon=0$ Eq. (8) becomes the conventional logistic map. So, what is observed along the line $\varepsilon=0$ is the usual period-doubling cascade, accumulated to the limit critical point of Feigenbaum (point $F$) [7, 8].

Let us take a value of $\lambda$ at which the unforced map has a stable fixed point. At nonzero $\varepsilon$ the fixed point will be transformed into a stable smooth invariant curve. In continuous-time dynamical systems such curves appear in the Poincaré cross-section for the motion on a torus, so, with commonly used abuse of the terminology, we speak about the torus-attractor T1.

If the external force of small amplitude effects a stable period-2 orbit, it gives rise to an attractor consisting of two closed smooth curves, the doubled torus T2. Period-4 orbit generates a four-part invariant curve (the torus T4), and so forth. In contrast to usual period-doubling, the sequency of torus-doubling transitions appears to be finite: the smaller amplitude of driving, the larger number of torus doublings seen in a course of increase of $\lambda$ [22-28].

If we keep $\lambda$ constant and increase the forcing amplitude, the smooth torus may transform into SNA: the Lyapunov exponent remains negative, but the geometrical structure of the attractor becomes complex, fractal-like. Also regimes with positive Lyapunov exponent arise for larger $\lambda$ and $\varepsilon$. With further increase of the parameters the orbits escape to infinity (white domain in Fig. 1).

As known, the parameter interval corresponding to existence of an attractive fixed point in the unforced logistic map $\lambda \in (-0.25, 0.75)$ is bounded from one side by the tangent bifurcation, collision of a pair of fixed points (stable and unstable) with their subsequent disappearance. From the other side it is bounded by the period-doubling bifurcation. Analogously, the bottom border of the domain T1 in Fig. 2 is the bifurcation curve of tori collision: attractor and repeller, represented by two invariant curves, approach one another, collide, and disappear. The top border is the bifurcation curve of torus doubling: instead of one attractive invariant curve attractor appears consisting of two closely placed curves; after the bifurcation they move one off another.

Let us start at $\varepsilon=0$, $\lambda=-0.25$ and go in the parameter plane along the torus collision bifurcation curve increasing $\varepsilon$. The situation of collision of smooth invariant curves takes place while the motion is confined on one side of the logistic parabola. At some value of $\varepsilon$ the invariant curve at the bifurcation threshold touches the extremum, $x=0$, and in accordance with argumentation of Ref. [16], it corresponds to the terminal point of the bifurcation line. This is critical situation of particular interest, the *TCT critical point* (TCT stands for «torus collision terminal») [16]:

$$\lambda_{TCT} = -0.09977122895..., \quad \varepsilon_{TCT} = 1.01105609099.... \tag{9}$$

Now, let us start at $\varepsilon=0$, $\lambda=0.75$ and move along the torus-doubling bifurcation curve. As in the previous case, this bifurcation of smooth invariant curve takes place only while the whole curve is placed on one side of the logistic parabola. At some value of $\varepsilon$ the invariant curve at the bifurcation threshold touches the extremum, $x=0$, and the torus-doubling bifurcation line is terminated. This is the *TDT critical point* (TDT stands for «torus-doubling terminal») [15]:

$$\lambda_{TDT} = 1.158096856726..., \quad \varepsilon_{TDT} = 0.360248020507.... \tag{10}$$

TCT and TDT critical point were found also in quasiperiodically forced circle map

$$x_{n+1} = x_n + r - (K/2\pi)\sin 2\pi x_n + \varepsilon\cos 2\pi n w \ (\mathrm{mod} 1) \tag{11}$$

in the supercritical case $K>1$ (near the extrema it looks locally like the logistic map). In some respects, this is a more convenient object for detailed study: no divergence can occur in this map because the variable $x$ is defined modulo 1.

Fig. 3 presents a chart of dynamical regimes for the driven circle map on a part of the parameter plane $(b,\varepsilon)$ including the TCT critical point [16]. Separately, two rectangular fragments of the chart are shown together with phase portraits of attractors at representative points.

The large gray domain in the diagram corresponds to existence of the localized torus attractor. The right border of this domain is the bifurcation curve of bifurcation of

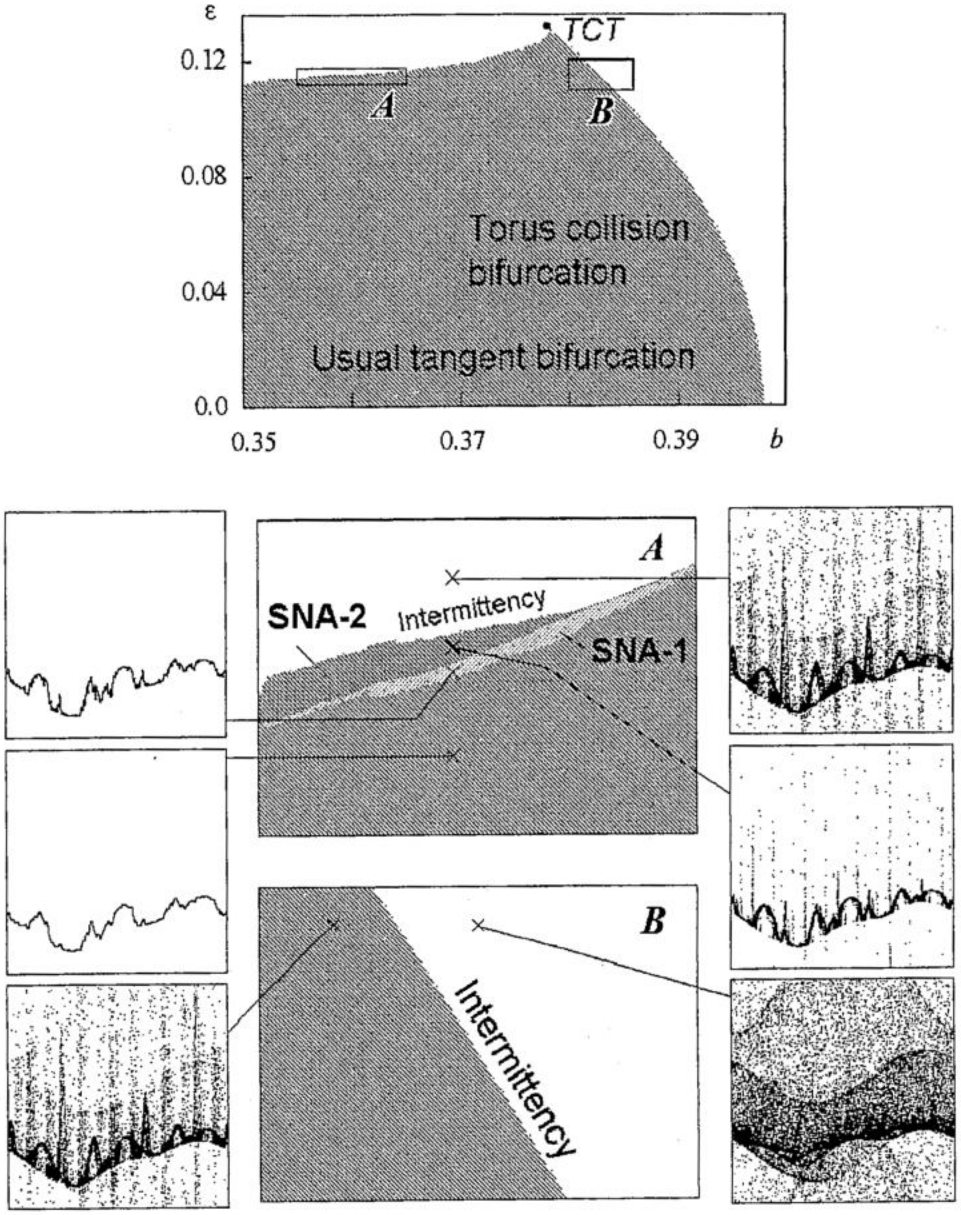

Fig. 3. Chart of dynamical regimes on the parameter plane $(b, \varepsilon)$ and two enlarged fragments with phase portraits of attractors on phase plane $(u,x)$ at representative points

collision of a pair of smooth tori, one stable and another unstable. After the event, both of them disappear, and intermittent regime arises, with long-time travel of the orbits through the region of former existence of attractor and repeller (the «channel»). Going along the bifurcation curve we observe that the semi-attractive invariant curve, formed at the moment of collision of stable and unstable tori, grows in size, and ultimately touches the minimum of the map; there we arrive to the TCT point. As found numerically, it is located at

$$r_{TCT} = 0.377866239..., \qquad \varepsilon_{TCT} = 0.132566321... \tag{12}$$

Another, upper border of the gray area corresponds to a situation when the stable and unstable invariant curves touch each other, but do not coincide. This means that at least one of the curves must be non-smooth («fractal torus»). From the figure one can see that both bifurcation lines of smooth and fractal tori-collision meet at the TCT critical point.

It was observed that fractalization of torus and transition to SNA in the forced circle map is possible also in the critical and subcritial domain ($K \le 1$) [29, 30]. This transition can not be associated with the TDT or TCT points because of absence of the quadratic extrema. Its nature was revealed in Ref. [19] as linked with the torus fractalization at the intermittency threshold. To describe the phenomenon it was convenient to use a model

$$x_{n+1} = f(x_n) + b + \varepsilon\cos 2\pi w n, \tag{13}$$

where $f(x)$ was defined as

$$f(x) = \begin{cases} x/(1-x), \; x \le 0.75 \\ 9/(2x) - 3, \; x > 0.75 \end{cases} \tag{14}$$

One branch of the mapping is selected in a form of the fractional-linear function, $x/(1-x)$, which naturally appears in analysis of dynamics near tangent bifurcation associated with intermittency (e.g. [31-34]). The other branch is attached somewhat arbitrarily to ensure presence of the «reinjection mechanism» in the dynamics and to exclude divergence.

Fig. 4 shows a chart of dynamical regimes for the model (13). The white area designates chaotic regime with positive Lyapunov exponent Λ. Gray regions correspond to negative Λ. In the bottom gray area attractor is localized and represented by a smooth torus. The upper border of this region is the bifurcation curve of transition to delocalized attractor via intermittency. The bifurcation consists in collision of smooth stable and unstable tori with their coincidence, and the Lyapunov exponent at the bifurcation is zero. In the right part of the diagram the bifurcation curve separates regimes of torus and SNA. The bifurcation corresponds to fractal collision of two invariant curves at some exceptional set of points, and the Lyapunov exponent at the bifurcation is negative. These two parts of the bifurcation border are separated by *the critical point of torus fractalization* (TF) that is located at

$$\varepsilon_{TF} = 2, \quad b_{TF} = -0.597515185376121... \tag{15}$$

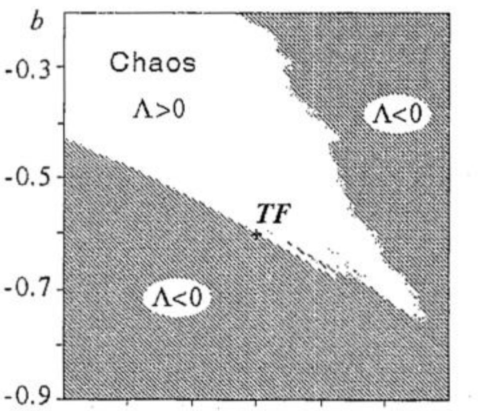

Fig. 4. Chart of dynamical regimes for the model (13). The bottom gray area corresponds to localized attractor represented by smooth torus. The upper border of the bottom area is the bifurcation curve of the intermittent transition. In the left part the bifurcation consists in collision of smooth stable and unstable tori with their coincidence, in the right part - to fractal collision at some exceptional set of points. White area designates chaos, and dark gray presumably corresponds to SNA. Sign of the Lyapunov exponent Λ is indicated in all three domains

## 3. The classic GM critical point

Critical behavior in the circle map associated with break-up of the golden-mean quasiperiodicity (GM critical point) was discovered first by Shenker [21] and studied in terms of RG analysis by Feigenbaum-Kadanoff-Shenker and Ostlund et al. [10-12]. Although the circle map is one-dimensional, it may be treated in terms of our general scheme, as a particular case of (1). We consider two decoupled maps

$$x_{n+1} = f(x_n),\quad u_{n+1} = u_n + w \ (\mathrm{mod} 1), \tag{16}$$

with $f(x)=x+r-(K/2\pi)\sin 2\pi x$. The function is independent of the second argument $u$, so, the GM criticality will correspond to a degenerate fixed point of our functional equation: $g_k(x,u)\equiv G(x)$. In this case Eq. (4) yields

$$G(x) = \alpha^2 G\,(\alpha^{-1}G(x/\alpha)), \tag{17}$$

the relation known as the Feigenbaum-Kadanoff-Shenker equation. It has been solved numerically (e.g. [10-12, 35, 36, 37, 9]), and the function is found in a form of high-precision expansion in powers of $x^3$. The scaling constant is

$$\alpha = -1.288574553954... \tag{18}$$

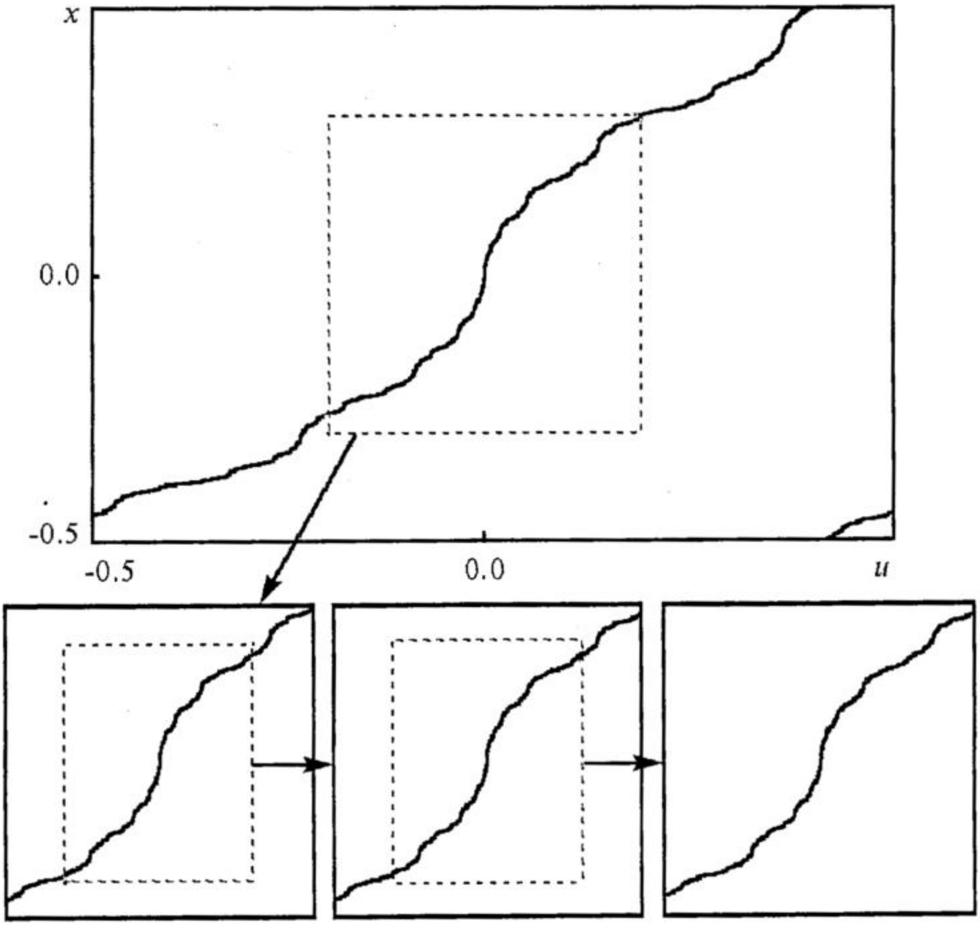

Fig. 5. Attractor of the two-dimensional map (16) at the GM critical point (top panel) and illustration of the basic local scaling property: the structure reproduces itself under magnification with factors $\alpha$=-1.28857... and $\beta$=-1.61803... along the vertical and the horizontal axes, respectively

Accounting representation of the circle map in the form (16) it is natural to depict the critical attractor in coordinates $(u,x)$ (Fig. 5). Observe that it is represented by a fractal-like curve. Locally, the basic scaling property of this fractal may be deduced from the RG analysis. Indeed, the evolution operators for time intervals increasing as Fibonacci numbers become identical, up to the scale change. For each next Fibonacci number the variables $x$ and $u$ are rescaled by $\alpha$ and $\beta=-w^{-1}$. As follows, attractor in coordinates $(u,x)$ must possess self-similarity: increasing resolution by factors $\alpha$ and $\beta$ along the vertical and the horizontal axes, respectively, one should observe the similar structures (see bottom panels of Fig. 5).

For perturbations of the GM fixed-point, which do not violate the unidirectional nature of the master-slave coupling, the equation (5) accepts the form

$$\delta^2 h(x) = \alpha\delta G'(G(x/\alpha))h(x/\alpha) + \alpha^2\,(\alpha^{-1}G(x/\alpha)). \tag{19}$$

As found (e.g. Refs [10-12, 35, 36, 37, 9]), there are two relevant eigenvalues,

$$\delta_1 = -\,2.8336106559... \quad \text{and} \quad \delta_2 = \alpha^2 = 1.660424381... \tag{20}$$

These are the constants responsible for the scaling properties of the parameter space structure near the GM critical point. However, to demonstrate them we need to define a special local coordinate system near the critical point - the scaling coordinates. (The same will be necessary for other types of criticality, see sections 4-6.) As argued in Refs [37, 9], this is a curvilinear system: one coordinate line goes along the critical line $k$=1, and the another - along the curve of constant rotational number. Numerically, the relation of new coordinates $(C_1, C_2)$ with parameters of the original map is expressed as

$$r = r_c + c_1 - 0.01749c_2 - 0.00148c_2^2, \quad k = k_c + c_2. \tag{21}$$

In these relations we account terms up to the second order because of the relation between $\delta_1$ and $\delta_2$: $\delta_2<\delta_1$ and $\delta_2<\delta_1^2$, but $\delta_2>\delta_1^3$ (see Refs [13, 16-19, 37] for explanation of the rules for selection of the scaling coordinates). Fig. 6 shows a chart of dynamical

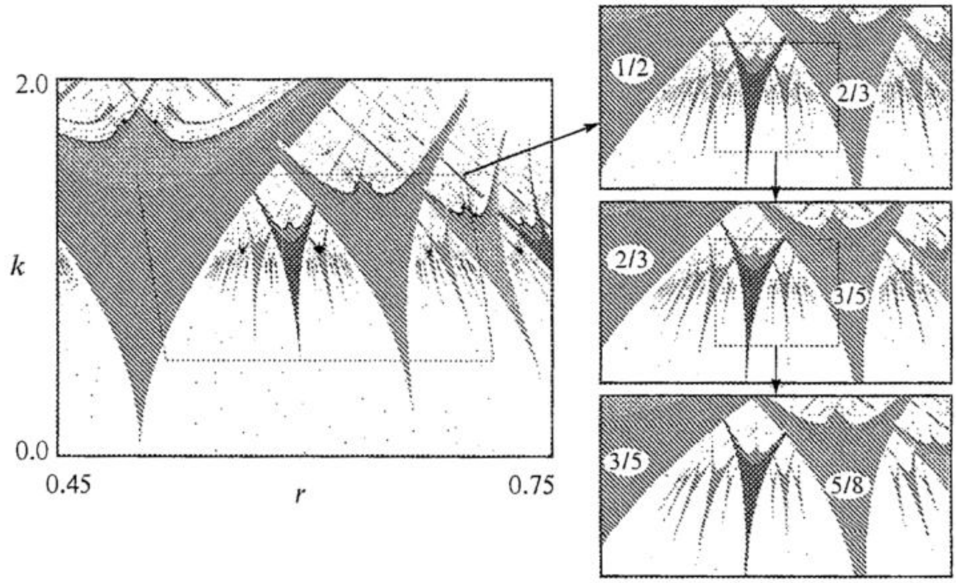

Fig. 6. Chart of dynamical regimes on the parameter plane of the sine circle map and a sequence of fragments for several steps of magnification of vicinity of the GM critical point in the scaling coordinates, with factors $\delta_1$ and $\delta_2$ along horizontal and vertical axes, respectively

regimes with Arnold tongues and a sequence of fragments for several steps of magnification in the scaling coordinates. Observe excellent repetition of the two-dimensional arrangement of the tongues at subsequent levels of resolution.

## 4. Critical point TCT

RG analysis of the torus-collision terminal point was developed in Ref. [16]. The critical behavior of this type was found in the forced logistic map (8) and in the forced supercritical circle map (11). Here we prefer to deal with the last one because divergence of iterations is excluded in this case. The equation may be written as

$$x_{n+1} = x_n + r - (K/2\pi)\sin 2\pi x_n + \varepsilon\cos(2\pi u) \pmod 1,$$
$$u_{n+1} = u_n + w \pmod 1, \tag{22}$$

and parameter $K$ is supposed to be supercritical and fixed, $K$=2.5. As mentioned in Sec.2, the TCT point is located at $(r, \varepsilon)_{TCT}$=(0.377866239, 0.132566321).

In the RG approach, the TCT point is associated with a fixed-point solution of the functional equation (4). This circumstance was checked accurately in numerical procedure based on iterations of the RG transformation (4). Also the multi-dimensional Newton technique was used to solve the fixed-point equation in respect to the coefficients of polynomial expansion of the universal function in an appropriately chosen domain in the $(u,x)$ plane (see [16] for details). The scaling constant $\alpha$ was found in the course of the computations, so

$$\alpha = 1.7109605... \text{ and } \beta = -w^{-1} = 1.6180339... \tag{23}$$

As seen from Fig. 7, the critical attractor in coordinates $(u, x)$ is represented by a non-smooth fractal-like curve. To observe scaling, we need to select properly the origin of local coordinate system (the «scaling center»). As found in Ref. [16], it is located at

$$u_c = 0.284109286 \text{ and } x_c = (2\pi)^{-1}\arctan(K^2 - 1)^{1/2} = 0.184505060. \tag{24}$$

Now, if we rescale $\Delta x$=$x$-$x_c$ and $\Delta u$=$u$-$u_c$ by factors $\alpha$ and $\beta$=-$w^{-1}$, respectively, the dynamical regimes remain of the same kind, but with rescaling of time by factor $w^{-1}$. The invariant curve also must be invariant under this transformation. Indeed, the picture inside a selected box in Fig. 7 reproduces itself under subsequent magnifications (with inversion in respect to the phase variable, due to the negative $\beta$). This scaling property implies that locally the behavior of the invariant curve obeys $\Delta x \propto |\Delta u|^\gamma$ with $\gamma$=log$\alpha$/log$\beta$≅1.117. The power $\gamma$ is close to one, so visually the curve looks like broken at the point of singularity.

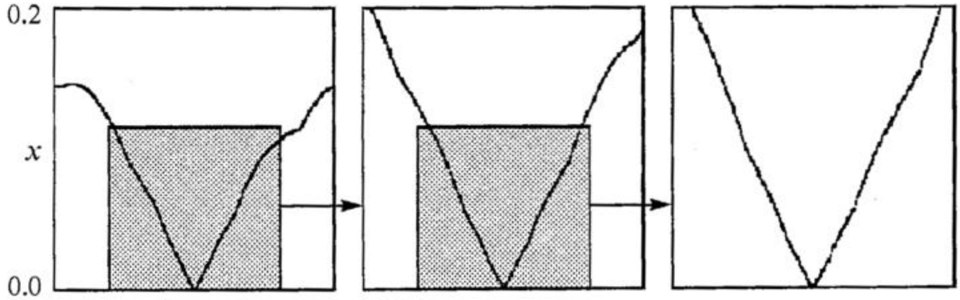

Fig. 7. Attractor of the forced circle map at the TCT critical point (the left panel) and illustration of the basic local scaling property: the structure reproduces itself under magnification with factors $\alpha$=1.71096... and $\beta$=-1.61803... along the vertical and the horizontal axes, respectively

Due to ergodicity ensured by irrationality of the frequency, the singularity at the origin implies existence of the same type of singularities over the whole invariant curve, in a dense set of points. Note that $\gamma>1$. It means that the singularity is weak: the invariant curve, apparently, remains differentiable, but not twice differentiable.

The next step is analysis of the linearized RG equation and of the corresponding eigenvalue problem (5). Numerical solution of the functional equation with substitution of $g(x,u)$ and constant $\alpha$ associated with the TCT criticality was performed with approximation of the eigenfunctions via finite power expansions in respect to $x$ and $u$. As found, two eigenvalues are relevant:

$$\delta_1 = 3.600810\ldots \text{ and } \delta_2 = 1.828329\ldots \tag{25}$$

These are scaling factors determining self-similarity of topography in a vicinity of the TCT point. To demonstrate the scaling property we define scaling coordinates in the parameter plane. Note that $\delta_2<\delta_1$ and $\delta_2<\delta_1^2$, but $\delta_2>\delta_1^3$. So, we account terms up to the second order in the parameter change. As suggested in Ref. [16] it may be chosen as

$$r = r_c + c_1 - 0.3121848c_2 - 2.047c_2^2, \quad \varepsilon = \varepsilon_c + c_2. \tag{26}$$

Fig. 8 shows a fragment of the chart of dynamical regimes near the TCT point for the forced circle map. Note similarity of the configurations represented in scaling coordinates.

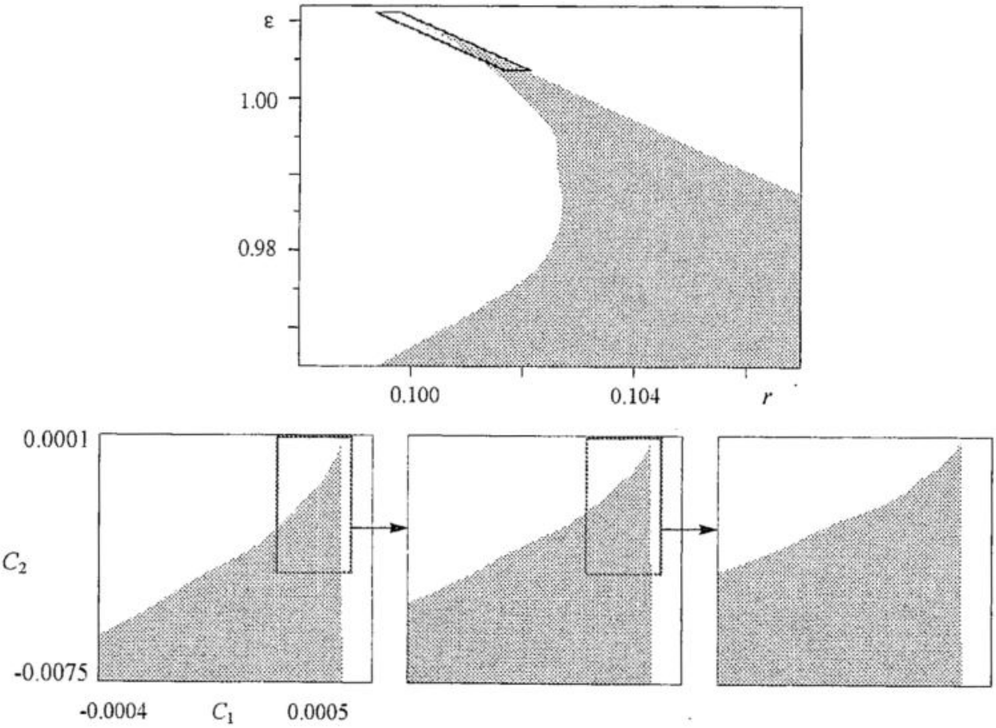

Fig. 8. Chart of dynamical regimes on the parameter plane of the quasiperiodically driven supercritical circle map and a sequence of fragments for several steps of magnification of a vicinity of the TCT critical point in the scaling coordinates, with factors $\delta_1$ and $\delta_2$ along horizontal and vertical axes, respectively. Gray area corresponds to localized attractor with negative Lyapunov exponent, and white to chaos

## 5. Critical point TDT

Let us turn now to the RG results relating to the torus-doubling terminal point [15, 38, 39]. The basic illustrative example will be the forced logistic map that may be rewritten as

$$x_{n+1} = \lambda - x_n^{\,2} + \varepsilon\cos 2\pi u_n, \quad u_{n+1} = u_n + w \pmod{1}. \tag{27}$$

As noted in Sec. 2, the TDT point is located at $(\lambda,\varepsilon)_{TDT}$=(1.158096856, 0.360248020).

It was found in Refs. [15, 38] that the TDT point is associated with a period-3 cycle of the RG equation (4): $g_1(x,u)\rightarrow g_2(x,u)\rightarrow g_3(x,u)\rightarrow g_1(x,u)$. To find this period-3 solution with high precision a numerical procedure was developed, the result was a representation of functional pair $\{g_1(x,u),g_2(x,u)\}$ in a form of polynomial expansion over the arguments $x$ and $u$ (see the table of coefficients in [38]). The rescaling constant is $\alpha$=1.58259341...

In coordinates $(u,x)$ the critical attractor looks like a fractal curve (Fig. 9). To observe scaling, the origin of the coordinate system must be placed at the «scaling center» [15, 38]

$$u_c = 0.3952188264 \text{ and } x_c = 0. \tag{28}$$

Due to the period-3 nature of the solution of the RG equation, observation of self-similarity of the critical attractor requires using the scaling factors

$$\alpha^3 = 3.96376647\ldots \text{ and } \beta^3 = -4.23606798\ldots. \tag{29}$$

If we rescale $x$ and $\Delta u=u-u_c$ by $\alpha^3$ and $\beta^3$, respectively, the dynamical regimes remain of the same kind, but with characteristic time rescaled by $w^{-3}$. The curve representing the attractor must be invariant under this transformation, and this is indeed the case, see Fig. 9.

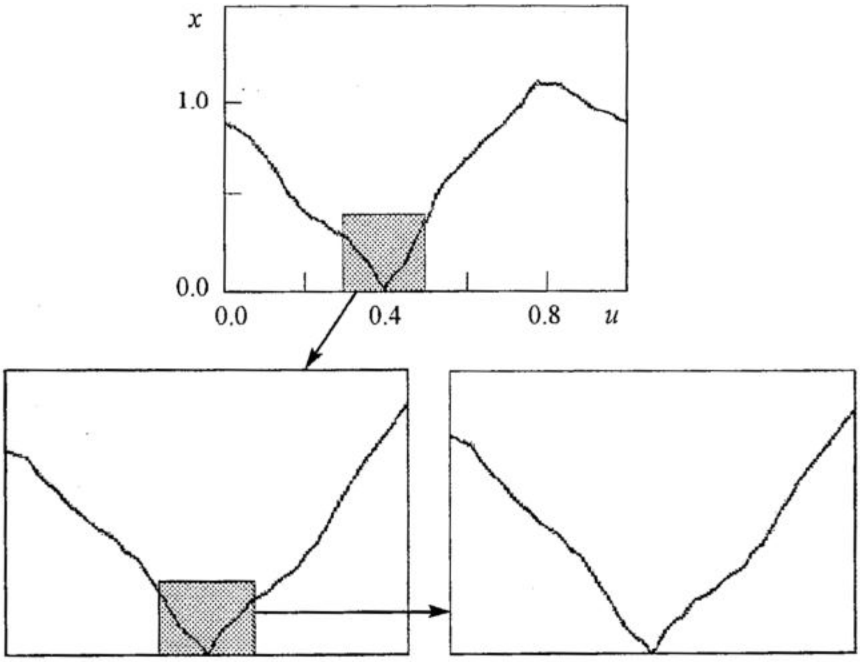

Fig. 9. Attractor of the forced logistic map at the TDT critical point (the left panel) and illustration of the basic local scaling property: the structure reproduces itself under magnification with factors$\alpha^3$=3.96376... and $\beta^3$=-4.2360... along the vertical and the horizontal axes, respectively

The picture inside a selected box reproduces itself under subsequent magnifications. Locally the invariant curve behaves as $x \propto |\Delta u|^{\gamma}$ with $\gamma = \log\alpha / \log|\beta| \cong 0.954$. The exponent is close to one, so the curve looks like broken at the point of singularity. Due to ergodicity of the quasiperiodic motion, the singularity at the origin implies presence of the same type of singularities in a dense set of points over the whole invariant curve.

Because of the period-3 nature of the solution, analysis of the linearized RG equation is more complicated than for a fixed point. The eigenvalue problem reads

$$\begin{aligned}
\delta^2 h_3(x,u) &= \alpha\delta g_1'\,(g_2(x/\alpha,\,-uw),\,w^2u+w)\,h_2(x/\alpha,\,-uw) + \alpha^2 h_1(\alpha^{-1}g_2(x/\alpha,\,-uw), w^2u+w),\\
\delta^2 h_1(x,u) &= \alpha\delta g_2'\,(g_3(x/\alpha,\,-uw),\,w^2u+w)\,h_3(x/\alpha,\,-uw) + \alpha^2 h_2(\alpha^{-1}g_3(x/\alpha,\,-uw), w^2u+w),\\
\delta^2 h_2(x,u) &= \alpha\delta g_3'\,(g_1(x/\alpha,\,-uw),\,w^2u+w)\,h_1(x/\alpha,\,-uw) + \alpha^2 h_3(\alpha^{-1}g_1(x/\alpha,\,-uw), w^2u+w).
\end{aligned} \tag{30}$$

Numerical solution of this problem with substitution of $g_{1,2,3}(x,u)$ and $\alpha$ associated with the TDT criticality yields two relevant eigenvalues [15, 38]:

$$\delta_1 = 10.5029\ldots \quad \text{and} \quad \delta_2 = 5.1881\ldots \tag{31}$$

To demonstrate scaling property in the parameter plane we need to define appropriate «scaling coordinates». In the present case $\delta_2 < \delta_1$ and $\delta_2 > \delta_1^{\,m}$ for $m$=2,3,... It

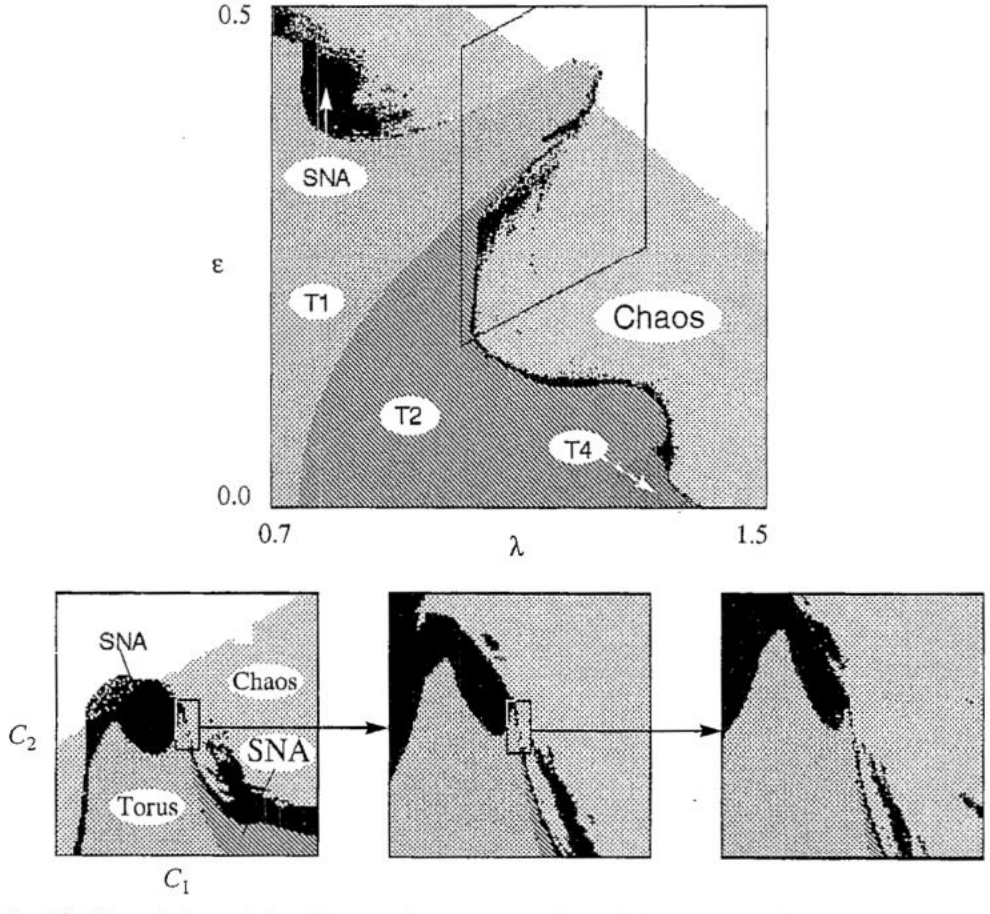

Fig. 10. Chart of dynamical regimes on the parameter plane of the quasiperiodically driven logistic map and a sequence of fragments for several steps of magnification of a vicinity of the TDT critical point in the scaling coordinates, with factors $\delta_1$ and $\delta_2$ along horizontal and vertical axes, respectively

means that a linear parameter change is sufficient. According to Refs [15, 38], it may be chosen as

$$\lambda = \lambda_{TDT} + c_2, \qquad \varepsilon = \varepsilon_{TDT} - c_1 + 0.3347c_2. \tag{32}$$

Fig. 10 shows a chart of dynamical regimes near the TDT in scaling coordinates for several steps of subsequent magnification.

## 6. Critical point TF

The transition from localized to delocalized attractor in the model map (13) is accompanied by appearance of intermittent regimes. While we are close to the point of bifurcation, the laminar stages of dynamics occupy an overwhelming part of observation time (like in the case of the usual Pomeau-Manneville intermittency). They correspond to dynamics on the left branch of the map (13). To study details of the transition we may concentrate on the laminar stages and consider a simplified map [19]

$$x_{n+1} = x_n/(1 - x_n) + b + \varepsilon\cos(2\pi(nw + u)), \; u_{n+1} = u_n + w \quad (\mathrm{mod}1). \tag{33}$$

As explained in Sec. 2, the bifurcation border in the plane $(\varepsilon,b)$ contains a critical point TF separating situations of smooth and fractal tori collision at $(\varepsilon,b)_{TF}$=(2, - 0.597515185).

An important note is that due to the fractional-linear nature of the map the functions obtained at subsequent steps of the RG transformation (4) will be fractional-linear too. The same is true for the fixed-point of the RG equation, associated with the TF critical point. It implies that we may search for the fixed-point solution in a form.

$$g(x,u) = (a(u)x + b(u))/(c(u)x + d(u)), \tag{34}$$

where $a$, $b$, $c$, $d$ are some functions of $u$. Without loss of generality we require them to satisfy additional conditions $a(u)d(u)-b(u)c(u)\equiv1$ and $c(0)=-1$. Substituting (34) into (4) we arrive at the fixed-point RG equation in terms of the functions $a$, $b$, $c$, $d$:

$$\begin{pmatrix} a(u) & b(u) \\ c(u) & d(u) \end{pmatrix} = \begin{pmatrix} a(w^2u + w) & \alpha^2 b(w^2u + w) \\ \alpha^{-2}c(w^2u + w) & d(w^2u + w) \end{pmatrix} \cdot \begin{pmatrix} a(-wu) & \alpha b(-wu) \\ \alpha^{-1}c(-wu) & d(-wu) \end{pmatrix}. \tag{35}$$

The solution was found numerically, the coefficients of polynomial expansions for $a(u)$, $b(u)$, $c(u)$, $d(u)$ are listed in Ref. [19]. The factor $\alpha$ was also computed, so

$$\alpha = 2.890053525... \quad \text{and} \quad \beta = -w^{-1} = -1.6180339.... \tag{36}$$

These two constants determine scaling properties of the critical attractor on the $(x,u)$-plane. In fact, the variable $x$ in the RG equation and in the original map are not the same: we need to introduce «scaling coordinates» in the $(x,u)$-plane. As found numerically [19], the variable change looks like

$$X \propto x + 2.34719526 + 5.92667u - 210.629u^2, \; U = u. \tag{37}$$

Fig. 11 illustrates scaling property of the critical attractor. Observe excellent reproduction of details of the structure in scaling coordinates $(X,u)$.

Numerical solution of the eigenvalue problem (5) for the fractional-linear fixed-point reveals two relevant eigenvalues

$$\delta_1 = 3.134272989... \quad \text{and} \quad \delta_2 = w^{-1} = 1.618033979... \tag{38}$$

responsible for scaling properties of the parameter space near the critical point. If we

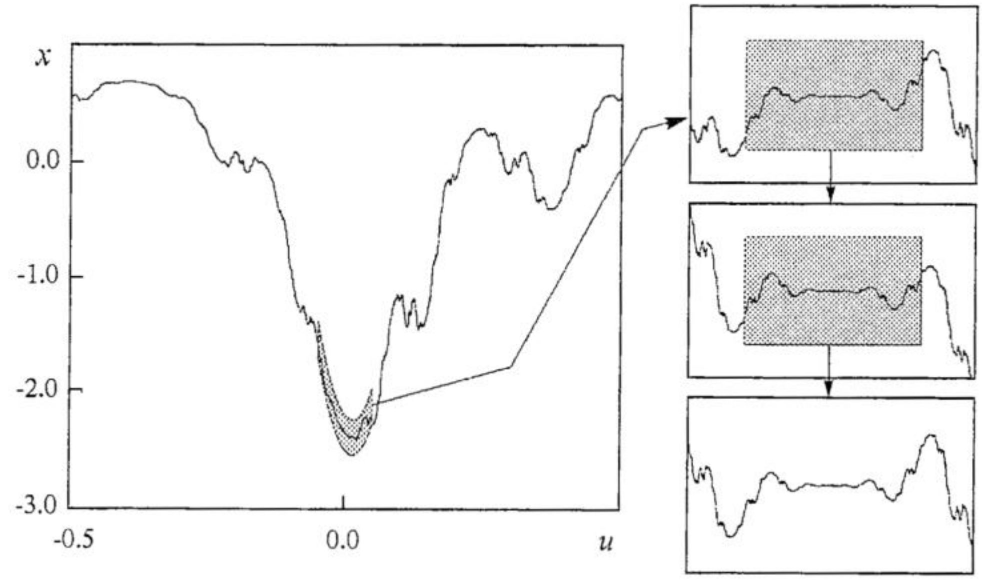

Fig. 11. Attractor of the forced fractional-linear map at the TF critical point (the left panel) and illustration of the basic local scaling property: the structure depicted in scaling coordinates reproduces itself under magnification with factors $\alpha$=2.89005... and $\beta$=-1.618034... along the vertical and the horizontal axes, respectively

depart from the critical point along the bifurcation curve of the attractor-repeller collision, the first eigenvector does not contribute, the relevant perturbation is associated with $\delta_2$. If we choose a transversal direction, say, along the axis $b$, the perturbation of the first kind appears.

In the case under consideration we have $\delta_1>\delta_2$ and $\delta_1>\delta_2^2$, but $\delta_1<\delta_2^3$, so quadratic terms must be taken into account in the parameter change; the scaling coordinates $(C_1,C_2)$ are linked with parameters of the original map as

$$b = b_{TF} + C_1 - 0.64938C_2 - 0.33692C_2^2, \qquad \varepsilon = 2 + C_2. \tag{39}$$

To illustrate scaling associated with nontrivial constant $\delta_1$ let us consider duration of laminar phases in a course of the intermittent dynamics generated by the map (33). In usual Pomeau - Manneville intermittency of type I the average duration of the laminar stages behaves as $\langle t_{\mathrm{lam}}\rangle \propto \Delta b^{\nu}$ with $\nu$=0.5 [31-34]. In presence of the quasiperiodic force the same law is valid in the subcritical region, $\varepsilon<2$. In the critical case $\varepsilon=2$ the exponent is distinct. Indeed, as follows from the RG results, to observe increase of characteristic time scale by factor $\theta=w^{-1}=1.61803$ we have to decrease a shift of parameter $b$ from the bifurcation threshold by factor $\delta_1$=3.13427. As follows, the exponent must be

$$\nu=\log\theta/\log\delta_1\cong 0.42123.$$

Fig. 12 shows data of numerical

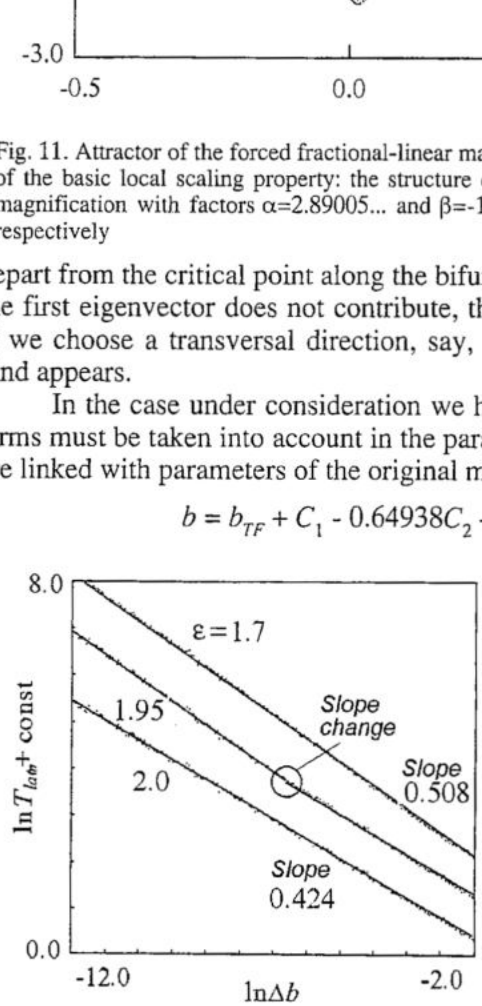

Fig. 12. Data of numerical experiments with the fractional-linear map: average duration of passage through the «channel» versus deflection from the bifurcation threshold for three values of $\varepsilon$ in the double logarithmic scale. Observe a «crossover» phenomenon, the slope change from critical to subcritical value at some intermediate value of $\Delta b$ for $\varepsilon$=1.95

experiments with the fractional-linear map. At each fixed ε an average duration of passage through the «channel» near the formerly existed attractor-repeller pair was computed in dependence on $\Delta b$ for ensemble of orbits with random initial conditions. Results are plotted in the double logarithmic scale. For particular $\varepsilon=1.7$ (subcritical) and 2 (critical) the dependencies fit the straight lines of a definite slope, estimated as 0.508 and 0.424, in good agreement with the theory. At subcritical ε slightly less than 2 one can observe a «crossover» phenomenon, that is the slope change from critical to subcritical value at some intermediate value of $\Delta b$.

## 7. Conclusion

The present paper was devoted to a review of critical situations at the onset of chaotic or strange nonchaotic behavior via quasiperiodicity, more concretely, in the case of the golden-mean ratio of the basic frequencies. We have derived a two-dimensional generalization of the Feigenbaum-Kadanoff-Shenker RG equation and demonstrate that it may be used to treat from the common point of view a number of critical situations, the conventional golden-mean criticality (GM), and the critical situations in quasiperiodically driven model maps: torus collision terminal (TCT), torus-doubling terminal (TDT), and torus fractalization at the intermittecy threshold (TF). All these critical situations are of obvious interest for a problem of synchronization in nonlinear systems, in context of study of transitions associated with break-up, or other bifurcations of complex generalized synchronous regimes. In perspective, it would be interesting to reveal details and regularities of coexistence and subordination of all the types of critical behavior.

As is common in situations allowing the RG analysis, one can expect that the quantitative regularities intrinsic to our model maps will be valid also in other systems relating to the same universality classes. It would be significant to find this type of behavior in systems of higher dimension, for example, in quasiperiodically driven invertible 2D maps, which could represent Poincare maps of some flow systems. It would be interesting to arrange special experiments on search and observation of the considered types of critical behavior. Since now, only two of them, GM and TDT critical behavior, were observed experimentally (see e.g. [40, 28, 41, 38, 39]).

I thank U.Feudel, E.Neumann, A.P.Kuznetsov, A.Pikovsky, and I.Sataev for fruitful collaboration, discussions, and valuable help during a work on different parts of the present research.

*This work was supported by RFBR (grant № 00-02-17509) and CRDF (award REC-006).*

## References

1. *L.D. Landau.* On the problem of turbulence // Doklady Akad. Nauk SSSR, 44, 1944. P. 311 (in Russian).

2. *E. Hopf.* A mathematical example displaying features of turbulence // Comm. Appl. Math. 1948. Vol. 1. P. 303.

3. *D. Ruelle and F. Takens.* On the nature of turbulence // Comm. Math. Phys. 20, 1971. P. 167.

4. *C. Grebogi, E. Ott, S. Pelikan and J.A. Yorke.* Strange attractors that are not chaotic // Physica D. 1984. Vol. 13. P. 261.

5. *F.J. Romeiras, A. Bondeson, E. Ott, T.M. Antonsen, and C. Grebogi.* Quasiperiodically forced dynamical systems with strange nonchaotic attractors // Physica D. 1987. Vol. 26. P. 277.

6. *A.S. Pikovsky and U. Feudel.* Characterizing strange nonchaotic attractors // Chaos. 1995. Vol. 5. P. 253.

7. *M.J. Feigenbaum.* Quantitative universality for a class of nonlinear transformations // J. Statist. Phys. 1978. Vol. 19. P. 25.

8. *M.J. Feigenbaum.* The universal metric properties of nonlinear transformations // J. Statist. Phys. 1979. Vol. 21. P. 669.

9. *S.P. Kuznetsov.* Dynamical Chaos. Moscow: Fizmatlit, 2001, 296 p. (In Russian.)

10. *M.J. Feigenbaum, L.P. Kadanoff, S.J. Shenker.* Quasiperiodicity in dissipative systems. A renormalization group analysis // Physica D. 1982. Vol. 5. P. 370.

11. *D. Rand, S. Ostlund, J. Sethna, and E.D. Siggia.* A universal transition from quasi-periodicity to chaos in dissipative systems // Phys. Rev. Lett. 1082. Vol. 49. P. 132.

12. *S. Ostlund, D. Rand, J. Sethna, and E.D. Siggia.* Universal properties of the tran sition from quasi-periodicity to chaos in dissipative systems // Physica D. 1983. Vol. 8. P. 303.

13. *A.P. Kuznetsov, S.P. Kuznetsov, I.R. Sataev.* A variety of period-doubling universality classes in multi-parameter analysis of transition to chaos // Physica D. 1997. Vol. 109. P. 91.

14. *S.P. Kunetsov, A.S. Pikovsky and U. Feudel.* Birth of a strange nonchaotic attractor: A renormalization group analysis // Phys. Rev. E. 1995. Vol. 51. R1629-R1632.

15. *S.P. Kunetsov, U. Feudel and A.S. Pikovsky.* Renormalization group for scaling at the torus-doubling terminal point // Phys. Rev. E. 1998. Vol. 57. P. 1585.

16. *S.P. Kuznetsov, E. Neumann, A. Pikovsky, I.R. Sataev.* Critical point of tori-collision in quasiperiodically forced systems // Phys. Rev. E. 2000. Vol. 62. № 2. P. 1995.

17. *A.P. Kuznetsov, S.P. Kuznetsov, I.R. Sataev.* Three-parameter scaling for one-dimensional maps // Phys. Lett A. 1994. Vol. 189. P. 367.

18. *A.P. Kuznetsov, S.P. Kuznetsov, I.R. Sataev.* Codimension and typicity in context of description of the period-doubling transition to chaos in dissipative dynamical systems // Regular and Chaotic Dynamics. 1997. Vol. 2. № 3-4. P. 90 (In Russian).

19. *S.P. Kuznetsov.* Torus fractalization and intermittency //Phys.Rev.E. 2002. Vol. 65. 066209.

20. *V.I. Arnold.* Cardiac arrythmias and circle mappings // CHAOS. 1991. Vol. 1. P. 20.

21. *S. J. Shenker.* Scaling behavior in a map of a circle onto itself. Empirical results // Physica D. 1982. Vol. 5. P. 405.

22. *K. Kaneko.* Doubling of torus // Progr. Theor. Phys. 1983. Vol. 69. P. 1806.

23. *S.P. Kuznetsov.* Effect of a periodic external perturbation on a system which exhibits an order-chaos transition through period-doubling bifurcations // JETP Lett. 1984. Vol. 39. № 3. P. 133.

24. *K. Kaneko.* Oscillation and doubling of torus // Progr.Theor.Phys. 1984. Vol. 72. № 2. P. 202.

25. *A. Arneodo.* Scaling for a periodic forcing of a period-doubling system // Phys. Rev. Lett. 1984. Vol. 53. P. 1240.

26. *S.P. Kuznetsov, A.S. Pikovsky.* Renormalization group for the response function and spectrum of the period-doubling system // Phys. Lett. A. 1989. Vol. 140. P. 166.

27. *A. Arneodo, P.H. Collet, E.A. Spiegel.* Cascade of period doublings of tori // Phys. Lett. A. 1983. Vol. 94. P. 1.

28. *V.S. Anishchenko.* Dynamical Chaos - Models and Experiments. Appearance, Routes and Structure of Chaos in Simple Dynamical Systems (World Scientific, Singapore, 1995).

29. *U. Feudel, A.S. Pikovsky, and J. Kurths.* Strange non-chaotic attractor in a quasiperiodically forced circle map // Physica D. 1995. Vol. 88. P. 176.

30. *H. Osinga, J. Wiersig, P. Glendinning and U. Feudel.* Multistability and nonsmooth bifurcations in the quasiperiodically forced circle map // Int. J. of Bifurcation and Chaos. 2001. Vol. 11. P. 3085.

31. *Pomeau Y., Manneville P.* Intermittent transition to turbulence in dissipative dynamical systems // Commun. Math. Phys. 1980. Vol. 74. P. 189.

32. *B. Hu, J. Rudnik.* Exact solution of the Feigenbaum renormalization group equations for intermittency // Phys. Rev. Lett. 1982. Vol. 48. P. 1645.

33. *J.E. Hirsch, B.A. Huberman, and D.J. Scalapino.* Theory of intermittency // Phys. Rev. A. 1982. Vol. 25. P. 519.

34. *F. Argoul and A. Arneodo.* Scaling for periodic forcing at the onset of intermittency // J. Phys. Lett. (Paris). 1985. Vol. 46. L901.

35. *K. M.Briggs, T.W. Dixon, G. Szekeres.* Analytic solution of the Cvitanovic-Feigenbaum and Feigenbaum-Kadanoff-Shenker equations // Int.J.of Bifurcation and Chaos. 1998. Vol. 8. P. 347.

36. *T.W. Dixon, T. Gherghetta, B.G. Kenny.* Universality in the quasiperiodic route to chaos // Chaos. 1996. Vol. 6. P. 32.

37. *N.Yu. Ivankov, S.P. Kuznetsov.* Complex periodic orbits, renormalization and scaling for quasiperiodic golden-mean transition to chaos // Phys. Rev. E. 2001. Vol. 63. 046210.

38. *B.P. Bezruchko, S.P. Kuznetsov, A.S. Pikovsky, Ye.P. Seleznev, U. Feudel.* On dynamics of nonlinear systems under external quasi-periodic force near the terminal point of the torus-doubling bifurcation curve // Yzv. Vuz. Applied Nonlinear Dynamics. 1997. Vol.5, № 6. P. 3. (In Russian.)

39. *B.P. Bezruchko, S.P. Kuznetsov, Ye.P. Seleznev.* Experimental observation of dynamics near the torus-doubling terminal critical point // Phys.Rev. E. 2000. Vol. 62. № 6. P. 7828.

40. *J.A. Glazier, G. Gunaratne, A. Libchaber.* $F(\alpha)$ curves - Experimental results // Phys. Rev. A. 1988. Vol. 37. P. 523.

41. *D.Barkley, A.Cumming.* Thermodynamics of the quasi-periodic parameter set at the borderline of chaos - Experimental results // Phys. Rev. Lett. 1990. Vol. 64. P. 327.

*Institute of Radio-Engineering and*
*Electronics of RAS, Saratov Branch*

*Received 07.05.2002*

УДК 517.9

# РАЗНООБРАЗИЕ КРИТИЧЕСКИХ ЯВЛЕНИЙ, АССОЦИИРУЮЩИХСЯ С КВАЗИПЕРИОДИЧЕСКИМ ДВИЖЕНИЕМ ПРИ СООТНОШЕНИИ ЧАСТОТ, РАВНОМ ЗОЛОТОМУ СРЕДНЕМУ

*С.П. Кузнецов*

В статье представлены несколько универсальных классов критического поведения, которые встречаются на пороге возникновения хаотической динамики или странного нехаотического аттрактора через квазипериодичность. Обсуждаются и иллюстрируются устройство пространства параметров и соответствующие его скейлинговые свойства.

*Kuznetsov Sergey Petrovich* was born in 1951. He is Doctor of Sciences, Corresponding Member of Russian Academy of Natural Sciences, head of laboratory in Saratov Branch of Institute of Radio-Engineering and Electronics of RAS. The main field of interests is nonlinear dynamics, transitions to chaos, and critical phenomena. S.P.Kuznetsov is an author of about 150 research articles, an author of a textbook «Dynamical Chaos», professor of Department of Nonlinear Processes of Saratov State University. He actively collaborates with research groups in Potsdam University (Germany), Technical University of Denmark, Loughboroug University (England).

Nonlinear waves. Solitons

Izv. VUZ «AND», vol.10, № 3, 2002

# NONLINEAR DYNAMICS OF SPATIAL AND TEMPORAL PATTERNS IN LASERS AND ATOM OPTICS: KERR-LENS MODE-LOCKED LASER, ZEEMAN LASER AND BOSE-EINSTEIN ATOMIC CONDENSATE

*L.A. Melnikov, A.I. Konukhov, I.V. Veshneva, V.L. Derbov, V.V. Serov*

Nonlinear dynamics of spatial and temporal behaviour of laser and atom optical systems is investigated numerically. Systems with nearly one scalar transverse mode (Kerr-lens mode-locked laser), with large number of vectorial transverse modes (Zeeman laser with large Fresnel number and anisotropic cavity), and non-ground collective states of Bose-Einstein condensate of trapped neutral atoms are considered. Attempts to classify the complex transverse polarization pattern dynamics are made basing on the vectorial Karhunen-Loeve modes and their singularity points character, including catastrophes and Newton diagrams. Excitation of non-ground states of atomic Bose-Einstein condensate via resonant perturbation is analyzed.

## Introduction

Nonlinear dynamics in lasers and optical systems is at present mainly addressed to the models which incorporate the distributed nature of these systems. Since the nonlinearity in lasers is not large, the laser field can be treated as a superposition of longitudinal and transverse empty-cavity modes coupled via linear and nonlinear elements in the cavity. Huge number of different regimes can be realized in lasers, depending on the active medium and cavity parameters. However, two different limit cases are of primary interest: (i) huge number of longitudinal modes and small number of transverse modes, and (ii) small number of longitudinal modes and large number of transverse modes. If all modes oscillate with definite phases, the laser output appears to be a regular sequence of ultra-short pulses for case (i) and a regular motion of light intensity spots in the transverse plane for case (ii). These regimes are often referred as mode-locked regimes, and the investigation of their stability and destruction is a challenging problem, taking the practical importance of these regimes into account. It is well known that mode locking is the only way to produce extremely short (a few femtoseconds) laser pulses.

On the other hand, there exist systems described by equations, similar to those of nonlinear paraxial optics, but with nonlinearity huge compared with that of optical systems. An important example of such a system is the Bose-Einstein condensate (BEC) of neutral trapped atoms whose wave function in the mean-field limit obeys the Schrödinger-type equation with large qubic nonlinear term proportional to the number of atoms. Investigations of the dynamics of BEC are of interest in the context of its promising applications in atom optics.

The study of the dynamics of these distributed systems in essentially nonlinear regimes is possible if we have (i) powerful methods for numerical modeling of the underlying physical processes, and (ii) means and approaches for the description of the resulting dynamics of distributed systems. The last condition is vital for the description of multitranverse polarization pattern dynamics. In this paper we present the models and numerical results related to the dynamics of the above-mentioned systems, the possible way for the classification of the regimes and excitation of nonlinear stationary states.

As an example of a laser system with large number of longitudinal modes we consider the Kerr-lens mode-locked laser. The full spatial-temporal model of this laser is presented and used for numerical investigations of the nonlinear dynamics of *Z*-cavity Ti:Sph laser with Kerr-lens mode locking (KLM).

In the mode-locked regime the laser output represents a pulse train with the repetition rate determined by the cavity round trip time $2L/c$, where $L$ is the cavity length. Kerr nonlinearity of intracavity elements provide intensity-dependent phase shift, thus inducing a lens-like medium with the intensity-dependent focal power. In specially designed cavities a spatially narrow gain profile or a physical aperture can provide intracavity losses which decrease almost instantaneously with the intensity. This makes the Kerr-lens mode locking to be a powerful technique for generating femtosecond pulses.

In time domain the Kerr nonlinearity in combination with the negative group velocity dispersion (GVD) leads to the solitonic pulse shaping [1, 2]. The pulse amplitude modulation due to Kerr-lens effect is usually treated as the effect of fast saturable absorber [5, 6]. For the mode locking process to be self-starting, the power-dependent losses must exceed a definite value [1, 7]. The optimum resonator parameters are derived with the help of the nonlinear ABCD-matrix formalism [5, 8, 9, 10, 11, 15].

The Schrödinger equation for the field envelope was completed with gain, losses, high-order dispersion terms [16, 17], Bloch equations for the coherent semiconductor absorber [18], stimulated Raman gain [19] and then either solved numerically or evaluated analytically using the hyperbolic secant ansatz for the solution [14, 3, 4]. This allows one to estimate the pulse chirp, pulse width and stability conditions. The pulse energy increase or the reduction of the negative group delay dispersion can result in the pulse instability [3], as well as the finite bandwidth of the gain and the reflecting mirrors [4] or the gain depletion and recovery during the pulse round-trip [20].

For certain conditions KLM lasers demonstrate instability of the pulse train [21, 22]. Quasi-periodic and chaotic oscillation regimes [26], bifurcation of the fundamental mode [27] arise due to the nonlinear coupling of geometrical and energetic characteristics of the beam due to Kerr effect. KLM lasers can keep a small portion of lasing energy in higher-order transverse modes [25]. The dynamical instabilities can be associated with the transverse mode beating [23, 24, 28].

The time-domain ABCD-law [29] in conjunction with ABCD-law for a Gaussian beam allows one to construct an iterative mapping for the beam and pulse parameters [30, 31, 32]. Numerical simulation reveals the evidence of quasi-periodical and chaotic behaviour of both the beam and the pulse parameters [30, 33].

In this paper we present a model with no limitations of pulse and beam shape. The transverse and temporal evolution of a pulsed beam is governed by the paraxial wave equation, which is solved in terms of Laguerre-Gauss modes. For simplicity we consider axially symmetric beams. A prominent feature of our model is that we take into consideration the temporal evolution of the active medium polarization (i.e., the gain and dispersion) during the pulse. The spatio-temporal profile of the gain is directly calculated from the density matrix equations for two-level media. Simultaneous treatment of spatial and temporal field distribution inside the cavity enables one to consider the dynamics and the transient processes during the build-up of the oscillation regime. Our model is not restricted to small round-trip changes of the transverse beam profile, round-trip gain, dispersion and amplitude modulation coefficient. It takes into account the amplitude modulation of the pulse due to self-focusing, the nonlinear mode coupling via the medium polarization, and the gain aperturing.

As an example of a laser system with large number of transverse mode we consider the Zeeman laser with anisotropic cavity [49]. Correct description of the polarization transverse pattern dynamics in lasers with large number of transverse modes is a challenging problem for laser dynamics [35, 28, 36, 37, 38]. For the classification of the structures of the laser field its singular points (zeroes, saddle points, maxima and minima) can be used [39, 40]. However, in these papers the models of the laser fields are far from reality. Another approach utilizing the hierarchy of symmetry breaking was also used for the classification of the regimes [41, 42].

An efficient approach to the analysis of very complicated signals and processes is based on Karhunen-Loeve procedure [44, 45, 46, 43, 47, 48, 49]. In [49] the laser regimes with rotating patterns were investigated and it was shown that these regimes are connected with catastrophes $A_n$ of $x \pm iy$ arguments, where $x$, $y$ are the transverse coordinates. In the present work we also used Karhunen-Loeve modes (KL-modes), however, we added the laser regimes corresponding to oscillating patterns. We introduce the vector Karhunen-Loeve modes, transform the four-dimensional vector field, representing the polarized laser transverse patterns, to the two-dimensional vector field, representing the transverse distribution of the Stokes parameters (2DSP), discuss some properties of this 2D vector field and try to classify the structures in accordance with the behaviour of the 2D vector field near the singularity points. For the oscillating patterns 2DSP does not belong to the gradient case [49]. We propose to use Newton diagram method for the investigation of singular points of the 2DSP vector field.

Bose-Einstein condensates of neutral trapped atoms have become a subject of numerous and extensive studies (see, e.g., the reviews [54, 55, 56]) as a new state of matter with properties opening new possibilities in atomic optics and related fields. One of the most exciting features is the possibility to construct atom lasers. In the present paper we report some new dynamical properties of the Bose-Einstein condensate of atoms in a harmonic trap. In contrast to the optical systems, the nonlinear terms in the equation governing the collective wave function, are typically dominating and, generally, cannot be treated as a perturbation, thus making the eigenfunction problem to be essentially nonlinear. In the present paper the non-ground stationary states of BEC are calculated, and the dynamics of these states under resonant perturbation of the trapping potential is investigated.

## 2. Kerr-lens mode-locked laser

***2.1. Theoretical model.*** The model was developed assuming the amplitude of the electric field $F$ to be varying slowly. For numerical simulations the $Z$-cavity configuration was taken (Fig. 1, *a*). To calculate the electric field envelope dynamics we consider the field passing the optical elements of the cavity from the plane of aperture $A_1$ to the plane of aperture $A_2$ and then returning back. For simplicity we consider the stigmatic case. Schematic equivalent diagram of the $Z$-cavity is shown in Fig. 1, *b*. The spherical mirrors of the folded cavity are replaced by lenses of the same focal power $F=2/R$, where $R$ is the curvature radius of the mirror. The round-trip change of the electric field envelope was obtained by applying transfer operators in the order of their action in the cavity.

Assuming the cylindrical symmetry of the cavity, the expression for the field at any

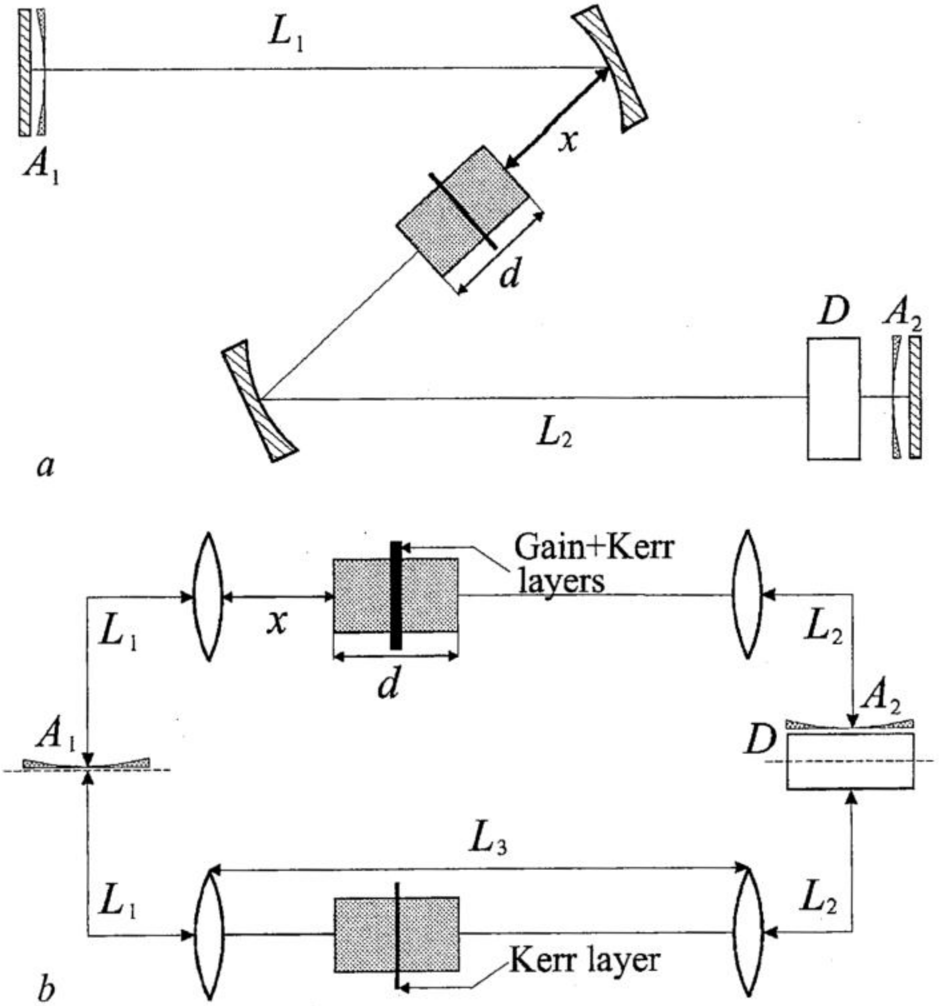

Fig. 1. Cavity configuration (*a*) and its equivalent diagram (*b*). $A_1$, $A_2$ are the Gaussian apertures near the plane mirrors. $L_1$, $L_2$, $L_3$ are the arm lengths of the cavity. $d$ is the rod length, $x$ is the distance between the mirror and the rod, $D$ denotes the dispersion element

transverse plane $z=z_0$=const may be written in terms of Laguerre-Gaussian mode amplitudes:

$$E\,(z_0,r,\tau) = \Sigma_j\ A_j(z_0,\tau)\,L_j(\eta(z_0)r^2)\,\exp(-P\,(z_0)r^2/2), \tag{1}$$

where $j$ is the mode index, $L_j$ are the Laguerre polynomials, $r$ is the transverse radius, $\tau=t-z/c$ is the local time in the running coordinate system $z$, $\tau$-$z/c$, $P(z)=\eta(z)+i\xi(z)$ is the complex beam parameter of the empty cavity, normalized to the value of $k/l$, where $k= =2\pi/\lambda$ is the wavenumber, $\lambda$=800 nm is the wavelength of the fluorescence peak, $l$=1 mm is the unit length of the propagation distance.

The mode amplitudes $A_j(0,\tau)$ at the initial plane $z=z_0$ are defined by the integral transformation

$$A_j\,(z_0,\tau) = 1/(2\eta)\int_0^\infty\ rdr\,E(z_0,r,\tau)\,L_j(\eta\,(z_0)r^2\exp(-P^*(z_0)r^2/2), \tag{2}$$

while the modal amplitudes and the beam parameters at arbitrary point $z$ during the free-space propagation are given by

$$A_j(z,\tau) = A_j(0,\tau)\,[1 + i(z/n)\,P(0)]^{-1} \exp(i\,\varphi_j),$$

$$P(z) = P(0)\,[1 + i\,(z/n)\,P(0)]^{-1}, \qquad (3)$$

$$\varphi_j = -2j \arg\,(1 + i\,(z/n)\,P(0)),$$

where $P(0)$ is the beam parameter at the initial plane $z=0$, $n$ is the refractive index.

The transformation of the beam parameter and mode amplitudes at the mirrors (lenses) is

$$P(2) = P(1) + iF, \quad A_j(2,\tau) = A_j(1,\tau)\,T^{1/2}, \qquad (4)$$

where 1, 2 denote the input and output planes of the mirror, $F=2/R$ is the mirror optical power, $T$ is the uniform power transmission coefficient.

The masking of the beam by the aperture with Gaussian transmission profile was taken into account in a way similar to [28]. For the transmission function of the aperture $T_a(r^2)=\exp(-\eta_a r^2/2)$

$$P(2) = P(1) + \eta_a,$$

$$A_j(2,\tau) = \Sigma_k\, A_k(1,\tau)\, L_{jk}\,,$$

$$L_{jk} = \int_0^\infty L_j(x')\,L_k(x)\exp(-x')\,dx' = \begin{cases} (-1)^k\,(j+k)!\ \sigma^{k-j}/(j\,!(-j-k)_k\,(1+\sigma)^k), & j \leq k \\ 0, & j > k, \end{cases}$$

where $x=\eta r^2$, $x'=(\eta+\eta_a)r^2$, $\eta$ is the real part of the beam parameter $P$ before the aperture, $\sigma=\eta_a/\eta$.

The transformation of the beam parameter per one round-trip obeys the well-known ABCD-law:

$$P(z+L) = P(z), \quad P(z+L) = (A(z)P(z) + B(z))\,/\,(C(z)P(z) + D(z)),$$

where $\begin{pmatrix} \mathrm{A} & \mathrm{B} \\ \mathrm{C} & \mathrm{D} \end{pmatrix}$ is the matrix of the cavity round-trip. This matrix is a product of the matrices

$$\begin{pmatrix} 1 & 0 \\ izn^{-1} & 1 \end{pmatrix}$$

for propagation through a homogeneous medium of the length $z$ and refractive index $n$,

$$\begin{pmatrix} 1 & iF \\ 0 & 1 \end{pmatrix} \qquad (5)$$

for a mirror with optical power $F$,

$$\begin{pmatrix} 1 & \eta_a \\ 0 & 1 \end{pmatrix}$$

for an aperture.

The thin dispersion element was placed near $A_2$ aperture of the right arm of the cavity (see Fig. 1). Assuming the effect of diffraction to be small, the equation for the mode amplitudes can be written as follows

$$\partial A_j(z,\tau)\,/\partial z = -i\,(\kappa_2/2)\,(\partial^2 A_j\,/\partial\tau^2).$$

For the chosen amplitude of electric field $E$ negative $\kappa_2$ corresponds to the negative group velocity dispersion. To calculate the modal amplitudes after the dispersion elements the Fourier transform method was used. It allows one to add linear dispersion terms of higher order and nonlinear group velocity dispersion [2].

For our calculations 15 Laguerre-Gaussian modes were used. After several thousands of the cavity round-trips the transient evolution was finished and the spatial and temporal dependencies were saved and analyzed.

To find the pulse transformation after the laser crystal the split-step method is used. The rod is divided in two parts (Fig. 1). We assume the active medium to be thin. The thin active layer is placed in the middle of the medium having the refractive index $n$. In the space of half rod length $d/2$ the mode amplitudes are calculated using (3). In the plane of the active layer the radial grid $(r_i)$ is chosen. In each of the grid points the field $E(r_i,\tau)$ is calculated using (1), then the field equation is solved:

$$\partial E(z,r,\tau)/\partial z = -(G/2)iP(z,r,\tau) + i\,\beta|E|^2E. \tag{6}$$

Here $G$ is the non-saturated power gain, $\beta$ is the Kerr constant, $P(z,r,\tau)$ is the medium polarization given by the density matrix equations (Bloch equations). In the thin layer the diffraction and dispersion are not taken into account.

We use the full set of Bloch equations for a two-level medium to simulate the oscillation regimes when the pulse width and the relaxation time of the medium polarization are of the same order.

$$\partial P/\partial\tau = -(\Gamma + i\,\Delta)P + iE(N_u - N_l)\Gamma, \tag{7}$$

$$\partial N_l\,(z,r,\tau)/\partial\tau = -\gamma_l N_l + \mathrm{Im}(E^*P)\gamma_l\gamma_u/(\gamma_l+\gamma_u), \tag{8}$$

$$\partial N_u\,(z,r,\tau)/\partial\tau = -\gamma_u\,(N_u - N_u{}^0) - \mathrm{Im}(E^*P)\gamma_l\gamma_u/(\gamma_l+\gamma_u), \tag{9}$$

where $\Gamma$, $\gamma_l$, $\gamma_u$, are the relaxation rates of the medium polarization and the populations of upper ($u$) and ($l$) lower levels, respectively, $N_l(z,r,\tau)$, $N_u(z,r,\tau)$ are the populations normalized to the unsaturated value of $N_u$, $\Delta=\omega_0-\nu_0$ is the frequency detuning, $\omega_0$ is the transition frequency. The field $E(z,r,\tau)$ is normalized so that $|E|^2$ is the dimensionless intensity. At each of the transverse grid points $r_i$ for given $E(r_i,\tau)$ the value of $P(r_i,\tau)$ is calculated using the second-order Adams scheme. In order to simulate the spontaneous emission effect the random short pulses are added to the field amplitude at each of the grid points. The effect of soft aperturing on the active medium is approximated by a Gaussian aperture placed near the thin active layer.

***2.2. The cavity parameters.*** For the empty cavity we chose the total power transmittance of the aperture to be $A_1$ ~75% (Fig. 1). The transmittance of the aperture $A_2$ did not exceed 99.5%, having no effect on the pulse formation. The coefficient in (4) was taken to be $T$=0.95. The focal power of the lenses was $F=2/R$, $R$=100 mm. We have performed the numerical calculations for the symmetric cavity with $L_1=L_2$=850 mm. The rod length was $d$=20 mm, the refractive index of the rod of Ti:Sph was $n$=1.76, the cavity detuning $\Delta$=0 (7), the relaxation rate of the medium polarization $\Gamma=0.31$ fs$^{-1}$, the relaxation rates for the upper and lower levels $\gamma_l=2\cdot10^{-4}$ fs$^{-1}$, $\gamma_u=2\cdot10^{-9}$ fs$^{-1}$, the dimensionless Kerr constant $\beta=(k/l)nn_2I_s$, where $n_2=3.2\cdot10^{-16}$ cm$^2$W$^{-1}$ [1], the saturation intensity $I_s$=290 kW/cm$^2$ [13].

The optimal configuration for mode locking gives the nonlinear loss coefficient [5, 6] $\delta=dL/dW$, where $L$ presents the differential cavity losses for the distributed laser model. For the discrete-element laser model the power dumping satisfies the round-trip equation $W^{(2)}=\Theta W^{(1)}$, where $W^{(1)}$ is the power before the cavity round trip and $W^{(2)}$ is the power after one round trip. Correspondingly,

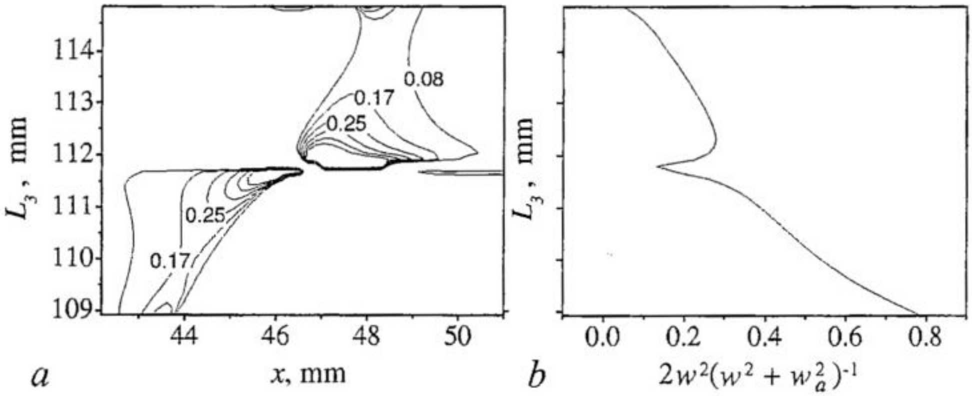

Fig. 2. Contour lines of the $w^{-1}(dw/dW)$ coefficient as a function of the rod position $x$ and of the folding distance $L_3$ (*a*). Only positive values are shown. Data labels are in $10^{-6}W^{-1}$ units. Coefficient $2w^2(w^2+w_a^2)^{-1}$ (11) for aperture $A_1$ (*b*). The dimensionless aperture width $w_a^2=2\eta_a^{-1}$ is fixed at the value $0.37\cdot10^4$

$$L = -\ln\Theta, \qquad \delta = -(1/\Theta)(d\Theta/dW)_{|W=0}. \tag{10}$$

For one intracavity aperture

$$\Theta = T\eta(\eta+\eta_a)^{-1}, \qquad \delta = -(2w^2/(w^2+w_a^2))\,(1/w)\,(dw/dW)_{|W=0}, \tag{11}$$

where $\eta=2w^{-2}$ is the real part of the beam parameter before the aperture, $\eta_d=2w_d^{-2}$ is the aperture parameter.

To calculate the value of $\delta$ the ABCD-matrix formalism was used. The thin Kerr layer was approximated by the lens (5) with the focal power $F=2\mathrm{Re}(P)^2\beta dW/\pi$, where $P$ is the stationary beam parameter in the middle of the laser rod, $dW$ is the power deviation from the zero value.

For $L_3$=111.8 the cavity is equivalent to the confocal one [6]. The upper half plane $L_3$>111.8 (Fig. 2, *a*) contains a wider region for stable mode locking. In the experiments [6, 12] this is referred as a region of low sensitivity to the misalignment of the mirrors and the laser rod.

***2.3. Numerical results and discussion.*** To characterize the output pulsed beam we expressed the intracavity power in Watts, while the pulse energy and the beam cross-section area were scaled to their stationary values. The field was calculated in the fixed time frame. We calculated also the pulse shift $s$ from the frame center and the pulse width $\tau_0$. For the chosen aperture transmission and uniform loss the differential losses are 0.35. For $G$ above this value we have obtained the mode-locking regime (Fig. 3).

As seen from Fig. 3, *a*, at the pulse peak the beam has the smallest transverse dimension. In addition to the solitonic pulse shaping this effect leads to the pulse shortening. In spite of the perfect pulse symmetry (Fig. 3, *b*) the relative beam area $\sigma(\tau)$ has an asymmetry with the respect to pulse peak. This asymmetry arises due to effect of finite relaxation time of the gain media. For longer pulses, which can be obtained for the same cavity configuration by increasing of the GVD-magnitude, such asymmetry is absent.

The relation between the solitonic pulse shaping and the pulse compression due to Kerr-lens effect is given by the factor [1]

$$R = (1/2\pi)(\beta J/|D|). \tag{12}$$

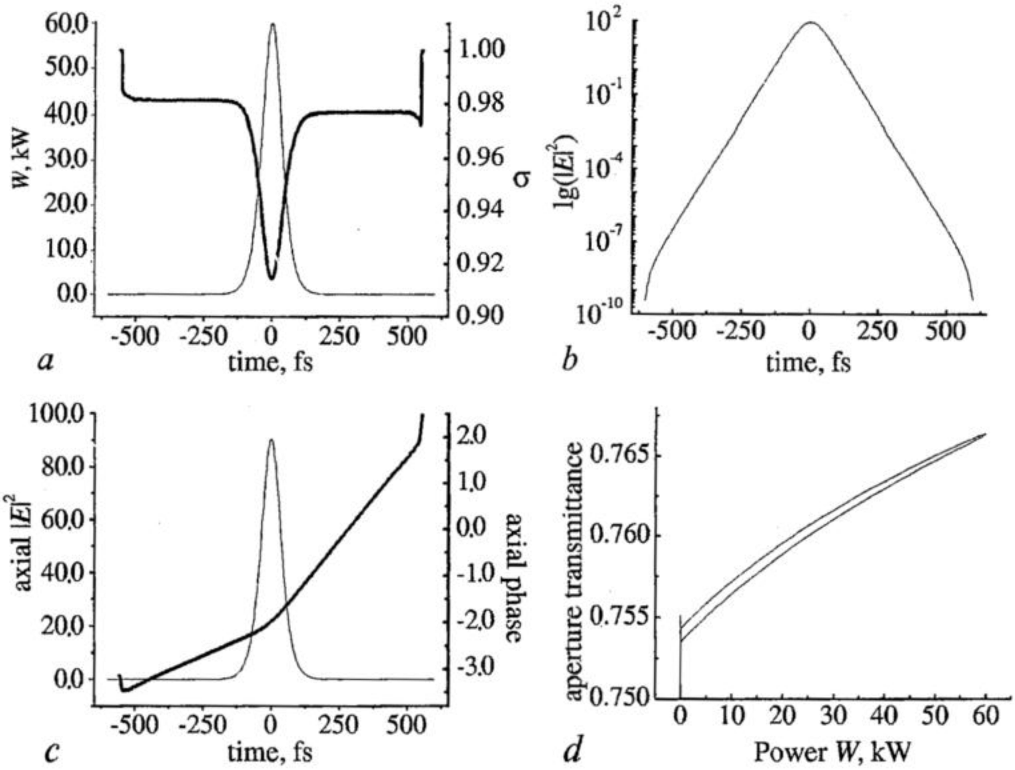

Fig. 3. Pulsed beam characteristics before the aperture $A_1$. The folding distance $L_3$=112 mm, the rod position $x$=47 mm. The round-trip power gain $G$=0.38. Power and relative beam area versus local time (*a*). Decimal logarithm of the axial intensity versus time (*b*). Axial intensity $|E|^2_{r=0}$ and axial phase $\arg(|E|^2)_{r=0}$ versus time (*c*). Aperture transmittance $w_a^2(w(\tau)^2+w_a^2)^{-1}$ versus beam power (*d*)

For the regime shown in Fig. 3 $J$=5 nJ which yields $R$=0.25. Therefore, the solitonic pulse shaping is predominate. Logarithmic plot versus the axial intensity reveals the pulse shape closer to sech $(\tau/\tau_0')^2$ (Fig. 3, *b*). The phase of the field shows the presence of pulse chirp. The linear part of the chirp corresponds to the pulse retardation with respect to the pulse propagation without the active medium. In other words, the pulse repetition rate is less than the reciprocal round trip time.

Estimating the power-dependent losses δ by means of the ABCD-matrix formalism for $L_3$=112 mm, $x$=47 mm we have found $\delta=0.43\cdot10^{-6}$ W$^{-1}$. To compare this value with the result of numerical simulations of mode-locking regime we have calculated the beam transmittance of the aperture $A_1$ (Fig. 3, *d*). Calculating the nonlinear loss coefficient (10) at $W$~0 we get $\delta=0.4\cdot10^{-6}$ W$^{-1}$, which is in agreement with our assumption. For higher power the weak saturation arises decreasing the magnitude of δ. Indeed, the effect of finite relaxation time causes a slight asymmetry in the transmission of the pulse front and the pulse train (Fig. 3, *d*).

The aperture transmittance can be calculated: i) by direct calculation of power before the aperture and after it; ii) as $w_a^2(w(\tau)^2+w_a^2)^{-1}$ in assumption of Gaussian intensity profile having the width $w(\tau)^2=\sigma(\tau)w_0^2$. Both methods give the same results, due to perfect approximation of the output beam by Gaussian. Besides, the analysis of spatio-temporal beam profile shows that the pulse width is independent of the radial coordinate.

The gain increase leads to the increase of the power dependent loss $W\delta$. As a consequence, the pulse width is decreased (Fig. 4, *a*).

We have calculated also the pulse shift $s$. The minimal pulse shift corresponds to

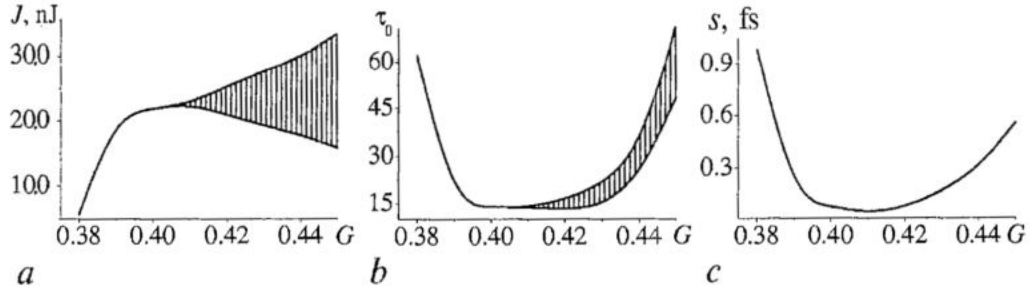

Fig. 4. Pulse width (*a*), averaged pulse shift per round trip (*b*) and pulse energy (*c*) versus round-trip power gain. The filled area shows the boundaries for the pulse energy (*a*) and pulse width (*b*) in the regime of pulse-train periodic instability

the maximal repetition rate, that corresponds to the minimum of the pulse width (Figs 4, *b, c*). This tendency is common for mode locking regimes. For example, at the rod position $x$=47 mm and the folded mirror distance $L_3$=112.5 mm the magnitude of the nonlinear loss coefficient $\delta$ is not sufficient to develop a pulse train instability up to $G$<0.6.

Before achieving the minimal width (Figs 4, *a*, 5, *a*) the pulse can be well approximated by the hyperbolic curve $\tau_0(J)=\pi/6^{1/2}\kappa_2(\beta J)^{-1}$ [1] as a function of the pulse energy. For higher gain values the parameter $R\geq 1$ (12), which corresponds to the breakdown of the weak-pulse-shaping approximation in the description of femtosecond pulses.

For given cavity configuration the phase delay per round-trip for each Laguerre-Gaussian mode of the empty cavity is close but not equal to $2\pi$. That is possible only for the unstable cavity configuration. Due to the mismatch between the phases of transverse modes quasiperiodic regimes are possible. Up to a definite value of gain the nonlinear medium gives rise to the locking of phases of mode amplitudes. Larger nonlinearity initiates distortion of the mode-locked regime. Earlier works [23, 24] have shown that very small amplitudes of higher-order transverse modes can give rise to quasiperiodic oscillation. Additional pulse instability arises due to the propagation of nonlinearly chirped pulse in the dispersive medium [1].

Pulse train periodic instability occurs starting with round-trip gain value $G$>0.41 (Fig.4, *a, b*). At the instability threshold we observed significant temporal variations of the spatial beam size (Fig. 6, *a*)

Logarithmic plot versus the axial intensity reveals the wing structure of the pulse (Fig. 6, *b*). The pulse shape significantly differs from sech$^2$. Moreover, the variation of the temporal profile from one transverse point to another was observed.

Due to the variation of the spatial beam size (Fig. 6, *a*) the pulse chirp has a

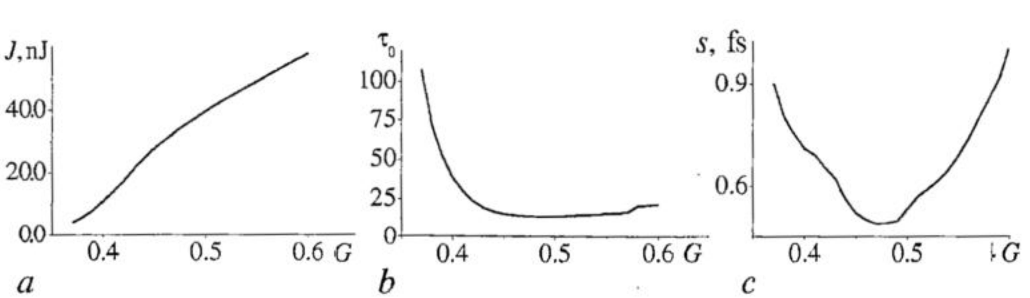

Fig. 5. $x$=47 mm, $L_3$=112.5 mm. Pulse width (*a*), averaged pulse shift per round trip (*b*), and pulse energy (*c*) versus round trip gain

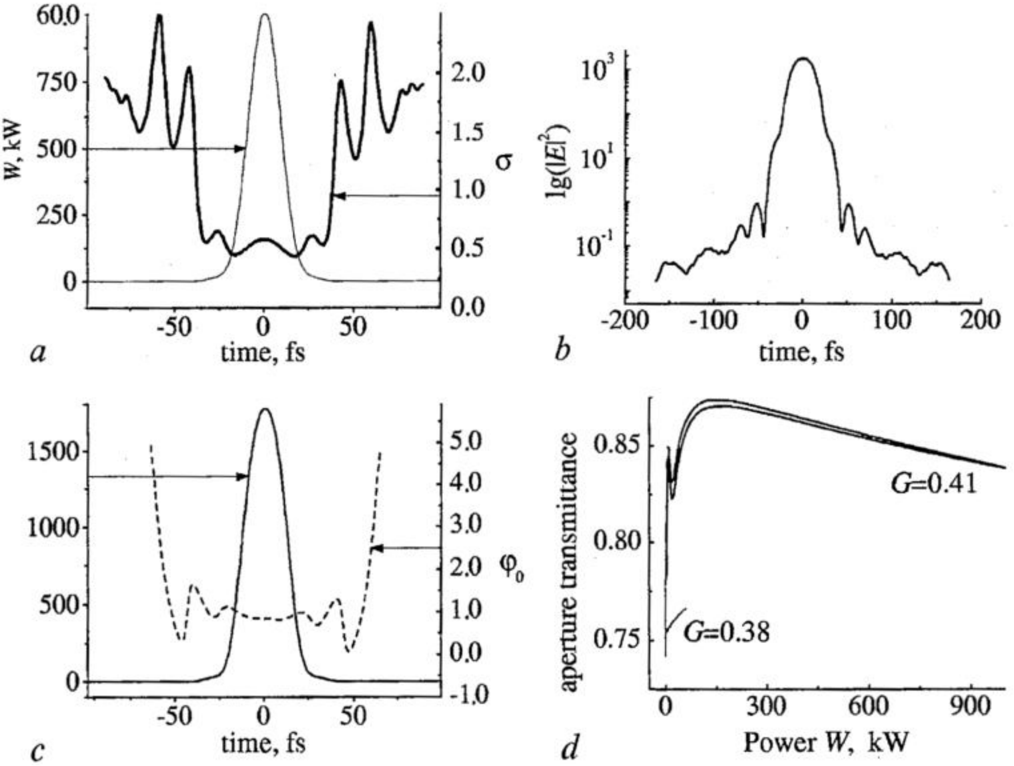

Fig. 6. Pulsed beam characteristics before the aperture $A_1$. The folded mirror distance and the rod position are unchanged. The round-trip power gain is $G$=0.41. Power and relative beam area versus local time (*a*). Logarithm of base 10 from axial intensity versus time (*b*). Axial intensity $|E|^2_{r=0}$ and axial phase $\arg(|E|^2)_{r=0}$ versus time (*c*). Aperture transmittance $w_a^2\,(w(\tau)^2+w_a^2)^{-1}$ versus beam power (*d*)

significant nonlinear part. However, for this regime the pulse shift has a minimum (Fig. 4, *c*).

Fig. 6, *d* shows the fractional power transmitted by the aperture $A_1$. For comparison two curves are shown: near the gain threshold ($G$=0.38) and close to the start of the pulse-train periodic instability ($G$=0.41).

The oscillation regime for $G$=0.43 is shown in Fig. 7. The curve showing the dynamics of pulse width (Fig. 7, *a*) has small spikes in front of one period of oscillations, but the pulse energy smoothly varies from one round trip to another.

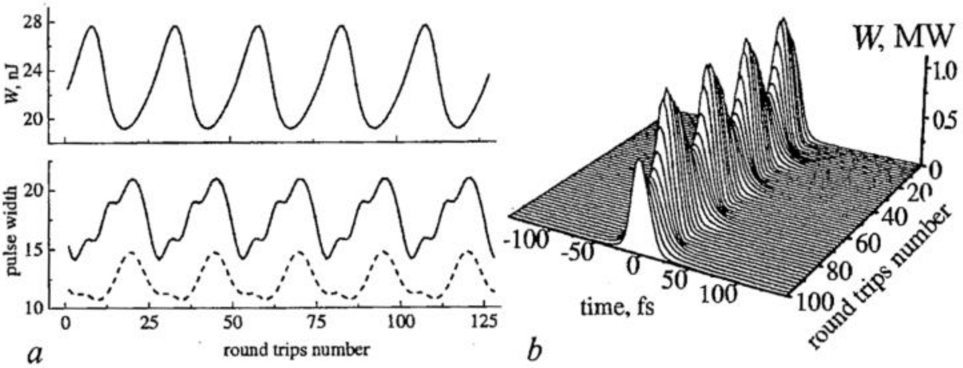

Fig. 7. $G$=0.43. Other parameters are unchanged. Pulse energy and pulse width versus round trips number (*a*). The pulse width shown by the solid curve was calculated as the second moment, the dashed curve corresponds to the pulse width defined at the $\mathrm{sech}(1)^2$ level. Temporal dynamics of the beam power (*b*)

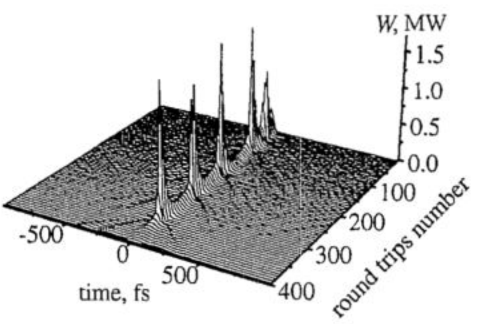

Fig. 8. Temporal dynamics of the beam power for $G=0.46$

At larger gain the magnitude of oscillations is growing (Fig. 8) which breaks the pulse train.

The growth of the oscillation magnitude is accompanied by successive excitation of several equidistant frequencies in the Fourier spectrum of the pulse energy evolution. The ground oscillation frequency depends on the GVD, the rod position and folded mirror distance.

## 3. Transverse pattern dynamics in Zeeman laser

***3.1. Karhunen-Loeve vectorial modes.*** The electric field vector in the transverse plane of a laser can be expressed in the paraxial approximation as follows:

$$\mathbf{E}(x,y,z,t) = \Sigma_{q=-1,1} (-1)^q E_q(t)\, \mathbf{e}_{-q}.$$

The spherical component of the field $E_q$ can be expressed in terms of the amplitudes of right and left polarized waves $A_q$

$$E_q = A_q\,(r, \varphi,z,t) \exp(i\nu t - iKz) + A_{-q}^{*}(r, \varphi,z,t) \exp(-i\nu t + iKz),$$

where $(r,\varphi)$ are the polar coordinates, $q=\pm1$.

To describe the complex spatio-temporal laser dynamics we use the Karhunen-Loeve procedure in which it is necessary to calculate the eigenvectors and eigenvalues of the normalized correlation matrix 2×2, obtained by time averaging of the product of normalized field components at two different points in the transverse plane. It is often more convenient to work with a matrix equation rather then with an integral equation. This can be done using the field decomposition in terms of Laguerre-Gaussian (LG) modes. For a fixed transverse plane $z$=const in the laser cavity

$$A_q(r,\varphi,t) = \Sigma_{m=-\infty}^{\infty} \Sigma_{n=0}^{\infty} A_n^{\ m}(t)_q\, \psi_n^{\ m}(r,\varphi), \tag{13}$$

where $A_n^{\ m}(t)_q$ is the mode amplitude,

$$\psi_n^{\ m}(r,\varphi) = L_n^{\ |m|}(\eta(z)r^2)\,(\eta r^2)^{|m|/2} \exp(-P(z)r^2/2 + im\varphi),$$

$$<\psi_n^{\ m} \,|\, \psi_{n'}^{\ m'*}> = N_n^{\ m}\, \delta_{mm'}\, \delta_{nn'}.$$

Here $P$ is the complex beam parameter at the chosen $z$ plane, $L_n^{\ m}$ is the Laguerre polynomial, $N_n^{\ m}=2\pi(n+m)!/n!$. It is convenient to introduce normalized mode amplitudes

$$(a_n^{\ m})_q = (A_n^{\ m})_q\, (N_n^{\ m}/W)^{1/2}. \tag{14}$$

In terms of Laguerre-Gaussian mode amplitudes the time-averaged total power of the beam can be written as $W=(2\eta)^{-1}<\Sigma_{m,n,q} N_n^{\ m} (A_n^{\ m})_q (A_n^{\ m})_q^{*}>_t$.

The matrix version of the integral equation can be easily derived

$$[\Lambda, \mathbf{b}] = \lambda \mathbf{b}, \tag{15}$$

where

$$\mathbf{b} = \begin{pmatrix} (b_n{}^m)_+ \\ \vdots \\ (b_n{}^m)_- \\ \vdots \end{pmatrix} , \qquad \Lambda = \overline{\begin{pmatrix} (a_n{}^m)_+ (a_n{}^m)_+^* & \cdots & (a_n{}^m)_+ (a_n{}^m)_-^* & \cdots \\ \vdots & \ddots & \vdots & \ddots \\ (a_n{}^m)_- (a_n{}^m)_+^* & \cdots & (a_n{}^m)_- (a_n{}^m)_-^* & \cdots \\ \vdots & \ddots & \vdots & \ddots \end{pmatrix}}^{\,t} . \tag{16}$$

Here the overline denotes the time averaging.

Due to the normalization chosen (14), the matrix $\Lambda$ is Hermitian and Spur($\Lambda$)=1. Hence $\Sigma_k \lambda_k = 1$, and the eigenvectors, corresponding to the different eigenvalues, are orthogonal:

$$\mathbf{b}_k \mathbf{b}_j^* = \Sigma_{m,n,q} \, (b_n{}^m)_{qk} \, (b_n{}^m)_{qj}{}^* = \delta_{k,j} \, .$$

The laser dynamics is dominated by the modes (**b**) whose sum of eigenvalues is close to unity. Obviously, for stationary fields the KL-modes include only one mode which coincides with the field itself with the eigenvalue $\lambda$=1. In LG basis the KL-modes coincide with LG modes with amplitudes $(b_n{}^m)_q W/N_n{}^m$ and eigenvalues which are the relative intensities of modes.

***3.2. Numerical model and results.*** We consider a Zeeman laser with nonplanar (image rotating) ring cavity with large Fresnel number [51, 49]. Fig. 9 shows the field transformation operator scheme used for numerical modeling.

For each slowly varying complex amplitude $A(r,\varphi,z,t)_q$ a paraxial wave equation similar to (6) is solved. We consider round-trip variations of the total field and describe the laser dynamics in the scale of round trip times. The field transformation during one round trip is a consequence of the following steps: i) free-space propagation; ii) image rotation; iii) Gaussian aperture and lens; iv) nonlinear active medium; v) linear cavity anisotropy.

In free-space part of the cavity we used the decomposition of each complex field amplitude in terms of Laguerre-Gauss orthogonal modes. The image rotation after one round-trip is described by the coordinate frame rotation by the angle $\theta$, $\varphi' = \varphi - \theta$, where $\varphi'$ is the azimuthal coordinate in the rotated coordinate frame

$$(A_n{}^m)_q{}' = (A_n{}^m)_q \exp(i\,(m - q)\theta).$$

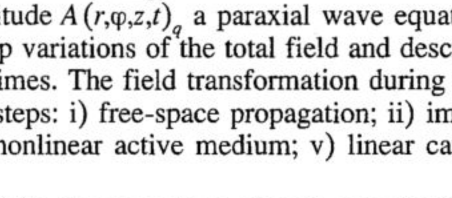

Fig. 9. Image rotating ring cavity model with axial maghetic field **H**

The field transformation at the Gaussian aperture and lens was also expressed in terms of the transverse mode amplitudes [28, 51]. For simplicity a stigmatic cavity was considered. Grid representation of the field in the active medium was used. In each of the transverse polar grid points $(r_i,\varphi_j)$, $i=1,\ldots,15$, $j=1,\ldots,20$ the field components $A_q$ were calculated. We suppose that the active medium is thin, $\partial A_q/\partial z = iG/2P(r_i,\varphi_j)_q$, where $P_q$ are the circular components of the medium polarization, $G$ is the round-trip power gain.

The active medium is supposed to have a transition $j=1 \leftrightarrow j=2$, where $j$ denotes the angular momentum quantum number, and is placed into the homogeneous magnetic field. The density matrix equation for the irreducible spherical tensors is solved algebraically.

$$P_q = A_q D_q \frac{1+[\alpha^{(+)} - \alpha^{(-)}]S_{-q}}{1+\alpha^{(+)}[S_q+S_{-q}] + [(\alpha^{(+)})^2-(\alpha^{(-)})^2]S_q\, S_{-q}},$$

where

$$D_q = \gamma/(\gamma + i\,(\omega-\nu+q\Omega)), \quad S_q = |A_q|^2\mathcal{L}_q, \quad \mathcal{L}_q = \mathrm{Re}[D_q].$$

Here $\gamma$ is the relaxation rate of the medium polarization, the frequency $\omega$ is associated with the energy gap in the absence of magnetic field, $\Omega$ is the Zeeman splitting, $\alpha^{(+)}=0.46$, $\alpha^{(-)}=(0.21/\gamma_u+0.01/\gamma_l)\gamma_u\gamma_l/(\gamma_u+\gamma_l)$, where $\gamma_u$ and $\gamma_l$ are the relaxation rates of the upper and lower level, respectively.

Phase anisotropy of the cavity was modeled by the birefringent plate. Corresponding expression can be found in [49].

We consider a high-gain active medium and a large number of transverse modes. In numerical studies we have used more than 200 transverse modes in both circularly polarized components of the field.

In numerical experiments we used the following set of parameters: the ratio of the beam area to the area of Gaussian aperture $\eta_A=0.05$, the normalized focal power of the effective lens in the cavity $F=L/f=1.5, 2.0, 2.5$, where $L$ is the cavity length, $f$ is the focal distance of the lens, the Zeeman splitting normalized to the transition line width $\mu=\Omega/\gamma=0.15$, the transmission coefficients responsible for the linear amplitude anisotropy of the cavity $t_x=0.95$, $t_y=0.94$, the linear phase anisotropy (phase retardation in the birefringent plate inside the cavity) $\delta=0.1$. The round-trip gain is $G=0.52$, corresponding to the relative excitation value close to 2.0. In the regimes considered the image rotation variation affected only the power modulation frequency, leaving unchanged the transverse pattern structures. Hence we used the zero value of the rotation angle.

***3.3. Classification of Karhunen-Loeve modes.*** We can use the Stokes parameters for the characterization of each KL mode polarization state:

$$\begin{aligned} X &= 2\mathrm{Re}(E_+E_-^*), \\ Y &= 2\mathrm{Im}(E_+E_-^*), \\ Z &= (E_+E_+^* - E_-E_-^*), \\ I &= (E_+E_+^* + E_-E_-^*), \end{aligned} \tag{17}$$

where $E_\pm$ represent the right and left circularly polarized components of the KL mode field.

Obviously, $X$, $Y$ can be expressed as polynomials in terms of coordinates $x$, $y$, thus defining a 2D vector field (2DSP) $X=X(x,y)$, $Y=Y(x,y)$. Of course, there exists the exponential factor appearing from Laguerre-Gaussian modes, but it has no influence on singular points. This 2D vector field can be associated with the autonomous dynamical system:

$$\dot{x} = X(x(t), y(t)), \quad \dot{y} = Y(x(t), y(t)), \tag{18}$$

and the classification of the KL-mode polarization pattern can be made investigating the character of the singular points (zeroes of $X$ and $Y$) of this system.

There are three possibilities [49]:

- The system is gradient,

$$\partial X/\partial y = \partial Y/\partial x.$$

There exists a potential function $V(x,y)$, which should be classified using the catastrophe theory [50].

- The system is Hamiltonian. The Hamiltonian $H(x,y)$ can be introduced in such a way that

$$dx/dt = \partial H/\partial y, \quad dy/dt = -\partial H/\partial x$$

and can be classified using Birkhoff-Gustavson normal forms [52].

- General case. The singular points $X=0$, $Y=0$ should be determined and their classification can be made using the methods [53].

In the previous paper [49] we have investigated the case $F=2.5$ which corresponds to rotating transverse patterns. These regimes belonged to the gradient case. Due to the rotation of the transverse pattern and the electric field vector $Y=0$, and the KL modes are linearly polarized. The results of numerical simulation of laser dynamics are summarized in the Table 1. *a*, *b*, *c*, *d* are nonzero coefficients, $r^2=x^2+y^2$. The type of catastrophe is presented in corresponding column, where «Morse» stands for Morse-type function, «QP» and «St» denote quasi-periodic and stationary regimes, respectively.

Table 1

Catastrophe classification of 2DSP for different gain and optical power

| $F$ | gain | number KL modes | X | catastrophe | regime |
|---|---|---|---|---|---|
| 1.5 | 0.4 | 1 | $a+br^2-cr^4$ | $A_{-3}$ | St |
| 1.5 | 0.5 | 1 | $-ar^4$ | $A_{-3}$ | QP |
| 1.5 | 0.5 | 2 | $-ar^6$ | $A_{-5}$ | QP |
| 1.5 | 0.5 | 3 | $ar^4$ | $A_3$ | QP |
| 1.5 | 0.5 | 4 | $-ar^2$ | Morse | QP |
| 1.5 | 0.5 | 5 | $-ar^{10}$ | $A_{-9}$ | QP |
| 1.5 | 0.6 | 1 | $a+br^2-cr^4$ | $A_{-3}$ | QP |
| 1.5 | 0.6 | 2 | $-ar^8$ | $A_{-9}$ | QP |
| 1.5 | 0.6 | 3 | $ar^4$ | $A_5$ | QP |
| 1.5 | 0.6 | 4 | $-ar^4$ | $A_{-5}$ | QP |
| 2.5 | 0.4 | 1 | $a-br^2+cr^4-dr^6$ | $A_{-7}$ | St |
| 2.5 | 0.5 | 1 | $a+br^2$ | Morse | QP |
| 2.5 | 0.5 | 2 | $-ar^6$ | $A_{-7}$ | QP |
| 2.5 | 0.5 | 3 | $ar^4$ | $A_{-5}$ | QP |
| 2.5 | 0.5 | 4 | $-ar^2$ | Morse | QP |
| 2.5 | 0.6 | 1 | $a+br^2$ | Morse | QP |
| 2.5 | 0.6 | 2 | $-ar^6$ | $A_{-7}$ | QP |
| 2.5 | 0.6 | 3 | $ar^4$ | $A_5$ | QP |
| 2.5 | 0.6 | 4 | $-ar^{10}$ | $A_{-11}$ | QP |
| 2.5 | 0.6 | 5 | $-ar^8$ | $A_{-9}$ | QP |
| 2.5 | 0.6 | 6 | $ar^8$ | $A_9$ | QP |
| 2.5 | 0.6 | 7 | $-ar^2$ | Morse | QP |
| 2.5 | 0.6 | 8 | $-ar^4$ | $A_{-5}$ | QP |

Another situation was observed for $F=2.0$. In this case the transverse patterns do not rotate but oscillate, changing the orientation of the pattern, while the polarization (the azimuth and eccentricity of the polarization ellipse) of the field in a given point of the transverse plane is almost unchanged. In Fig. 10 the corresponding instant laser patterns for right and left polarization are shown.

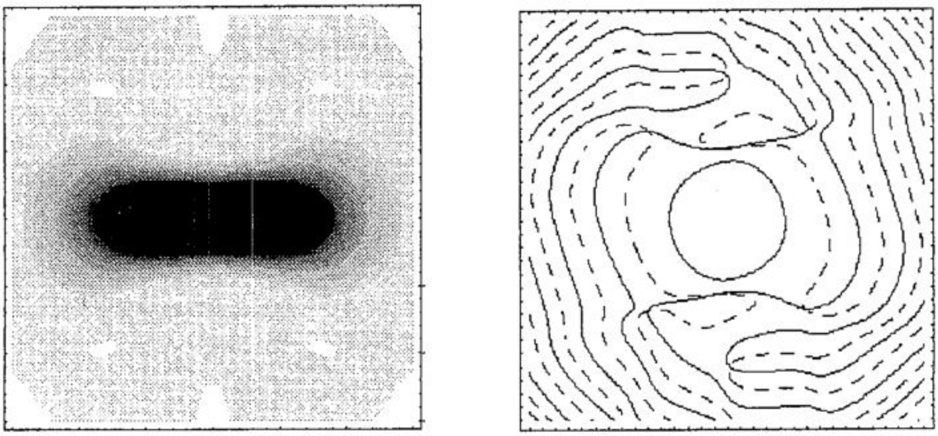

*a* *b*

Fig. 10. Transverse laser patterns for right-hand circular component of the electric field vector. Transverse intensity distribution $|E_+|^2$ (*a*). The curves $\mathrm{Re}(E_+)=0$ are solid and $\mathrm{Im}(E_+)=0$ are dashed (*b*)

There exist two KL modes at $F=2$, $g=0.7$ (Fig. 11).

In this case both $X$ and $Y$ parts of the 2D vector field of Stokes parameters are nonzero. Explicit expressions for $X$, $Y$ can be written as:

$$\begin{aligned} \dot{x} &= \Sigma_{i=0}^{6}\Sigma_{j=0}^{6} a_{ij}\, x^{2i} y^{2j}, \\ \dot{y} &= \Sigma_{i=0}^{6}\Sigma_{j=0}^{6} b_{ij}\, x^{2i} y^{2j}. \end{aligned} \tag{19}$$

For the classification of these regimes we can use the procedure [53], which includes some steps explained below. First we should find the so-called *carrier* of the system Eq.(19). We should multiply the first equation by $y$ and the second equation by $x$.

The resulting monomials $x^n y^m$ can be labeled by its powers $(n,m)$, representing the corresponding point in the plane of variables $(n,m)$. The set of all these points is the *carrier* of the system. The set of coefficients of a given monomial appearing in the right-hand part of the system is called *vector coefficients*. The points in the plane $n,m$ form the *Newton polygon* of the system, and the part of this polygon which «looks» at the origin is *Newton diagram*.

The second step consists in simplifying the Newton diagram. The polygons can be transformed using the change of variables of the special kind ($z$ is no more the longitudinal coordinate starting from here):

$$x = z^{p_1} w^{q_1}, \quad y = z^{p_2} w^{q_2}.$$

The matrix of indices $C$ associated with this transformation looks as follows:

$$C = \begin{pmatrix} p_1 & q_1 \\ p_2 & q_2 \end{pmatrix}. \tag{20}$$

In our specific case it was convenient to use $C$ =1, 0, 1, 1. Under the transformation of coordinates the system is subjected to the corresponding transformation too:

$$\begin{aligned} \dot{z}w &= \Sigma_{i=2,6}\, w^{2i} z\, \Sigma_{j=0,6}\, a_{i,j}\, z^{2j} \\ z\dot{w} &= \Sigma_{i=2,6}\, w^{2i} z\, \Sigma_{j=0,6}\, b_{i,j}\, z^{2j} \end{aligned} \tag{21}$$

and, therefore, the Newton diagram can be simplified (Fig. 12).

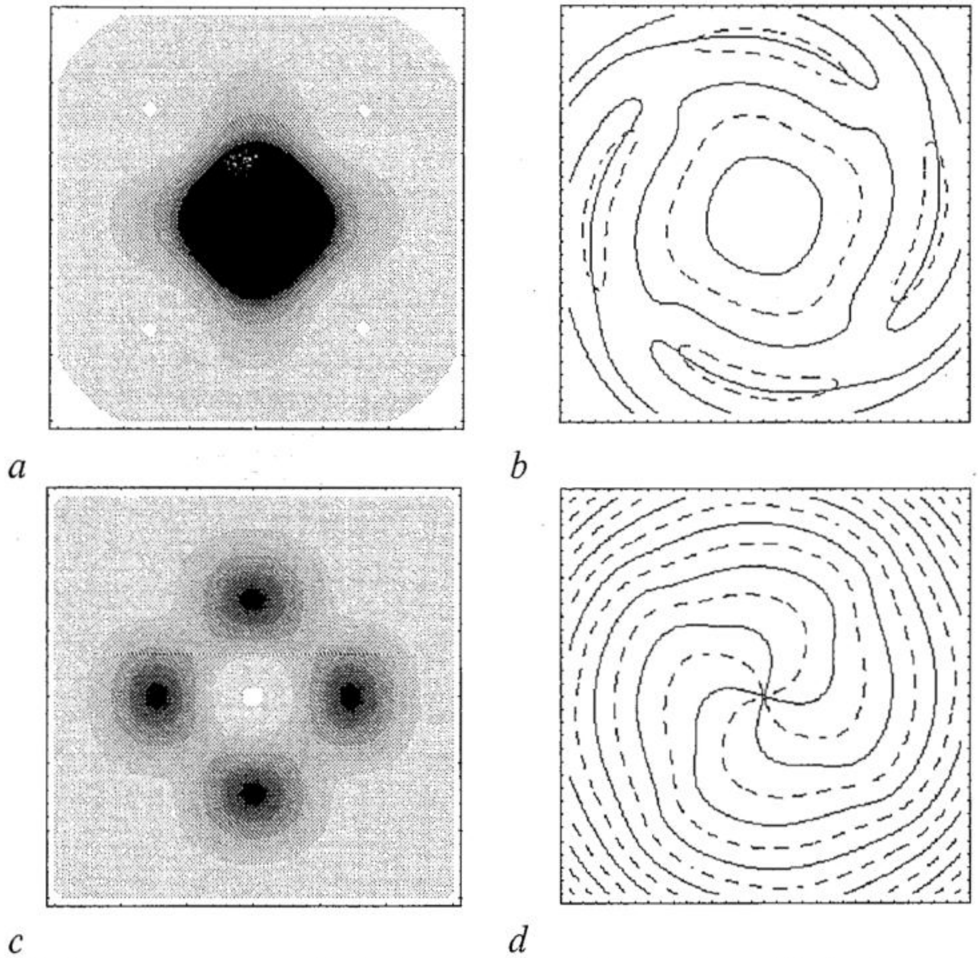

Fig. 11. The transverse patterns of the right-hand circularly polarized component of the first (*a*, *b*) and the second (*c*, *d*) Karhunen-Loeve modes. The correspondent tranverse pattern of the field is shown in Fig. 10. The eigenvalues $\lambda_1$=0.650072, $\lambda_2$=0.349926. The density (*a*, *c*) plot shows intensity of right-hand circularly polarized component of Karhunen-Loeve mode. Solid curves (*b*, *d*) shows the point of transverse plane where the real part of right-hand circularly polarized component of KL-mode is zero. Dashed curves shows the zeros of imaginary part of the same

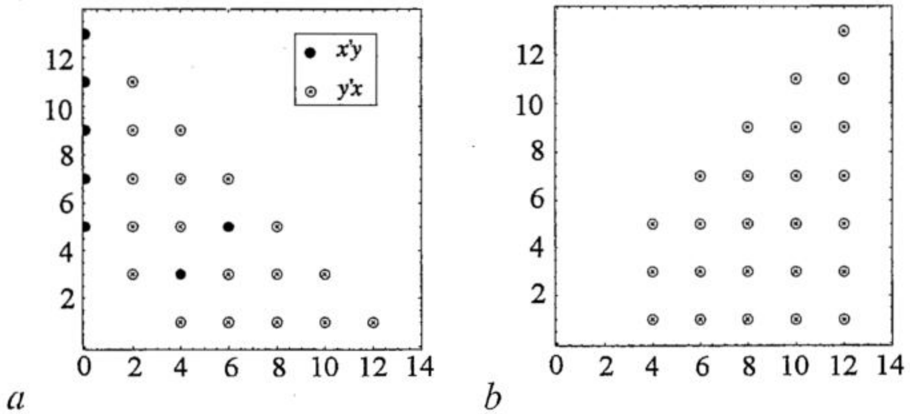

Fig. 12. Newton diagram for the right - (*a*) and the left-polarized (*b*) components of the second KL-mode after the transformation

After these transformations we can calculate the eigenvalues of the linearized system $\kappa_1$, $\kappa_2$. The signature of $\kappa$ set shows the type of singularity (in our case at $z=w=0$). In this case $\kappa_1=0$,......., therefore the type of singularity is saddle-node. Using the described algorithm we can study in general the behaviour of the transverse polarization structure near the singularities of 2D vector field of Stokes parameters, which, of course, correspond to peculiarities of electric field polarization patterns. Further classification of singular points of the field is possible in the spirit of catastrophe theory for the transformed fields with linear Newton diagrams.

## 4. Stationary modes in boson traps

***4.1. Nonground stationary states.*** Consider an ensemble of neutral atoms trapped in a parabolic potential. At low temperatures the Bose-Einstein condensation is possible. In the mean-field limit and s-scattering approximation the condensate is described by the collective wave function $\Phi$ that obeys the Gross-Pitaevskii (GP) equation [55]

$$i\ \partial\Phi(\mathbf{r},t)/\partial t = \hat{H}_0\Phi(\mathbf{r},t) + g|\Phi(\mathbf{r},t)|^2\Phi(\mathbf{r},t), \tag{22}$$

where $g$ is proportional to the number of the atoms and the length of scattering,

$$\hat{H}_0 = -\tfrac{1}{2}\nabla^2 + (\omega_x^{\,2}x^2 + \omega_y^{\,2}y^2 + \omega_z^{\,2}z^2)/2, \tag{23}$$

x, $y$, $z$ are the coordinates. The initial condition to solve Eq. (22) is

$$\Phi(\mathbf{r},t=0) = \Phi_0(\mathbf{r}). \tag{24}$$

The wave function can be normalized

$$\int_{R^3}|\Phi(\mathbf{r},t)|^2 d\mathbf{r} = 1. \tag{25}$$

Let us seek the stationary solution of Eq. (22) in the form

$$\Phi^{\mathrm{stat}}(\mathbf{r},t) = \exp\,(-i\,\mu t)\,\phi(\mathbf{r}). \tag{26}$$

The stationary states $\phi$ satisfy the stationary GP equation

$$\hat{H}_0\phi(\mathbf{r}) + g|\phi(\mathbf{r})|^2\phi(\mathbf{r}) = \mu\phi(\mathbf{r}). \tag{27}$$

For cylindrical traps $\omega_x=\omega_y=\omega_\perp$, $\omega_z<<1$. In all examples we consider $\omega_\perp=1$, $\omega_z=0$. Obviously, in this case Eq. (22) is similar to the scalar paraxial wave equation for a beam in a parabolic waveguide with Kerr nonlinearity. In contrast to optics, the nonlinear term in Eq. (22) is typically very large. Our aim here is to investigate the stationary mode with one transverse node (Fig. 13) and the possibility of a resonance transition to this state from the ground state.

For a weakly perturbed stationary state

$$\Phi^{\mathrm{pert}}(\mathbf{r},t) = \exp(-i\,\mu t)\{\phi(\mathbf{r}) + [Cu(\mathbf{r})\exp(-i\,\omega t) + C^{*}v^{*}(\mathbf{r})\exp(i\,\omega t)]\}, \tag{28}$$

corresponding to small oscillations of the order parameter around the stationary-state value, the linearized GP equation is reduced to the simultaneous Bogoliubov equations [55]

$$\omega u = (\hat{H}_0 - \mu + 2g|\phi|^2)u + g\phi^2 v; \tag{29}$$

$$-\omega v = (\hat{H}_0 - \mu + 2g|\phi|^2)v + g\phi^{*2}u, \tag{30}$$

with the orthonormalization condition

$$\int_{R^3} (u_i^* u_j - v_i^* v_j) d\mathbf{r} = \delta_{ij}. \tag{31}$$

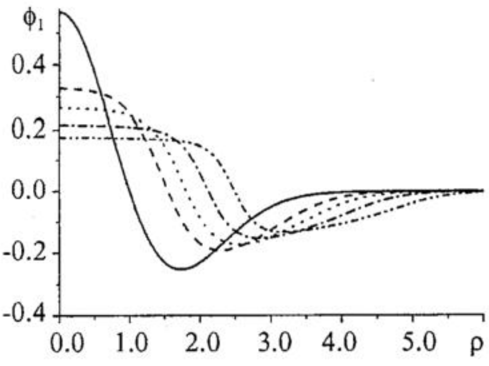

Fig. 13. One-node stationary wave function versus the distance from the trap axis. $g$=0 (solid line), $g$=50 (dashed line), $g$=100 (dot line), $g$=200 (dash dot), $g$=400 (dash dot dot)

The oscillations (collective modes) for the one-node state considered possess some specific features in comparison with those for the ground state. One of the functions $(u,v)$ must have no nodes, while the other has two. So we can identify the normal state by indicating the quantum numbers of the base state and of the function $u$. For $(u,v)_{1,2}$ (Fig. 14, *a*) the result of the numerical calculation (dotted line in Fig. 15) shows that $\omega=2\omega_\perp$ at any $g$. Therefore, this state is an analog of the monopole mode of the ground state. For $(u,v)_{1,0}$ (Fig. 14, *b*) the dependence of the frequency upon $g$ is shown in Fig. 15 with dashed line. This mode, corresponding to exotic oscillations, should occur with the package radius and, therefore, the potential energy, being constant, while the kinetic energy exchanging with the energy of atomic interaction.

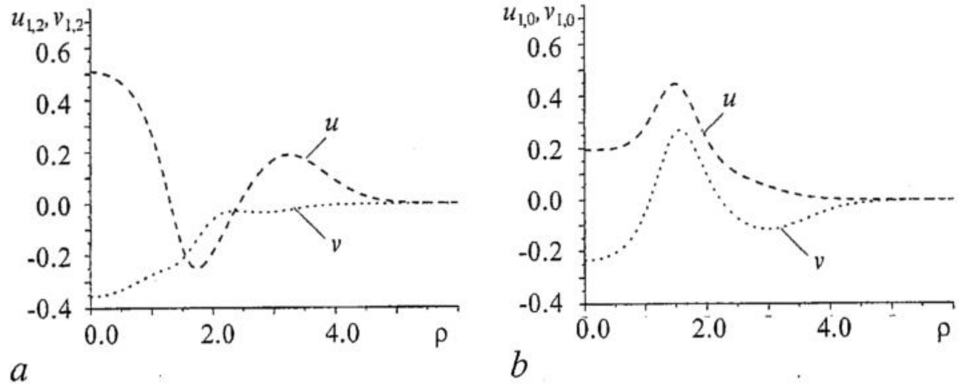

Fig. 14. Collective modes for one-node stationary state,$g$=50

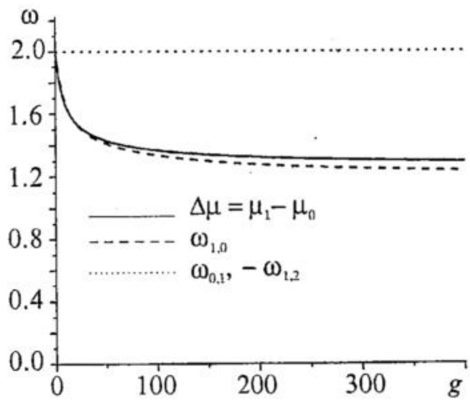

Fig. 15. Characteristic frequencies: the difference between the potentials corresponding to one-node stationary state and the ground state (solid line); the kinetic-interaction exchanging frequency (dashed line); the averaged square radius oscillation frequency(dotted line)

***4.2. Excitation of the non-ground states.*** Consider a harmonic external perturbation that may be caused, e.g., by the variation of the trap parameters. In this case the GP equation may be written in the form

$$i\,(\partial\Phi(\mathbf{r},t)/\partial t) = [\hat{H}_0 + g|\Phi(\mathbf{r},t)|^2 + \kappa\sin\Omega t\,(x^2+y^2)]\Phi(\mathbf{r},t). \tag{32}$$

Let us take the ground state as the initial one

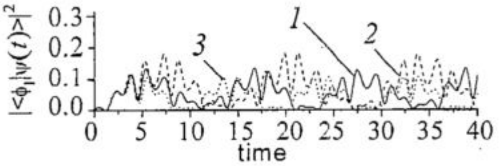

Fig. 16. Dynamics of the projection of the ground state to the one-node state under the harmonic excitation: «on-resonance» frequency (*1*, $\Omega=\Delta\mu=1.43017$), positive detuning (*2*, $\Omega=\Delta\mu+0.1$), negative detuning (*3*, $\Omega=\Delta\mu-0.1$). The maximal value is achieved for the positive detuning, because the corresponding $\Omega$ is the closest to the collective mode frequency $\omega_{0,1}=2$, $g=50$, $\kappa=0.1$

$$\Phi(\mathbf{r},t=0)=\phi_0(\mathbf{r}). \qquad (33)$$

Earlier it was supposed [56] that the transitions between the stationary states are possible under the action of a resonance external field. It is well known that for linear oscillator the maximal rate of a transition to a fixed state is limited because the energy spectrum is equidistant. Nonlinear operator eigenvalue problem (27) yields a non-equidistant spectrum. This fact was noted in [56] as the case for the applicability of the two-level approximation and possibility of creating the non-ground state. However, the results of our direct numerical solution (32, 33) contradict to this hypothesis. We found that, firstly, there is no resonance at $\Omega=\Delta\mu=\mu_i-\mu_0$ for any $i$ and any $g$, and, secondly, the population of the non-ground state is oscillating from 0 to some maximal value, which increases with the growth of $\kappa$, but tends to the saturated value <40%, that accords with the maximal transition rate for a simple linear oscillator (see Fig. 16). We observed only resonances associated with the collective modes, i.e., at $\Omega=\omega$, see Eqs .(29, 30). This result is easy to explain. While the wave function of the system is close to a certain stationary state, another stationary states does not exist, because of the different effective potential in Eq.(27). The result of [56] can be a consequence of using one-parametric variational functions for the solution of Eq.(27). As a result, the authors of [56] found that $\Delta\mu\rightarrow\infty$ when $g\rightarrow\infty$, so, the averaging technique and the two-level approximation hold when $g$ is big enough. Actually, as seen in Fig. 15, $\Delta\mu$ tends to a constant for big $g$.

## Conclusions

Using the numerical simulations within the framework of full spatio-temporal model, we have analysed the pulse train characteristics of the Kerr-lens mode-locked laser. At the threshold the pulses have the hyperbolic secant shape. We have found that the gain depletion due to the finite relaxation time of the medium response leads to the asymmetry in the beam size variation. The gain increase leads to the distortion of the hyperbolic secant pulse shape and to deep beam size variation during the pulse. The effect of finite-time relaxation and gain saturation leads to the nonlinearity in the calculated beam transmittance at the output aperture.

In the absence of the third-order dispersion the pulse remains symmetric, but the beam size demonstrates pronounced asymmetry.

We have found that in the mode-locked regime only single solitonic solutions are stable. The gain increase leads to instabilities of pulse train. The threshold of the non-periodical oscillations of the beam shape is decreased with the decrease of the GVD and with the increase of the amplitude modulation coefficient. In quasi-periodical regimes the output power spectrum depends on the GVD coefficient and the frequency spacing between the transverse modes of the empty cavity. The coupling of multiple transverse modes leads to the sweeping of the beam size. This result is in agreement with experimental investigations.

The presented model makes it possible to obtain the full information about the spatio-temporal evolution of the pulse train. The temporal and transverse beam reshaping becomes important for femtosecond pulses. Our approach to the description of pulsed beams can be applied in modeling femtosecond laser dynamics without the approximation of slowly varying amplitude.

We present the algorithm for the classification of different dynamics of transverse polarization patterns based on the calculation of eigenmodes (Karhunen-Loeve modes) and eigenvalues of the two-point correlation matrix, expressed via the time average of the products of the electric field components. The use of the vector Karhunen-Loeve modes allows one to select the group of transverse modes which determine the laser dynamics. These KL modes form the orthogonal basis and provide the optimal description of the dynamics of the vector field laser. Using numerical simulation of the polarization transverse pattern dynamics in a Zeeman laser, it was demonstrated that the number of essential KL modes is not so large (four in the regimes considered), while the number of Laguerre-Gaussian modes necessary to reproduce the laser dynamics is several hundreds. The regimes corresponding to the rotation of the pattern with nearly constant angular velocity were investigated as well as the regimes with oscillating patterns and nearly constant polarization parameters.

For the classification of vector transverse patterns we propose to investigate the behaviour of the polynomials representing the KL modes or the total field in the vicinity of its singular points in the transverse plane, namely, to investigate the 2D vector field of the Stokes parameters $X$, $Y$.

Non-ground stationary states of Bose-Einstein condensate of trapped atoms were studied numerically solving the strongly nonlinear Gross-Pitaevskii equation for the collective wave function. Small harmonic perturbations of these states described by Bogoliubov equations revealed essential difference between the ground stationary state and the ones having one transverse node. In contrast to earlier assumptions, we have demonstrated that in the strongly nonlinear system under consideration the periodic perturbations are unable to produce resonant transitions from the ground state to one-node non-ground states.

*This work was supported in part by grant REC-006 of the US Civilian Research and Development Foundation for the Independent States of the Former Soviet Union (CRDF).*

## References

1. *Krausz F., Fermann M.E., Brabec T., Curley P.F., Hofer M., Ober M.H., Spielman C., Winter E. and Schmidt A.J.* // IEEE J. of Quantum Electron. 1992. Vol. 28. P. 2097.

2. *Akhmanov S.A., Vysloukh V.A., Chirkin A.S.* Optics of femtosecond laser pulses, Springer, New Yourk, 1992.

3. *Brabec T. , Spielmann C. , Krausz F.* // Opt. Lett. V. 16. P. 1961 (1991).

4. *Haus H.A., Fujimoto J.G., Ippen E.P.* // J.Opt. Soc.Am. B, Vol.8, № 10, P.2069 (1991).

5. *Magni V. , Cerullo G. , De Silvesrtri S.* // Opt. Commun. 101, P. 365, 1993.

6. *Cerullo G., De Silvesrtri S. and Magni V.* // Opt. Letters. 19, № 14, pp.1040-1042, 1994.

7. *Krausz F., Brabec T., Spielman Ch.* // Opt. Lett. Vol. 16., № 4. P. 235 (1991).

8. *Haus H.A., Fujimoto J.G., Ippen E.P.* // IEEE J. of Quantum Electron. 28, pp. 2086-2096, 1992.

9. *Bouma B.E., Ramaswamy-Paye M., Fujimoto J.G.* // Appl. Phys. B. Vol. 65, P. 213-220 (1997).

10. *Barbosa E.A., Vierra N. D.*// Optics Commun. V. 188. P. 205-211 (2001).

11. *Bohn M.J., Jones R.J., Diels J.-C.* // Optics Communications, V. 170, P.85-92, (1999).

12. *Cerullo G., De Silvesrtri S., Magni, Pallaro L.* // Opt. Letters. 19, № 11, pp. 807-809, 1994.

13. Alfrey A.J. // IEEE J. of Quantum Electron. 35, pp. 760-766, 1989.

14. Hermann J. // J.Opt.Soc.Am.B, Vol. 11, № 3, P. 498-512, (1994).

15. *Garduno-Mejia J., Mohebi M., Jamasbi N*// Opt. Comm. Vol. 171. P.263-269, (1999).

16. *KalashnikovV.L., Sorokin E., Sorokina I.T.* // e-print arXiv: physics/0101004 V. 2, Jul. 2001.

17. *Kalashnikov V., Sorokin E., Sorokina I.T.* // J. Opt. Soc. Am. B. Vol. 18 (2001), № 11, P. 1732.

18. *Kalashnikov V.L.* // Optics Communications, Vol. 192, P. 323-331 (2001).

19. *Haus H.A., Sorokina I., Sorokin E.* // J. Opt. Soc. Am. B. Vol. 15 (1998). P.223.

20. *Kutz J.N., Collings B.C., Bergman K. and Knox W.H.* // IEEE Journal of Quant. Electron., Vol . 34, № 9. P. 1749-1757, (1998).

21. *Xing Q., Chai L., Zhang W. and Wang C.* // Opt.Comm. V. 162, P. 71, (1999).

22. *Kovalsky M.G., Hnilo A.A., Gonzlez Inchauspe C.M.F.* // Opt. Lett. Vol. 24, 22. P.1638-1640 (1999).

23. *Cote D., van Dier H.M.* // Opt. Lett V.23, N.9, P.715-717, (1998).

24. *Bolton S.R., Jenks R.A., Elknton C.N., Sucha G.* // J.Opt.Soc.Am. B. Vol. 16. P.339, (1999).

25. *Spence D.E., Kean P.N., Sibbet W.* // Opt. Lett. Vol. 16. P.42 (1991).

26. *Kalashnikov V.L., Poloyko I.G., Mikhailov V.P., von der Linde D.* // J.Opt.Soc.Am B. Vol. 14, N.10, (1997).

27. *Ming-Dar Wei, Wen-Feng Hsieh* // Opt. Comm. Vol. 168, P. 161-166, (1999).

28. *Melnikov L. A., Veshneva I.V., Konukhov A.I.* // Chaos, Solitons & Fractals 4, pp. 1535-1546, 1994.

29. *Nakazawa M., Kubota H., Tamura K.* // IEEE J. Quant. Electron. V.34, № 7, P.1075-1081, (1998).

30. *Bolton S.R., Acton M.R.* // Phys. Rev. A. V.62., 063803, (2000).

31. *Konstenbauder A.G.* // IEEE J. Quant. Electron. V.26, P.1148, (1990).

32. *Dijaili S., Dienes A., Smith J.S.* // IEEE J. Quant. Electron. V.26, P.1158, (1990).

33. *Sanchez L.M., Hnilo A.A.* // Opt. Comm. V.199, P.189-199, (2001).

34. *Borisevich N.A., Buganov O.V, Tikhomirov S.A., Tolstorozhev G.B., Shkred G.L.* // Quantum Electronics. V.29, N.9, P.780-786, (1999).

35. *Brambilla M., Lugiato L.A., Penna V., Prati F., Tamm C., Weiss C.O.* 1991 Phys. Rev. A 43. 5090.

36. *Martin-Regalado J., Prati F., San Miguel M., Abraham N.B.*// 1997 IEEE J. of Quantum Electron. 33, 765.

37. *Abraham N.B., Arimondo E., San Miguel* // M. 1995. Opt. Comm. 117. 344.

38. *Serrat C., Abraham N.B., San Miguel M., Vilaseca R., Martin-Regalado J.* // 1996. Phys. Rev. A. 53. R3731.

39. *Freund I.* Optics Coomunications. 159. 99.

40. *Freund I.* 1999. Optics Communications. 163. 230.

41. *Lugiato L.A., Oppo G.L., Pernigo M.A., Tredicci J.R., Narducci L. M. and Bandy D. K.* // 1988 Optics Communications. 68. 63.

42. *Green C., Mindlin G.B., D'Angelo E.J., Solari H.G. and Tredicce J.R.* // 1990. Phis.Rev.Lett. 65. 3124.

43. *Stanley W.D.* // Digital Signal Processing. 1975. Reston Publishing Company, Inc.

44. *Reed I.S., Lan L.S.* 1994. // Journal of Visual Communication and Image Representation. 5. 304.

45. *Carevic D., Caelli T.* // 1997. Graphical Models and Image Processing. 59. 27.

46. *Wolf S.G., Ginosar R., Zeevi Y.Y.* // 1998. Journal of Visual Communication and Image Representation. 9. 25.

47. *Alessandro G., Oppo G.L.* // 1992. Optics Communications. 88. 130.

48. *Konukhov A.I., Ryabinina M.V., Veshneva I.V., Melnikov L.A.* // 1999. Proc. SPIE. 3726. 237.

49. *Konukhov A.I., Ryabinina M.V., Veshneva I.V., Melnikov L.A.* // 2001. Journal of Optics B: Quantum & Semicl. Optics. 3. S209-S214.

50. *Gilmore R.* Catastrophe theory for scientists and engineers. 1981. A Wiley-Interscience Publication John Wiley & Sons. 1981.

51. *Melnikov L.A., Konukhov A.I., Ryabinina M.V.* // 1998. Quantum and Semiclassical Optics. 10. 167.

52. *Moser J.K.* // Lectures on Hamiltonian systems. 1968. Mem. Amer. Math. Soc.

53. *Bruno A.D.* // 1979 M.: Nauka. 256 p.

54. *Parkins A.S. and Walls D.F.* The physics of trapped dilute-gas Bose-Einstein condensates // Phys. Reports, 303, pp.1-80,1998.

55. *Dalfovo F., Giorgini S., Pitaevskii L.P. and Stringari S.* Theory of Bose-Einstein condensation in trapped gases // Rev. Mod. Phys, 1, pp. 463-512, 1999.

56. *Courteille Ph.W. , Bagnato V.S. and Yukalov V.I.* Bose-Einstein condensation of trapped atomic gases // Laser Physics,{textbf 11}, pp. 659-800, 2001.

*Saratov State University*
*Saratov Branch of the Institute of*
*Radio-Engineering and Electronics of RAS*

*Recieved 19.06.2002*

УДК: 621.373.826

# НЕЛИНЕЙНАЯ ДИНАМИКА ПРОСТРАНСТВЕННЫХ И ВРЕМЕННЫХ СТРУКТУР В ЛАЗЕРАХ И АТОМНОЙ ОПТИКЕ: ЛАЗЕРЫ С КЕРРОВСКОЙ СИНХРОНИЗАЦИЕЙ МОД, ЗЕЕМАНОВСКИЙ ЛАЗЕР, АТОМНЫЙ КОНДЕНСАТ БОЗЕ - ЭЙНШТЕЙНА

*Л.А. Мельников, А.И. Конюхов, И.В. Вешнева, В.Л. Дербов, В.В. Серов*

Путем математического моделирования исследованы пространственное и временное поведение лазерных и атомно-оптических систем. Рассмотрены системы в режиме возбуждения небольшого числа скалярных поперечных мод (лазер с Керровской синхронизацией мод), с неоднородным распределеним поляризации по поперечному сечению пучка в режиме возбуждения высших поперечных мод (Зеемановский лазер с большим числом Френеля и анизотропным резонатором) и возбужденные коллективные состояния конденсата Бозе - Эйнштейна нейтральных атомов, захваченных в ловушку. В работе предприняты попытки классифицировать динамику сложных поляризационных структур поля в лазере. Подходы к классификации основаны на вычислении векторных мод Карунена - Лова и описании их сингулярных точек с использованием теории катастроф, диаграмм Ньютона. Проанализировано возбуждение неосновных состояний атомного конденсата Бозе - Эйнштейна через резонансное возмущение.

*Melnikov Leonid Arkad'evich* was born in 1949, graduated from the Faculty of Physics of Saratov State University in 1971. Candidate of Science in Physics and Mathemathics since 1978, Doctor of Sciences in Physics and Mathematics since 1992. He is the member of the Optical Society of America and SPIE. He is head of Chair of Laser and Computer Physics of Saratov university, head of Laser and Fiber Optics Systems lab of Saratov Branch of the Institute of Radio-Engeneering and Electronics of Russian Academy of Sciences. His research and teaching interests include laser physic, laser spectroscopy, fiber optics, optical gyroscopes, nonlinear dynamics of lasers and optical systems, nonlinear propagation of lihgt beams and pulses in waveguides and resonance medium, lasers with short pulses and transverse nonlinear optics, laser diagnostics, photonic crystals and photonic crystal fibers, programming, computer physics. He is the author of more than 100 scientific papers.

*Konukhov Andrey Ivanovich* was born in 1972, graduated from Saratov State University in 1994. Candidate of Science in Physics and Mathemathics since 1998. He is a senior researcher of Laser and Fiber Optics Systems lab of Saratov Branch of the Institute of Radioengeneering of Russian Academy of Sciences. His research and teaching interests include nonlinear dynamics of lasers and optical systems, lasers with short pulses and transverse nonlinear optics.

*Veshneva Irina Vladimirovna* was born in 1966, graduated from Saratov State University in 1989. Candidate of Science in Physics and Mathemathics since 1996. Her research interests include nonlinear dynamics of lasers and optical systems. She is the grantee of 1995,1996 Soros graduate student program contest. She is a lecturer of Physic Depatment of Saratov State University.

*Derbov Vladimir Leonardovich* was born in 1949, graduated from the Faculty of Physics of Saratov State University in 1972. Candidate of Science in Physics and Mathematics since 1977, Doctor of Science in Physics and Mathematics since 1999. A member of SPIE. Head of Chair of Theoretical and Nuclear Physics of Saratov State University. His research and teaching interests include quantum theory of atoms and molecules in strong electromagnetic fields, laser spectroscopy, nonlinear optics, nonlinear dynamics of laser beams and pulses in resonance media, numerical modeling of nonlinear optical phenomena. He is the author of more than 120 scientific publications.

*Serov Vladislav Victorovich* was born in Ussuriysk (1976), graduated from Saratov State University in 1999. In the present time he is a post-graduated student of the chair of Theoretical and Nuclear Physics of the Saratov State University. He is the author of the 10 articles. Research interests and specialization: numerical modeling, atomic and laser physics.

Izv. VUZ «AND», vol.10, № 3, 2002

# MULTISTABILITY, IN-PHASE AND ANTI-PHASE CHAOS SYNCHRONIZATION IN PERIOD-DOUBLING SYSTEMS

*V. Astakhov, A. Shabunin, P. Stalmakhov*

We consider mechanisms of multistability formation and complete chaos synchronization loss in mutually coupled period-doubling maps. Cases of in-phase and anti-phase synchronization are investigated. Influence of non-identity of partial oscillators is also discussed.

## 1. Introduction

Phenomenon of complete synchronization of chaos has being intensively investigated for the last time. Majority of authors consider a case of in-phase synchronization when oscillations of subsystems are equal or almost equal to each other in the every moment of time [1, 2]. The other case of complete synchronization is antiphase synchronization when the subsystems oscillate identically but with opposite signs: $x_1(t) = -x_2(t)$. The antiphase synchronization of chaos was considered in the work [3]. The authors investigated «master - slave» synchronization [4], when one subsystem unidirectionally influences on the other one.

Bifurcational mechanisms of both in-phase and antiphase complete chaotic synchronization are in close connection with bifurcations of saddle periodic orbits embedded in the synchronous chaotic attractor. In a system of symmetrically coupled identical oscillators a limit set relating to synchronous oscillations locates in the symmetric subspace ($\mathbf{x}_1 = \mathbf{x}_2$) (for the in-phase synchronization) or in the antisymmetric subspace ($\mathbf{x}_1 = - \mathbf{x}_2$) (for the antiphase synchronization) of the whole phase space of the system, where $\mathbf{x}_1$ and $\mathbf{x}_2$ are vectors of identical dynamical variables of interacting subsystems. If a chaotic set is attracting in the normal to the subspace direction, namely when its largest transversal Lyapunov exponent is negative, the synchronous oscillations are observed in experiment. When the exponent changes its sign to the positive, the chaotic attractor becomes non-attracting in the normal direction and transforms to a chaotic saddle. The synchronous oscillations are not observed in experiment further. However, the case is possible when the largest transversal Lyapunov exponent on the chaotic attractor is negative, but the exponents on some limit sets encapsulated in the attractor are positive. In this case the synchronous regime remains stable but becomes unrobust. Any infinitesimal noise or the parameters mismatch can lead to the «bubbling» of the attractor. Time-series of the oscillations related to motions in the normal to the subspace direction becomes an intermittency process when the phase point moves in vicinity of the symmetric subspace for a long time (laminar phase) and leaves it from time to time (turbulent bursts) [12]. The bubbling of attractor is the first step to the desynchronization of chaos. Then, with changing of the controlling parameters more quantity of encapsulated cycles lose their stability in the normal direction. This enforces the process of bubbling and then the averaged on the attractor largest normal Lyapunov exponent can become positive. As a result, the chaotic set in the symmetric subspace becomes non-attractive. This phenomenon is called the blowout bifurcation [5]. The bubbling of attractor can be followed also by the riddling of its basins when «holes» from the basins of another attractor appear in infinitesimly small vicinity of the attractor . In this case, the presence of small noise or the parameters mismatch leads to leaving of the phase point to the another attractor. Regimes which accompany the process of chaotic synchronization loss in the coupled logistic maps were described in works [13], [14].

In the paper we detaily describe phenomena and mechanisms of in- and anti-phase complete synchronization of chaos in period-doubling maps with symmetric diffusive coupling. The paper is organized as a follows: The section one describes bifurcational mechanisms of destruction of in-phase synchronization and formation of multistability in system of symmetrically coupled cubic maps. The found regularities are compared with that in other systems. In the second section we consider the influence of small parameter's mismatch on mechanisms of synchronization loss in logistic maps. In the third section we hold comparing mechanisms of in-phase and anti-phase synchronization of regular regimes in coupled cubic maps. We propose a method of control for anti-phase chaos synchronization and describe the phenomena which accompany it. The conclusion summarises main results of the paper.

## 2. Mechanisms of destruction of in-phase synchronization and formation of multistability in coupled cubic maps

Let's consider a system of two identical discrete maps with symmetrical diffusive coupling:

$$x_{n+1} = f(x_n) + \gamma\,(f(y_n) - f(x_n)). \tag{1}$$

$$y_{n+1} = f(y_n) + \gamma\,(f(x_n) - f(y_n)). \tag{2}$$

It is seen, that this system is invariant to the transformation ($x \leftrightarrow y$) and therefore the subspace ($x=y$) is invariant to the operator of the evolution of the system. For investigation of the stability properties of symmetric solutions it is convenient to use «normal» variables: $u = (x+y)/2$, $v = (x-y)/2$.

Adding and subtracting equations (1) and (2) and then linearizing results in the vicinity of the symmetric subspace we get:

$$u_{n+1} = f(u_n). \tag{3}$$

$$v_{n+1} = (1-2\gamma)\,f'(u_n)\,v_n\,. \tag{4}$$

The equation (3) describes the dynamics inside the symmetric subspace. It is evidently the equation of the single map. The tangent stability of the synchronous solution is described by the tangent Lyapunov exponent:

$$\Lambda_\tau^{l} = \lim_{N\to\infty} (1/N)\,\Sigma_{n=1}^{N} \ln |f'(u_n)|. \tag{5}$$

The equation (4) describes the dynamics in the normal direction to the symmetric subspace in its small vicinity. The transversal stability of the synchronous solution is determined by the transversal Lyapunov exponent:

$$\Lambda_{\perp}^{i} = \lim_{N\to\infty} (1/N) \Sigma_{n=1}^{N} \ln| (1\text{-}2\gamma) f'(u_n)|. \tag{6}$$

Comparing (3) and (4) we see that the tangential and the transversal Lyapunov exponents satisfy the relation:

$$\Lambda_{\perp}^{i} = \Lambda_{\tau}^{i} + \ln |1\text{-}2\gamma| \tag{7}$$

and hence, for small positive coupling ($0<\gamma<0.5$) the normal Lyapunov exponent is smaller than the tangent one. Any in-phase regular oscillations are normally stable and in-phase chaotic oscillations are stable only at sufficient large coupling. Let the single map be a period-doubling one. In this case in the symmetric subspace a cascade of period-doubling bifurcations leading to formation of synchronous chaos takes place. The resulting chaotic attractor contains infinite number of saddle periodic orbits taken part in its formation. According to (7) every orbit in the cascade can undergo one more period-doubling bifurcation which takes place in the normal direction to the symmetric subspace. As a result the saddle orbits which undergo the bifurcation become repellers and saddle orbits of double periods appear in their neighborhood. Then, the new saddle orbits become stable with further parameter changing. Hence, if first period-doubling bifurcations lead to complicating of synchronous oscillations, the second ones lead both to multistability and to transforming synchronous saddles into repellers.

In the Fig. 1 we built an example of a scheme of bifurcations that begin the formation of multistability. For better clarity we use here the following notation: the first index denotes the period of the orbit (or Cycle), the upper number is the number of steps on which oscillation in $y$ map is delayed from that in $x$ one. Obviously, synchronous oscillations have zero upper index. The bottom index identifies the orbit if there are several ones. Firstly, we observe the situation (Fig. 1, *a*) when there are two saddle orbits: period-one $C^0$), period-two ($2C^0$) and one stable period-four orbit ($4C^0$) in the symmetrical subspace. Then, the saddle orbit ($C^0$) undergoes the second period-doubling bifurcation in the normal to the subspace direction. As a result it becomes a repeller and a saddle orbit of period-two $2C^1$ appears outside the diagonal ($x=y$) (Fg. 1, *b*). With further parameters change it undergoes pitchfork bifurcation in the result of which the orbit $2C^1$ becomes stable and two symmetrical orbits $2C_1^{s1}$ and $2C_2^{s2}$ appears near it (Fig. 1, *c*). Then, similar series of bifurcations occurs with orbits of higher periods (Fig. 1, *d*).

The considered scheme is a typical one. It is observed for a number of different period-doubling oscillators. Here we consider a coupled cubic maps system:

$$f(x) = (a\text{-}1)\,x - ax^3. \tag{8}$$

We investigate bifurcations of the periodic orbits located inside the symmetrical subspace and of periodic orbits appeared from them. The structure of lines of tangential and transversal period-doubling bifurcations on the parameters plane is represented in the Fig. 2.

Horizontal lines $l_{01}$, $l_{02}$, $l_{03}$ marks period-doubling bifurcations of periodic orbits $C^0$, $2C^0$ and $4C^0$ inside the symmetric subspace. On the line $l_0$ the periodic orbit $C^0$ undergoes tangent period-doubling bifurcation. As a result, it transforms to saddle and a stable periodic orbit of double period $2C^0$ appears in its neighborhood. Then, on the line $l_1$ the saddle $C^0$ undergoes the transversal period-doubling bifurcation. As a result, it loses stability in transversal direction and transforms to repeller. In its neighborhood, outside the symmetrical subspace a period-two saddle orbit $2C^1$ appears. With further parameter change this orbit becomes stable through pitchfork bifurcation on line $l_2$. The similar bifurcations take place with other periodic orbits in the symmetric subspace (see lines $l_{03}$, $l_3$, $l_4$ and lines $l_{04}$, $l_5$). Choosing value of the coupling we can observe different sequences of tangent and transversal bifurcations with the parameter $a$ change. For example, the scheme described in the Fig. 1 corresponds to $\gamma \simeq 0.18$. Further increasing of the

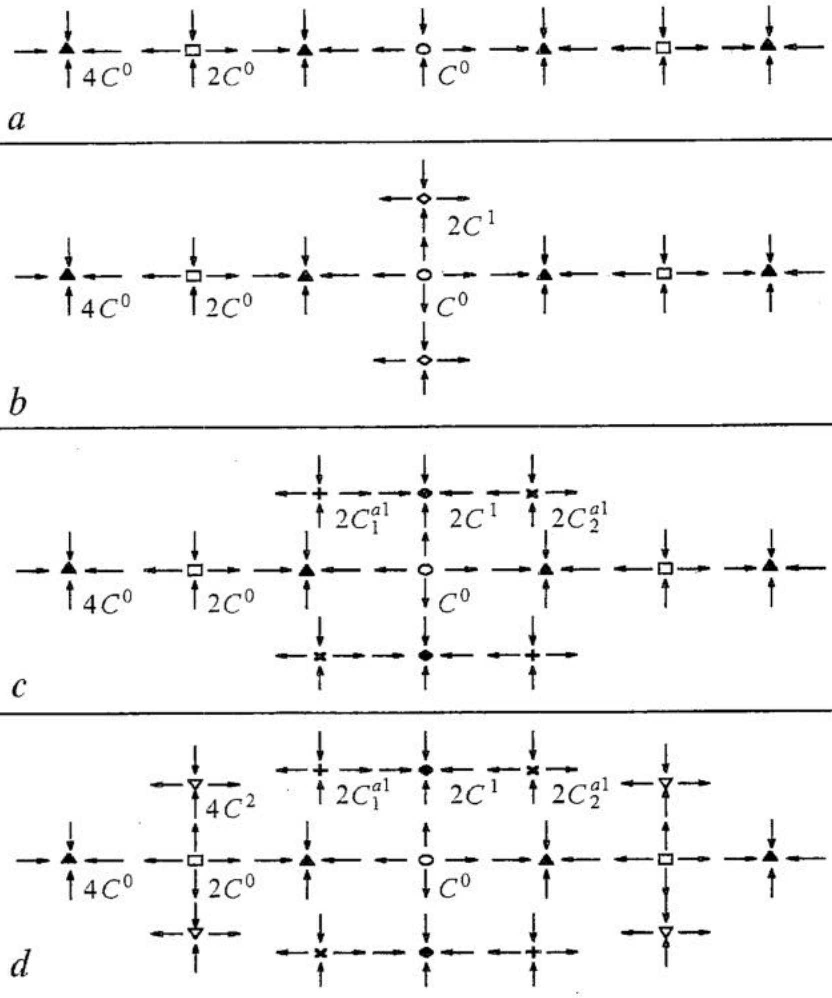

Fig. 1. Scheme of multistability formation beginning in the system of two logistic maps. Orbits $1C^0$ (o) $2C^0$ (□) $4C^0$ (Δ) are located inside the symmetric subspace. Orbits $2C^1$ (◇) $4C^2$ (∇) $2C_1$ (+) and $2C_2$ (×) are outside it

parameter of nonlinearity (line $l_{04}$ in the Fig. 2) leads to transition to synchronous chaos $2^NA^0$ ($2^NA^k$ is $2^N$ *-band* self-symmetric chaotic attractor originated on the base of the periodic orbit $2^NC^k$). Inside chaotic region band-merging bifurcations and windows of periodicity are observed. On the line $l_{05}$ the system transits to one-band synchronous chaos $A^0$.

Every transversal period-doubling bifurcation for a periodic orbit $2^N C^0$ located in the symmetric subspace, which is accompanied by its transformation to repeller adds points of local transversal instability to the chaotic attractor $2^NA^0$. From these points phase trajectory leaves the symmetric subspace at transversal perturbations. The regime of synchronous oscillations becomes unrobust. Any small noise and mismatch of the subsystems lead to destroying of the complete synchronization. Time-series of the difference ($x_n$ -$y_n$) becomes intermittency process (on-off intermittency), when motion in the symmetric subspace is intermittent by bursts from it. As a result a boundary of the synchronous region in the system with any small noise is shifted relatively to one in the system without noise. We have hold numeric investigations on determination of the boundary of the synchronization region. In these investigations we define oscillations as synchronous if the time-series of the subsystems are equal with precision of (ε) during the whole time interval of observations:

$$\max |x_n - y_n| < \varepsilon,\ n=1,2,3,\ldots,N_{observ}.$$

at chosen values: $\varepsilon = 0.0001$, $N_{observ} = 2000000$ iterations. In the Fig. 2 (o) mark the experimentally determined boundary of the robust synchronization region. From the right side of it stable synchronous chaotic oscillations take place. Under the line $l_{05}$ the system demonstrates many-band synchronous chaotic attractors $2^N A^0$, over it there is one-band synchronous chaotic attractor $A^0$. Adding small noise with intensity ~ 0.00001 to the system doesn't lead to desynchronization.

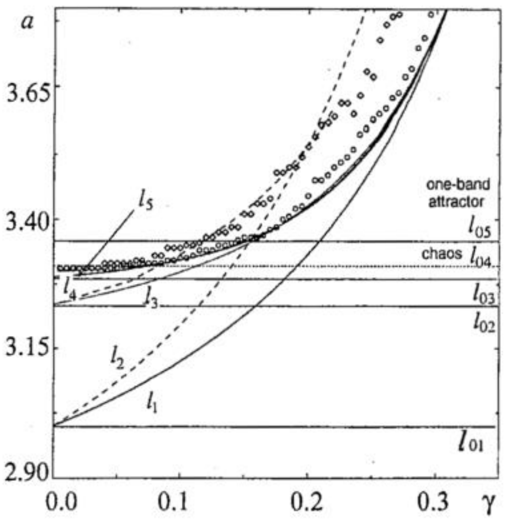

Fig. 2. Location of bifurcational lines on the plane «coupling - nonlinearity» for the system of coupled cubic maps. $l_{01}$, $l_{02}$, $l_{03}$ are lines of tangent period-doubling bifurcations of orbits $C^0$, $2C^0$ and $4C^0$ respectively, $l_1$, $l_3$ and $l_5$ are lines of transversal period-doubling bifurcations of the same orbits, $l_2$ and $l_4$ are lines of pitch-fork bifurcations of orbits $2C^1$ and $4C^2$. Line $l_{04}$ marks transition to synchronous chaos; line $l_{05}$ - transition to one-band the synchronous chaotic attractor. Symbol smark destroying of chaotic synchronization: (o) - bubbling process, (◇) - riddled basins

From the left side of this boundary and from the right side of the boundary marked by (◇) there is a region of unrobust synchronous chaos. The synchronous regime is observed only in the absence of noise. The transition process to this regime has the form of intermittency. Its duration essentially depends on the chosen initial conditions. Adding very small noise to the system destructs the synchronous regime. The system demonstrates bubbling behaviour. In the region from the left side of the boundary (◇) we observe riddling of the basins of the synchronous chaotic attractor. The basins is riddled with holes that belong to basins of other regular or chaotic attractors.

Comparing mechanisms of multistability formation for different systems (coupled cubic maps, logistic maps [10, 11], Hennon maps [18], Chua's self-oscillators [19], Rossler oscillators [20]) we have concluded that:

1. It is common for period-doubling oscillators with diffusive symmetrical coupling including invertible and non-invertible discrete maps and continuous time oscillators.
2. The same bifurcations of the same periodic cycles form the basis of both appearing of new stable oscillatory regimes and destroying of the regime of in-phase chaotic synchronization.
3. The main mechanism of multistability formation and synchronization loss is based on the cascade of transversal period-doubling bifurcations which take place with orbits of main family forming the skeleton of the synchronous chaotic attractor.
4. Bifurcations of synchronous periodic orbits initiate and then enforce the bubbling process of the chaotic attractor. Bifurcations of unsynchronous orbits appeared from synchronous ones lead to riddled basins of the attractor.

## 3. Synchronization of chaos in weakly non-identical oscillators

Real oscillators are non-identical. Hence, there is a reasonable question: is it possible to apply theory of synchronization based on symmetry properties to real systems. At what conditions idealized pure identical systems will behave similarly to real objects. For investigation of the complete synchronization phenomenon identical interacting systems are usually used as mathematical models. Then obtained in the frameworks of such idealization results are applied to explain behavior of real experimental systems. If the regime of synchronization is stable and the used mathematical model is rough it is observable in real experiments. Intervals of synchronization on the coupling parameter are practically similar for identical and slightly mismatched systems. In this sense the behaviors of the identical and slightly mismatched systems correspond to each other. However, when we investigate more exact effects such as mechanism of the synchronization loss from the point of view of bifurcations of saddle periodic orbits embedded in the chaotic attractor, there are differences in the scenario for identical and weakly non-identical systems. This situation can take place when the symmetry breaking bifurcations take part in the process of synchronization loss. For example this is the pitch-fork bifurcation. From the bifurcation and catastrophe theory it is well-known (see [21, 22]) that the point of this bifurcation is the cusp catastrophe. At slight non-identity between interacting systems the bifurcation is eliminated by the certain ways. Non-identity can qualitatively change behavior of orbits in dependence on a parameter of the system.

We consider this subject on the example of coupled logistic maps with weak non-identity between elements:

$$\begin{aligned} x_{n+1} &= \lambda - x_n^2 + \gamma\,(x_n^2 - y_n^2) \\ y_{n+1} &= \lambda\delta - y_n^2 + \gamma\,(y_n^2 - x_n^2) \end{aligned} \qquad (9)$$

here $\delta$ is a detuning parameter. The considered system has no more subspace of symmetry. Hence, we can not define synchronous oscillations as motions inside the surface $x=y$. In this case we must use «experimental» description of oscillating regimes in asymmetric system. In the frameworks of the present description we call the chaotic regime synchronous, if $|x_n - y_n| < \Delta$, at any moment of time $n$, where $\Delta$ is a suitable given value that is small with respect to the intensity of the chaotic oscillation. In our investigations we use the following value of the parameters: $\lambda=1.56$, $\delta=1$ (identical oscillators) and $0.995 \le \delta < 1$ (non-identical oscillators). These values correspond to regime of one-band chaotic attractors in both oscillators at zero coupling.

Let's consider firstly the identical case ($\delta=1$). In the system (9) the synchronization region has a finite interval. The stability loss of the symmetric one-band chaotic attractor $A^0$ in the transversal direction occurs both at decreasing ($\gamma<0.5$) and at increasing ($\gamma>0.5$) of the coupling coefficient $\gamma$. The synchronization loss is induced by bifurcations of saddle orbits $2^N C^0$ which are embedded in the chaotic attractor and form its skeleton. In the both cases of coupling increasing and decreasing the loss of stability begins with a bifurcation of the saddle point $1C^0$, which induces the bubbling transition in the system.

With $\gamma$ decreasing the saddle point $1C^0$ undergoes the period-doubling bifurcation. In the result it becomes a repeller and the saddle period-2 orbit $2C^1$ appears in its vicinity outside the symmetric subspace. This bifurcation induces the bubbling transition in the system. With further $\gamma$ decreasing the saddle orbits $2^N C^0$ of higher periods undergo the same bifurcations. This enforces the bubbling phenomenon.

Then the saddle orbit $2C^1$ located outside the symmetric subspace undergoes one more bifurcation. It becomes stable and a pair of period-2 saddle symmetric to each other orbits appear in its vicinity (at inverse parameter changing this bifurcation is the subcritical pitch-fork bifurcation). The bifurcation of the orbit $2C^1$ induces the riddling transition in the system. With further decreasing of the coupling the chaotic attractor gradually «loses» its basins and transforms into a chaotic saddle. The described mechanism fully repeats one of the cubic maps. At the coupling increasing we observe the other mechanism: The point $1C^0$ undergoes the pitch-fork bifurcation. In the result it becomes a repeller and in its vicinity a pair of saddle points $C_1$ and $C_2$ symmetric to each other appear. This bifurcation induces the bubbling transition. With further increasing of $\gamma$ other saddle orbits $2^N C^0$ undergo the period-doubling bifurcations similarly as in the case of coupling decreasing. The riddling phenomenon of the $A^0$ basins is a result of the bifurcation of the saddle points $C_1$ and $C_2$. They become stable and in their vicinities saddle orbits of double period appear (at inverse parameter changing this bifurcation is the subcritical period-doubling bifurcation). In the cases of both the coupling decreasing and the coupling increasing bifurcational scenario of the synchronization loss are very similar. The difference is only in the following. At weak coupling $1C^0$ undergoes the period-doubling bifurcation, but at strong coupling - the pitch-fork bifurcation. Other saddle orbits $2^N C^0$ undergo the period-doubling bifurcations in the both cases. At $\gamma$ decreasing the process of riddling basins of $A^0$ begins with the pitch-fork bifurcation of the orbit $2C^1$, but at $\gamma$ increasing - with the period-doubling bifurcations of $C_1$ and $C_2$.

The depended on coupling sequence of bifurcations of periodic orbits which begin the bubbling of the attractor and then the riddling of its basins is built in the Fig. 3, *a*.

Let's now consider the parameter mismatch effect on the bifurcational scenario of the synchronization loss of the system (9) when $\delta \neq 1$. We consider the synchronization loss both at decreasing and increasing of the coefficient of coupling $\gamma$. At small value of $\delta$ we investigate bifurcations of unstable periodic orbits which lead to breaking of regime of nearly identical chaotic oscillations in the coupled systems.

At $\gamma$ decreasing a period-doubling bifurcation of the saddle point $C^0$ induces the transition to the bubbling behavior. After this bifurcation a rebuilding of the phase space structure occurs in the vicinity of the $A^0$. Namely, inside the quasi-symmetric region the saddle $C^0$ transforms to repeller and a saddle orbit $2C^1$ appears outside it. Stable manifolds of the saddle $2C^1$ lean on the repeller $C^0$ and unstable manifolds leave to the quasi-symmetric region. The appearance of such structure changes the character of motions from nearly identical oscillations to the bubbling behavior. At increasing of coupling scenario of the transition to the bubbling behavior is different. With increasing of $\gamma$ firstly we observe a gradual displacement of the saddle $C^0$ in the normal direction. It leaves the quasi-symmetric region. Other saddle orbits $2^N C^0$ practically do not change their locations. Then the saddle-repeller bifurcation takes place in the system. In the vicinity of the quasi-symmetric region a repeller $C_r^0$ and a saddle $C_s^0$ appear. With further increasing of $\gamma$ the fixed points diverge. The repeller $C_r^0$ enters the quasi-symmetric region and the saddle $C_s^0$ moves away from it. As a result there is the same structure of the phase space in the vicinity of the $A^0$ as in the case of identical oscillators, but it is formed on the base of other bifurcations. In the quasi-symmetric region there is the repeller $C_s^0$ on which stable manifolds of the saddles $C^0$ and $C_s^0$ lean. Their unstable manifolds leave to the quasi-symmetric region. This phase space structure also leads to the bubbling behavior. Then, with further coupling increasing both saddles $C^0$ and $C_s^0$ undergoes subcritical period-doubling bifurcations. As a result they become stable and the trajectory from vicinity of the ex-attractor $A^0$ transits to one of them. This process is very similar to the case of identical oscillators except the fact that now we do not observe riddled basins more. A trajectory leaves $A^0$ from any its neighborhood. But the duration of the transition process can be extremely large and essentially depends on the initial values. The scheme of bifurcations that take place in the mismatched system are represented in the Fig. 3, *b*.

Comparing the behaviors of the system (9) at $\delta=0.995$ and at $\delta=1$ we see good qualitative correspondence. The regime of complete synchronization corresponds to nearly identical chaotic oscillations. The bubbling transitions in the symmetric system corresponds appearance of bubbling behavior in the system with mismatch. With further coupling change the same stable orbits appear both in the symmetric and asymmetric systems. In the asymmetric systems there is no riddled basins but one can observe the

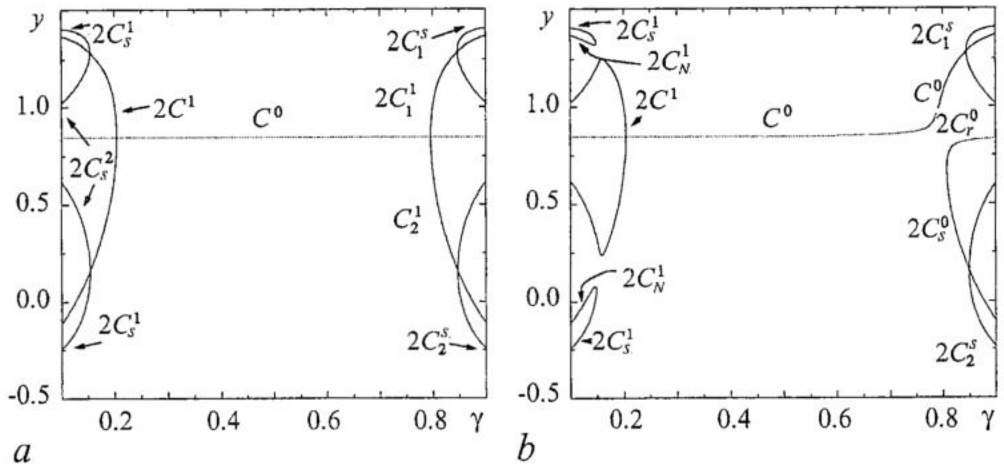

Fig. 3. The scheme of bifurcations on coupling which initiate bubbling and then riddling process in the system of identical (*a*) and weakly non-identical (*b*) logistic maps

sensitive dependence of the transition process time on initial conditions. However, comparing the results quantitatively one need take into account the following: At the coupling decrease the value $|x_n - y_n|$ exceeds the chosen threshold value $\Delta$ almost at the same value of $\gamma$ that corresponds to the bubbling transition in the identical systems. At the coupling increase the corresponding values of $\gamma$ are very different. This difference of changing of left and right boundaries of the synchronization interval is a result of difference of behavior of unstable periodic orbits embedded in the chaotic attractor which takes place at decreasing and increasing of $\gamma$. This difference appears as a result of elimination of the bifurcation conditioned by the symmetry of the system. Thus, if the bubbling transition in the symmetric system is induced by «uneliminated» bifurcation (the period-doubling bifurcation of the saddle $C^0$ at the coupling decreasing) weak asymmetry does not influence on the bifurcational scenario of the transition to the bubbling behavior. If the bubbling transition is determined by the bifurcation conditioned by the symmetry of the system (the pitch-fork bifurcation of the saddle $C^0$ at the couplingin creasing) the weak non-identity of the subsystems eliminates it and the bubbling behavior appears according to another scenario.The determined structure of the phase space in the vicinity of $A^0$ is formated not as a result of the bifurcation of the saddle $C^0$, but after saddle-repeller bifurcation of birth of new unstable points, namely the repeller $C_r^0$ and the saddle $C_s^0$. The completion of the process of the chaos synchronization loss occurs according to different scenario in the symmetric and non-symmetric systems. At the coupling decreasing slight non-identity eliminates the bifurcation of the saddle $2C^1$. Besides it the saddle-node bifurcation of the new stable period-2 orbits $2C_N^1$ and $2C_s^1$ birth take place. Starting from the vicinity of $A^0$ phase trajectories move to this stable orbit. At the coupling increasing the loss of synchronization in the non-symmetric system is completed by the bifurcation of the saddle $C^0$. After the bifurcation the point $C^0$ becomes stable.

## 4. Antiphase complete synchronization of chaos

In this section we consider another case of complete synchronization of chaos: the antiphase synchronization on example of the coupled cubic maps (1, 2, 8). The single cubic map has a symmetry to transformation of the coordinate:

$$I:\ x \leftrightarrow -x.$$

The system of the coupled maps posses the symmetric property of the single map to the transformation:

$$I:\quad x \leftrightarrow -x, \quad y \leftrightarrow -y,$$

and due to the symmetric coupling and identity of the subsystem sit also posses symmetry to transformation:

$$R:\ x \leftrightarrow y.$$

Because $I$ and $R$ commutate with each other, their combination is also a symmetric transformation for the system (1, 2, 8):

$$I \circ R:\ x \leftrightarrow -y,\ y \leftrightarrow -x.$$

Consequence of the symmetry of the system to the transformation $R \circ I$ is a possibility of existence there anti-phase oscillations, which are satisfied condition $x=-y$.

Let's consider the stability properties of the antiphase motions in the coupled maps. In this case we also use normal variables.The equations in the small vicinity of the antisymmetric subspace ($x=-y$) have the form:

$$u_{n+1} = f'(v_n)u_n \tag{10}$$

$$v_{n+1} = (1-2\gamma) f(v_n). \tag{11}$$

In this case the dynamics inside the antisymmetric subspace is described by the equation (11). Contrary to the case of in-phase synchronization it depends on the coupling coefficient $\gamma$. Stability of an antisymmetric solution to the tangent perturbations is determined by the tangent Lyapunov exponent:

$$\Lambda_\tau^a = \lim_{N\to\infty} (1/N)\, \Sigma_{n=1}^{N} \ln|(1-2\gamma) f'(v_n)|. \tag{12}$$

The equation (10) determines dynamics in the normal direction to the antisymmetric subspace in its vicinity. It has no obvious dependence on the coupling coefficient $\gamma$ but it depend on it through the variable $v_n$, which is determined by the eq. (11). The normal Lyapunov exponent which determines transversal stability of the antiphase oscillations has the form:

$$\Lambda_\perp^a = \lim_{N\to\infty}(1/N)\, \Sigma_{n=1}^{N} \ln|f'(v_n)|. \tag{13}$$

It is seen that the normal and tangent Lyapunov exponents are connected with each other:

$$\Lambda_\tau^a = \Lambda_\perp^a + \ln|1-2\gamma|. \tag{14}$$

This relation is the opposite to the in-phase case. Here $\Lambda_\tau^a \le \Lambda_\perp^a$ and hence, the every antiphase oscillating regime firstly loses its stability in the normal to the antisymmetric subspace direction and secondly in the tangent direction. Because of relation (14) the antiphase self-synchronization of chaos is impossible in the considered systems. For a chaotic attractor $\Lambda_\tau^a>0$ and therefore the normal Lyapunov exponent must be positive. Hence chaotic antiphase oscillations can not be transversally stable.

Oscillating regimes inside the antisymmetric subspace are formed on the base of the fixed points $C_{10}$ and $C_{20}$ which appeared from the trivial fixed point $C_{00} = (0; 0)$. Limit sets formed on the base of these points are identical up to symmetry transformation. Therefore we consider only one family of the regimes (for example, near the point $C_{10}$).

The saddle fixed point $C_{10}$ appears from the saddle fixed point $C_{00}$ in the result of the symmetry breaking bifurcation. It is unstable to the perturbations directed transversally to the antisymmetric subspace. On the line $l_{tp}^1$ (Fig. 4) it becomes stable

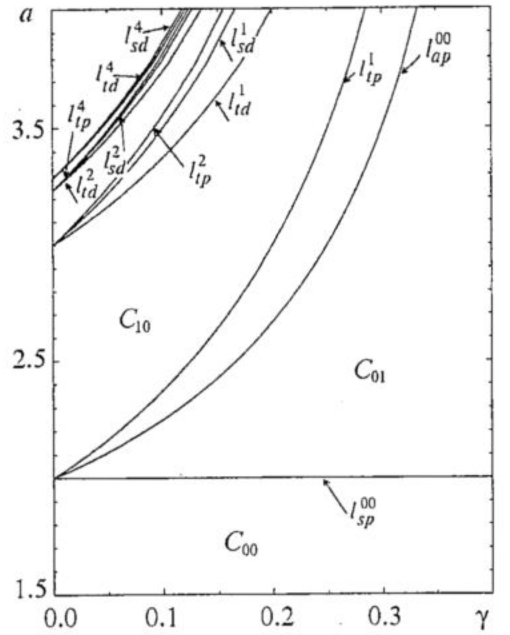

Fig. 4. Bifurcational lines of antisymmetric periodic orbits on the pane of the parameters $\gamma$ - $a$

through pitchfork bifurcation. With changing of the parameters $a$ and $\gamma$ on the base of this fixed point there is a cascade of period doubling bifurcations which leads to formation of a chaotic set inside the antisymmetric subspace. The every orbit undergoes the period-doubling bifurcation twice in the cascade. Firstly, as stable orbit on the first multiplier, secondly as saddle orbit on the second multiplier. As a result of the first period doubling the orbit loses its stability in the normal to the subspace direction. In its vicinity, outside the antisymmetric subspace a stable orbit of double period appears. As a result of the second period doubling the saddle orbit loses stability in the tangent direction and becomes repeller. In its vicinity, inside the antisymmetric subspace a saddle periodic orbit of double period appears. In the Fig. 4 the lines of the first period doubling bifurcations are denoted: $l_{td}^{\ 1}$ (for the orbit of the period-one), $l_{td}^{\ 2}$ (for the orbit of the period-two), $l_{td}^{\ 4}$ (for the orbit of the period-four), and the lines of the second period doubling bifurcations as $l_{tsd}^{\ 1}$, $l_{tsd}^{\ 2}$, $l_{tsd}^{\ 4}$ respectively. Then, with further parameters changing, the appeared saddle antisymmetric orbits become stable through the subcritical pitchfork bifurcations. In the Fig. 4 these lines are denoted as $l_{tp}^{\ 2}$ and $l_{tp}^{\ 4}$. Therefore, on the parameters plane there is a stable antiphase period-one orbit in the region between the lines $l_{tp}^{\ 1}$ and $l_{td}^{\ 1}$, a stable antiphase period-two orbit between the lines $l_{tp}^{\ 2}$ and $l_{td}^{\ 2}$ and a stable antiphase period-four orbit between the lines $l_{tp}^{\ 4}$ and $l_{td}^{\ 4}$. Bifurcations of orbits of higher periods take place by similar way. Hence, on the plane of the parameters there are bounds of stability for regular antiphase regimes, between which bounds of transversal instability exist.

The considered bifurcational scenarium is very similar to the one for in-phase orbits. However, in the case of in-phase synchronization the bifurcations inside the symmetric subspace precede the bifurcations in the normal direction. Therefore, in the case of antiphase synchronization, contrary to the in-phase synchronization:

- regions of transversal stability are divided by the regions of transversal instability;
- in the symmetrical subspace the transversally stable chaotic attractor is not formed.

Antiphase synchronous system in the diffusively coupled period-doubling maps is impossible. However, for stabilization of antiphase chaotic oscillations one can apply feedback controlling technics. We want to find the controlling function in the form which does not change the form of antiphase oscillations, but changes their stability. Hence, the controlling function $\Psi(x, y)$ must be equal to zero inside the antisymmetric subspace, namely: $\Psi(x, -x) = 0$. In our work we suggest the function in the form: $\Psi(x, y) = r[f(x) + f(y)]$. The controlling term is added to the right side of the first equation of the system (1, 2):

$$x_{n+1} = f(x_n) + \gamma(f(y_n) - f(x_n)) + r(f(x_n) + f(y_n)) \tag{15}$$

$$y_{n+1} = f(y_n) + \gamma(f(x_n) - f(y_n)). \tag{16}$$

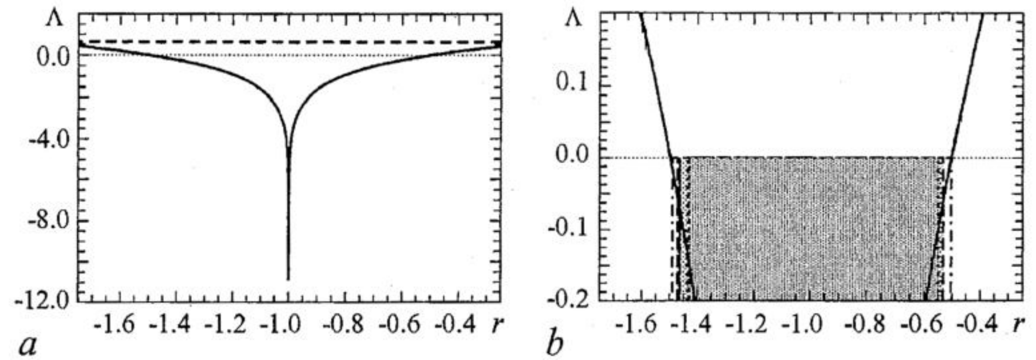

Fig. 5. Dependence of the normal Lyapunov exponent for antiphase chaotic attractor on the controlling parameter *r* (*a*) at $a$=3.8, $\gamma$ =0.04. Dashed line denotes the values of the tangent Lyapunov exponent. In the (*b*) this dependence is presented in larger scale with regions of the antiphase controlled synchronization

The term $r(f(x_n)+f(y_n))$ can be considered as another coupling loop with coupling coefficient *r*.

The equations in the normal variables for the system with the control have the form (near the antisymmetric subspace):

$$u_{n+1} = (1+r)\,f'(v_n)u_n \tag{17}$$

$$v_{n+1} = (1\text{-}2\gamma)\,f(v_n) + rf'\,(v_n)u_n\,. \tag{18}$$

In the case of antiphase oscillations $u_n$ =0 and equation (18) transforms to the (11). The normal Lyapunov exponent for the system with the control is:

$$\Lambda_{\perp\ contr}^{\ a} = \lim_{N\to\infty}(1/N)\,\Sigma_{n=1}^{N}\ \text{ln}|\,(1+r)f'(v_n)| \tag{19}$$

and hence:

$$\Lambda_{\perp\ contr}^{\ a} = \Lambda_{\perp} + \text{ln}|1+r|. \tag{20}$$

We chose parameter *r* near value -1 to make the normal Lyapunov exponent sufficiently small and hence, the synchronous chaotic regime transversally stable. The Fig. 5, *a* represents the dependences of the normal Lyapunov exponent on the controlling parameter *r*. Values of the other parameters corresponds to the regime of the developed chaotic attractor: $a$=3.8, $\gamma$ =0.04. To transit to regime of antiphase synchronization we use the following procedure: We chose initial conditions from the basins of the chaotic attractor. In the every moment of time we appreciate the distance between the phase point and the antisymmetric subspace: $\rho = |x_n + y_n|$. The distance was compared with the chosen value $\varepsilon$. If $\rho > \varepsilon$, the phase point is far from the subspace and the controlling influence is switched off. The trajectory evolves on the unsynchronous chaotic attractor. When phase point appears near the antisymmetric subspace ($\rho \le \delta$), the controlling influence is switched on. If the controlling parameter *r* locates in the interval where $\Lambda_{\perp contr} < 0$ the chaotic set inside the antisymmetric subspace becomes stable to transversal perturbation and the trajectory is attracted to the subspace. After this the controlling influence tends to zero. In our numerical experiments we chose $\varepsilon$ =0.01. In the Fig. 6 phase portraits of the oscillations without control (*a*) , with control (*c*, *e*) and correspondent time-series of $x_n+y_n$ (*b*, *d*, *f*) are represented. The original chaotic attractor (Fig. 6, *a*) corresponds to the regime of unsynchronous chaos. The phase trajectory draws the square-like region. With applying small controlling influence the diagonal line $x$=-$y$ appears on the region (Fig. 6, *c*). The time-series has interval of synchronous behavior (Fig. 6, *d*). With further changing $r$ the interval of synchronous behavior grows and as a result the system transits to fully synchronous oscillations (Fig. 6, *e*, *f*). In this case the resulting chaotic attractor is a one-band attractor located in the antisymmetric subspace. In the Fig. 5, *b* the intervals of the parameter $r$ sufficient for complete synchronization at different intensities of noise are presented. The more dark color corresponds to larger noise. Without noise the interval of the synchronization coincides with the interval of $r$ where the normal Lyapunov exponent is negative. With noise the controlled synchronization region becomes more narrow (Fig 5, *b*).

As we have demonstrated before the process of the in-phase synchronization loss is accompanied by the bubbling phenomenon and riddled basins. It is reasonable question: Do these phenomena exist in the case of antiphase synchronization loss? To answer this question we consider the evolution of the chaotic attractor with changing of the coefficient $r$. In the numerical experiments we chose initial values near the

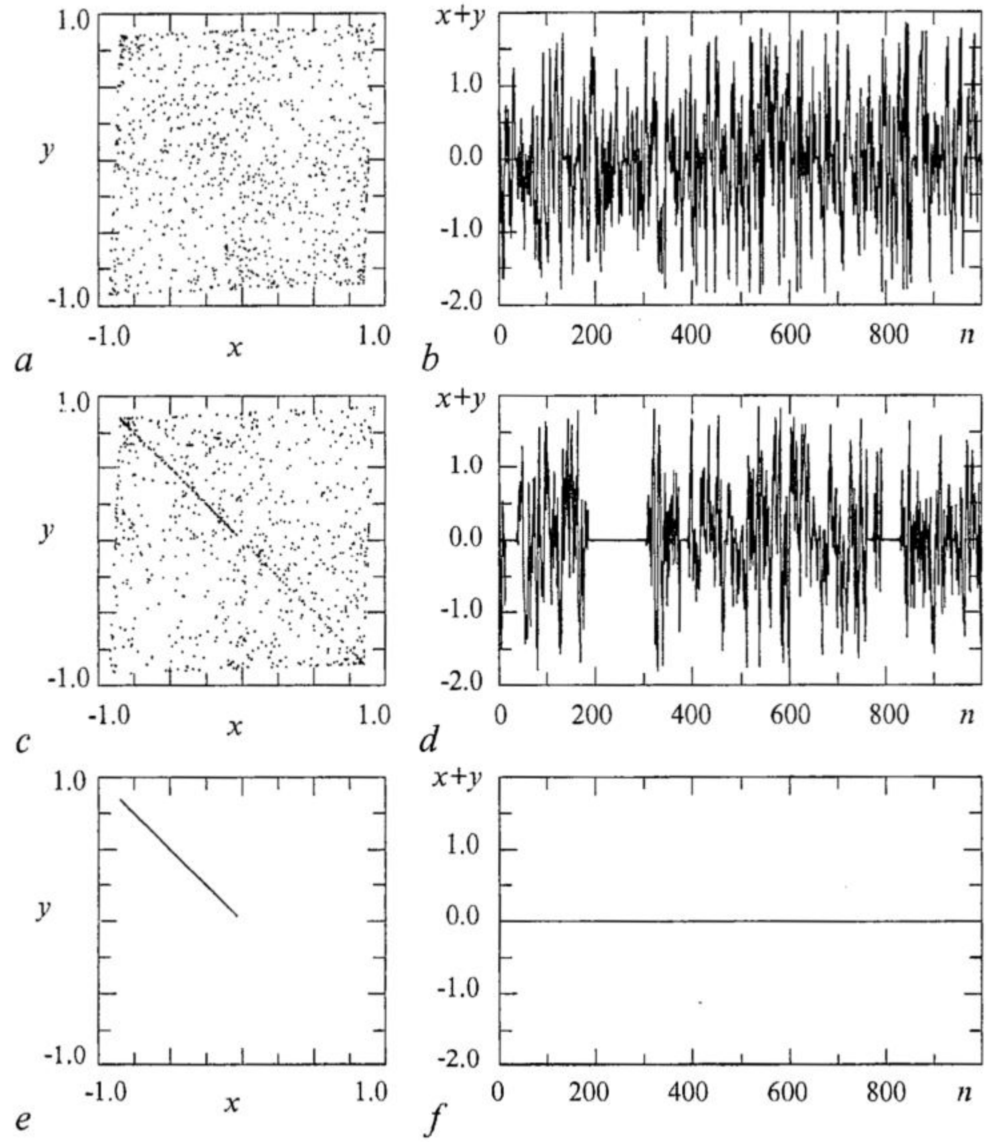

Fig. 6. The phase portraits and time-series of the oscillating regimes without control (*a*, *b*), with partial control (*c*, *d*) and in the regime of the complete antiphase synchronization (*e*, *f*)

antisymmetric subspace. The controlling influence is switched on during the whole time of observation (not depending on nearness $\rho$ of the phase point to the subspace). At $-1.46<r<-0.525$ the chaotic attractor inside the antisymmetric subspace is stable to transversal perturbations. The synchronous regime is robust. Adding noise of small intensity (~ 0.00001) doesn't lead to visible changing in the systems behavior. With increasing of the controlling parameter at $r>-0.525$ a bubbling attractor is observed in the system. The chaotic attractor remains stable to transversal perturbations but the time of transient process becomes extremely large (hundreds of thousands iterations) and it sensibly depends on the initial values. Adding noise of small intensity leads to essential rebuilding of the phase portrait of the oscillations. The attractor gets finite transversal size. Phase point begins to visit neighborhoods of the both fixed points $C_{10}$ and $C_{20}$. The corresponding time-series of $x_n + y_n$ is the on-off intermittency process [12]. The Fig. 7 demonstrates phase portraits of the attractor without noise (*a*) and with small noise (*c*). In

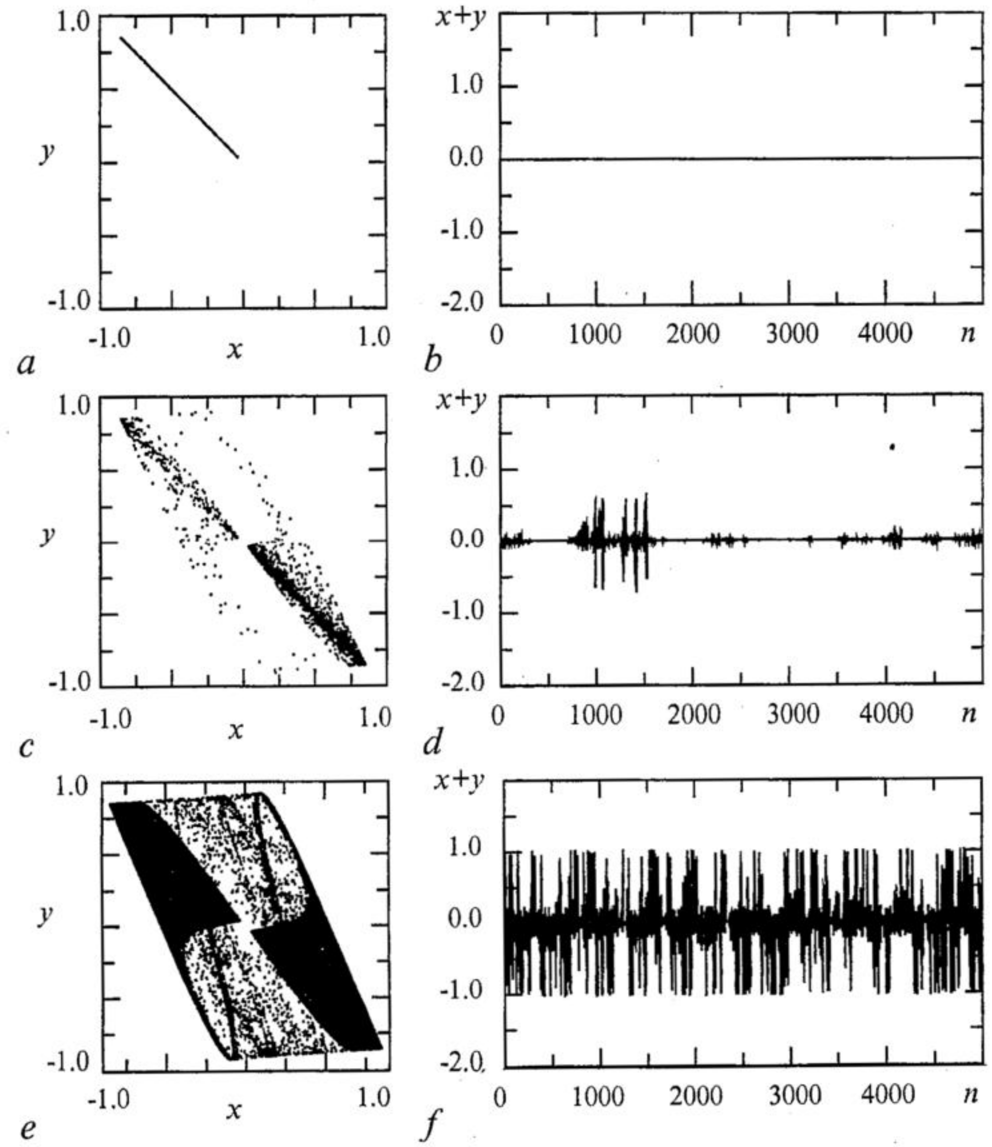

Fig. 7. The phase portraits and time-series of antiphase oscillations without noise (*a*, *b*) and with noise (*c*, *d*). In (*e*, *f*) there is chaotic oscillations resulted from the blowout bifurcation

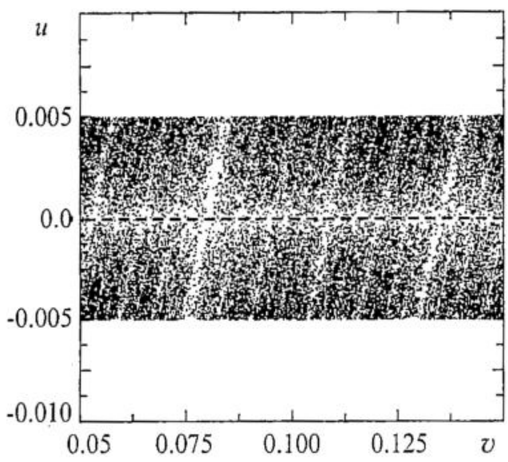

Fig. 8. A part of the basins of the chaotic attractor inside the antisymmetric subspace (white color) at $r$ =-1.485. The black color denotes regions relating to the basins of the attractor in the infinite

the ($b$, $d$) there are corresponding time-series. With small noise phase point moves along the antisymmetric subspace for a long time. Then, it is short burst apart from the subspace, after which the phase point return to the vicinity of the antisymmetric subspace. The averaged frequency of the bursts increase with increasing of the parameter $r$. Finally, at $r$ =-0.406 the blowout bifurcation [5] takes place when the chaotic attractor is not already stable in the normal direction and it transforms to the chaotic saddle. The synchronous oscillations are not observed further in the system both with noise and without it. The phase portrait of oscillations looks like the bubbling attractor in presence of noise (Fig. 7, $e$).

With decreasing $r$ from the synchronization region, at $r$ <-1.46 we observed the transition from the robust stable synchronous regime to the bubbling behavior. Then, at $r$ <-1.472 the basins of the synchronous attractor is riddled by holes of the basins of the attractor in the infinity.

In the Fig. 8 we present a fragment of the basins of the chaotic attractor in the antisymmetric subspace (white color) with holes from the basins of the infinity attractor (black color) wedged in it. This basins is represented in the normal coordinates $u$ and $v$, the antisymmetric subspace is marked by the dashed line. The results were obtained for the parameters values: $a$ =3.8, $\gamma$ =0.04, $r$=-1.485.

Comparing in-phase and anti-phase synchronization of chaos we demonstrate that bifurcational mechanism inside the antisymmetric subspace is similar to the one in the symmetric subspace except the order of bifurcations taking place tangently and normally to the subspace. The anti-phase self-synchronization in similar systems is possible only for regular regimes. The chaotic synchronization can be achieved with applying methods of chaos control. We demonstrate that the process of loss of this type of synchronization can be similar to the case of in-phase synchronization. It demonstrates bubbling behavior, riddled basins and blowout bifurcation.

## Conclusion

We consider in- and anti-phase complete synchronization of chaos in dissipativelly coupled periodic-doubling oscillators. For in-phase synchronization cases of purely identical and slightly mismatched subsystems are investigated.

We demonstrate that the processes of loss of in-phase and anti-phase synchronization are very similar. The both ones go through stages of bubbling attractor and riddled basins. Structures of bifurcations inside symmetric and antisymmetric subspaces are similar to each other except the order of their bifurcations. In the both cases every periodic orbit undergoes two period-doubling bifurcations: in tangent and normal direction to the subspace. In the case of symmetric subspace the tangent bifurcations proceed the transversal ones. In the case of antisymmetric subspace the transversal bifurcations proceed the tangent ones. Two period-doubling cascades lead to formation of multistability. The bifurcations inside the symmetric subspace form the synchronous chaotic attractor. The similar bifurcations in antisymmetric subspace form synchronous chaotic saddle which can be stabilized in normal direction by using control of chaos technic. In the both cases the transversal period-doubling bifurcations lead to (*a*) loss of transversal stability and (*b*) forming new periodic regimes outside the corresponding subspace.

Comparison of identical and slightly mismatched systems demonstrates that in the both cases the loss of in-phase synchronization goes through similar steps with small differences: bubbling attractor and riddled basins for identical systems and bubbling behavior and essential dependence of the duration of transition process to another attractor for mismatched ones. In the both cases we observe similar structure of the phase space near the symmetric subspace. However, this structure can be following of different bifurcational mechanisms: pitch-fork bifurcation in the case of identical oscillators and saddle-repeller bifurcation in the mismatched ones.

### Acknowledgments

The authors thanks to the Fond of Civil Research Development (Grant REC 006) and Russian Fond of Basic Researching (Grant 00-02-17512) for financial support.

### Reference

1. *Fujisaka H., Yamada T.* Stability theory of synchronized motion in coupled-oscillator systems // Progress of Theoretical Physics. 1983. Vol. 69. P. 32.

2. *Pikovsky A.S., Grassberger P.* Symmetry breaking bifurcation for coupled chaotic attractors // J. Phys. A: Math.. 1991. Vol. 24. P. 4587.

3. *Cao L.-Y., Lai Y.-C.* Antiphase synchronism in chaotic systems // Phys. Rev. E. 1998. Vol. 58. P. 382.

4. *Pecora L.M., Caroll T.L.* Synchronization in chaotic systems // Phys. Rev. Lett. 1990. Vol. 64. P. 821.

5. *Ashvin P., Buescu J., Stewart I.* Bubbling of attractors and synchronization of chaotic oscillators // Physics Letters A. 1994. № 193. P. 126.

6. *Ashvin P., Buescu J., Stewart I.* From attractors to chaotic saddle: a tale of transverse instability // Nonlinearity. 1996. Vol. 9. P. 703.

7. *Lai Y.C., Grebogi C., Yorke J.A.. Venkataramani S.C..* Riddling bifurcation in chaotic dynamical systems // Phys. Rev. Lett. 1996. Vol. 77, № 1. P. 55.

8. *Pikovsky A., Osipov G., Rosenblum M., Zaks M., Kurths J.* Attractor-repeller collision and eyelet intermittency at the transition to phase synchronization // Phys. Rev. Lett. Vol. 79, 1997.

9. *Sushchik M.M., Rulkov N.F., Abarbanel H.D.I.* Robustness and stability of synchronized chaos: an illustrative model // IEEE Transactions on circuits and systems. 1997. Vol. 44, № 10. P. 866.

10. *Astakhov V., Shabunin A., Kapitaniak T., Anishchenko V* . Loss of chaos synchronization through the sequence of bifurcations of saddle periodic orbits // Phys.Rev. Lett. 1997. Vol. 79, № 6. P. 1014.

11. *Astakhov V., Hasler M., Kapitaniak T., Shabunin A., AnishchenkoV.* Effect of parameter mismatch on the mechanism of chaos synchronization loss in coupled systems // Phys. Rev. E. 1998. Vol. 58, № 5. P. 5620.

12. *Platt N., Spiegel E.A., Tresser C.* On-off intermittency:a mechanism for bursting // Phys. Rev. Lett.. 1993. Vol.. 70. P. 279.

13. *Fujisaka H., Yamada T.* A new intermittency in coupled dynamical systems // Progr. Theor.Phys. 1985. Vol. 74, № 4. P. 918.

14. *Kuznetzov S.P.* Universality and similarity in behavior of coupled Feigenbaum systems // Radiophizika. 1985. Vol. 28, № 8. P. 991.

15. *Maistrenko Y.L., Maistrenko V.L., Popovich A.* Transverse instability and riddled basins in a system of two coupled logistic maps // Phys. rev. E. 1998. Vol. 57, № 3. P. 2713.

16. *Maistrenko Y.L., Maistrenko V.L., Popovich A., Mosekilde E.* Desynchronization of chaos in coupled logistic maps // Phys. Rev. E. 1999. Vol. 60, № 3. P. 2817.

17. *Astakhov V.V. , Bezruchko B.P., Ponomarenko V.I., Seleznev E.P.* // Izv. Vuzov. Radiofizika. 1988. 31 (5), 627.

18. *Astakhov V., Shabunin A., Uhm W., Kim S.* Multistability formation and synchronization loss in coupled Hennon maps: Two sides of the single bifurcational mechanism // Phys.Rev. E. 2001. Vol. 63. 056212.

19. *Anishchenko V.S., Astakhov V.V., Nikolaev V.V., Shabunin A.V.* Chaotic synchronization in a network of symmetrically coupled oscillators // Journal of Communications Technology and Electronics. 2000. Vol. 45, № 2. P. 179.

20. *Astakhov V.V., Balanov A.G., Sosnovtzeva O.V., Vadivasova T.E.* Loss of Synchronization in coupled Rossler systems // Applied Nonlinear Dynamics. 1999. Vol. 7, № 5. P. 26.

21. *Arnold V.I.* Theory of ordinary differential equations. Part II. Moscow: Nauka, 1978 (in Russian).

22. *Iooss G., Joseph D.D.* Elementary Stability and Bifurcation Theory // Springer Verlag, New York, Heidelberg, Berlin 1980.

*Saratov State University*

*Received 3.06.2002*

УДК 537.86

# Мультистабильность, синфазная и противофазная синхронизация в системах с бифуркациями удвоения периода

*В.В. Астахов, А.В. Шабунин, П.А. Стальмахов*

В статье рассматриваются механизмы образования мультистабильности и потери полной синхронизации хаоса в диффузионно связанных отображениях с бифуркациями удвоения периода. Рассматриваются случаи синфазной и противофазной синхронизации. Для синфазной синхронизации исследуется влияние неидентичности между осцилляторами на механизм потери синхронизации хаоса.

*Astakhov Vladimir Vladimirovich* graduated from Saratov State University in 1980. He is a Doctor of Science in Physics and Mathematics since 1999. He works as a professor of Radiophysics and Nonlinear Dynamics department on the Physical faculty of the Saratov State University. His scientific interests are: nonlinear dynamics, theory of oscillations, chaotic behavior, synchronization and chaos control. He is an author of more than 60 scientific publications.

*Shabunin Alexey Vladimirovich* graduated from Saratov State University in 1990. He is an associate professor of Radiophysics and Nonlinear Dynamics Department of the Saratov State University, Candidate of Science in Physics and Mathematics since 1998. His scientific interests include nonlinear dynamics, theory of oscillations, chaotic behavior, synchronization and chaos control. He is an author of more than 30 scientific publications.

*Stalmakhov Peter Andreevich* graduated from Saratov State University in 2001. He is a PhD student of Radiophysics and Nonlinear Dynamics Department of the Saratov State University. His scientific interests include chaotic behavior, synchronization and chaos control. Stalmakhov is an author of 2 scientific publications.

Deterministic chaos

Izv. VUZ «AND», vol.10, № 3, 2002

# MULTI-PARAMETER PICTURE OF TRANSITION TO CHAOS

*A.P. Kuznetsov, L.V. Turukina, A.V. Savin, I.R. Sataev,*
*J.V. Sedova, S.V. Milovanov*

In this paper we outline several research directions linked with multi-parameter analysis of complex dynamics of nonlinear systems. In particular, we discuss examples of realistic models of multi-parameter systems, critical phenomena at the chaos threshold, correspondence of features of differential equations and maps etc.

## Introduction

The commonly recognized conception of a scenario of transition to chaos suggests that this term designates some sequence of bifurcations observing under variation of one control parameter. For example, in a driven nonlinear oscillator increase of the amplitude of the external force is accompanied by a period-doubling cascade with subsequent transition to chaos. However, in a system with two or more control parameters we should imagine a picture on parameter plane or in parameter space. (For example, in the case of the mentioned oscillator it is natural to use a plane of amplitude versus frequency of the external force.) A study of arrangement of the parameter space implies revealing of typical bifurcations, regularities of their coexistence and subordination, characteristic forms of phase portraits at representative points of the parameter space, plotting bifurcation trees associated with definite paths in the parameter space, consideration of plots of Lyapunov exponents etc.

Moreover, it is natural to develop and generalize the concept of scenario of transition to chaos in application to multi-parameter systems. Let us imagine some three-parameter nonlinear system demonstrating transition to chaos via the period-doubling cascade. It is clear that in general the period-doubling bifurcations in such system will occur at some curved surfaces, and they will accumulate to the limit, *the Feigenbaum critical surface*, which corresponds to the border of chaos. It may be expected that in some cases this surface may have an edge, some *critical curve*. In a neighborhood of this curve some special regularities of coexistence of bifurcations and scaling laws should be observed distinct from those of Feigenbaum. In turn, on the critical curve some critical points may occur, etc. The corresponding classification and discussion may be found in reviews [1-5].

Multi-parameter approach to a study of nonlinear systems is proven to be productive and has induced a number of research directions, which will be discussed in the present article.

## 1. Two-parameter analysis of physical systems

First of all, we must outline the search for physical systems with complex dynamics, for which the multi-parameter analysis is of importance. Very often researches working in nonlinear dynamics tend to use rather formal models like logistic map, Henon map, Arnold's cat map, etc. An alternative is constructing maps describing dynamics of physical systems from «first principles», that is, from their fundamental evolution equations (Newton equations, Maxwell equations, etc). For physically motivated maps dynamical variables and parameters have usually a clear sense, and this circumstance increases its value and significance. For example, to account noise in such models we turn to physical argumentation and mechanisms, while in abstract models the fluctuations are introduced rather in formal and artificial manner.

***Periodically kicked nonlinear oscillator.*** As a first example let us consider the Duffing oscillator excited by a periodic sequence of δ-pulses

$$\ddot{x} + \gamma\dot{x} + \omega_0^2 x + \beta x^3 = \Sigma\, C\delta(t - nT). \qquad (1)$$

Here $x$ is a coordinate of the oscillator, $\gamma$ - is coefficient of decay, $\omega_0$ is frequency of free linear oscillations, $T$ is a period of pulses, $C$ is their amplitude. For intervals between the kicks one can derive an approximate analytical solution using the method of slow amplitudes. It yields a 2D map:

$$z_{n+1} = A + Bz_n \exp(i\,(|z_n|^2 + \psi)), \qquad (2)$$

where $z_n$ is complex amplitude just before the $n$-th kick, and dimensionless parameters $A$, $B$ and $\psi$ are expressed via parameters of the original oscillator as follows:

$$A = (C/\omega_0)[(3\beta T/8\omega_0)(1-e^{-\gamma T})/\gamma T]^{1/2}, \quad B = e^{-\gamma T/2}, \quad \psi = \omega_0 T. \qquad (3)$$

***System of Ikeda.*** It appears that the map (2) also describes dynamics of the optical system considered by Ikeda et al. It is a circular optical resonator containing medium with phase nonlinearity and excited by laser beam [6]. In this case parameter $A$ represents a dimensionless intensity of the incident light, and $B$ characterizes dissipation in the resonator. Fig. 1, *a* shows a chart of dynamical regimes in the parameter plane $(A, B)$ for $\Psi=0$.

The gray tones designate domains of definite period of motion generated by the map. Fig. 1, *b* is a magnified fragment of the chart, it presents a very wide-spread pattern of parameter-space structure called the «crossroad area».

In Fig. 1, *a* together with the chart we present several phase portraits of the Ikeda map. There is some domain in the parameter plane where the phase portrait tends to turn to a circle; it indicates that the description in terms of 1D map becomes appropriate. The explicit form of this map may be derived from (2) [7, 8] and reads

$$x_{n+1} = \lambda\cos x_n + \varphi. \qquad (4)$$

Here $x=\lambda\xi+\varphi$, $\mathrm{Re}\tilde{z}_n=\xi_n$. New parameters $\lambda$ and $\varphi$ are expressed via parameters of the original map as

$$\lambda = 2A^2B, \quad \varphi = A^2 + \psi. \qquad (5)$$

We see that the kicked nonlinear oscillator allows description in terms of differential equations and in terms of analytically derived (approximate) 2D and 1D mappings.

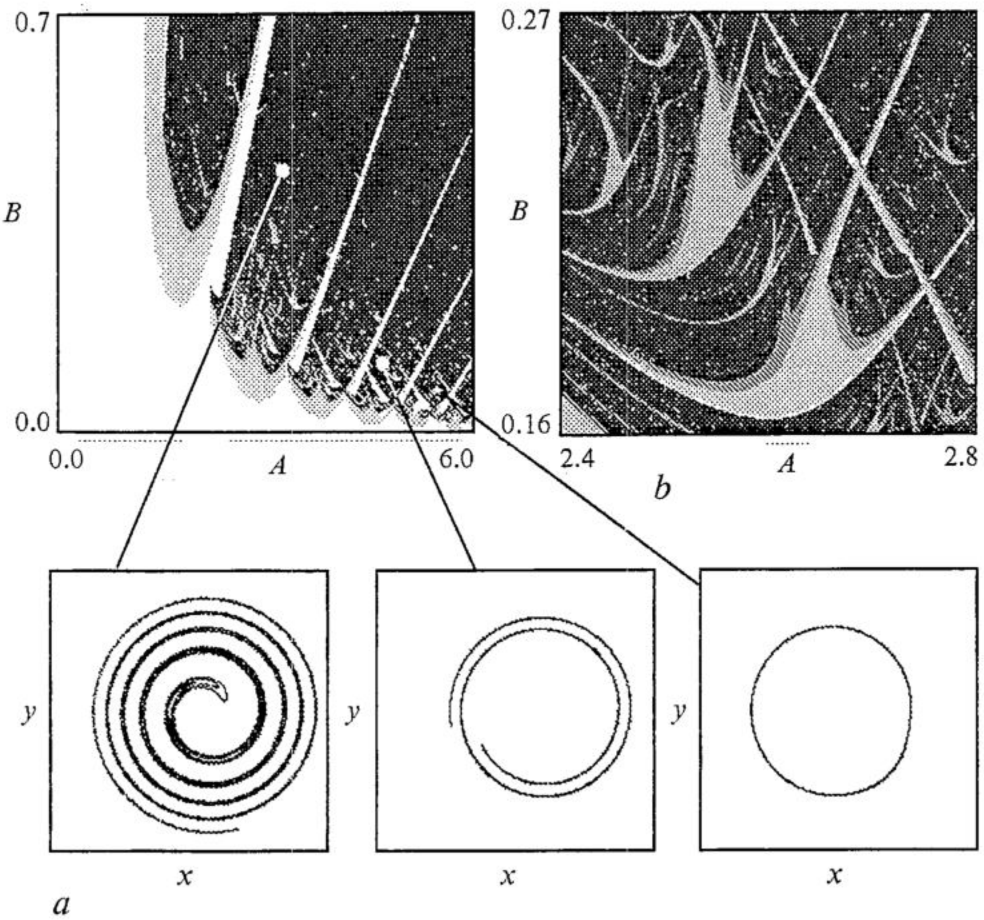

Fig. 1. *a* - Parameter plane for the Ikeda map (2) and typical phase portraits in select points; *b* - magnified fragment of parameter plane

***Gravitational machine of Zaslavsky (bouncing ball on a vibration table).*** Originally, the idea of gravitational machine was formulated in context of astrophysics and celestial mechanics and consists in a use of alternating gravitational field (e.g. of a double star) for acceleration of a spaceship or a celestial body [9]. The model suggested by Zaslavsky is a ball of mass *m* bouncing up and falling down under the gravitational force on a horizontal plate, oscillating in the vertical direction. A traditional simplification used in a course of derivation of the basic dynamical equation (map) consists in neglecting displacement of coordinate of the plate in the moment of impact. It seems a very natural assumption, as the amplitude is small enough. The resulting map is rather simple and looks like [9]

$$\begin{aligned} v_{n+1} &= (1 - \varepsilon)v_n + k\sin\phi_n, \\ \phi_{n+1} &= \phi_n + v_{n+1}, \quad (\mathrm{mod} 2\pi). \end{aligned} \tag{6}$$

Here dimensionless variables and parameters are introduced: $v_{n+1}$ is a velocity of the ball just after an impact, $\varphi_n=\omega t_n$ is dimensionless time of the impact, $k=2(2-\varepsilon)V_0\omega/g$ is amplitude of the oscillating velocity of the plate, $\varepsilon$ is a coefficient characterizing a fraction of energy loss in an impact of the ball with nonmoving plate. In particular, this approximate mapping was discussed in books of Moon [10], Lichtenberg and Liberman [11], Guckenheimer and Holms [12] as one of classic examples of chaotic systems.

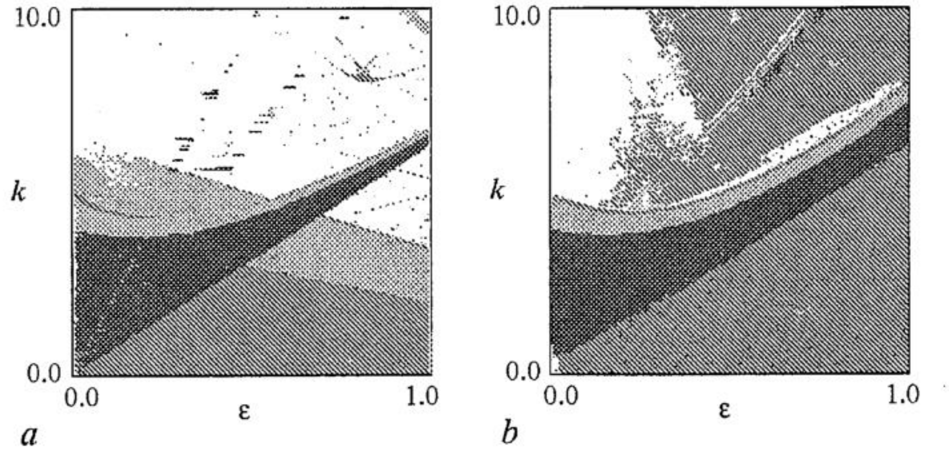

Fig. 2 Parameter planes: *a* - approximate (6) and *b* - exact (7) maps of bouncing ball

Alternatively, one can undertake more accurate analysis and obtain a map without the restriction in respect to the amplitude of the plate vibrations [13]. It is an implicit relation

$$\begin{aligned} &v_{n+1} = -(1-\varepsilon)v_n - k\sin\phi_n + 2(\phi_{n+1} - \phi_n), \\ &[(1-\varepsilon)v_n + k\sin\phi_n](\phi_{n+1} - \phi_n) - (\phi_{n+1} - \phi_n)^2 = [k/(2-\varepsilon)](\cos\phi_n - \cos\phi_{n+1}). \end{aligned} \tag{7}$$

The charts of dynamical regimes both for the approximate and accurate models, the maps (6) and (7), are shown in Fig.2.

***Relativistic electron beam interacting with a backward electromagnetic wave.*** As known, in the system of electron beam interacting with a backward wave a generation of the electromagnetic oscillations is possible. A very rough approach to description of the dynamics is based on assumption that the electromagnetic field effects the electron beam only in a narrow spatial domain near the input edge of the device, and the beam radiates energy into the backward wave in a narrow domain near the opposite end. In other words, we assume that the interaction takes place only in two gaps (δ-functions). In this case the dynamical equations can be reduced to a 1D map. In the relativistic case it was obtained and studied in Ref. [14]:

$$\begin{aligned} &A_{n+1} = F(A_n), \\ &F(A) = (L/2\pi)\,|\int_0^{2\pi} \exp(-i\,(\alpha + (L/\nu)[1+(L\nu A/4)\cos\alpha]^{-2}(-L/\nu))d\alpha|. \end{aligned} \tag{8}$$

Here $A_n$ is a dimensionless amplitude of the wave at the input of the electron beam, $L$ is a dimensionless length of the interaction space (proportional to the cube of the beam current), $\nu$ is the relativistic parameter. The chart of dynamical regimes on the parameter plane $L$, $\nu$ exhibits an obvious resemblance with the chart for the kicked oscillator and for the Ikeda model (Fig. 3, upper panel). The bottom panel in Fig. 3 shows magnified fragment of the parameter plane and demonstrates formation of crossroad area type on a base of the period-3 cycle. Also, several graphs of the map at some representative points are shown.

***Free-electron laser in regime of mode selection.*** Using approximation analogous to that discussed above, it is possible to derive a map for description of interaction of two modes (a basic mode and a parasitic one) in a free-electron laser [15]

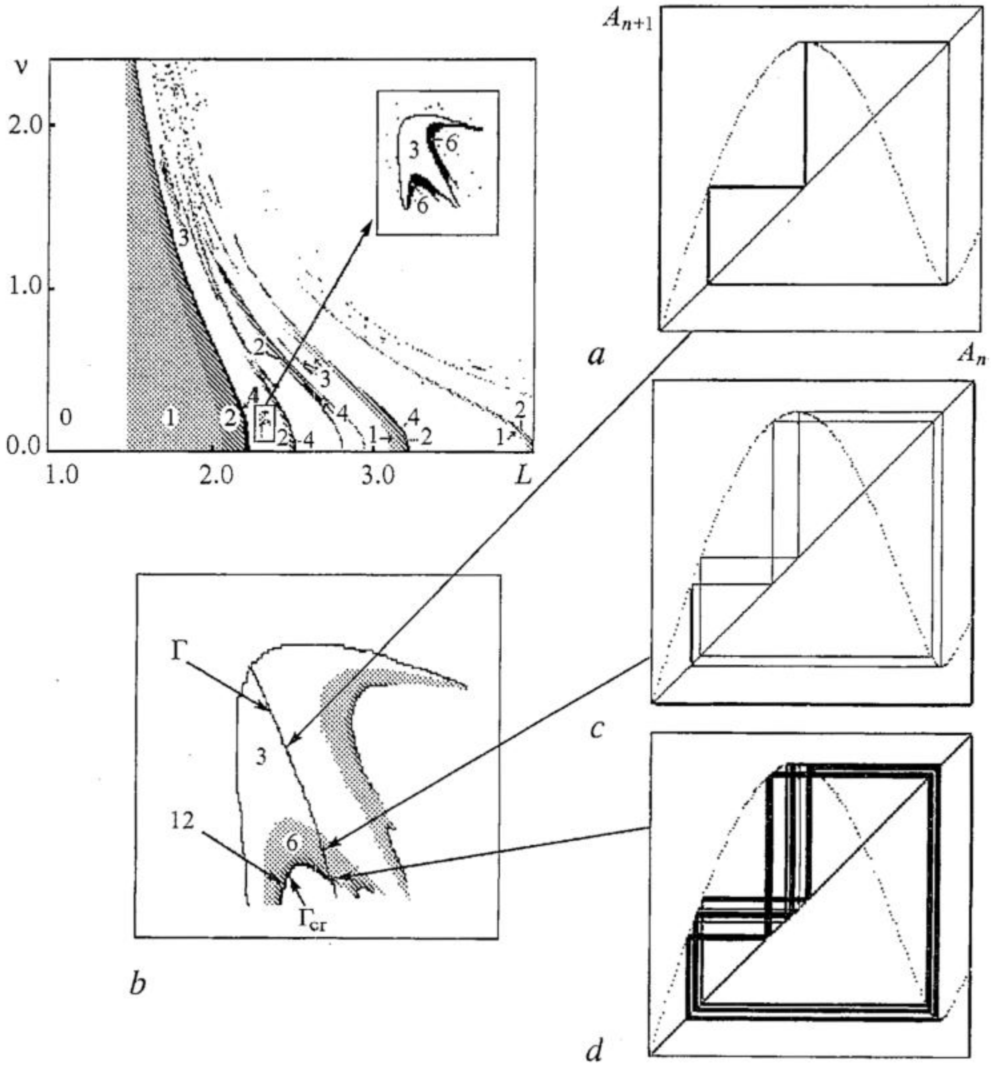

Fig. 3. At the top of figure - parameter plane of the map (8) for the relativistic electron beam interacting with a backward electromagnetic wave. At the foot of figure (on the left) (b) - its fragment. Line Γ, which corresponds to mapping the maximum onto minimum, and Feigenbaum critical line $\Gamma_{cr}$ are shown. Figures *a*, *c*, *d* - iteration diagrams in typical points. Figure *d* corresponds to tricritical point. Lines Γ и $\Gamma_{cr}$ are converged, and Feigenbaum critical line is terminated

$$\begin{aligned} R^{-1}x_{n+1} - x_n &= L^3 | J_0(y_n) J_1(x_n)|, \\ R^{-1}y_{n+1} - y_n &= L^3 | J_0(x_n) J_1(y_n)|, \end{aligned} \tag{9}$$

where $x_n$ and $y_n$ are dimensionless amplitudes of the basic and parasitic modes, respectively, $J_0$ and $J_1$ are the Bessel functions, $L$ is the normalized length of the interaction space, $R$ is a combination of reflection coefficients at the input and output edges of the system. The arrangement of the parameter plane for the model (9) was studied and discussed in Refs [16, 17].

## 2. On an effectiveness of the analytical methods in nonlinear dynamics

As we see, the analytical derivation of a map is possible usually with use of some assumptions and physical approximations. How effective they are? Due to concepts of universality (Feigenbaum and other authors) investigators tend to regard as a habitual fact that the realistic systems should demonstrate the same phenomena as simple formal models, like logistic or cubic maps. When we construct a map analytically, we assume definite assumptions, which may seem very natural and justified. However, speaking about regimes of strong nonlinearity and high sensitivity in respect to initial conditions, we must be extremely careful: quite logical approximations may appear to be unsuccessful or to have a disappointingly restricted domain of application.

In Ref. [13] an example of such situation was demonstrated for the gravitational machine of Zaslavsky. Fig. 4, *a* shows attractors of the approximate and exact mappings (left and right panels, respectively) for several parameter values. Observe that they are absolutely different although the selected parameters are from domain traditionally used by researchers. Analogous situation occurs in a conservative case (Fig. 4, *b*).

We conclude that investigation of models of realistic physical systems in context of nonlinear dynamics requires careful handling and attentive revealing conditions of validness of the accepted assumptions. The last may turn to be a separate voluminous

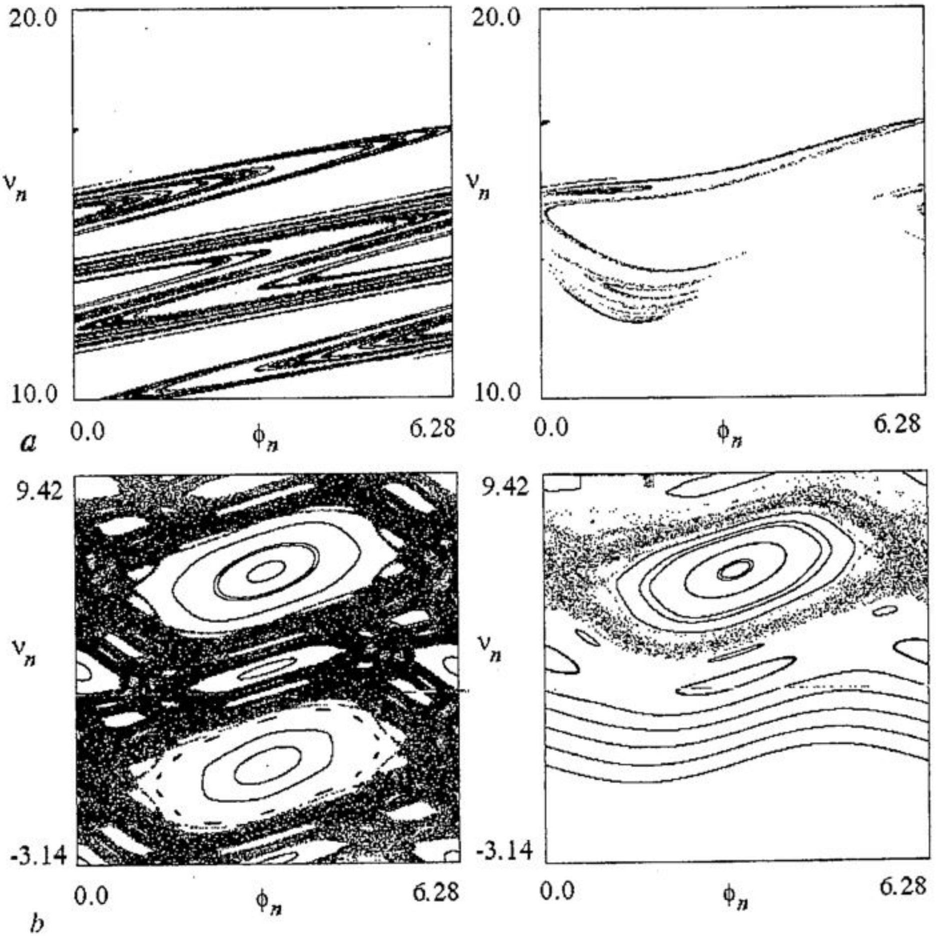

Fig. 4. At the top of figure (*a*) - phase portraits for approximate (on the left) and exact (on the right) dissipative map of bouncing ball. Parameter values are $\varepsilon=0.4$, $k=6.5$. At the foot of figure (*b*) - phase portraits in the conservative case parameter values are $\varepsilon=0$, $k=1.2$

research. For example, such a study of the original differential system (1), the 2D map (2), and 1D map (4) was presented in Ref. [7, 8].

## 3. Critical points in the parameter plane

One of the simplest critical phenomena mentioned in the Introduction is the so-called tricritical dynamics. This is a phenomenon that may occur in two-parameter analysis of bimodal (with two extrema) one-dimensional maps. In parameter plane the tricritical point appears as a terminal point of the Feigenbaum critical line. Also a line comes to this point associated in the parameter plane with a condition that one quadratic extremum is mapped precisely to another. On this line, obviously, the twice iterated map has a quartic extremum. Hence, moving along this line we will observe period-doubling cascade, but the scaling constant will be $\delta_T$=7.284686... and it is distinct from the well-known Feigenbaum value $\delta_F$=4.6692016...

As an example, let us consider Fig. 3. In the parameter plane of the system of relativistic electron beam and electromagnetic wave one can see the Feigenbaum critical line and the line of existence of the quartic extremum in the twice iterated map. These two lines intersect at the tricritical point. Fig. 3, *d* shows typical iteration diagrams at these lines and precisely at the tricritical point. Detailed two-parameter analysis and discussion of scaling properties of the system may be found in Ref. [14].

Usually, a tricritical point is not unique, but there exists an infinite number of such points forming a complex nontrivial set in the parameter plane. To study and classify them, MacKay and Van Zeijtz suggested a specific procedure of constructing «a binary tree of superstable orbits» [5]. In Fig. 5 this tree is plotted on the parameter plane of the map (4), which describes approximately dynamics of the kicked nonlinear oscillator. In a sense, the «crown» of the tree organizes the complex form of the chaos border in the parameter plane. Detailed study of the tricritical dynamics in this system and illustrations of scaling may be found in Refs [7, 8, 18].

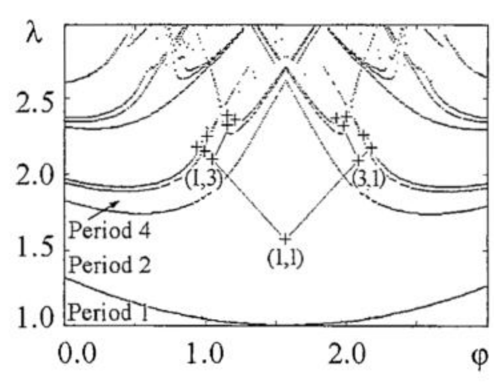

Fig. 5. Binary tree of superstable orbits in the parameter plane of «cosine map» (4) the branch of the tree are lines, which corresponds to mapping the maximum onto minimum after some iterations. The type of doubly superstable cycles associated with the branching points at the tree are indicated in brackets

It is worth noting that the maps for the gravitational machine (6) and (7) demonstrate one more type of critical behavior. In these maps, Feigenbaum's critical line in the parameter plane comes to the point *H*, where the dissipation vanishes. This point may be found as limit of period-doubling cascade in the Hamiltonian system (along the line $\varepsilon$=0). A neighborhood of the critical point *H* on the parameter plane is characterized by a two-parameter scaling, with universal constants $\delta_1$= 8.721097... and $\delta_2$=2.

## 4. Comparative description of complex dynamics in terms of mappings and differential equations

Correspondence between description of physical systems with three-dimensional phase space in terms of differential equations and of 2D maps is, in a sense, perfect. Indeed, the 2D map may be thought as obtained from the Poincare cross-section

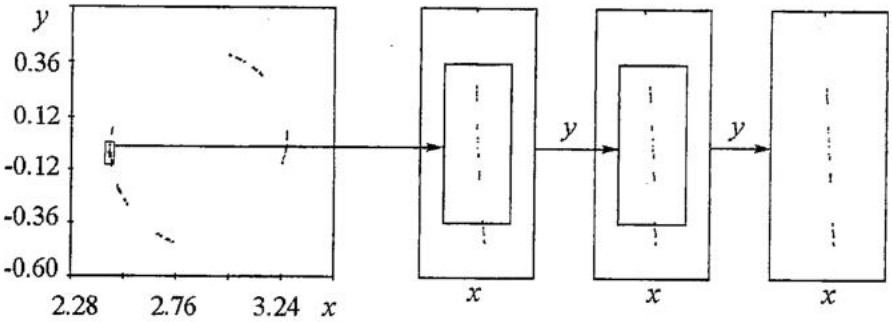

Fig. 6. Scaling properties on the three level of resolution on the attractor for the Ikeda map (2) at the pseudo - tricritical point $A$=2.8988007984, $B$=0.1445571961. We magnify each fragment by $\alpha$= =-1.69030297...

construction. However, passage from a 2D map to a 1D map may lead to principal differences in subtle details of dynamics. In particular, it relates to critical behavior of the maps at the chaos threshold, as mentioned in the Introduction.

In Ref. [18] the related matters were discussed by means of comparison of the Ikeda map (2) and of its 1D approximation (4). As we know, both Feigenbaum's and tricritical dynamics allow description in terms of the renormalization group. On this basis, one could expect that the exact 2D maps and the approximate 1D maps will relate to the same universality class and demonstrate identical scaling regularities. The only notable difference would be in some displacement of the Feigenbaum critical lines and tricritical points due to the approximate nature of the 1D map. However, the attempt to find the tricritical points in the 2D Ikeda map appears to be unsuccessful! It occurs that the tricritical behavior in the 2D map survives only in a sense of somewhat an *intermediate asymptotics*, perhaps over a sufficiently large number of period doublings. In the last case it is convenient to speak on the so-called *«pseudo-tricritical» points* In computations performed in Ref. [18] they have been located in the parameter plane of the Ikeda map, and tricritical scaling has been illustrated in the attractor structure at several levels of its resolution (see Fig. 6). However, the tricritical scaling behavior at those points is destroyed inevitably at some level of the resolution. The larger parameter of dissipation $B$, the less number of levels at which the tricritical scaling is valid.

So, in the picture of scenarios of transition to chaos a number of phenomena exists that can not be extended from 1D maps onto 2D maps, and further, onto the differential equations.

## 5. Universality and scaling in presence of noise

As known, in early 80-th Crutchfield et al. have revealed the property of universality and scaling for Feigenbaum's period doubling scenario in presence of noise [19]. The appropriate version of the renormalization group analysis was developed, and a new universal constant was estimated, $\gamma(2)$=6.6190365: to observe one more level of the period doubling one has to decrease the noise magnitude by this factor. Due to the universality intrinsic to the critical behavior, the regularities are in a high degree insensitive in respect to correlation properties of noise and to details of the form of the distribution function.

Naturally, analogous problem concerning the effect of noise arises in respect of the critical behaviors relating to other classes of universality, which may appear in the multi-parameter analysis of the transition to chaos.

First, we may consider an effect of noise onto 1D maps with extrema of different degree $\chi$: $x_{n+1}=1-\lambda|x_n|^\chi+\varepsilon\xi_n$, where $\xi_n$ is a random sequence. The scaling property consists in the following: to observe each one new level of the fractal structure of the attractor at the critical point, it is necessary to decrease the noise amplitude $\varepsilon$ by a definite factor $\gamma$ that depends (in a universal manner) on the degree $\chi$ [20].

As noted, in two-parameter analysis of smooth 1D maps situations can be met, when the twice iterated map has an extremum of degree 4 and the period-doubling accumulation lead to the tricritical point. Analogously, in three-parameter analysis of 1D maps additional critical situations may appear, when a twofold iteration yields a map with extremum of the 6-th degree, or a threefold iteration gives rise to an extremum of the 8-th degree. These situations correspond to certain critical points of codimension three [4]. In all these cases the constants responsible for scaling properties in respect to noise differ from that of Crutchfield et alt. The respective numbers have been computed in Ref. [20] and summarized in the Table. Also charts of the Lyapunov exponent on the parameter plane of the noisy maps were plotted, and illustrations of the scaling properties in presence of noise were given.

Table

Universal constants responsible for scaling in respect to noise for different types of criticality in 1D maps

| Type of criticality | $\chi$ | $\gamma(\chi)$ |
|---|---|---|
| Feigenbaum | 2 | 6.6190365 |
| Tricritical | 4 | 8.2439109 |
| Type S («six power») | 6 | 10.037886 |
| Type E («eight power») | 8 | 11.523865 |

Also we have revealed and illustrated in numerical experiments the scaling properties associated with the effect of noise at the so-called *bicritical point B*. This type of criticality occurs in a system of two unidirectionally coupled period-doubling subsystems as we bring both of them to the threshold of chaos by tuning their control parameters [21, 22]. The model equations are of the following form:

$$x_{n+1} = 1 - \lambda x_n{}^2 + \kappa\xi_n, \quad y_{n+1} = 1 - Ay_n{}^2 - Bx_n{}^2 + \varepsilon\eta_n, \tag{10}$$

where $\xi_n$ and $\eta_n$ are random sequences effecting the master and slave subsystems, respectively. An essential qualitative and quantitative difference was noted between the respond of the system to the noise added either into the first, or into the second subsystem. The universal constants responsible for the scaling in respect to the noise intensity are $\gamma$=6.619036 and $\nu$=2.713695, respectively. (The first one, naturally, coincides with the constant of Crutchfield et al.) Fig.7 illustrates scaling regularities on the charts of the Lyapunov exponents.

## 6. Complex dynamics of nonlinear oscillators and catastrophe theory

Concept of the multi-parameter analysis allows formulation of a novel and original view onto a study of complex dynamics of nonlinear oscillators. Traditionally, researc-

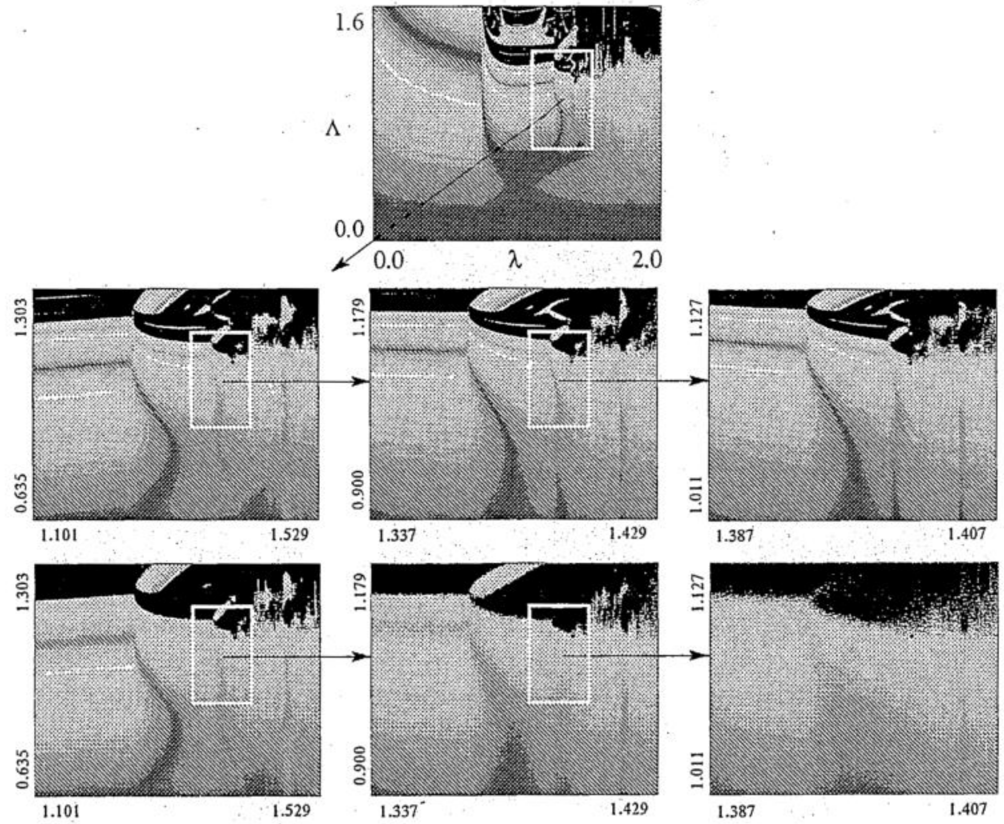

Fig. 7. Charts of the largest Lyapunov exponent in the parameter plane for two unidirectionally coupled logistic maps with noise (10) (the grey tones designate magnitude of the Lyapunov exponent). Values of noise amplitude are $k=0$, $\varepsilon=0.005$. Top row of the fragments are demonstrated scaling properties. We magnify fragments by 4.6692016 along $\lambda$ and by 2.392724 along $A$ in the vicinity of the bicritical point $\lambda=1.4011552$, $A=1.0900943$ and rescale value of noise by 2.713695. Lower row of fragments are demonstrated role of the noise in case if its amplitude is not rescale

hers fix a form of the potential relief for the oscillator and regard amplitude and frequency of the external force, or the dissipation coefficient, as variable control parameters. We suggest an alternative approach based on ideas of the catastrophe theory. Let us assume that a function that defines the potential relief is controlled by one, two, or more parameters. Classification of such functions is delivered by the catastrophe theory and, in particular, by the Rene Thom classification theorem. This approach gives an opportunity to formulate and study a sequence of situations of increasing codimension corresponding to potentials associated with canonical catastrophe theory forms: fold, cusp, swallow tail, etc. For example, a potential function $U(x) = -bx - (1/2)ax^2 - (1/3)x^3$ depending on two parameters $a$ and $b$ corresponds to the fold catastrophe. It generates a family of nonlinear oscillators which are governed (in presence of dissipation and of periodic external force) by the following equation:

$$\ddot{x} + \gamma\dot{x} + b + ax + x^3 = B\cos\omega t. \tag{11}$$

The main object of attention is now an analysis of dynamics of the system in dependence on parameters $a$ and $b$ responsible for configuration of the potential relief. Concrete examples of nonlinear oscillators considered in literature may be regarded now as particular representatives in a frame of the suggested generalized scheme. A study of complex dynamics for forced dissipative oscillators with potential functions associated with different elementary catastrophes may be found in Ref. [23].

## 7. Non-invertible 2D maps

Mappings constructed in a course of the Poincare cross-section procedure appear to be invertible because the differential equations themselves allow continuation of solutions back and forth in time. Nevertheless, noninvertible 2D maps are of interest too. They may arise in a straightforward way in some physical problems [24]. The simplest example, however, is a pair of coupled logistic maps (coupled period-doubling systems):

$$\begin{aligned} x_{n+1} &= 1 - \lambda x_n^2 - C y_n^2, \\ y_{n+1} &= 1 - A y_n^2 - B x_n^2. \end{aligned} \qquad (12)$$

Here λ and $A$ are control parameters of two subsystems, $C$ and $D$ are coupling constants, and the coupling is supposed to be quadratic.

Fig. 8, *a* presents examples of charts of dynamical regimes on parameter plane (λ, $A$). One can see there bifurcation points of codimension 2, where the bifurcation lines of Andronov-Hopf (birth of quasiperiodic regimes) and those of period-doubling meet together. The sequence of the codimension 2 bifurcation points converge to somewhat new critical point called the *FQ critical point* [4]. (FQ stands for «Feigenbaum» and «Quasiperiodicity».) A magnified fragment of the chart (Fig. 8, *b*) demonstrates that the system is characterized by an unusual form of the synchronization tongues. More detailed study shows their nontrivial metamorphoses. For instance, Fig. 8, *c* and *d* present examples of tongues of ring-like form. Yet more fascinating picture can be obtained for coupled 2D maps, say Hénon maps.

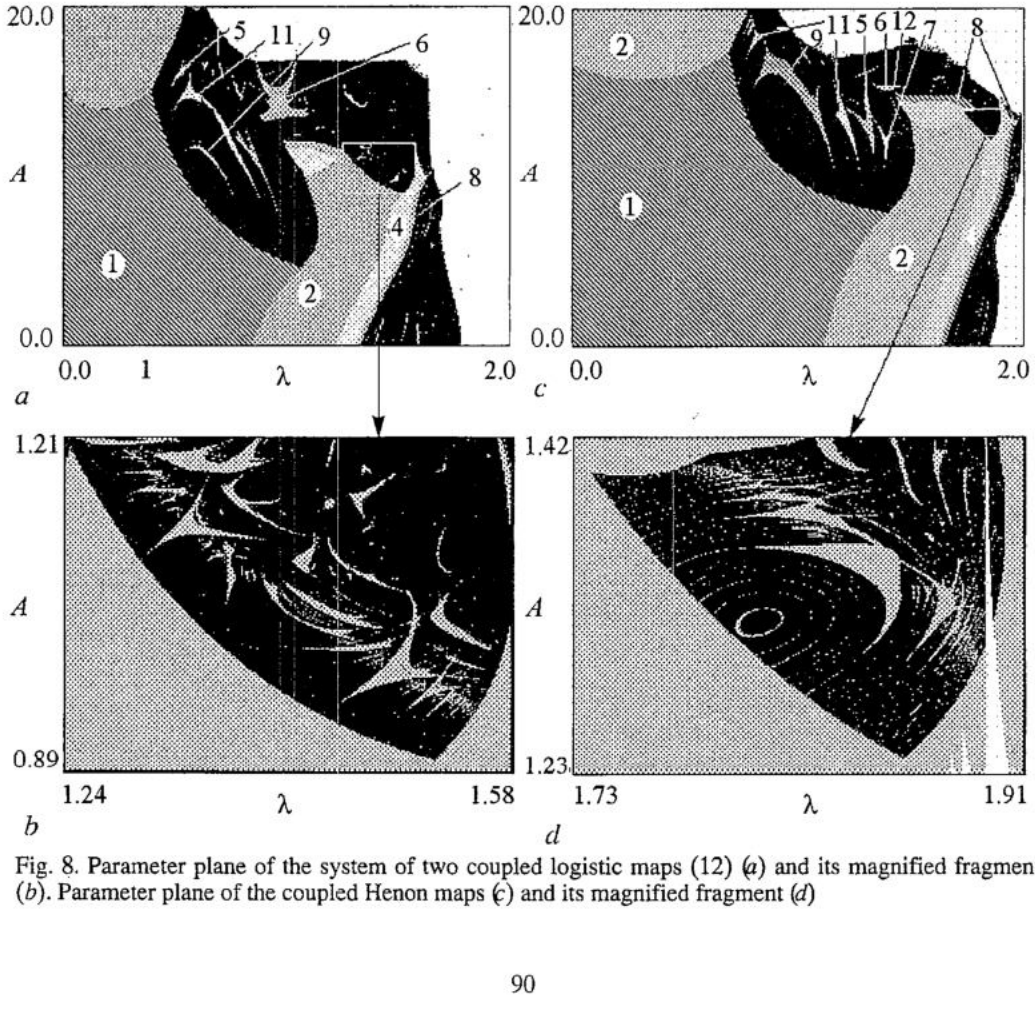

Fig. 8. Parameter plane of the system of two coupled logistic maps (12) (*a*) and its magnified fragment (*b*). Parameter plane of the coupled Henon maps (*c*) and its magnified fragment (*d*)

Interesting features of synchronization of noninvertible maps challenge us to elaborate a «universal» 2D map, which would demonstrate all basic bifurcations typical for two-dimensional phase space. To construct such a map, let us start with a note that a fixed point of any 2D map has a stability domain in the parameter plane of trace $S$ and determinant $J$ of the Jacobian matrix represented by a triangle with borders $\{J=1, S-J=1, S+J=-1\}$. Now, we construct the model to have S and J as natural parameters of the linearized part of the map, and add arbitrarily some quadratic nonlinearity:

$$\begin{aligned} x_{n+1} &= Sx_n - y_n - (x_n^2 + y_n^2), \\ y_{n+1} &= Jx_n - (1/5)(x_n^2 + y_n^2). \end{aligned} \tag{13}$$

Chart of dynamical regimes for this «universal» map is shown in Fig. 9. One can see a set of synchronization tongues with sharp edges at the upper side of the triangle, representing the Andronov-Hopf bifurcation line. Observe that the arrangement of the tongues differ from that intrinsic, for example, to the circle map and to the ring map. In particular, bifurcations occur, for which two multipliers are equal to 1 and -1, respectively. These codimension-2 bifurcation points may accumulate to somewhat new critical point called *the critical points of C-type* [4].

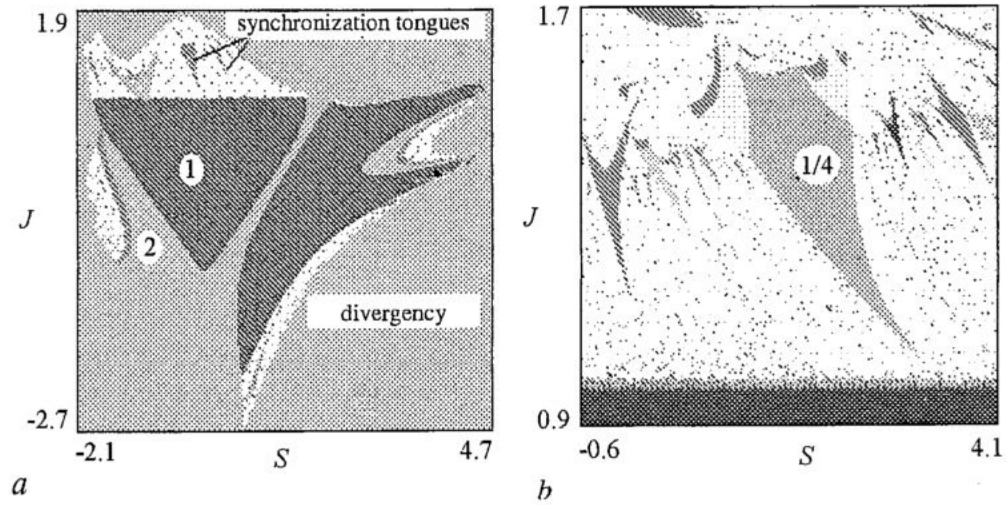

Fig. 9. Parameter plane $S$, $J$ «universal» 2D map (13). One can see «triangle of stability», which is formed by lines of tangent bifurcation, period doubling bifurcation and Neimark bifurcation. Inside of synchronization tongues there are the points of C-type, which corresponded to accumulation of the points, in which lines of the period doubling are terminated in the bounds of synchronization tongue

## 8. Synchronization and bifurcations of cycles

The idea of multi-parameter study opens new possibilities in research of the phenomenon of synchronization. Indeed, let a non-autonomous system be characterized by one or several control parameters, and undergoes some bifurcations under their variation. Then, the metamorphoses of synchronization regimes should be studied naturally in a parameter space of dimension increased by 2. (We add amplitude $A$ and frequency $\omega$ of the external force to a number of internal parameters of the system.) The simplest example is a situation of a unique control parameter of the autonomous system $\lambda$; let us suppose that its variation gives rise to a period-doubling bifurcation cascade. Then, in a cross-section of the parameter space by a plane $(\omega, r)$ the period-doubling bifurcation lines are terminated at edges of the synchronization tongues, these are

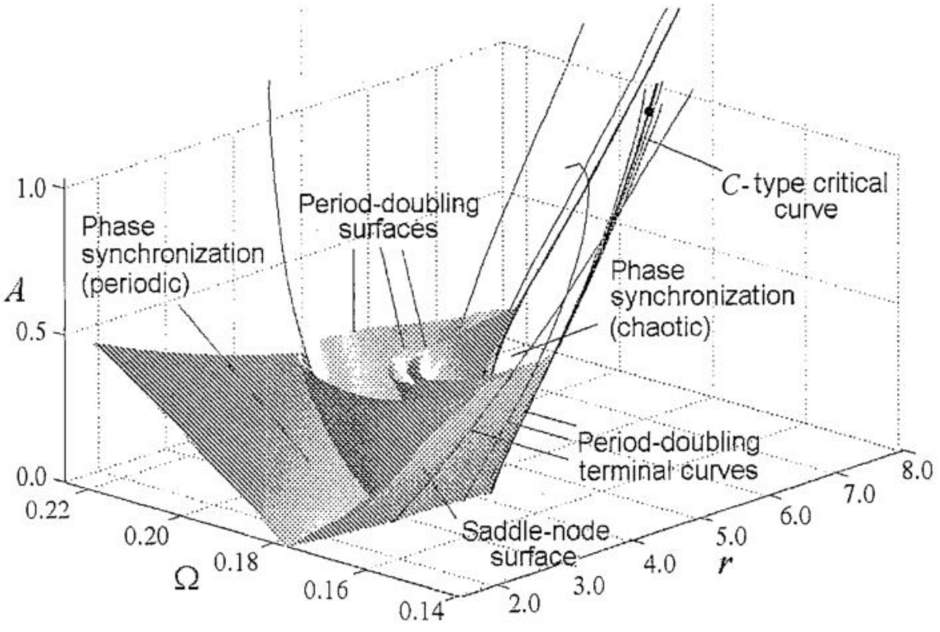

Fig. 10. Synchronization tongue for the forced Rössler system (14) and its interior arrangement in the parameter space; ω is frequency, $A$ is amplitude of the external force, $r$ is the parameter, controlled period doubling. One can see surfaces of tangent and period-doubling bifurcations. These surfaces are intersected along the lines, which are accumulated to critical lines of C-type as the number of period-doubling increase

codimension-2 bifurcation points. In 3-dimensional parameter space $(\omega,r,A)$ they correspond to codimension-2 bifurcation lines accumulated towards some critical line. The respective picture for the forced Rössler system [24]

$$\dot{x} = -y - z + A\sin 2\pi\Omega t, \quad \dot{y} = x + ay, \quad \dot{z} = b + z(x - r), \tag{14}$$

is reproduced in Fig. 10. The critical line obtained as a limit of codimension-2 bifurcation lines corresponds to the criticality of C-type [4] mentioned in the previous section. In Ref. [24] the respective scaling properties intrinsic to this criticality are revealed and discussed.

Next, let us consider a self-oscillator with hard excitation under external periodic force governed by an equation

$$\ddot{x} + (\lambda - x^2 + \alpha x^4)\dot{x} + x + \beta x^3 = b\sin\omega t. \tag{15}$$

Note that in autonomous case variation of a control parameter gives rise to bifurcation of collision of a stable and unstable limit cycles in this system.

Using a method of slow amplitudes one can derive the following reduced equation:

$$\dot{R} = -R + R^3 - kR^5 - \varepsilon\cos\varphi, \quad \dot{\varphi} = -\Delta + 3\beta R^2 + (\varepsilon/R)\sin\varphi. \tag{16}$$

Here ε is a dimensionless amplitude of the external force, Δ is a dimensionless deviation of the external frequency from the frequency of self-oscillations, parameter $k$ controls mutual location of the stable and unstable limit cycles, $k=\gamma\lambda$. At $k=0.25$ they collide and disappear.

Bifurcation analysis in the parameter space of the model (15) reveals a fascinating picture. At small values of $k$ there exist two synchronization tongues, one corresponds to a stable, and another to an unstable regime. With increase of $k$ one observes their

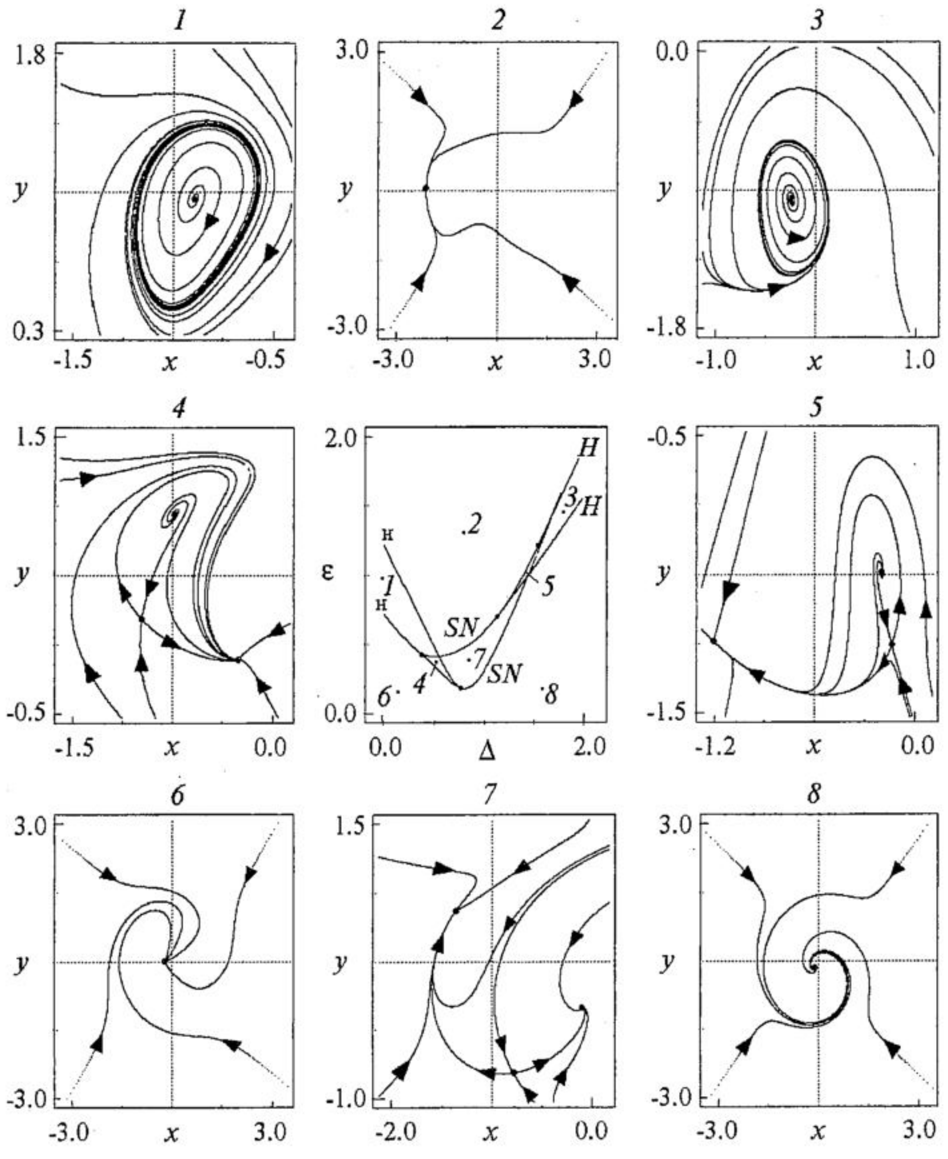

Fig. 11. Parameter plane (ε is a dimensionless amplitude and Δ is dimensionless deviation of the frequency) for system (15) after collision of the limit cycles in the autonomous system. $k$=0.29

unification via bifurcation situations of codimension 3. In particular, a known catastrophe of «swallow tail» [25] is observed. At the bifurcation of the autonomous system the synchronization tongue loses touch with the frequency axis and forms a singularity known in the catastrophe theory called «lips» [25]. In this situation the quasiperiodic regimes at small amplitudes of the external force disappear. The respective picture is shown on the central panel of Fig. 11. Also the Andronov-Hopf bifurcation lines are shown there, which have common points with the tongue edge (the Bogdanov-Takens points). It may be seen that above the bifurcation threshold of the autonomous system the quasiperiodic regimes are possible yet at large amplitudes of driving. They are observed in a region between the Andronov-Hopf bifurcation lines. Only at $k$=0.3 one more codimension-3 bifurcation occurs, when the pairs of the Andronov-Hopf bifurcation lines collide and disappear.

*The authors thank S.P. Kuznetsov for discussions. The work was supported by CRDF and Ministry of Education of Russian Federation (grant REC-006), by Russian Foundation of Basic Research (grants 00-02-17509 and 02-02-06469) and Russian Foundation of assistance to science fo our country.*

## References

1. *A.P. Kuznetsov, S.P. Kuznetsov.* Critical dynamics of the lattices coupled map at the onset of chaos (review). Izvestiya VUZ. - Radiophysics. Vol. 34, 1991, № 10 - 12. P. 1079 - 1115.

2. *A.P. Kuznetsov, S.P. Kuznetsov.* Critical dynamics for 1D maps. Part I. Feigenbaum's scenario. Izvestiya VUZ. Applied Nonlinear Dynamics, 1993. Vol. 1, № 1. P. 15 - 32.

3. *A.P. Kuznetsov, S.P. Kuznetsov, I. R. Sataev.* Critical dynamics for 1D maps. Part II. Two-parameter transition to chaos. Izvestiya VUZ. Applied Nonlinear Dynamics, 1993. Vol. 1, № 3 - 4. P. 17 - 35.

4. *A.P. Kuznetsov, S.P. Kuznetsov, I.R. Sataev.* A variety of period-doubling universality classes in multi-parameter analysis of transition to chaos. Physica D. Vol. 109, 1997. P. 91 - 112.

5. *A.P. Kuznetsov, S. P. Kuznetsov, I. R. Sataev.* Codimension and Typicity in a Context of Description of Transition to Chaos via Period - Doubling in Dissipative Dynamical Systems. Regular and Chaotic Dynamic. 1997. Vol. 2, № 3 - 4. P. 90 - 105.

6. *Ikeda K., Daido H., Akimoto O.* Optical turbulence: chaotic behavior of transmitted light from a ring cavity. Phys. Rev. Lett. 1980. Vol. 45. P. 709

7. *A.P. Kuznetsov, L.V. Turukina.* Dynamical systems of different classes as models of the kicked nonlinear oscillator. Izvestiya VUZ. Applied Nonlinear Dynamics. Vol. 8, 2000, № 2. P. 31 - 42.

8. *A.P. Kuznetsov, L.V. Turukina, E. Mosekilde.* Dynamical systems of different classes as models of the kicked nonlinear oscillator. International Journal of Bifurcation and Chaos. Vol. 11, 2001, № 4. P. 1065 - 1078.

9. *Tufillaro N.B., Albano A.M.* Chaotic Dynamics of a Bouncing Ball. Am. J. Phys. Vol. 54, 1986, №. 10. P. 939 - 944.

10. *Moon F.* Chaotic vibrations. 1987, Wiley and Sons.

11. *Lieberman M., Lichtenberg A.* Stochastic and Adiabatic Behavior of Particles Accelerated by Periodic Forces. Phys. Rev. Vol. 5, 1972. P. 1852 - 1866.

12. *Guckenheimer J., Holmes P.* Nonlinear Oscillations, Dynamical Systems, and bifurcations of Vector Fields. 1997, Springer.

13. *A.P. Kuznetsov, A.P. Shirokov.* Comparative analysis of the approximate and precise mapping for «bouncing ball» . Izvestiya VUZ. Applied Nonlinear Dynamics. Vol. 8, 2000, № 5. P. 72 - 81.

14. *A.P. Kuznetsov, A.P. Shirokov.* Discrete model of a backward - wave tube. Izvestiya VUZ. Applied Nonlinear Dynamics, 1997. Vol. 5, №. 6. P. 76 - 84

15. *V.L. Bratman, A.V. Savilov.* Scenario of transition to the multi - frequency regime in the FEL - oscillator with a low-Q microwave system. Izvestiya VUZ. Applied Nonlinear Dynamics, 1994. Vol. 2, №. 6. P. 27 - 39.

16. *A.P. Kuznetsov, A.P. Shirokov.* Complex dynamics of two - mode low - dimension model of the free electron laser. Izvestiya VUZ. Applied Nonlinear Dynamics, 1999, № 1. P. 3 - 11.

17. *Kuznetsov A.P., Shirokov A.P.* Analysis of the scenarios of transition to chaos in the discrete two - mode model of free electron laser. Letters in the J. of Technical Physics, 1999. Vol. 25, №. 12. P. 17 - 21.

18. *A.P. Kuznetsov, S.P. Kuznetsov, L.V. Turukina, E. Mosekilde.* Two-parameter analysis of the scaling behavior at the onset of chaos: Tricritical and pseudo-tricritical points. Physica A300, № 3 - 4, 2001. P. 367 - 385.

19. *Crutchfield J.P., Farmer J.D., Huberman B.A.* Fluctuations and simple chaotic dynamics. Phys. Rep., 1982. Vol. 92 №. 2. P. 45 - 82

20. *A.P. Kuznetsov, J.V. Kapustina.* Scaling properties at transition to chaos in model maps in the presence of noise. Izvestiya VUZ. Applied Nonlinear Dynamics. Vol. 8, 2000, № 6. P.78 - 87.

21. *J.V. Gulyaev, J.V. Kapustina, A.P. Kuznetsov, S.P. Kuznetsov.* On scaling properties in unidirectionally coupled period-doubling systems in the presence of noise. Letters in the J. of Technical Physics, 2001. Vol. 27, № 22. P. 58 - 65.

22. *Julia V. Kapustina, Alexandr P. Kuznetsov, Sergey P. Kuznetsov, and Erik Mosekilde.* Scaling properties of bicritical dynamics in unidirectionally coupled period-doubling systems in the presence of noise. Physical Review E. Vol. 64, № 6, 2001, 066207 (12 pages).

23. *A.P. Kuznetsov, A.Yu. Potapova.* Features of the complex dynamics of the nonlinear oscillations with Thom's catastrophes. Izvestiya VUZ. Applied Nonlinear Dynamics. Vol. 8, 2000, № 6. P. 94 - 120.

24. *S.P. Kuznetsov, I.R. Sataev.* Universality and scaling for the breakup of phase synchronization at the onset of chaos in a periodically driven Rössler oscillator. Phys.Rev.E. Vol. 64, №. 4, 2001, 046214 (7 pages).

25. *Arnold V. I.* Catastrophe theory. Moscow: Science, 1990. 128 p.

*Saratov State University*
*Institute of Radio-Engineering and*
*Electronics of RAS, Saratov Branch*

*Received 18.05.2002*

УДК 517.9

# МНОГОПАРАМЕТРИЧЕСКАЯ КАРТИНА ПЕРЕХОДА К ХАОСУ

*А.П. Кузнецов, Л.В.Тюрюкина, А.В. Савин, И.Р. Сатаев,*
*Ю.В. Седова, С.В. Милованов*

В работе представлен ряд направлений исследований сложной динамики нелинейных систем, связанных с многопараметрическим исследованием. В частности, обсуждаются примеры реалистичных моделей многопараметрических систем, критические явления на пороге хаоса, сопоставление свойств дифференциальных систем и отображений и др.

*Alexander P. Kuznetsov* was born in 1957. He is a Doctor of Sciences, Head Researcher of the Laboratory of Theoretical Nonlinear Dynamics of Saratov Branch of IRE RAS, Head of the Chair of Dynamical Systems of Nonlinear Processes Department of Saratov State University, Professor of Nonlinear Processes Department. A.P.Kuznetsov specializes in nonlinear dynamics, dynamical chaos and critical phenomena theory. He is Soros Professor (2000, 2001), scientific leader of the student's laboratory «Theoretical Nonlinear Dynamics» at SSU and SB of IRE RAS, member of Editorial board of the Journal «Empire of Mathematics». Sphere of his scientific interest includes applications of bifurcation and catastrophe theory, development of the concept of the multi-parameter criticality which is a generalization of the idea of scenario of transition to chaos onto multi-parameter nonlinear systems, investigation of features of signals with hierarchical organization («the fractal signals»). A.P.Kuznetsov is an author of more than 100 published works in Russian and International scientific press, an author of several teaching courses for the Nonlinear Processes Department of SSU and five popular scientific books and textbooks.

*Ludmila V. Turukina* was born in 1977. She is a Postgraduate student of the Nonlinear Processes Department of Saratov State University, a Laureate of Fellowship of RF President for students and post-graduate students (1999-2000, 2001-2002), Soros Student (1998, 1999, 2000), Soros Graduate Student (2001). Her scientific interest includes study of dynamical chaos, critical phenomena at the transition to chaos, comparative analysis of dynamical systems description with the help of mathematical models of different classes. She is an author of 17 publications in Russian and International scientific press. L.V. Turukina took part in 23 scientific conferences, including 10 international conferences. She made several working visits to the Technical University of Denmark and to the Potsdam University (Germany).

*Alexey V. Savin* was born in 1980 in Saratov, graduated from the Physical Department of Saratov State University. Now A. Savin is post-graduate student. His main scientific interests are the numerical investigations of model of nonlinear dynamics systems, particularly, coupled systems. A. Savin participated in 4 international conferences and has one publication.

*Igor R. Sataev* was born in 1959, graduated from the Moscow Physical-Technical Institute (1982). He is a Candidate of Sciences (PhD), Senior scientific researcher at the SB of IRE RAS. His basic scientific interests include numerical methods for solving renormalization group equations, numerical simulations of dynamics at the chaos threshold, critical phenomena in nonlinear systems. Sataev I.R. is an author of more than 30 publications in Russian and International scientific press.

*Julia V. Sedova (Kapustina)* was born in 1979. She is a Postgraduate student of the Nonlinear Processes Department of Saratov State University. Her basic scientific interest includes a noise influence on dynamical systems. She is a Soros Student (1999, 2000, 2001), the winner of the nominal prize fellowship of Saratov administration (1999-2000, 2000-2001 academic years). She made working visit to the Potsdam University, Germany (2002). She is an author of 4 scientific publications in Russian and International scientific press.

*Sergey V. Milovanov* was born in 1980. He is a fifth-year student of the Nonlinear Processes Department of Saratov State University. His basic scientific interests connect with topological methods in nonlinear dynamics, complex dynamics of non-autonomous systems and two-parameter maps. S. Milovanov took part in 10 scientific conferences, including 2 international conferences. Soros Student (2000, 2001).

Izv. VUZ «AND», vol.10, № 3, 2002

# INVESTIGATION OF TRANSIENT CHAOS IN GYRO-BACKWARD-WAVE-OSCILLATOR SYNCHRONIZED BY THE EXTERNAL SIGNAL

*A.E. Hramov, A.A. Koronovskii, I.S. Rempen, D.I. Trubetskov*

In this work we explore the transient chaos in non-autonomous, distributed active medium (gyro-backward-wave oscillator synchronized by the external signal). The transient chaos characteristics near the synchronization tongue boundaries are investigated. Special attention is payed to the building of long time series which is used to appreciate the characteristics of system dynamics. The time series is constructed by gluing of short time realizations which characterize the transient chaos observed in the distributed system.

## Introduction

In our days great interest causes the questions of microwave signals generation and amplification in gyroresonance devices with the travelling wave and the backward wave, based on the interaction of the unmoderated electromagnetic waves with the spiral electron beam (gyro-BWO and gyro-BWT). Such devices are actively examined theoretically and experimentally [1-5].

The non-autonomous active medium «spiral electron beam - backward electromagnetic wave» demonstrates several non-linear effects like periodical and chaotical modulation of the output signal, synchronization of the gyro-BWO by the external signal etc. [5-9]. In this work we show the possibility of appearance of a phenomenon of transient chaos in such system. As distinct from the «classic» dynamical chaos (its image in phase space is strange attractor and the phase trajectories tend to it with $t \to \infty$), under the term «transient chaos» [10-12] the follow phenomena is ment: in the phase space of the system there exists the so-called chaotic saddle - a chaotic set which is unstable in one of directions. The phase path starting from the points situated near the chaotic saddle for a long time demonstrates chaotic behaviour and henceforth quits from its vicinity and reaches the attractor which may be regular of chaotic.

The unstable chaotic set might be characterized by the same parameters as a strange attractor (dimension, Lyapunov exponent etc.) In this case the characteristics can be carried out from ensemble of short time series describing the transient chaotic process in the investigated system. In this case usually the procedure of gluing of the time series is used. Mostly, the transient chaos is investigated in simple finite-dimensional systems with discrete and continuous time.

In this work we investigate transient chaos in a distributed (and therefore, infinite-dimensional) active medium containing oscillations-electrons. The characteristics of transient chaos in non-autonomous gyro-BWO are examined. Special attention is payed to the problem of correct building of long time series using the short series derived from the distributed system.

The structure of the work is the follows. In sec. 1 the mathematical model of the investigated system is set, the admissions used in its constructing and the boundaries of its adaptability are discussed. In sec. 2 the oscillation regimes in non-autonomous gyro-generator with backward wave are discussed. The parameters' interval, in which the regime of transient chaos realizes, is explored. Sec.3 is devoted to the question of building of long time series produced by distributed system in transient chaos regime. In sec. 4 some characteristics of transient chaos (dimension, maximal Lyapunov exponent) are derived from the constructed time series.

## 1. General formalism

When the spiral electron beam interacts with the TE-modes of the waveguide and the waves synchronizm condition is fulfiled

$$\omega \approx \hat{\omega}, \quad \hat{\omega} + \beta_0(\hat{\omega})v_{\parallel} - \omega_c = 0, \tag{1}$$

we can observe high-frequency generation [13, 14]. Here $\hat{\omega}$ is the synchronism frequency, $\omega_c$ is the cyclotron frequency, $v_{\parallel}$ is the electrons longitudinal velocity, i.e. the velocity which is parallel with the applied magnetic field, $\beta_0(\hat{\omega})$ is the distribution constant of the waveguide without electron beam.

In such system accelerative grouping of the electrons takes place. It is caused by relativistic non-isochronism of the electrons-oscillators of the spiral (or polyspiral) beam. One of the peculiarities of this system is the possibility of retuning the generation frequency by the changing of the longitudinal electrons velocity $v_{\parallel}$ or the static magnetic field $B_0$. In real systems for such purpose it is necessary to change the geometry of the waveguide and the value of the magnetic field along the interaction space [15, 16]. From this sight the model described in our paper is idealized.

The interaction between the weakly relativistic spiral beam and the backward wave is described by the self-consistent system of movement equation [13] and stimulation equation [17]

$$d\beta/d\xi - j\,\mu(1 - |\beta|^2\beta = F, \tag{2}$$

$$\partial F/\partial\tau - \partial F/\partial\xi = -I, \quad I = {}^1\!/_{2\pi}\int_0^{2\pi} \beta d\theta_0, \tag{3}$$

where $\beta=r\exp(j\theta)$ is the complex radius of the trajectories of the ensemble electrons, which are initially distributed by phases relatively the HF field, $F=F(\xi,\tau)$ is the slowly changing complex non-dimensional amplitude of the field in the beam section, $I=I(\xi,\tau)$ is the first harmony of the grouped current, $\xi=\beta_0(\hat{\omega})\varepsilon z$ is the nondimensional longitudinal coordinate, $\tau=\hat{\omega}\varepsilon(t-z/v_{\parallel})(1+v_{\parallel}/|v_g|)^{-1}$ is the non-dimensional time in the coordinate system moving with the longitudinal beam velocity $v_{\parallel}$, $\hat{\omega}$ is the frequency satisfying the synchronism condition (1), $\beta_0(\hat{\omega})$ is the coefficient of propagation of the backward wave with the frequency $\hat{\omega}$ in the system without electron beam, $v_g$ is the wave group velocity on the frequency $\hat{\omega}$.

Besides we bring in the following parameters: $\mu=(v_{\parallel}/c)/2\varepsilon$ is the non-isochronism parameter, characterizing the system phase non-linearity,

$$\varepsilon = [(I_0K/4V_0)(1 + v^2_{\perp 0}/v^2_{\parallel})]^{0.5} << 1$$

is the interaction parameter,

$$\omega_c = (eB_0/m_0c)(1 - {}^1\!/\!{}_2(v_{\parallel}^{\,2} + v^2_{\perp 0})/c^2)$$

is the cyclotron frequency with $\xi=0$, $K$ is the coupling impedance, $v_{\perp 0}$ is the initial transversal electron velocity, $I_0$ and $V_0$ are the constant constituents of the beam current and voltage.

Equations (2) and (3) are solved within the follow initial and boundary conditions:

$$F(\xi,\tau=0) = f^0(\xi), \qquad I(\xi,\tau=0) = 0, \tag{4}$$

$$\beta(\xi=0) = \exp(j\,\theta_0), \qquad \theta_0 \in [0, 2\pi], \tag{5}$$

where the initial distribution $f^{\,0}$ is taken as

$$f^{\,0}(\xi) = \delta_0\sin(\pi(A - \xi)/2). \tag{6}$$

The external controlling signal

$$F(\xi=A,\tau) = F_0\exp[j\,\Omega\tau] \tag{7}$$

is added on the collector boundary of the system $\xi=A$, where $A$ is the length of the system, $F_0$ is the external signal amplitude, $\Omega$ is the mismatch between the external signal frequency and the «cold» synchronism frequency $\hat{\omega}$.

The model described by the equations (2)-(5), is correct only within the following conditions: the EM field in the beam cross section is uniform, the longitudinal velocity $v_{\parallel}\approx$const (i.e. the interaction between the electrons-oscillators and the HF components of the magnetic field is neglected), the non-stationary process is assumed to be narrow-band, hence in the active frequency band it is necessary to take into account only the interaction of the spiral beam with the backward wave.

In our work we investigate the gyro-BWO within the following parameter values: $\mu=4$ and A=3.0. In the autonomous system these values correspond to the regime of a periodical self-modulation of the exit signal. The numerical scheme parameters for the equations (2) and (3) were taken as $\Delta\xi=8\cdot10^{-3}$ (coordinate step), $\Delta\tau=4\cdot10^{-3}$ (time step).

## 2. Oscillation regimes and the transient chaos in gyro-BWO

In the works [9, 18, 19] the influence of different types of external control signal on the dynamics of the simple gyro-BWO model is investigated. In reference [20] the problem of chaotic auto-oscillation synchronization in the system «spiral electron beam - backward elecrtomagnetic wave» is analyzed. The importance of this problem is conditioned by the practical aspects of elaborating gyro-devices with controlled parameters and also by theoretical interest attracted to the investigation of auto-oscillation synhronization in distributed active medium.

In Fig. 1 we introduce the regimes map of the gyro-BWO synchronized by the external signal on the parameters plane «frequency - amplitude of the external influence» (the external signal parameters are foregoing) [18]. Different symbols on the map marks the areas of different oscillation regimes. With $\Omega>-2.0$ we derive the synchronization regime, i.e. stationary generation on the frequency of external signal. The dashed line marks the boundary of frequency capture area. In this case the device may demonstrate periodical or chaotic self-modulation of the output signal.

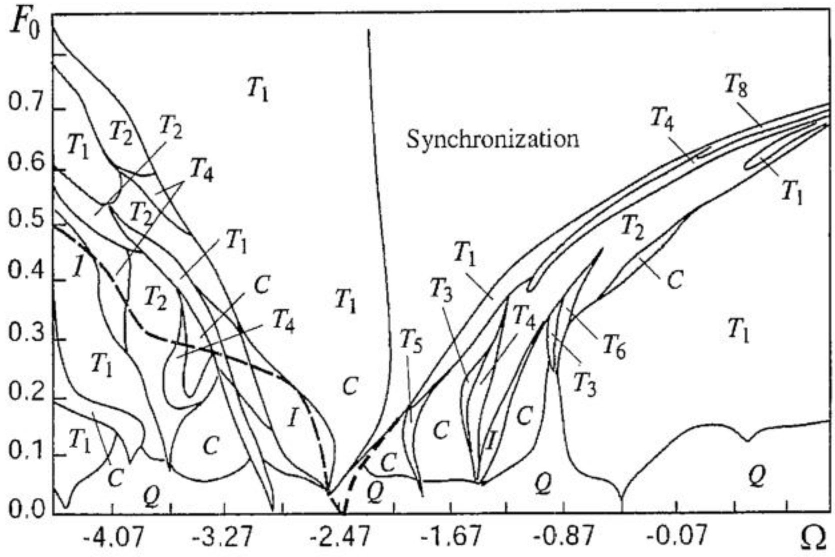

Fig. 1. Typical regimes of the non-autonomous oscillations in gyro-BWO on the controlling parameters plane frequency Ω - amplitude $F_0$. By the dashed line the quasi-synchronization area is marked

The region of frequency capture from the side of higher frequencies coincides with the boundary of the self-modulation region (and, accordingly, the synchronization region), and, on the side of smaller frequencies, the frequency of the external signal, at which the frequency capture takes place lays, essentially more to the left of from the boundary of the stationary generation regime. The regions of the regimes map marked by the symbols $T_n$ corresponds to the periodic automodulation of the output signal with the period $n$. And, at last, the regions marked by the symbols $C$ and $Q$ corresponds to the chaotic generation and generation with several incommensurable automodulation base spectral components (quasiperiodic automodulation).

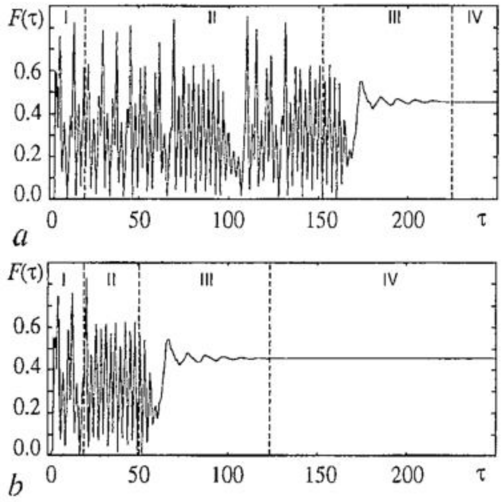

Fig. 2. Typical time series of the output signal amplitude of non-autonomous gyro-BWO. The signals are constructed at the following values of the initial perturbation amplitude: (*a*) $\delta_0=0.0019$ and (*b*) $\delta_0=0.0072$. By vertical shaped lines the typical parts of time series are divided: the part II is the region of the transient chaos which we analyse

Near the right boundary of the synchronization tongue (in the region of larger frequencies) the appearance of transient chaos considered the Introduction takes place. We explore the transient chaos in the regimes map point with the following values of the external signal control parameters: $\Omega=2.0$ and $F_0=0.62$. In Fig. 2 we represent the typical time series of the output signal $F(\xi=0,\tau)$ in the transient chaos regime obtained at the different starting conditions (6), namely at different amplitudes of initial perturbation $\delta_0$.

In Fig. 2 one can see that depending on the initial perturbation amplitude $\delta_0$ the transient time duration is various, but finally the regime of stationary generation on the external signal frequency is stated. The transient process is rather irregular, what testifies the presence of the phenomenon of transient chaos in a system.

We analyse the transient chaos characteristics, for which it is necessary to create an artificially long time series consisting of the «sewed» short segments of time series corresponding to the transient chaos. For analysing the transient chaos regime and the procedure of gluing of short time series characterizing the unstable transient chaos regime we use the time series generated by the field amplitude oscillations $|F(\tau)|$, taken from the exit of the system $\xi=0$.

## 3. Constructing of an artificially long time series

Time series generated by the explored system in the transient chaos regime, can be «divided» into four parts (see Fig. 2): I - evolution of the system from the initial state to the unstable chaotic state, II - naturally, the transient chaos regime, III - the exiting of the system on an asymptotic regime and IV - the final asymptotically stable state. The information concerning the unstable chaotic saddle we can obtain from the part II of the time series, while the parts I, III and IV correspond to other states of the system. Therefore, for the analysis of characteristics of the chaotic saddle existing in the system phase space, we need to «cut out» the parts I, III and IV of the time series [12], and then to «sew» the parts corresponding to the chaotic unstable regime. This approach allows then to apply the standard methods of the analysis to the obtained artificially long time series (see, for example, [21, 22, 23]).

One of possible methods of deriving an artificially long time series is immediate combination of the truncated time series with each other. In this case the variable $F$ of the derived new time series can have break points i.e.

$$\lim_{t\to T_n - 0} F(t) \neq \lim_{t\to T_n+0} F(t), \tag{8}$$

Where $T_n$ are the points of the uniting of the series.

Yet when we restore an attractor using the delay method (Takens method) [24, 25] by an artificially derived long time series, $J$ false points appear on an attractor [12]:

$$J = d(T/\Delta\tau)(n - 1), \tag{9}$$

where $T$ is the delay time of the Takens method, $n$ is the amount of the truncated time series, $d$ is the dimension of the space of embedding, $\Delta\tau$ is the time step.

Another, more correct method of deriving of similar long time realization is the method of «gluing» of two different time series. Let $x(t)$ and $y(t)$ be the «glued» time series. If the attractor is restored in $d$-measure phase space, the following condition must be fulfilled for the «gluing» of the phase trajectories:

$$[\Sigma_{i=0}^{d-1} (x(t_1 + i\times T) - y(t_2 + i\times T))^2]^{1/2} < \varepsilon, \tag{10}$$

where $\varepsilon$ is the «gluing» precision (we have chosen $\varepsilon=2.5\times10^{-3}$), $t_1$ and $t_2$ are the times of «gluing» for $x(t)$ and $y(t)$. The condition (10) can be replaced by the similar

$$|x(t_1 + i\times T) - y(t_2 + i\times T)| < \varepsilon, \quad i = \overline{0,\dots,d-1}. \tag{11}$$

For procedure (11) it is required the value of the phase space dimension $d$, in which the attractor corresponding to the transient chaos is embedded. Let's estimate the value of $d$, calculating the correlation dimension $D$ [21, 22], of an attractor restored by an artificially long time series derived without special method of «gluing» for different, increasing values of embedding space dimension $d$=2,3,4,.... The phase space dimension is equal to the value of embedding space dimension $d$ with which the correlation dimension $D$ is saturated [26].

Of course, such estimation is not absolutely precise, taking into account the presence of «false» points in the phase space. However, as was shown in [27], the estimation of correlation dimension by short segments of chaotic time series is rather reliable. Therefore the offered procedure can be used for the estimation of phase space dimension $d$. Further, using the procedure of correct gluing of short time series, we shall test the obtained results on calculation correlation dimension using simulated long chaotic time series.

The correlation dimension of an attractor $D$ is a function of a scale of observation $\varepsilon$:

$$D(\varepsilon) = \lim_{\varepsilon\to 0} (\ln C(\varepsilon,d) /\ln\varepsilon), \tag{12}$$

where $C(\varepsilon,d)$, the number of pairs of points, distance between which in $d$-measured phase space is less than $\varepsilon$ (the reduced correlation integral), is derived from the following relation

$$C(\varepsilon,d) = (1/MN)\, \Sigma_{j=1}^{M} \Sigma_{i=1, i\neq j}^{N} H(\varepsilon - \|\mathbf{x}_i - \mathbf{x}_j\|). \tag{13}$$

Here $M$ is the number of reduction points, $N$ is the number of points in the time series, $H$ is the Heviside function, $\mathbf{x}$ is the position vector in the phase space restored by Takens method.

In Fig. 3, *a* one can see the results of calculation of the correlation dimension $D(\varepsilon)$ by the transient chaos time series combined without «gluing» for different values of embedding space dimension $d$. Time series length was chosen $N=6\cdot 10^4$, and number of points of a reduction $M=10^4$. The time series is combined from three short ones and the number of false points in pseudo-phase space $J=3200$ according to (9).

From fig. 3 one can see that the chaotic attractor corresponding to the transient chaos, is strongly inhomogeneous, because there is no scaling region on the function of correlation integral inclination depending on the scale of observation. However, beginning from the embedding space dimension $d=3\div 4$ the shape of curves $D(\varepsilon)$ does not vary. Therefore as an estimate of embedding space dimension $d=4$ can be taken. This value would further be used for constructing artificially long time series by gluing the short ones.

When the parts of short time series are glued it's necessary to obtain the value of the $T$. We realized the glue of short time series with different values of $T$ and analysed the effectiveness of the method in each case. One of the time series $x(t)$ (we shall call it «$x$-realization») was cut into two parts $x_1(t)$ and $x_2(t)$ at the time $\hat{t}$ so, that

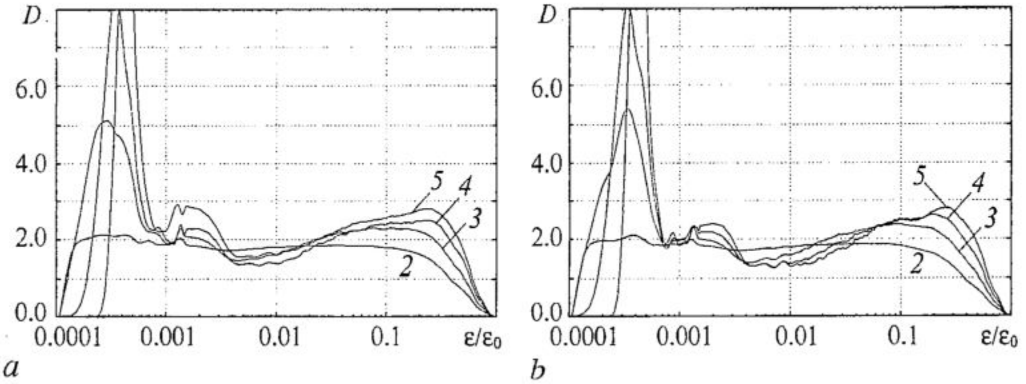

Fig. 3. Correlation dimension $D$ as a function of observation scale: (*a*) for attractor restored on the time series derived by simple combining of short ones without special «gluing» method (11) and (*b*) for attractor restored on correctly glued long time series. The numbers correspond to different embedding space dimensions $d$

$$x(t) = \begin{cases} x_1(t), & \text{if } t \le \hat{t}, \\ x_2(t), & \text{if } t > \hat{t}. \end{cases} \tag{14}$$

After that the time series $x_1(t)$ was glued together with another time series $y(\theta)$, which we shall call «$y$-realization» (see (11)), so that the following condition should be satisfied:

$$\hat{t}_1 = t - (d-1) \times T. \tag{16}$$

In the case of $x$- and $y$-realizations are equivalent, i.e. $x(t) \equiv y(\theta)$, the following relation takes place

$$x_2(t) \equiv y(t_2 + (d-1) \times T + (t - \hat{t})), \qquad t \ge \hat{t}. \tag{16}$$

In a case of phase trajectories corresponding to $x$- and $y$-realizations are close to each other in $d$ - measured phase space (but are not equivalent), by virtue of instability they will disperse with time and after a slice of time $\Delta t$ will separate on distance exceeding some value $\varepsilon_2$ (in our case $\varepsilon_2 = 2.5 \times 10^{-2}$):

$$|x_2(\hat{t} + \Delta t) - y(t_2 + (d-1) \times T + \Delta t)| > \varepsilon_2. \tag{17}$$

The value of time interval during which the difference between «glued» time series $x(t)$ and $y(\theta)$ is less than $\varepsilon_2$, characterizes quality of the procedure of time series «gluing».

In Fig. 4 the dependance of the average value of $\Delta t$ on the delay time $T$ is represented. One can see that the average value of interval $\Delta t$ during which the glued time series becomes practically identical, does not depend on the chosen magnitude of a delay time $T$. Only at small delay times the average value $\Delta t$ diminishes.

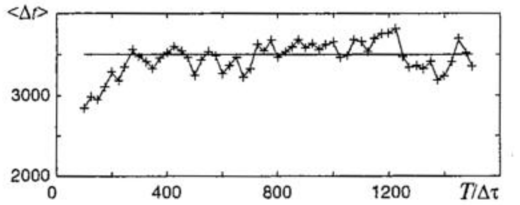

Fig. 4. Dependence of the average magnitude $\langle \Delta t \rangle$ on the value of a delay time $T$. Average was carried out on 300 points of «gluing»

The analysis of normalized distribution (see Fig. 5) of the magnitude of $\Delta t$ shows that at a delay time $T=1.6$ the part of «unsuccessfully» glued time series is minimal. In this case the number of glued time series with little interval $\Delta t$ is small. Simultaneously, the exploration carries out that with the increase of the delay time $T$ the number of glue points diminishes. Therefore the delay time for the procedure of gluing is chosen $T=1.6$. Besides, with such a choice of delay time $T=1.6$ the duration of time interval $(d-1) \cdot T$ becomes comparable with the typical oscillations time scale.

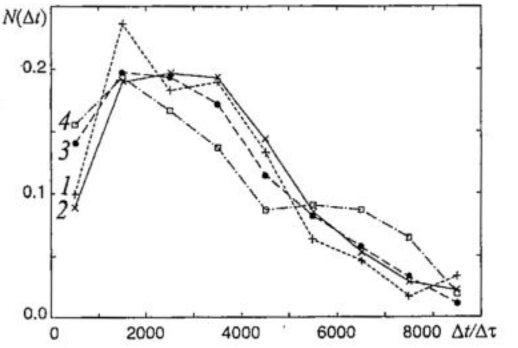

Fig. 5. Normalized distribution of $\Delta t$ at the different values of a delay time $T$: curve 1 (+) corresponds to the delay time $T=0.8$; curve 2 (×) - to the $T=1.6$; curve 3 (•) - to the $T=2.4$; curve 4 (□) - to the $T=3.2$. The allocations are constructed on 300 glued time series for each delay time $T$

Let's consider now the glued time series. On Fig. 6 the examples of the most successful ($a$) and unsuccessful ($b$) gluing with delay time $T=1.6$ are represented. One can see from the figure that even in case of «unsuccessful» glue the $y$-realization well agrees with the $x$-realization, with which it is glued.

The important circumstance is that all the time series used to construct the artificially long one are generated by the distributed system. Hence, that fact, that two time series are well glued, yet does not guarantee that the states of an initial distributed system are close in times $t_1$ and $t_2$ for $x$- and $y$-realizations, accordingly. Therefore it is necessary to consider the spatial distributions of amplitude of the field $|F(\xi)|$ and current $|I(\xi)|$ in gyro-BWO at the time corresponding to the points of glue of time series $x(t)$ and $y(\theta)$.

Fig. 7 illustrates the spatial distributions of the values $|F(\xi)|$ and $|I(\xi)|$ in the case of «successful» glue of time series at the chosen value of delay time $T$=1.6 (see also Fig. 6, *a*) and the corresponding distributions after the time $\Delta t_a$=30.09 passes and the $x$- and $y$-realizations dispersed on the distance $\varepsilon_2$. Similar dependences for the most «unsuccessful» glue are represented on Fig. 8 (see Fig. 6, *b*); the time interval $\Delta t_a$ is chosen the same $\Delta t_a$=30.09. In spite of the fact that in a case of unsuccessful glue of $x$- and $y$-realizations, the spatial distributions $|F(\xi)|$ and $|I(\xi)|$ explicitly differ from each other, these differences are quantitative but not

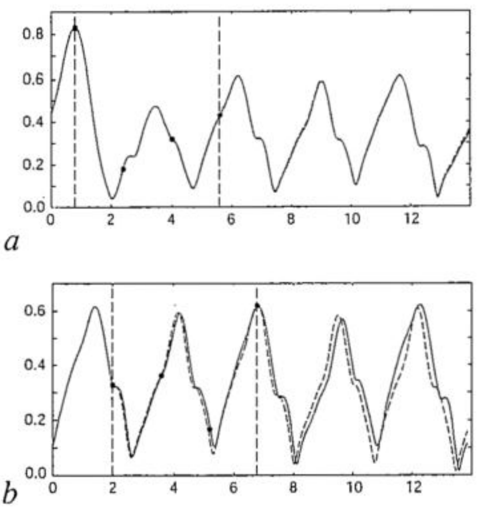

Fig. 6. Successful (*a*) and unsuccessful (*b*) gluing of the time series. The delay time in both cases $T$=1.6. Time interval $\Delta t$, during which the distinction between $x$- and $y$-realizations does not exceed the value $\varepsilon_2$, is equal to $\Delta t_a$=30.09 and $\Delta t_b$=0.28 time unities, accordingly. The vertical dashed lines restrict the time interval $(d\text{-}1)T$, on which the glue of the $x$- and $y$-time series is carried out. The circles (•) correspond to the points of gluing (see relation (11)). $x$-realization is shown by solid line, $y$-realization - by dashed one

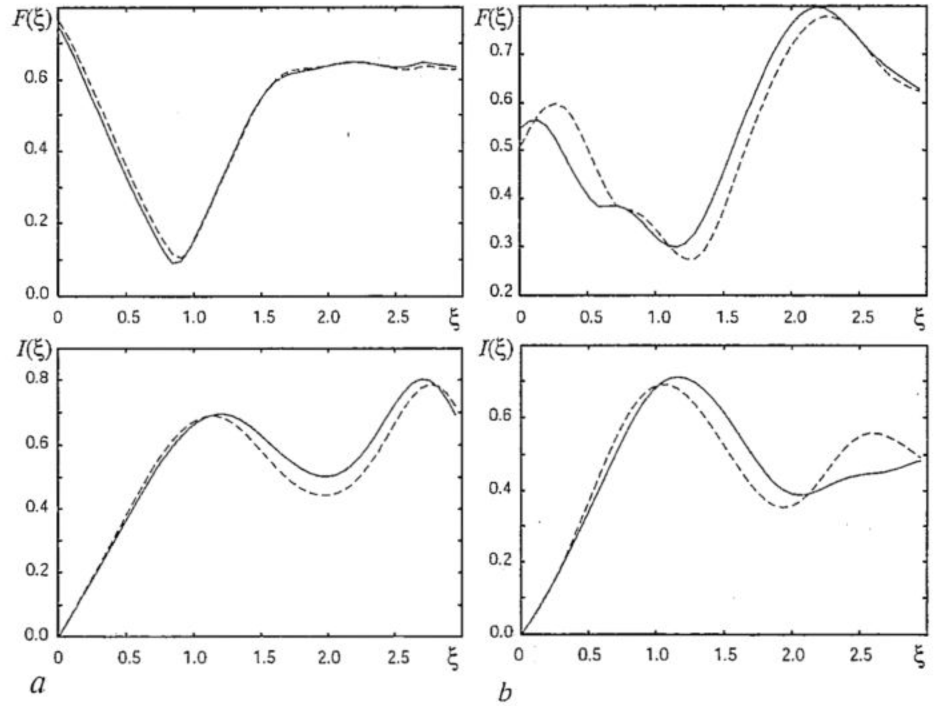

Fig. 7. Spatial distributions of the field amplitude $F$ and current $I$ for the case of «successful» glue of time series with $T$=1.6. The time series with initial amplitude $\Delta_0$=0.0041 (solid line) at time $\tau$=29.36 and $\Delta_0$=0.0012 (dashed line) at the time $\tau$=106.16 (Fig. *a*) are glued. The Fig. *b* illustrates the divergence of time series and corresponds to the time interval passed from the moment corresponding to Fig. *a*, $\Delta t_a$=30.09

qualitative. At the same time the structures existing in a distributed system which generates $x$- and $y$- realizations, at the moment of gluing agree with each other. In the case of «good» glue after the disperse of the two time series on distance $\varepsilon_2$ in both cases we derive the double-peak distribution of the first harmonic of the grouped current, what is equal to two electronic structures (two phase bundles of electrons - oscillators of the spiral beam) on the length of interaction space, though the value of the second maximum of the grouped current strongly differs in both cases.

For the case of «bad» glue of time series after the pass of the same time $\Delta t_a$, as in the first case, essentially stronger discrepancy of system dynamics takes place. Comparing the distributions introduced in Fig. 8, *a* and the Fig. 8, *b*, one can see that not only quantitative, but also qualitative distinction of the interior beam and field structures takes place. However, if we take the time interval $\Delta t_b$=0.28, through which the time series disperse on the distance $\varepsilon_2$, it is possible to make the same deduction, as earlier: the difference between states is only quantitative. Qualitatively the behaviour of the system is identical in both cases. Thus, the quality of gluing first of all renders influence on the length of the time interval $\Delta t$, during which it is possible to consider the two time series identical (compare the times $\Delta t_a$ and $\Delta t_b$ for the case of a good and bag glue accordingly). It is obvious, that the duration $\Delta t$ is defined, first of all, by quality of gluing, and, then, by the magnitude of the maximum Lyapunov index $\lambda_1$, which is the measure of the velocity of the disperse of neighboring phase trajectories of a chaotic set corresponding to transient chaos.

In a view of above-stated it is possible to make a deduction that the offered procedure of glue of truncated time series generated by a distributed system, allows to create a correct long time series, on which it is possible to determine the characteristics of transient chaos.

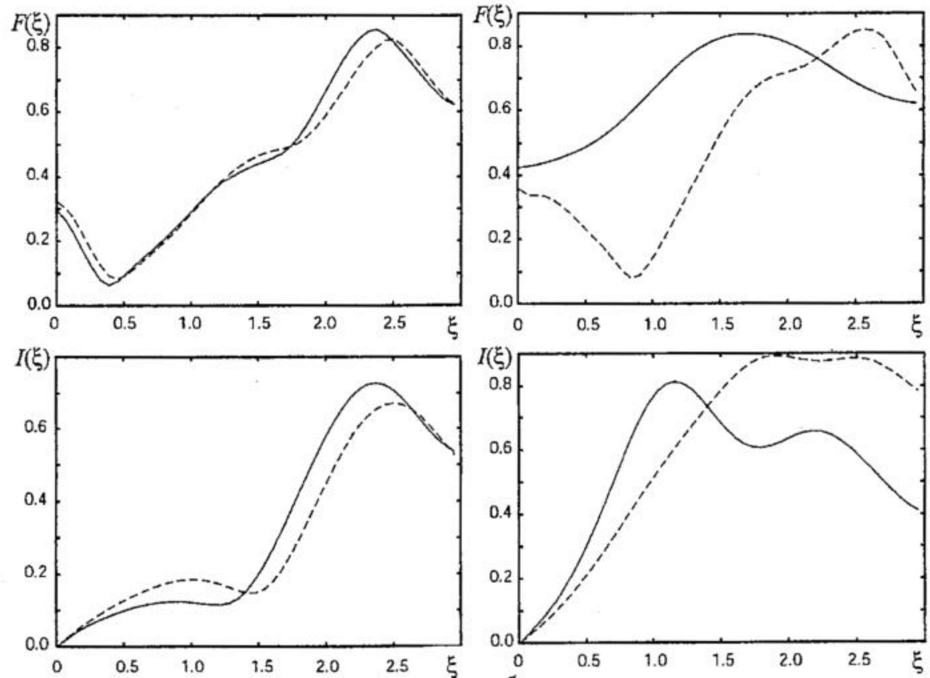

*a*

*б*

Fig. 8. Spatial distributions of the field amplitude $F$ and current $I$ for the case of «bad» glue of time series with delay time $T$=1.6. The time series with initial amplitude $\Delta_0$=0.0033 (solid line) at time $\tau$=54.97 and $\delta_0$=0.0012 (dashed line) at the time $\tau$=111.80 (Fig. *a*) are glued. The Fig. *b* illustrates the divergence of time series and corresponds to the time interval passed from the moment corresponding to Fig. *a*, $\Delta t_a$=30.09

## 4. Characteristics of transient chaos

Let's compare the results obtained at calculation of the correlation dimension of the attractor restored by «not glued» long time series at presence of false points, and the result calculated from correctly glued time series. For correct comparison the time series length $N=6\cdot 10^4$ and the number of points of reduction $M=10\cdot 4$ were chosen the same, as in the previous case. The results of calculation are represented in fig. 3, *b*, on which one can see the curves $D(\varepsilon)$ for the embedding space dimension $d=2,3,4$ and 5. It is obvious that the earlier obtained estimated results agree with the more precise calculation of correlation dimension. The embedding space dimension $d$ in this case also don't exceed 4. The last means that the pseudo-phase spaces dimension, evaluated in previous section, was chosen correctly.

Also it is possible to make a conclusion that for the estimation of correlation dimension of the attractor restored from short time series the procedure of glue is not required and the small number of false points in the phase space does not render essential influence to the calculation of correlation dimension.

Let's consider now such important characteristics of transient chaos as the maximum Lyapunov exponent $\lambda_1$. Its estimation was produced with the help of procedure offered in [28, 29]. According to it the magnitude of $\lambda_1$ is defined as

$$\lambda_1 = \lim_{t\to\infty}(1/t)\ \ln(\chi(t)/\chi(t_0)), \qquad (18)$$

where $\chi(t)$ is the distance between two points $\mathbf{x}'$ and $\mathbf{x}''$ in phase space at the time $t$. We suppose that at the initial time these points are close, i.e. $\|\mathbf{x}'-\mathbf{x}''\|=\chi(t_0)<<R$, where $R$ is the typical geometrical size of an attractor in phase space. The positive value of the maximum Lyapunov index $\lambda$ is evidence of the chaotic dynamics of the system. Through the time interval $\tau\approx\ln(R/\chi(t_0))/\lambda$ the behaviour of the system becomes unpredictable, i.e. the magnitude of the Lyapunov index characterizes the measure of instability and complexity of the chaotic process.

Now, keeping up for the system dynamics after starting from the points $\mathbf{x}'$ and $\mathbf{x}''$ and analyzing the distance $\chi(t_0+m\Delta\tau)=\|\mathbf{x}'(t_0+m\Delta\tau)-\mathbf{x}''(t_0+m\Delta\tau)\|$ between the current states of the system, we find the time interval $m\Delta\tau$, during which the trajectories disperse on the distance larger than $\chi_{\max}$. Then a new point $\mathbf{x}_m''$ on the attractor, which is close to the point $\mathbf{x}'(t_0+m\Delta\tau)(\|\mathbf{x}'(t_0+m\Delta\tau)-\mathbf{x}_m''\|=\chi(t_0+m\Delta t)<<R)$, also is moved from it to the direction of the vector $\mathbf{x}''(t_0+m\Delta\tau)-\mathbf{x}'(t_0+m\Delta\tau)$ is found. Then the procedure is repeated.

To define the value of the maximum Lyapunov index average on the attractor the above described procedure it is necessary to iterate $M$ times before reaching by magnitude

$$\langle\lambda_1\rangle = (1/M\Delta\tau)\ \Sigma_{m=1}^{M}\ln(\chi(t_0+m\Delta\tau)/\chi(t_0+(m-1)\Delta\tau)) \qquad (19)$$

the asymptotic value.

Using the above described procedure for the «correctly» glued time series we obtained the value of the maximum Lyapunov index $\lambda_1=0.098\pm0.011$.

Let's remark, that if we are moving a little bit to the area of the chaotic generation by changing the generation parameters $\Omega=0.1$, $F_0=0.62$ (let's remind that we have studied the transient chaos with $\Omega=2.0$, $F_0=0.62$), the typical characteristics of the chaotic attractor as the restored attractor and Fourier power spectrum are similar to the characteristics of the transient chaos.

However, the maximum Lyapunov exponent of the chaotic attractor $\lambda_1=0.002$. I.e. the chaotic set (transient chaos) is a more unstable (and, hence, more «chaotic») regime than the chaotic attractor existing «at neighbourhood» in the parameters space.

## Conclusion

In this work the transitional chaos found in non-autonomous distributed active medium «spiral electron beam - electromagnetic wave» (gyro-BWO, synchronized by external signal) near the boundary of synchronization tongue was investigated. The analysis of the characteristics of the transient chaos in explored distributed system was carried out. For this purpose we modified the procedure of combining of short time series generated by the distributed auto-oscillation system and obtained at the different starting conditions of integration of the model equations (2)-(6). Great attention was payed to the examination of the correctness of procedure of short time series «gluing» for the purpose of constructing an artificially long time series. It is possible to make a conclusion that the procedure of gluing offered in our paper is effective at constructing the long time series by a set of short time series generated by distributed systems.

*This work is supported by Russian Foundation for Basic Research, projects 01-02-17392, MAS 02-02-06067, 00-15-96673 and U.S. Civilian Research & Development Foundation for the Independent States of the Former Soviet Union (CRDF), grant REC-006.*

## References

1. *Nusinovich G.S., Walter M.* Linear theory of multistage forward-wave amplifiers // Phys.Rev.E. 1999. Vol. 60, № 4. P. 4811.

2. *Rodgers J., Guo H., Nusinovich G.S., Granatstein V.L.* Experimental Study of Phase Deviation and Pushing in a Frequency Doubling, Second Harmonic Gyro-Amplifier // IEEE Trans. on Plasma Sci. 2001. Vol. 48, № 10. P. 2434.

3. *Nusinovich G.S., Chen W., Granatstein V.L.* Analytical theory of frequency-multiplying gyro-travelling-wave-tubes // Phys.Plasmas. 2001. Vol. 8, № 2. P. 631.

4. *Nusinovich G.S., Sinitsyn O.V., Kesar A.* Linear theory of gyro-travelling-wave-tubes with distributed losses // Phys.Plasmas. 2001. Vol. 8, № 7. P. 3427.

5. *Nusinovich G.S., Vlasov A.N., Antonsen T.M.* Nonstationary Phenomena in Tapered Gyro-Backward-Wave Oscillators // Phys.Rev.Let. 2001. Vol. 87, № 21. 218301-1.

6. *Dmitriev A.Yu., Trubetskov D.I., Chetverikov A.P.* // Izv. vuzov. Radiofizika. 1991. Vol. 34, № 9. P. 595.

7. *Trubetskov D.I., Chetverikov A.P.* // Izv. vuzov. Prikladnaja Nelinejnaja Dinamika. 1994. Vol. 2, № 5. P. 3.

8. *McCurdy A.H.* Nonlinear theory of large-signal mode locking in a girotron oscillator // Appl.Phys.Let. 1995. Vol. 66, № 14. P. 1845.

9. *Trubetskov D.I., Hramov A.E.* // Tech.Phys.Let. (to be published).

10. *Grebogi C., Ott E., Yorke J.A.* Crises, sudden changes in chaotic attractors and chaotic transients // Physica D. 1983. Vol. 7. P. 181.

11. *T'el T.* // In: Directions in Chaos / Edited by Bai-lin Hao, Vol. 3, World Scientific, Singapore, 1990.

12. *J'anosi I.M., T'el T.* Time series analysis of transient chaos. Phys. Rev. E. 1994. Vol. 49. P. 2756.

13. *Yulpatov V.K.* // Voprosu radioelectroniki. Ser.I. Electronika. 1965. №12. P. 15.

14. *Yulpatov V.K.* // Voprosu radioelectroniki. Ser.I. Electronika. 1965. №12. P. 24.

15. *Bratman V.L., Novogilov S.L., Petelin M.I.* // Electronnaja Tekhnika. Ser. I. Electronika SVCH. 1976. № 11. P. 46.

16. *Chu K.R., Chen H.Y., Hung C.L., Chang T.H., Barnett L.R.* Ultrahigh Gain Gyrotron Traveling Wave Amplifier // Phys.Rev.Let. 1998. Vol. 21, № 21. P. 4760.

17. *Kyznetsov S.P., Trubetskov D.I.* / Backward Wave Oscillators Electronics. Saratov: SSU Press, 1975. P. 135. (In Russian)

18. *Koronovskii A.A., Trubetskov D.I., Hramov A.E.* // Izv. vuzov. Radiofizika (to be published).

19. *Koronovskii A.A., Trubetskov D.I., Hramov A.E.* // Izv. vuzov. Prikladnaja Nelinejnaja Dinamika (to be published).

20. *Trubetskov D.I., Hramov A.E.* // Journal of Communication Technology and Electronics (to be published).

21. *Grassberger P., Procaccia I.*Characterization of Strange Attractors. Phys. Rev.Lett. 1983. Vol. 50. P. 346.

22. *Grassberger P., Procaccia I.* Measuring the Strangeness of Strange Attractors, 1983. Physica 9D. P. 189.

23. *Dhamala M., Ying-Cheng Lai, Kostelich E.J.* Analyses of transient chaotic time series // Phys.Rev.E. 2001. Vol. 64 056207.

24. *N.H. Packard, J.P. Crutchfield, J.D. Farmer and R.S. Shaw.*Geometry from a Time Series, Phys. Rev. Lett. 45 (1980) 712-716.

25. *Takens F.* Detecting Strange Attractors in Turbulence // Proceedings of the Symposion on Dynamical Systems and Turbulence, University of Warwick, 1979 (1980, edited by D.A. Rand and L.S. Young (Springer, Berlin, 1981).

26. *Babin A.V., Vishik M.I.* // Yspekhi Matematicheskikh Nayk. 1983. Vol. 38, № 4. P. 133.

27. *Kipchatov A.A., Krasichkov L.V.* On Reconstruction of Chaotic Attractor from Time Series Represented as «Clusters» // Proceedings of the International Conference on Dynamical Systems and Chaos, edited by Aizawa Y., Saito S. and Shiraiwa K., Singapore: World Scientific. Vol. 2. 1995. P. 355.

28. *Wolf A., Swift J., Swinney H.L., Vastano J.* Determining Lyapunov exponents from a time series // Physica D. 1989. Vol. 16. P. 285.

29. *Elsmann J.-P., Kamphorst S.O., Ruelle D., Gilberto D.* Lyapunov exponents from a time series // Phys.Rev.A. 1986. Vol. 34. P. 4971.

*Saratov State University*

*Received 17.07.2002*

---

УДК 621.385

# ИССЛЕДОВАНИЕ ПЕРЕХОДНОГО ХАОСА В ГИРОЛАМПЕ СО ВСТРЕЧНОЙ ВОЛНОЙ, СИНХРОНИЗИРУЕМОЙ ВНЕШНИМ СИГНАЛОМ

*Храмов А.Е., Короновский А.А., Ремпен И.С., Трубецков Д.И.*

В работе изучается переходный хаос в неавтономной распределенной активной среде (гиролампа со встречной волной (гиро-ЛВВ), синхронизируемая внешним сигналом). Исследуются характеристики переходного хаоса в гиро-ЛВВ вблизи границы области синхронизации. Особое внимание уделяется проблеме построения искусственной длинной временной реализации, по которой оцениваются характеристики хаотической динамики, и которая строится путем сшивания коротких временных реализаций, характеризующих переходный хаос, порождаемый распределенный системой.

*Hramov Alexander Evgen'evich* was graduated from the Physical Department of the Saratov State University in 1996. Now he is the Associate Professor of the chair of Electronics, Oscillations and Waves of Nonlinear Processes Department. The area of scientific interest is nonlinear dynamics of distributed electron and plasma systems and also the methods of modelling and analysis of the nonlinear systems. He has many scientific publications in Russian and foreign journals.

*Koronovskii Alexei Alexandrovich* was born in 1972, graduated from the Physical Department of the Saratov State University in 1995. Now he is the Associate Professor of the chair of Electronics, Oscillations and Waves. His scientific interest is connected with nonlinear dynamics and its applications in different spheres of life, including socio-economical processes. Koronovskii is the author and co-author of many scientific publications, including the educational edition «Non-linear dynamics in actions» (together with D.I. Trubetskov: Saratov, 1995; the 2nd edition - 2002).

*Rempen Irina Sergeevna* was born in 1974, graduated from the Physical Department of the Saratov State University in 1996. Now she is the lecturer at the chair of Electronics, Oscillations and Waves. The area of scientific interest is a modelling and analysis of nonlinear dynamics of distributed systems.

*Trubetskov Dmitry Ivanovich* was born in 1938, graduated from Saratov State University (SSU) in 1960. He is a Doctor of Science in Physics and Mathematics since 1978, Corresponding Member of RAS, Head of Chair of Electronics, Oscillation and Waves SSU, Rector of SSU. His scientific interests include electronics of ultrahigh frequencies, quantum electronics, methods of mathematical optimization, theory of wave processes, theory of vacuum microelectronic devices, high-frequency relativistic electronics, chaos and structures. He is the supervisor of studies Liceum of Applied Sciences SSU, the author of a lot of papers and monographs. E-mail:Trubetskov@cas.ssu.runnet.ru

Izv. VUZ «AND», vol.10, № 3, 2002

# CLUSTER AND GLOBAL SYNCHRONIZATION IN A QUASI-HARMONIC SELF-OSCILLATORY CHAIN IN THE PRESENCE OF NOISE

*T.E. Vadivasova, V.S. Anishchenko, G.I. Strelkova, A.I. Fomin*

We study numerically effects of noise on synchronization phenomena in a chain of Van der Pol oscillators. A structure of frequency clusters in the non-homogeneous noisy chain is analyzed. We generalize the notion of effective synchronization to the case of a spatially extended system. The effect of amplitude relations on the phase dynamics is also explored. The possibility of realizing external synchronization of the homogeneous chain was considered. We clear up a role of two components of coupling (diffusive and one-direct coupling) and a noise sources in relation to the global synchronization.

## 1. Introduction

The phenomenon of synchronization plays an important role in the behavior of ensembles of interacting nonlinear oscillators. This effect provides the basis for self-organization of ensembles' dynamics and is associated with a variety of phenomena, such as multistability, growth restriction of the Kolmogorov entropy and attractor dimension, spatio-temporal structure formation, etc. The theory of synchronization, originally proposed for quasi-harmonic oscillations [1-4], was generalized to a wide range of systems including chaotic [5-11] and stochastic [11-15] ones.

Phase synchronization in ensembles of locally and globally coupled interacting periodic oscillators has been studied for a long time but these investigations still attract a growing interest of many researchers [4, 16-29]. Ensembles of periodic oscillators have found wide applications in mathematical modeling of physical [30-33], chemical [4, 16], and biological [34-38] processes.

Even the simplest quasi-harmonic oscillators coupled in a large ensemble generate a lot of complicated nonlinear effects such as a phase and frequency synchronization [20, 23, 24, 28, 29, 35, 40], an oscillatory death [21, 22, 27, 29, 40, 41], frozen states [28], formation of a collective chaotic behavior [27, 33, 39] e.t.c. All these effects are the manifestations of the phase - frequency synchronization phenomena.

It is known that fluctuations are inevitably present in real ensembles and a parameter mismatch (random or definitely specified) of partial systems also takes place. Effects of noise and parameter mismatch on phase locking in an ensemble of oscillators are considered in [4, 17, 18, 20-22, 24, 25, 29, 31, 40, 42, 43]. The presence of a linear gradient of native unperturbed frequencies along the medium consisting of locally coupled oscillators leads to the formation of so-called frequency clusters of synchronization [20, 29, 40].

Recently, numerous works have appeared devoted to the study of ensembles of chaotic oscillators [30, 44-52]. It has been shown that the synchronization effect also plays an important role in the dynamics of chaotic ensembles. They demonstrate a number of phenomena which appear to be quite similar to those occurred in ensembles of periodic oscillators. Particularly, effects of phase-locking and cluster phase synchronization have been found in ensembles of chaotic oscillators [50-52]. This fact testifies that the effect of synchronization is generic for a variety of oscillatory systems.

However, even in the case of quasi-harmonic oscillatory ensembles it remains a number of unresolved problems, which devote a special attention. One part of these problems concerns the cluster synchronization in a chain of non-identical oscillators. How much can cluster synchronization be stable to the influence of fluctuations? Is it possible to generalize the notion of effective synchronization of self-sustained oscillations in the presence of noise [54, 55] to spatially extended systems? It is interesting to elucidate how significant may it be if a variation of instantaneous amplitude values of oscillators is taken into consideration? Can the behavior of an ensemble be qualitatively described by the phase equations only? The other part of the problems is connected with the global external synchronization of a chain (i.e. the synchronization of all oscillators of the chain at the external frequency force). What are the conditions of global synchronization of the chain by a harmonic external force applied to the first oscillator? How does the type of coupling between oscillators influence on the global synchronization effect? Is the global synchronization possible in the presence of noise?

Some of these problems were considered in [56, 57]. In the present work we try to answer the above stated questions and this is the main objective of this paper.

The paper is organized as follows. In Sec. I we study the effects of cluster synchronization in a chain of non-identical Van der Pol oscillators with diffusive coupling. The effect of noise on clusters structure is analyzed. In Sec. II we explore the peculiarities of the behavior of the chain of diffusively coupled non-identical Van der Pol oscillators described by the phase equations only. Sec.III is devoted to the external synchronization of a chain of identical Van der Pol oscillators with a harmonic force applied to the first element of the chain. The role of two coupling components (diffusive and one-direct) is discussed. The global synchronization of the chain in the presence of noise is studied. And finally, we give our conclusions in Sec. IV.

## 2. Effect of noise on cluster synchronization in a chain of non-identical Van der Pol oscillators

The model to study is a chain of Van der Pol oscillators, being similar to that considered in [29, 40] and including additive noise on the chain elements. The chain is described by a system of equations which, in a truncated form, are as follows:

$$\dot{\rho}_j = r(1-\rho_j^2)\rho_j + g(\rho_{j-1}\cos(\phi_j-\phi_{j-1}) + \rho_{j+1}\cos(\phi_{j+1}-\phi_j) - 2\rho_j) + D/\rho_j + (2D)^{1/2}\xi_j(t), \tag{1}$$

$$\dot{\phi}_j = \omega_j + g(\rho_{j+1}/\rho_j \sin(\phi_{j+1}-\phi_j) - \rho_{j-1}/\rho_j \sin(\phi_j-\phi_{j-1})) + (2D)^{1/2}\eta_j(t)/\rho_j,$$

$$j = 1, 2, 3, \ldots, m,$$

where $j$ is the number of an oscillator, representing a discrete spatial coordinate, $\rho_j$ and $\phi_j$ are the amplitude and the phase of oscillations of the $j$th oscillator, respectively. $\xi_j(t)$ and

$\eta_j(t)$ are assumed to be identical uncorrelated Gaussian white noise sources with zero means and with the same intensity $D$*.

The boundary conditions were chosen to correspond to a free-ended chain, i.e., $\rho_0=\rho_1$, $\phi_0=\phi_1$, $\rho_{m+1}=\rho_m$, $\phi_{m+1}=\phi_m$. The initial conditions for the oscillators are chosen to be close to homogeneous ones with a small random dispersion within $\delta=0.1$.

The model (1) has the following parameters: $r$ is the excitation parameter (in computation, we fix $r=0.5$), $\omega_j$ is the unperturbed frequency of the $j$th oscillator, i.e., oscillation frequency without coupling and external forcing, $g$ is the parameter of diffusive coupling of nearest-neighbor oscillators. For the model (1) we suppose a case of linear dependences of the unperturbed frequencies on spatial coordinate $j$, i.e., $\omega_j=\omega_1+(j-1)\Delta$, where $\Delta$ is the frequency mismatch of two neighboring oscillators. The peculiarities of the chain dynamics do not depend on the choice of the frequency origin. Therefore, we can set $\omega_1=1$.

We study numerically the chain (1) with $m=100$ elements using a fourth-order Runge-Kutta routine. In the course of numerical experiments, we analyze the dynamics of each element, estimate the variation of phases $\phi_j$ during a large enough time $T$ and compute the average (perturbed) frequencies $\tilde{\omega}_j$ of the partial oscillators:

$$\tilde{\omega}_j = \langle \dot{\phi}_j(t) \rangle = \lim_{T\to\infty} [(\phi_j(t_0+T) - \phi_j(t_0))/T\,]. \tag{2}$$

The angle brackets mean time averaging.

Equality of the mean frequencies $\tilde{\omega}_j$ and $\tilde{\omega}_{j+1}$ corresponds to the limitation of the phase difference of the oscillators $\theta_j=\phi_{j+1}(t)-\phi_j(t)$ in time:

$$\lim_{t\to\infty} |\theta_j(t)| < M, \quad \text{where } 0 \neq M \neq \infty. \tag{3}$$

The condition (3) is the generalization of the phase locking definition [9]. So defined phase locking notion may be applied not only to harmonic oscillations but also to non-periodic selfsustained oscillations. The group of oscillators $(j=k_1,\dots,k_2)$ synchronized in the sense (3) is named as a frequency cluster. The instant values of the frequencies $\dot{\phi}_j(t)$ of partial oscillators belonging to the same cluster may be different but their time averaged values $\tilde{\omega}_j$ must be equal.

For the chain (1) with a linear frequency gradient along the spatial coordinate $j$, one can observe frequency cluster formation in a certain range of coupling parameter $g$ values [29, 40]. The partial oscillators exhibit the quasi-periodic oscillations $x_j(t)=\rho_j(t)\cos\phi_j(t)$ and $y_j(t)=\rho_j(t)\sin\phi_j(t)$, and the number of independent frequencies is determined by the number of synchronized clusters. Fig. 1, *a*, *b* illustrate $(x_j,y_j)$ projections of oscillations in the regime of cluster synchronization, which are characteristic for the center and the boundary of a cluster, respectively. If we consider the oscillators within the same cluster, then a representative point rotates around the origin, $x_j=0$, $y_j=0$, on the average, with the same frequency and a bounded phase shift. Oscillators belonging to different clusters have distinct rotation frequencies. Consequently, the form of phase projections $(x_j,x_k)$ is qualitatively different when $j$th and $k$th oscillators belong to one cluster (Fig. 1, *c*) and to different clusters (Fig. 1, *d*).

Now we are going to elucidate how the noise influences the cluster synchronization. We fix $\Delta=0.002$ and compute the distribution of perturbed frequencies

---

* In fact, in numerical experiments the same pseudo-random number generator was used having a Gaussian distribution. Successive values produced by the generator may be treated as practically independent. To make sure that the noise disturbances are uncorrelated, the noise source added to each subsequent element of the chain was shifted with respect to the previous one by five iterations of the pseudo-random number generator.

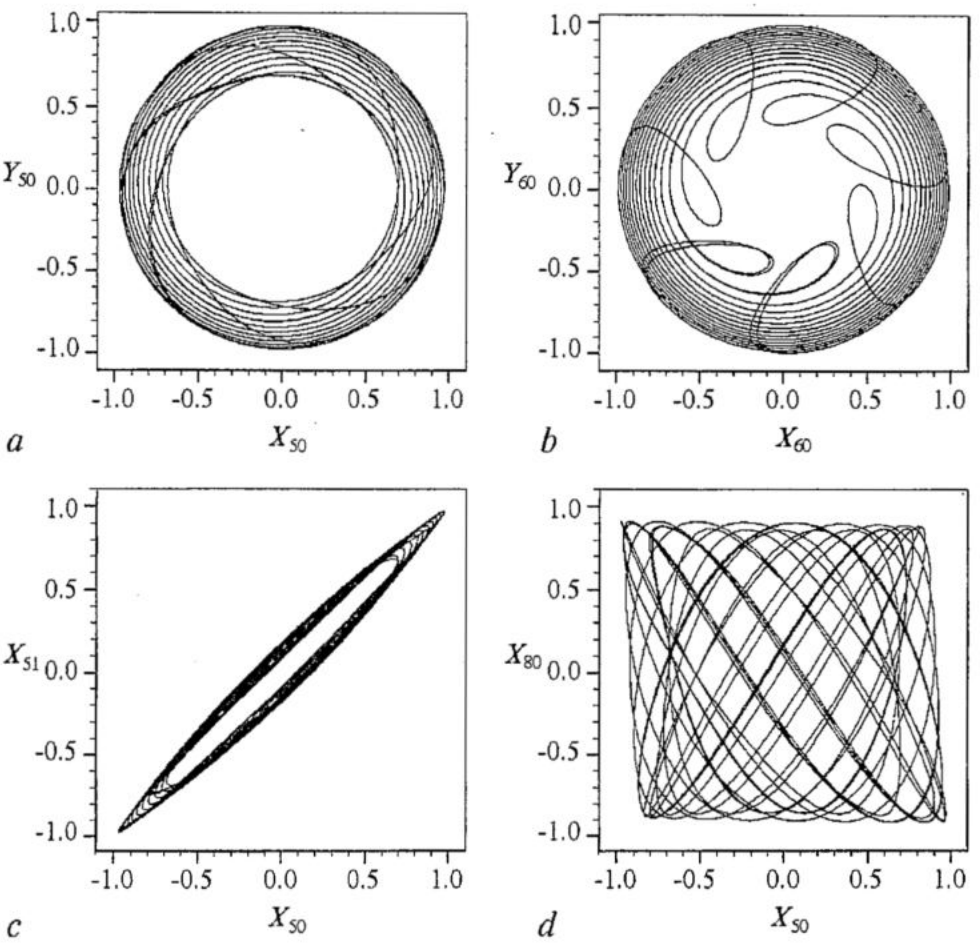

Fig. 1. Phase projections of oscillations of partial oscillators in the regime of cluster synchronization for $\Delta$=0.002 and $g$=3.8

$\tilde{\omega}_j$ of oscillators along the chain without and in the presence of noise. The calculation results, shown in Fig. 2, *a* (I), *b* (I) for two different values of the coupling parameter $g$, clearly demonstrate the effect of cluster synchronization in the noise-free chain ($D$=0) and completely correspond to the analogous results presented in [29, 40].

Now consider the case when all oscillators are subjected to noisy perturbations. Fig. 2, *a* (II), *b* (II) and *a* (III), *b* (III) presents the distributions of the perturbed frequencies for two different noise intensities $D$=0.00001 and $D$=0.001, respectively. It is clearly seen that for both coupling parameters, the clusters of synchronization are destroyed as the noise intensity increases. If the noise is weak, the clusters' boundaries are only smoothing slightly (graphs II). Both smoothing and gradual destruction of the clusters begin with the chain center. For sufficiently large noise (graphs III), all middle clusters are completely destroyed. However, our computations have shown that the first and the last clusters appear to be highly stable to noisy disturbances and only a very strong noise is needed to destroy them.

The effect of noise on cluster synchronization can be more clearly understood by considering how the phase differences $\theta_j(t)$ of neighboring oscillators, located near the clusters boundary, change with time without and in the presence of noise. Without noise,

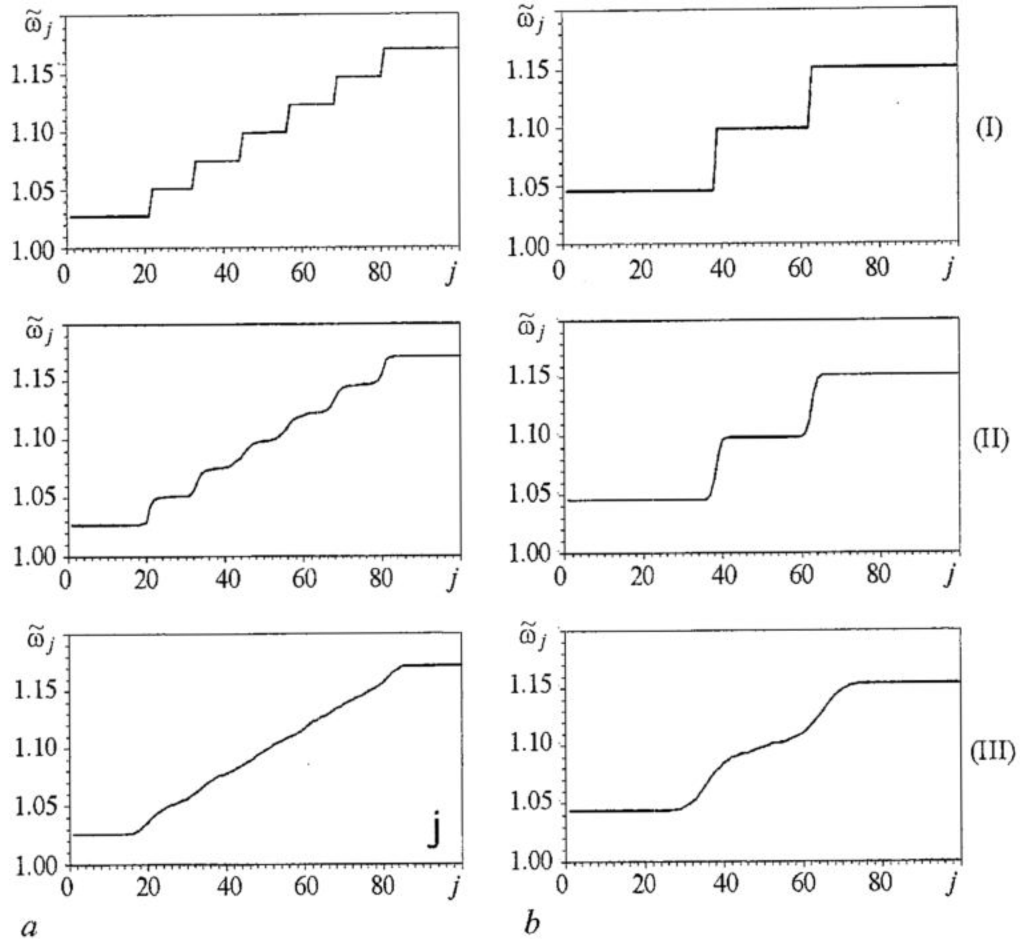

Fig. 2. Distributions of the perturbed oscillator frequencies for $\Delta$=0.002 and for different strengths of coupling: (a) $g$=0.55; (b) $g$=3.8. Dependences (I), (II) and (III) are obtained for the chain in the presence of noise with intensity $D$=0, $D$=0.00001, and $D$=0.001, respectively

the phase difference of oscillators belonging to different clusters increases, on the average, linearly as the time goes on. At the same time, the phase difference remains strictly bounded if the oscillators considered belong to the same cluster. When the noise is added, the phase difference of any neighboring oscillators grows indefinitely with time but this growth is linear for none of $j$. The average growth rate of phase difference is different for different $j$. This fact allows one to find certain segments of the chain, for which this rate is low. Hence, we can identify clusters of effective synchronization in the presence of noise [55].

The clusters' boundaries in the presence of noise can be estimated by using the effective diffusion coefficient $D_{\text{eff}}$ of the phase difference of neighboring oscillators [54]. $D_{\text{eff}}$ defines the average rate with which the variance $\sigma_{\theta_j}^2(t)$ of phase difference $\theta_j$ increases in time. Its mean value can be calculated as follows:

$$\begin{aligned} D_{\text{eff}}(j) &= \lim_{t\to\infty} \tfrac{1}{2}\big((\sigma^2_{\theta_j}(t) - \sigma^2_{\theta_j}(t_0))/(t - t_0)\big), \\ \sigma^2_{\theta_j}(t) &= \langle\theta_j^2(t)\rangle - \langle\theta_j(t)\rangle^2. \end{aligned} \tag{4}$$

We compute the effective diffusion coefficient versus the spatial coordinate within one cluster (39≤$j$≤62) for three different values of noise intensity $D$. Numerical results are presented in Fig. 3. They testify a gradual destruction of the clusters boundaries as the noise intensity increases. One can note that the dependence $D_{\text{eff}}(j)$ is quite similar (taking into account that $j$ is a discrete variable) to a well-known dependence of the diffusion coefficient of the phase difference between a self-sustained system and an external forcing versus detuning. The clusters boundaries of effective synchronization can be defined by specifying some tolerable level of the diffusion coefficient $D_{\text{eff}}^{\max}$. In this case oscillators for which $D_{\text{eff}} \leq D_{\text{eff}}^{\max}$ can be considered as belonging to the same cluster. Such a determination of clusters boundaries is enough arbitrary since the value of $D_{\text{eff}}^{\max}$ can be given in different ways depending on a particular task. However, in any case the length of a cluster decreases with increasing noise intensity. For example, given $D_{\text{eff}}^{\max}=0.001$, the boundaries of the cluster shown in Fig. 3 for $D=0.0001$ correspond to the 44th and the 56th oscillators.

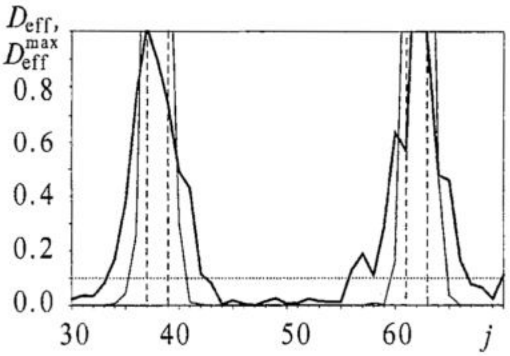

Fig. 3. Effective diffusion coefficient $D_{\text{eff}}$ as a function of spatial coordinate $j$ for $D=10^{-8}$ (*thin dashed line*), $D=10^{-5}$ (*thin solid line*), and $D=10^{-4}$ (*thick solid line*). The horizontal dotted line marks the level of $D_{\text{eff}}^{\max}$, defining the clusters boundaries. The detuning and the coupling strength are $\Delta=0.002$ and $g=3.8$

## 3. Phase dynamics approach

In the previous section we have numerically studied the chain of Van der Pol oscillators, which is described by the system of truncated equations (1) where amplitude and phase dynamics are combined. However, in many cases only phase equations are often used assuming amplitudes to be equal and constant in time. Such an approach allows one to qualitatively describe effects of frequency and phase locking and to simplify numerical simulation. Besides, in some cases the problem can be solved analytically using the phase equations only [4, 16, 20, 24, 25, 27]. Nevertheless, the dynamics of an ensemble may be distorted and some effects may be lost such as, for example, «oscillator death» [21, 22, 29, 53], if the amplitude dynamics is excluded from consideration. In particular, as emphasized in [29, 40], amplitude effects may influence the cluster structure formation. To reveal such an effect, we analyze first cluster synchronization in the enforced chain described by the phase equations only and then compare it with relevant results obtained for the full system of truncated equations (1). The system of phase equations can easily be derived from (1) by setting $\rho_j=1$ for any $j$. This means that the amplitudes of all oscillators are taken to be equal to their unperturbed value. The system of phase equations reads:

$$\dot{\phi}_j = \omega_1 + (j-1)\,\Delta + g(\sin(\phi_{j+1} - \phi_j) - \sin(\phi_j - \phi_{j-1})) + (2D)^{1/2}\eta_j(t), \quad j = 1,2,\ldots,m. \qquad (5)$$

The boundary conditions corresponding to free ends are: $\phi_0=\phi_1$, $\phi_{m+1}=\phi_m$. The detuning is fixed as $\Delta=0.002$. The frequency distributions calculated from (5) are shown in Fig. 4 for different strengths of coupling. The first three plots correspond to the noise-free case. In Fig. 4, *a* illustrating the frequency distribution for $g=0.55$ only two clusters can be observed being formed at the boundaries of the chain. The analogous distribution, presented in Fig. 1, *a* (I) for the full system (1), reflects a more rich synchronization picture. With increasing strength of the coupling the middle clusters also appear (Fig. 4, *b*, *c*) but their structure is somewhat different from that formed when integrating the system (1). As seen from Fig. 4, *b*, *c*, the extreme clusters are extended, while the middle

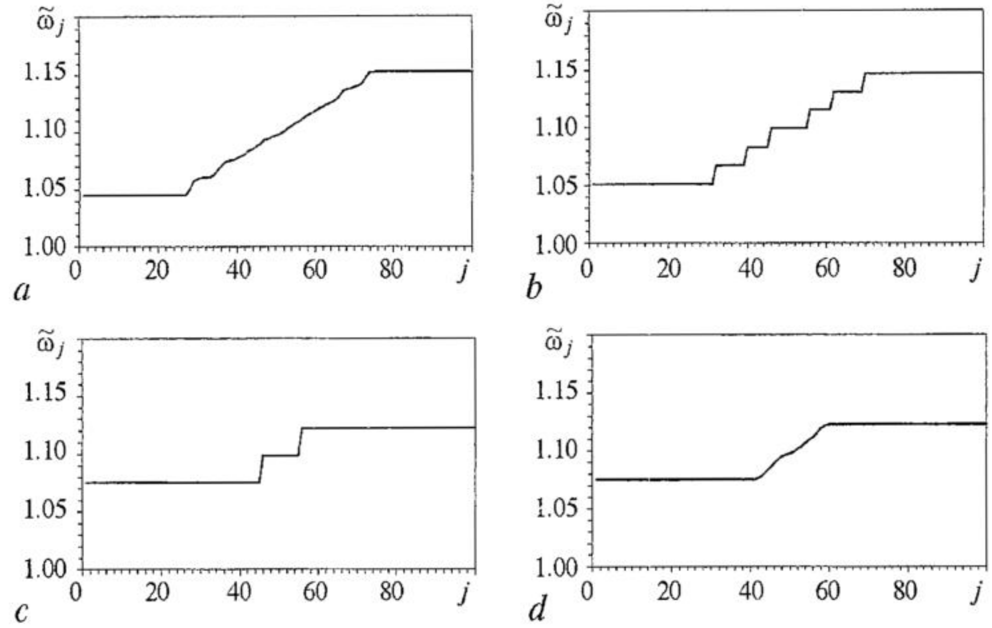

Fig. 4. Distributions of the perturbed frequencies in the chain, described by the phase equations (5), for $\Delta=0.002$ and for different strengths of the coupling: *a*) $g=0.55$; *b*) $g=0.7$; *c*) $g=1.5$ without noise, and *d*) $g=1.5$ in the presence of noise with intensity $D=0.00001$

ones become more shorter. The height of clusters' steps, i.e., the difference between the frequencies of neighboring clusters, is less than that for system (1) and decreases rapidly as the strength of coupling increases. Thus, the region of cluster synchronization significantly shrinks when only phase dynamics is taken into consideration. Moreover, in this case the cluster structure appears to be more sensitive to noise perturbations. This is illustrated in Fig. 4, *d* when a weak noise of intensity $D=0.00001$ is added to the system (5). As follows from the figure, the noise causes the middle clusters to be destroyed.

## 4. External synchronization of a chain of identical Van der Pol oscillators

To study effects of external synchronization in a chain of quasi-harmonic self-sustained oscillators we use the following model:

$$\begin{aligned}\dot{\rho_j} &= 0.5(1-\rho_j^2)\,\rho_j + g_1(\rho_{j-1}\cos(\phi_j-\phi_{j-1}) + \rho_{j+1}\cos(\phi_{j+1}-\phi_j) - 2\rho_j) + \\ &+ g_2(\rho_{j-1}\cos(\phi_j-\phi_{j-1}) - \rho_j) + D/\rho_j + F_j(t), \\ \dot{\phi}_j &= \omega_j + (g_1/\rho_j)\,(\rho_{j+1}\sin(\phi_{j+1}-\phi_j) - \rho_{j-1}\sin(\phi_j-\phi_{j-1})) - \\ &- g_2(\rho_{j-1}/\rho_j)\sin(\varphi_j - \phi_{j-1}) + P_j(t),\ j=1,2,3\ldots m.\end{aligned} \tag{6}$$

Here the same signs are used as in the model (1). The functions $F_j(t)$ and $P_j(t)$, $j=1,2,\ldots,m$, describe forces which are applied to the oscillators of the chain. These forces include independent sources of Gaussian $\delta$-correlated noise $\xi_j(t)$ and $\eta_j(t)$ for all oscillators of the chain, and also the harmonic force applied only to the first oscillator. So, $F_j(t)$ and $P_j(t)$ are

$$F_1(t) = C\sin(\omega_{ex}t - \phi_1) + (2D)^{1/2}\xi_1(t),$$
$$P_1(t) = (-C/\rho_1)\cos(\omega_{ex}t - \phi_1) + (2D)^{1/2}\eta_1(t)/\rho_1,$$
$$F_j(t) = (2D)^{1/2}\xi_j(t),\ \ P_j(t) = (2D)^{1/2}\eta_j(t)/\rho_j,\ \ j = 2,3\ldots m,$$

where $D$ is the intensity of noise sources, $C$ and $\omega_{ex}$ are the amplitude and the frequency of the external force, respectively. The boundary conditions are chosen as: $\rho_0=\rho_1$, $\phi_0=\phi_1$, $\rho_{m+1}=\rho_m$, $\phi_{m+1}=\phi_m$. The initial conditions for the oscillators are chosen to be close to homogeneous ones ($\rho_j(0)=0.5$, $\phi_j(0)=0.1$) with a small random dispersion within $\delta=0.1$.

The parameters of the chain are the unperturbed frequencies of partial oscillators $\omega_j$, the external force parameters (amplitude $C$ and frequency $\omega_{ex}$), the coupling parameters $g_1$ and $g_2$, and also the noise intensity $D$. In the model (6) two types of coupling are used: diffusive coupling and one-direction coupling. So, $g_1$ is the diffusion coefficient, and $g_2$ characterizes a propagation of perturbations along the chain.

Let us consider first the effects of external synchronization in the homogeneous chain (6) with fixed length $m=100$ without noise sources ($D=0$). The homogeneous chain consists of identical elements. So, we suppose that $\omega_j=\omega_0=1$, $j=1,2,\ldots m$. The value $\Delta_{ex}=\omega_{ex}-\omega_0$ determines the mismatch of the excitation frequency from the unperturbed frequencies of oscillators. We also introduce the phase differences $\theta_j(t)=\phi_{j+1}(t)-\phi_j(t)$, $\theta_{ex}(t)=\omega_{ex}t-\phi_1(t)$. A perfect phase locking of oscillators on the main tone is given by the following conditions:

$$\dot{\theta}_j \equiv 0,\quad \dot{\theta}_{ex} \equiv 0,\quad \dot{\rho}_j \equiv 0,\quad j = 1,2,\ldots m. \tag{7}$$

In this case the phase differences are constant, and the oscillations are harmonic with the period equal to the period of the external force. According to a more general definition of the phase locking [9] only the phase differences limitation (3) are needed.

The synchronization of the $j$-th oscillator on the external frequency was detected numerically by the condition

$$|p_j - 1| \leq 10^{-4}, \tag{8}$$

where $p_j=\tilde{\omega}_j/\omega_{ex}$ is the relative mean frequency (winding number) of the $j$-th oscillator. We consider the validity of condition (8) for all oscillators of the chain as a numerical criterium of a global synchronization of a chain (i.e. synchronization of all chain elements). In the case of global synchronization the condition (7) must also be valid for all oscillators. If only a part of oscillators is synchronized, the oscillations are not perfectly periodic (as in the case of frequency clusters exist). In this situation the synchronization in the sense of (8) does not correspond to (7).

We will study a region of the global synchronization as the parameters $\Delta_{ex}$, $C$, $g_1$, $g_2$ are varied. Disregarding perturbations of the partial amplitudes $\rho_j$ it is possible to estimate the region of global synchronization. Supposing in (6) that $\rho_j=1$, $j=1,2,\ldots m$ we obtain from (7) the approximate synchronization conditions:

$$C \leq |\Delta_{ex}|\,(g_1+g_2)\,/\,g_2;\quad |\Delta_{ex}| \leq g_2. \tag{9}$$

The equality $C=|\Delta_{ex}|(g_1+g_2)/g_2$ at $|\Delta_{ex}|\leq g_2$ determines the external synchronization boundary of the first oscillator of the chain, assuming that all elements of the chain are mutually synchronized. The equality $|\Delta_{ex}|=g_2$ at $C\leq|\Delta_{ex}|(g_1+g_2)/g_2$ corresponds to the boundary of mutual synchronization of all chain elements in condition that the first oscillator is synchronized with the external force. The estimation of the global synchronization region in accordance with (9) does not reflect the dependence of synchronization effect on a chain length $m$. Notwithstanding, in some cases these estimations agree rather well with results of numerical simulations. The conditions (9) result in the impossibility of global synchronization of the chain with purely diffusive interaction of oscillators ($g_2$=0). On the contrary, numerical simulation shows that the finite length chain can be synchronized. But the synchronization region is very small even for a short chain ($m$=10-20).

The calculation results of the global synchronization boundaries are given in Fig. 5, *a*. The global synchronization region $S$ is obtained for a chain with $m$=100 elements on the parameter plane ($\Delta_{ex}$,$C$). The signs (∘) and (∗) mean the numerically obtained points of a boundary for the cases of one-direction and combined coupling, respectively. Dashed lines mark the boundaries described by (9). The estimation (9) for the case of Fig. 5, *a* is in a well agreement with the numerical data. When a diffusive component of coupling prevails the one-direction coupling, then a distribution of partial amplitudes $\rho_j$ influences essentially on the dynamics of phases $\phi_j$. In these circumstances relations (9) do not give a satisfactory estimation for synchronization boundaries. As it follows from simulation data, there exists a certain maximal value of the diffusive coupling parameter value $g_1^{max}$ when global synchronization is yet possible in a chain of any length. Fig. 5, *b* shows the numerically calculated values of a half-width band $\Delta_s$ of global synchronization as functions of a chain length at fixed external amplitude and different coupling component relations. The signs (∘), (∗), (×) mark the results for the cases of one-direction coupling, combined coupling and purely diffusive coupling, respectively. It is well seen that the value $\Delta_s$ tends to the certain constant level as the $m$ increases. For $m \geq 20$ a value of $\Delta_s$ does not practically depend on the next increasing of a chain length. So, it is reasonable to suppose that in the presence of one-direction interaction of oscillators directed from an external excited element, a global synchronization can be observed for the chain of an infinite length. It takes place in the band of external frequencies of nonzero width. This width essentially depends on the relationship between the coupling parameters $g_1$ and $g_2$. As the diffusive coupling parameter $g_1$ increases, the synchronization band becomes more narrow. For the pure diffusive interaction the band width quickly goes to zero with $m$ increasing.

With crossing different parts of the region $S$ boundaries two scenarios of the transition to global synchronization may be realized. In Fig. 5 two routes ($Q$ and $R$) on the parameter plane corresponding to these scenarios are marked with arrows. The rout $R$ corresponds to the gradual simultaneous approaching of the mean frequencies $\tilde{\omega}_j$ of all partial oscillators to the external frequency $\omega_{ex}$. Approaching to the boundary of the region $S$ from outside along direction $Q$ we can observe external synchronization of several first oscillators in the chain. If $g_1 \neq 0$, the synchronization of the first oscillators

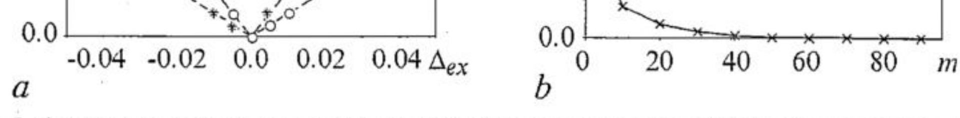

Fig. 5. *a*) Region $S$ of global synchronization of the homogeneous chain of self-sustained oscillators (6) on the parameter plane ($\Delta_{ex}$,$C$) for $g_1$=0, $g_2$=0.04 (∘) and $g_1$=$g_2$=0.04 (∗). The dashed lines denote the boundaries of region $S$, defined by the conditions (9). The directions $Q$ and $R$ marked by arrows correspond to different scenarios of global synchronization; *b*) dependence of the half-width of the global synchronization band on the chain length$m$ for $g_1$=0, $g_2$=0.04 (∘); $g_1$=0.08, $g_2$=0.04 (∗); $g_1$=0.08, $g_2$=0 (×). The amplitude of excitation is assumed to be equal $C$=0.1

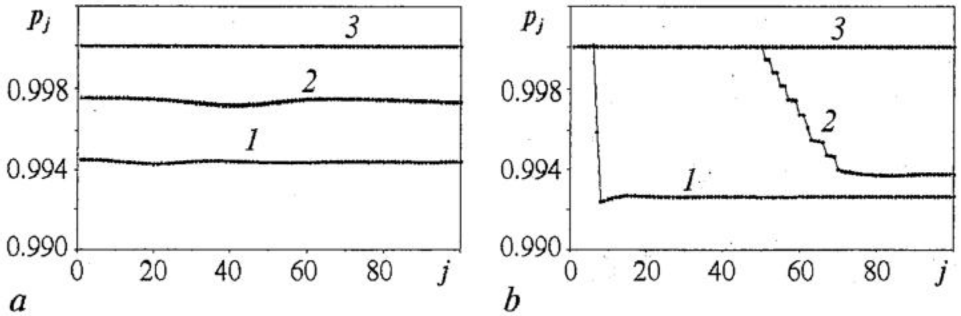

Fig. 6. Distribution of relative mean frequencies $p_j=\tilde{\omega}_j/\omega_{ex}$ along the chain when crossing different parts of the region $S$ boundary on the parameter plane $(\Delta_{ex},C)$ for $g_1=g_2=0.04$: *a*) direction $R$ (Fig. 5, *a*), $\Delta_{ex}=0.031$; 0.0315; 0.0305; *b*) direction $Q$ ( Fig.5, *a*), $\Delta_{ex}=0.04$; 0.0395; 0.039

must be understood in a sense of (3). The frequency synchronization cluster is formed ($j=1, 2,\dots k,m$). For all oscillators belonging to the cluster the relative frequencies $p_j$ satisfy the condition (8). Oscillatory regimes for all elements of the chain (including the synchronized ones) are quasi-periodic. With a distance till the synchronization boundary decreases a length of cluster $k$ increases tending to $m$. The evolution of the distribution of the relative frequencies $p_j$ along the chain with approaching to the region $S$ boundary is given in Fig. 6, *a*, *b*.

Consider the noise influence on the effect of global chain synchronization with the external frequency. In the presence of Gaussian δ-correlated noise sources the perfect synchronization is impossible. In this case we can speak about effective synchronization of self-oscillator only, i.e. about a phase locking during finite time intervals. However, if the noise intensity is small enough, the times of locking may be very long for some nonzero region of mismatch $\Delta_{ex}$ values, and a mean frequency of self-sustained oscillations is equal to the external force frequency with high accuracy. Therefore, the usage of (8) as a criterion of the $j$-th oscillator synchronization is justified from an experimental point of view both without noise and in the presence of noise.

We will study the robustness of global synchronization effect in the presence of independent sources of Gaussian δ-correlated noise in each oscillator of a chain. Consider the chain (6) of fixed length $m=100$ consists of identical oscillators with combined type of interaction. In Fig. 7, *a* some curves illustrate the dependence of relative frequency of oscillator with number $j=100$ on mismatch $\Delta_{ex}$ for different noise levels. It is well seen

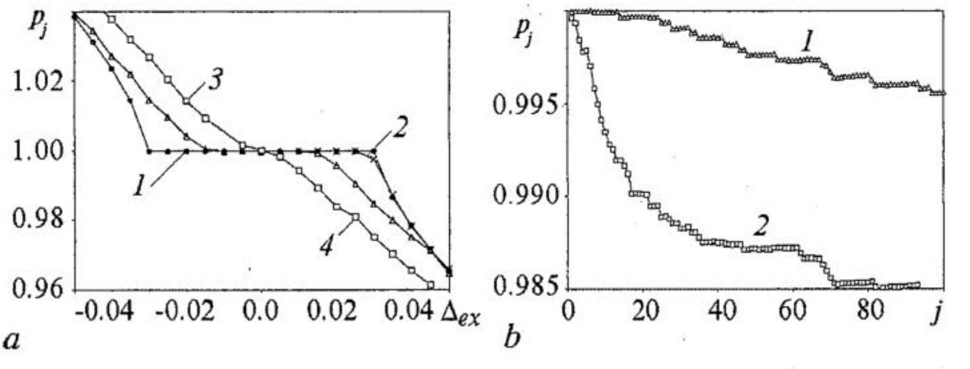

Fig. 7. Effect of noise on global synchronization of the chain with $g_1=g_2=0.04$, $C=0.06$. *a*) Dependences of the relative frequency of the self-sustained oscillator with $j=100$ on mismatch $\Delta_{ex}$, obtained for different noise levels: $D=0.0$ (curve *1*), $D=0.001$ (curve *2*), $D=0.005$ (curve *3*), $D=0.01$ (curve *4*); *b*) variation of the relative frequency $p_j$ along the chain for the given value of mismatch $\Delta_{ex}=0.02$ and for two different noise intensities $D=0.005$ (curve *1*) and $D=0.01$ (curve *2*)

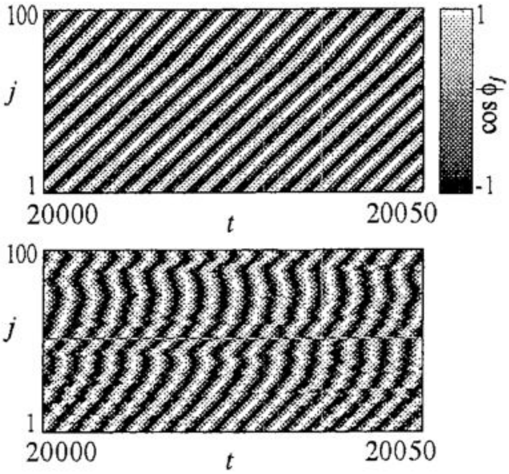

Fig. 8. Spatio-time diagrams of the phase behavior in a chain (6) at $g_1=g_2=0.04$, $C=0.06$, $\Delta_{ex}=0.02$ without noise (*a*) and with a noise of intensity $D=0.01$ the tone of gray colour correspond to a value of $\cos\phi_j$ from -1 (black) till +1 (white)

that the noise influence on the chain synchronization is analogous to the case of one noisy oscillator synchronization. The region of effective synchronization diminishes when the noise intensity $D$ increases. For a small enough noise $D=0.001$ (×) the width of a global synchronization region consists nearly 80% (○). For the noise $D=0.005$ (△) it is nearly 30%. For the case of $D=0.01$ (□) there is no any synchronization region because the condition (8) is valid for all oscillators of the chain only if $\Delta_{ex}=0$. However, a few first oscillators are still remain synchronized. Fig. 7, *b* illu-strates how values of $p_j$ change along the chain for the given mismatch $\Delta_{ex}=0.02$ and two different noise levels: $D=0.005$, and $D=0.01$. In a case of $D=0.005$ the $k=13$ first oscillators can be considered as synchronized ones. At $D=0.01$ the condition (8) is not satisfied even for the first oscillator of the chain. In Fig. 8 the spatio-temporal diagrams of the chain are given. They show the behavior of phases of all oscillators of the chain in a region of global synchronization. Without noise excitation a well- distinguishable structure of diagonal strips is observed (Fig. 8, *a*). It corresponds to the regime of a phase wave propagation along a chain. The noise excitation destroys this structure (Fig. 8, *b*). It is clear, that in the presence of any noise (even very small) synchronization with the external frequency $\omega_{ex}\neq\omega_0$ can be achieved only for a finite number (thought it may be very large) of the first oscillators of the chain.

## 5. Conclusions

In this paper we have numerically studied the synchronization phenomena in a chain of coupled Van der Pol oscillators with noise. The numerical results obtained allow us to make a number of important conclusions.

The frequency cluster structure observed in a chain of non-identical elements with diffusive coupling appears to be sufficiently stable against uncorrelated Gaussian fluctuations added to each element. The cluster structure can be considerably destroyed in the presence of noise of large intensities.

Cluster synchronization in the chain in the presence of fluctuations should be understood as effective synchronization and characterized by the effective diffusion coefficient $D_{\text{eff}}$.

The amplitude dynamics may play an essential role in creating the cluster structure. Cluster synchronization can also be observed in a chain modeled by the phase equations only. But this effect is realized in a considerably narrow range of coupling parameter values. Besides, the cluster structure appears to be more sensitive to noise perturbations.

In a case of harmonic external excitation of the first chain element the character of interaction of oscillators plays the principal role. The presence of one-direction component of coupling results in a possibility of a realizing global synchronization with an external frequency for a chain of any length. There exists a region of external frequency variations in which the synchronization is observed. The width of this region tends to a constant level when the chain length $m$ increases. In the case of pure diffusive coupling external synchronization is possible only for the chain of a finite length.

Two scenarios of the chain transition to the regime of global external synchronization are observed. One of them corresponds to simultaneous frequency synchronization for all oscillators, and the other one - to the formation of group of externally synchronized oscillators. The number of elements of this group (cluster) increases with approaching to the synchronization boundary.

And finally, the action of independent sources of Gaussian δ-correlated noise restricts a number of chain elements which can be considered as synchronized in the sense of effective synchronization. The synchronization of a chain of infinite length becomes impossible in the presence of noise.

*This work is supported by Grant № REC-006 of the U.S. Civilian Research and Development Foundation (CRDF) and the RFBR (Grant № 00-02-17512).*

## References

1. *Van der Pol B.* Theory of the amplitude of free and forced triode vibration // Radio Rev. 1920. Vol. 1. P. 701-710.

2. *Andronov A.A., Vitt A.A.* To the Theory of Locking of the Van der Pol Oscillator / in works of A.A. Andronov. AS USSR, Moscow, 1956 (in Russian).

3. *Blekhman I.I.* Synchronization in Nature and Engineering. Nauka, Moscow, 1981 (in Russian).

4. *Kuramoto Y.* Chemical Oscillations Waves and Turbulence. Springer-Verlag, Berlin, 1984.

5. *Fujisaka H., Yamada Y.* Stability theory of synchronized motions in coupled oscillatory systems // Progr. Theor. Phys. 1983. Vol. 69. P. 32-46.

6. *Afraimovich V.S., Verichev N.N., Rabinovich M.I.* Stochastic synchronization of oscillations in dissipative systems // Radiophyzika. 1986. Vol. 29, № 9. P. 1050-1060 (in Russian).

7. *Pecora L. and Carroll T.*Synchronization of chaotic systems // Phys. Rev. Lett. 1990. Vol. 64. P. 821-823.

8. *Anishchenko V.S., Vadivasova T.E., Postnov D.E., Safonova M.A* . Synchronization of chaos // Int. J. of Bifurcation and Chaos. 1992. Vol.2, № 3. P. 633-644.

9. *Rosenblum M.G., Pikovsky A., Kurths J.* Phase synchronization of chaotic oscillations // Phys. Rev. Lett. 1996. Vol. 76, № 11. P.1804-1807.

10. *Rulkov N.F., Sushchik M.M., Tsimring L.S., Abarbanel H.D.I.* Generalized synchronization of chaos in unidirectorally coupled chaotic systems // Phys. Rev. E. 1995. Vol. 51. P.980-995.

11. *Anishchenko V.S., Vadivasova T.E.* Synchronization of self-oscillations and noise-induced oscillations // Radiophys. and Quantum Electronics. 2002. Vol. 47, №2. P.1-33.

12. *Neiman A.B.* Synchronization-like phenomena in coupled stochastic bistable systems // Phys. Rev. E. 1994. Vol. 49. P. 3484-3488.

13. *Shulgin B.V., Neiman A.B., Anishchenko V.S.* Mean switching frequency locking in stochastic bistable systems driven by periodic force // Phys. Rev. Lett. 1995. Vol. 75. P. 4157-4160.

14. *Han S.K., Yim T.G., Postnov D.E., Sosnovtseva O.V.* Interacting coherence resonance oscillators // Phys. Rev. Lett. 1999. Vol. 83, № 9. P. 1771-1774.

15. *Anishchenko V.S., Neiman A.B., Moss F., Schimansky-Geier L.* Stochastic resonance: noise-induced order // Phys. Uspekhi. 1999. Vol. 42, № 1. P. 7-36.

16. *Kuramoto Y.* Progr. Theor. Phys. 1974. Vol. 79. P. 212.

17. *Kostin I.K., Romanovsky Yu.M.* Fluctuations in systems of many coupled generators // Vestnik MGU. 1972. Vol. 13, № 6. P. 698-705 (in Russian).

18. *Malafeev V.M., Polyakova M.S., Romanovsky Yu.M.* Izv.VUZ. Radiophysics. 1970. Vol. 13, № 6. P. 936-940 (in Russian).

19. *Aizawa Y.* Synergetic approach to the phenomena of mode-locking in nonlinear systems // Progr. Theor. Phys. 1976. V. 56, № 3. P. 703-716.

20. *Ermentrout G.B., Kopell N.* Frequency plateaus in a chain of weakly coupled oscillators // SIAM J. Math. Ann. 1984. Vol. 15. P. 215-237.

21. *Yamaguchi Y., Shimizu H.* Theory of self-synchronization in the presence of native frequency distribution and external noises // Physica D. 1984. V. 11. P. 212-226.

22. *Ermentrout G.B., Troy W.C.* Phase-locking in a reaction-diffusion system with a linear frequency gradient // SIAM J. Appl. Math. 1986. Vol. 39. P. 623-660.

23. *Sakaguchi H., Shinomoto S., Kuramoto Y.* Local and global self-entrainments in oscillator lattices // Progr. Theor. Phys. 1987. Vol. 77. P. 1005-1010.

24. *Strogatz S.H., Mirollo R.E.* Phase-locking and critical phenomena in lattices of coupled nonlinear oscillators with random intrinsic frequencies // Physica D. 1988. V. 31. P. 143-168.

25. *Strogatz S.H., Mirollo R.E.* Collective synchronization in lattices of nonlinear oscillators with randomness // J. Phys. A. 1988. V. 21. P. L699-L705.

26. *Afraimovich V.S., Nekorkin V.I., Osipov G.V., Shalfeev V.D.* Stability, structures and chaos in nonlinear network of synchronization. - IPPh RAN, N.Novgorod, 1989 (in Russian).

27. *Matthews P.C., Mirollo R.E., Strogatz S.H.* Dynamics of a large system of coupled nonlinear oscillators // Physica D. 1991. Vol. 51. P. 293-331.

28. *Tass P.* Phase and frequency shifts in a population of phase oscillators // Phys. Rev. E. 1997. Vol. 56, № 2. P. 2043-2059.

29. *Osipov G.V., Sushchik M.M.* Synchronized clusters and multistabylity in arrays of oscillators with different natural frequencies // Phys. Rev. E. 1998. Vol. 58, № 6. P. 7198-7207.

30. *Anishchenko V.S., Aranson I.S., Postnov D.E., Rabinovich M.I.* Spatial synchronization and bifurcations of chaos development in a chain of coupled self-oscillators // DAN USSR. 1986. Vol. 286, № 5. P.1120-1124 (in Russian).

31. *Braiman Y., Linder J.F., Ditto W.L.* Taming spatiotemporal chaos with disorder // Nature. 1995. Vol. 378. P. 465-467.

32. *Braiman Y., Ditto W.L.,Wiesenfeld K., Spano M.L.* Disorder-enhanced synchronization // Phys. Lett A. 1995. Vol. 206. P. 54-60.

33. *Wiesenfeld K., Bracikowski C., James G., Ray R.* Observation of anti-phase states in a multi-mode laser// Phys. Rev. Lett. 1990. Vol. 65, № 14. P. 1749-1752.

34. *Romanovsky Yu.M., Stepanova N.V., Chernavsky D.S.* Mathematical biophysics. - Nauka, Moscow, 1984 (in Russian).

35. *Winfree A.T* . The geometry of biological time. - Springer, New York, 1980.

36. *Murray J.D.* Mathematical Biology .- Springer, Berlin-Heidelberg, 1989.

37. Modeling the Dynamics of Biological Systems. - Ed. by E. Mosekilde and O.G. Mouritsen (Springer, Berlin, 1995.

38. *Abarbanel G.D.I, Rabinovich M.I., Silverstone A. et al.* Synchronization in neural assembles // Phys.Uspekhi. 1996. Vol. 4, № 4. P. 365-390 (in Russian).

39. *Hakim V., Rappel W.-J.* Dynamics of the globally coupled complex Ginzburg - Landau equation // Phys. Rev. A. 1992. Vol. 46, № 12. P. R7347-R7350.

40. *Осипов Г.В., Сущик М.М.* Synchronization and controlling in chain of coupled self-oscillators // Vestnik NNGU. Nonlinear dynamics and chaos -II. 1997. P.5-23 (in Russian).

41. *Ermentrout G.B.* Oscillator death in populations of «all to all» coupled nonlinear oscillators // Physica D. 1990. Vol. 41. P. 219-231.

42. *Rubchinsky L., Sushchik M.* Disorder can eliminate oscillator death // Phys. Rev. E. 2000. Vol. 62, № 5. P. 6440-6446.

43. *Lorenzo M.N., Perez-Munuzuri V.* Influence of low intensity noise on assemblies of diffusively coupled chaotic cells // Chaos. 2001. Vol. 11, № 2. P. 371-376.

44. *Gaponov-Grekhov A.V., Rabinovich M.I.* Dynamic Chaos in Ensembles of Structures and Spatial Development of Turbulence. In: Unbounded Systems, ed. W.Ebeling. New York. Springer. 1986.

45. *Kaneko K.* Spatio-temporal chaos in one- and two-dimensional coupled map lattices // Physica D. 1989. Vol. 37. P. 60-82.

46. *Kuznetsov A.P., Kuznetsov S.P.* Critical dynamics of the coupled map lattices on the threshold of chaos // Izv. VUZ. Radiophysics. 1991. Vol .34, № 10-12. P. 1079-1115 (in Russian).

47. *Astakhov V.V., Bezruchko B.P., Ponomarenko V.I.* Multistabylity formation, classification of isomers and their evolution in coupled Feigenbaum's systems // Izv. VUZ. Radiophysics. 1991. Vol. 34, № 1. P. 35-39 (in Russian).

48. *Heagi J.F., Caroll T.L., Pecora L.M.* Synchronous chaos in coupled oscillator systems // Phys. Rev. E. 1994. Vol. 50, № 3. P. 1874-1885.

49. *Kocarev L., Parlitz U.* Generalized synchronization, predictability, and equivalence of unidirectionally coupled dynamical systems // Phys. Rev. Lett. 1996. Vol. 76, № 11. P. 1816-1819.

50. *Pikovsky A.S., Rosenblum M.G., Kurths J.* Synchronization in a population of globally coupled chaotic oscillators // Europhys. Lett. 1996. Vol. 34, № 3. P. 165-170.

51. *Osipov G.V., Pikovsky A.S., Rosenblum M.G., Kurths J.* Phase synchronization effects in a lattice of non-identical Rössler oscillators // Phys. Rev. E. 1997. Vol. 55. P. 2353-2361.

52. *Fomin A.I., Vadivasova T.E.. Sosnovtseva O.V., Anishchenko V.S.* External phase synchronization of a chaotic oscillator chain // Izv. VUZ. AND. 2000. Vol. 8, № 4. P. 103-112 (in Russian).

53. *Aranson D.G., Ermentrout G.B., Kopell N.* Amplitude response of coupled oscillators // Physica D. 1990. Vol. 41. 403-449.

54. *Stratonovich R.L.* Selected Problems of Fluctuation Theory in Radiotechnics. - Sov. Radio, Moscow, 1961 (in Russian).

55. *Malakhov A.N.* Fluctuations in Self-Sustained Systems. - Nauka, Moscow, 1968 (in Russian).

56. *Vadivasova T.E., Strelkova G.I., Anishchenko V.S.* Phase - frequency synchronization in a chain of periodic oscillators in the presence of noise and harmonic forcing // Phys. Rev. E. 2001. Vol. 63. P. 036225 (1-8).

57. *Vadivasova T.E., Anishchenko V.S.* Effects of synchronization in a chain of quasi-harmonic oscillators in the presence of random and harmonic forces // In Proceeding of the Conference «Modern problems of Electronics an Radiophisycs», Saratov. 2001. P.23-25 (in Russian).

*Saratov State University*

*Received 20.05.2002*

УДК: 537.86:621.373

# КЛАСТЕРНАЯ И ГЛОБАЛЬНАЯ СИНХРОНИЗАЦИЯ В ЦЕПОЧКЕ КВАЗИГАРМОНИЧЕСКИХ АВТОГЕНЕРАТОРОВ С ШУМОМ

*Т. Е. Вадивасова, В.С. Анищенко, Г.И. Стрелкова, А.И. Фомин*

В работе исследуется влияние шума на эффекты синхронизации в цепочке осцилляторов Ван дер Поля. Анализируется режим частотных кластеров в неодно-

родной цепочке с шумом. Понятие эффективной синхронизации обобщается на случай пространственно распределенной системы. Исследуется также влияние амплитудных соотношений на поведение фаз осцилляторов. Рассматривается возможность вынужденной синхронизации однородной цепочки. Выясняется роль двух компонент связи (диффузионной и однонаправленной) и источников шума по отношению к эффекту глобальной синхронизации.

*Vadivasova Tatyana Evgenevna* is an Associated Professor of Radiophysics and Nonlinear Dynamics Chair of SSU. Her scientific interests are related with nonlinear oscillation theory, theory of deterministic chaos and theory of stochastic processes. She has about 60 scientific publications including 2 monographs.

*Anishchenko Vadim Semenovich* is the full Professor, Doctor of Sciences in Physics and Mathematics, the Honored Man of Science of Russia (1995), academician of the Russian Academy of Natural Sciences (2002), the Humboldt Prize Awarded on Physics (1999), Head of Radiophysics and Nonlinear Dynamics Chair. He is the author of 8 scientific monographs and more than 300 scientific papers. Since 2000 he is Director of the Scientific and Educational Center on Nonlinear Dynamics and Biophysics. He is a leading and well-known specialist in the field of oscillation theory and statistical radiophysics. He is a supervisor of the Laboratory of Nonlinear Dynamics of SSU.

*Strelkova Galina Ivanovna* graduated from Saratov State University in 1993 on the specialty «radiophysics». In 1998 she defended her PhD thesis on the topic of properties and characteristics of nonhyperbolic chaos. Since 1994 she has been working as a leading engineer and a senior researcher at the Laboratory of Nonlinear Dynamics of SSU. Her scientific interests include nonlinear dynamics, deterministic chaos, statistical radiophysics, synchronization, noise-induced transitions. She has 19 scientific papers in leading Russian and foreign journals.

*Fomin Anton Igorevich* graduated from Saratov State University in 1998 on the specialty «radiophysics». He is working at the plant as a program engineer and continues his studies as a post-graduate student of Radiophysics and Nonlinear Dynamics Chair. His scientific interests are connected with the nonlinear dynamics and behavior of oscillatory ensembles.

Autowaves. Self-organization

Izv. VUZ «AND», vol.10, № 3, 2002

# NOISE-INDUCED SPATIAL STRUCTURES IN EXCITABLE MEDIA

*O.V. Sosnovtseva, D.E. Postnov, A.I. Fomin*

The paper considers the formation of coherent structures in a population of excitable systems driven by noise. We focus on two effects. (i) A one-dimensional lattice with at least one inhomogeneous unit demonstrates noise-induced excitation waves. The degree of coherence in such a spatial structure can be enhanced by tuning the noise intensity. (ii) A random distribution of the parameters responsible for the excitatory properties and the interaction strength leads to self-organization in the form of cluster synchronization.

## 1. Introduction

Together with self-sustained oscillators, excitable units serve as an important paradigm in the study of nonlinear dynamic phenomena. To understand electrical signaling in cells, it is helpful to divide all cell types into two groups: excitable cells and nonexcitable cells. Many cells maintain a stable equilibrium potential. For some of these, if a current is applied to the cell for a short period of time, the potential returns *directly* to its equilibrium value after the applied current has been removed. Such cells are called nonexcitable. Typical examples are the epithelial cells that line the walls of the gut. However, there are other cells for which, if the applied current is sufficiently strong, the membrane potential goes through a *large excursion*, called an action potential, before eventually returning to rest. Such cells are called excitable. Excitable cells include cardiac cells, smooth and skeleton muscle cells, secretory cells, and most neurons.

The underlying excitability determines, for example, the propagation of an action potential along the axon of a nerve, the reverberating cortical depression waves in the brain cortex [1], waves in muscle tissue (particularly the heart muscle: in their two- and three-dimensional manifestations these excitable waves are intimately related to the problem of atrial flutter and fibrillation [2]), or waves in colonies of microorganisms [3]. In this context, a number of interesting problems arise for experimental and numerical investigations of excitable media. Both the response of a single excitable functional unit and the overall dynamics of an ensemble of such units to an external stimulus are now well understood [3-5].

Noise is inevitably present in all natural oscillators. The positive (that is creative), ordering role of noise was recently demonstrated for a wide range of natural systems, including systems of physical, chemical, and biological origin. The phenomena of stochastic resonance, noise-induced transitions, and stochastic synchronization have been observed experimentally in various biological systems [6, 7]. Our topic here is the phenomenon of coherence resonance that is induced *purely by noise without an external signal* [8-10]. At a certain noise amplitude the regularity of the noise-induced dynamics is maximal. This is witnessed by a well-pronounced peak in the Fourier power spectrum and by a ring-like structure of probability density distribution in the phase space of the system. Recently, Postnov *et al.* [11-13] described synchronization mechanisms of coupled coherence resonance oscillators.

Cooperative dynamics of an ensemble of interacting self-sustained systems manifests itself in the form of synchronization phenomena and wave propagation. Clustering, i.e. the formation of groups of functional units with similar properties (amplitudes, phases or frequencies) is an important phenomenon which is assumed, for instance, to underlie perception and the processing of information by the brain [14]. The problem of clustering was formulated and analyzed in a general context within the framework of phase equations [15], self-sustained periodic oscillators [16], chaotic dynamical networks [17], or of a chain of bistable elements [18]. Vadivasova *et al.* [19] showed that cluster synchronization is structurally stable to small fluctuations.

In the present paper we focus on the questions: what are the types of noise-induced ordering that can be observed in ensembles of *stochastic* excitable systems? What are the common, respectively the specific properties of chains of coupled excitable and self-sustained systems? With this aim we investigate the generation and propagation of excitable waves caused by the presence of an inhomogeneus element with a low excitation threshold. Then we analyze cluster formation caused by the random distribution of excitation parameters and coupling strengths.

## 2. Model and Method

Let us take FitzHugh-Nagumo model as the unit in an array. Being originally suggested for the description of nerve pulses [20], this model is commonly applied to describe excitable dynamics in different fields ranging from chemical reactions to biological processes.

With $x$ and $y$ being a fast and a slow variable, respectively, the model reads

$$\begin{aligned} \varepsilon dx_j/dt &= x_j - x^3_j/3 - y_j + g_j(x_{j+1} + x_{j-1} - 2x_j), \\ dy_j/dt &= x_j + a_j + D\xi_j(t), \quad j = 1,\ldots, N. \end{aligned} \tag{1}$$

Here, $j$ numbers the excitable unit in the chain, and $\varepsilon=0.01$ is the small time-scale ratio of the two variables. The parameter $a$ governs the character of the solutions and is responsible for the excitatory properties of the individual dynamics, and $g$ denotes the coupling strength. Each functional unit is subjected to stochastic forcing by Gaussian white noise $\xi_j(t)$ which is statistically independent in space and with zero mean value, i.e. $\langle\xi_j(t)\xi_i(t')\rangle=\delta_{ij}\delta(t-t')$ and $\langle\xi_j(t)\rangle=0$. We use free boundaries and random initial conditions.

With noise, an excitable system generates a random sequence of pulses, i.e. firing events, whose properties can be described by Eq. (1). We characterize the process via the distribution of the time intervals between pulses, the periodicity of their occurrence, and the mean frequency. The mean frequency of noise-induced oscillations in the $j$-th element is defined as $\langle f_j\rangle=1/\langle\tau_j\rangle$, where $\langle\tau_j\rangle$ is the time averaged pulse duration specified as the sum of the activation time needed to excite the system from the stable fixed point and the excursion time needed to return from the excited state.

In order to quantitatively characterize the effect of coherence resonance, different methods can be used, including the signal-to-noise ratio [8, 9] and a properly defined entropy-like measure [13]. In this paper, we calculate the regularity of an individual unit as [10]:

$$R_j = \langle\tau_j\rangle/[Var(\tau_j)]^{1/2}. \tag{2}$$

Overall dynamics of the whole array is described by the regularity averaged over all functional units $R_t=\bar{R}_j$.

## 3. Wave structures

In the deterministic case, due to the local coupling between neighboring elements, excitation waves can propagate through the medium. In the one-dimensional lattice, such waves propagate without any decrement of their amplitude and velocity until they reach the boundary of the medium. Note, that excitable systems are characterized by both excitability and refractoriness. That is, after the system has responded to a superthreshold stimulus with a large excursion from rest, there is a period of refractoriness during which no subsequent response can be evoked followed by a period of recovery during which excitability is gradually rebuilt. Once excitability is restored, another wave of excitation can be evoked. The wave velocity is the higher the stronger the coupling and the lower the excitation threshold of the individual functional units. Moreover, it strongly depends on the time allowed for recovery of excitability.

With noise added to each system, the formation and propagation of excitation waves are changed. Random excitation can happen in any element at any time. This element then becomes the center of a wave propagating to both sides. The propagation stops as soon as it reaches the array boundary or an element in the excitatory (or refractory) state. Depending on the relation between the mean frequency of noise-induced firings and the wave velocity, the wave can pass a shorter or longer distance along the array before it disappears in a collision with another wave propagating in the opposite direction.

For identical units and equal noise intensity, the above process is completely unpredictable. In this paper we investigate the case when the one-dimensional lattice of excitable systems contains an inhomogeneous element with lower excitation threshold. This element is more frequently excited by noise and becomes the center of wave propagation. In our simulations, the inhomogeneous unit with $a_1=1.01$ is located at the beginning of a chain ($j=1$). For $j=2,...100$, the excitation parameter is fixed at $a_j=1.05$.

Fig. 1 presents the spatio-temporal pattern of noise-induced waves in the system (1) for weak noise ($D=0.0002$). Black dots represent the firing state. The gray arrow indicates a center of wave birth. The black arrow points at an event of wave suppression after collision with another wave. One can observe how a wave is annihilated when it reaches elements in the refractory state.

In spite of a large number of excitation and annihilation points, the cooperative spatiotemporal dynamics looks fairly regular (Fig. 2, *a*). In this case, wave propagation precedes the mean time between noise-induced firings for any (except the first) unit in an array. As a result, spatiotemporal structures in the form of excitation waves running in different directions can be observed. Along such waves each element operates in a more

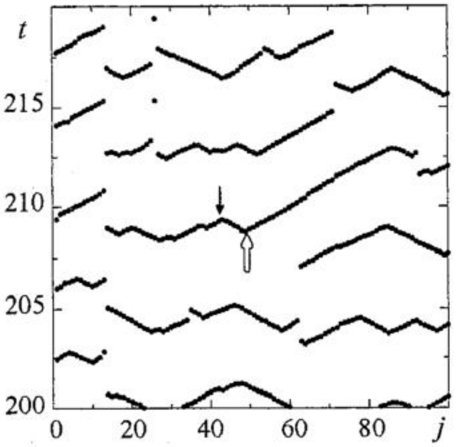

Fig. 1. Spatiotemporal pattern for $D=0.0002$ and $g=0.015$. Black dots indicate firing events. Apperence (gray arrow) and annihilation (black arrow) as well as interruption of excitation waves are clearly observed

regular way than it would be possible for the same noise intensity, but without spatial communications. For strong interaction and weak noise, the first unit becomes the single excitation center and waves propagate without annihilation for long distances. With stronger noise as well as with weaker coupling, the structure is changed. Increasing noise leads to interruption of wave fronts (Fig. 2, *b*). This is related both to effects of refractoriness and to an instantaneously increase of the excitation threshold caused by noise. Subsequent waves can not cause firings. Figs 2, *b*, *c*, and *d* illustrate how wave fronts are interrupted more and more frequently with decreasing coupling strength. Thus, the regime in Fig. 2, *a* in spite of wave fronts consisting of combinations of oppositely-propagating waves, is seen to be more regular than the structures in Fig. 2, *b*, *c*, and *d*.

To characterize the observed structures, we introduce a causality principle for firing events in two neighboring units if their phases overlap in time (Fig. 3). Let us call a group consisting of $L$ paired elements a mutually-conditioned discharge. Obviously, large (in average) values of $L$ correspond to a well-pronounced spatial structure. Hereafter the spatial regularity can be defined as the ratio between the mean length of the mutually-conditioned discharge and its maximal value $L=N$ (i.e. the length of the chain):

$$R_s = \langle L \rangle / N . \qquad (3)$$

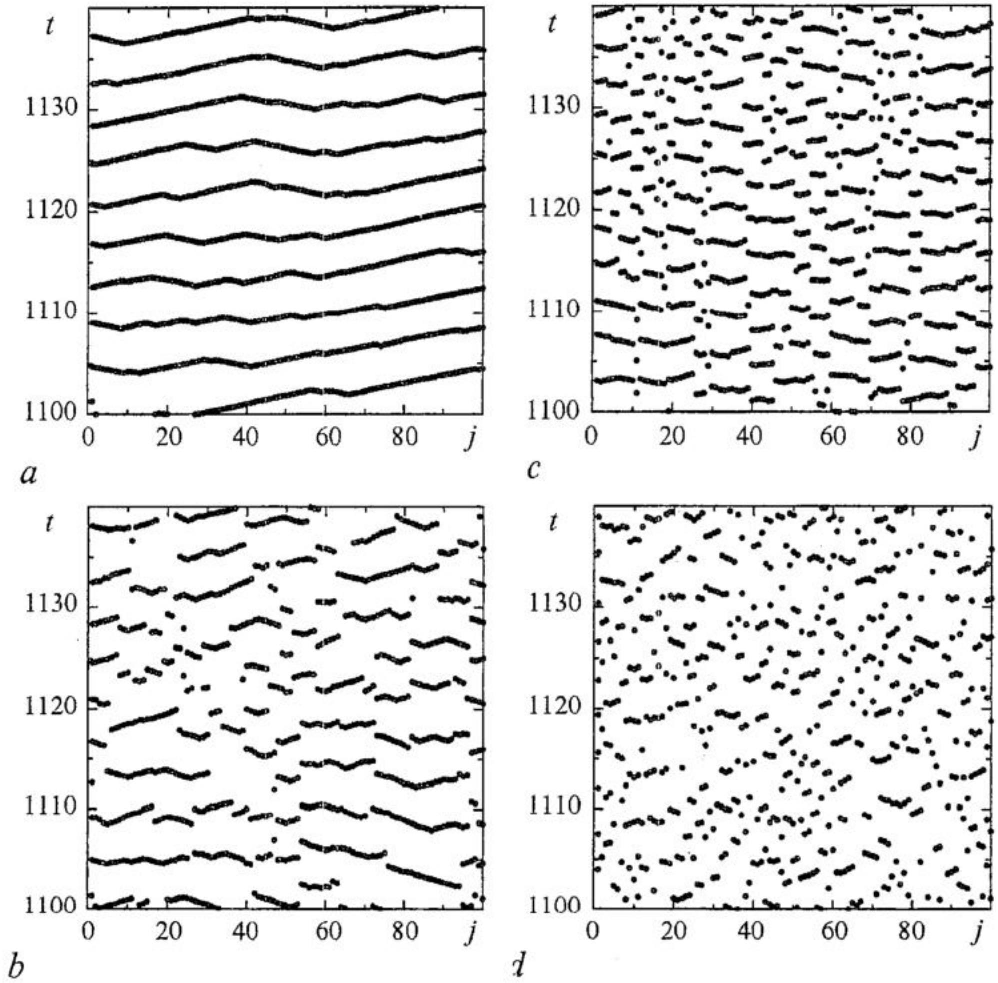

Fig. 2. Spatiotemporal structures for (*a*) $g=0.02$, $D=0.0002$; (*b*) $g=0.02$, $D=0.001$; (*c*) $g=0.01$, $D=0.0002$; (*d*) $g=0.005$, $D=0.0002$

Both temporal $R_t$ and spatial $R_s$ coherence measures characterize to what degree noise-induced spatiotemporal motions in a one-dimensional lattice can be regularized by tuning the coupling strength $g$ and noise intensity $D$ (Fig. 4). For fixed noise intensity, one can distinguish different behaviors of $R_t$ as function of the coupling strength $g$. For weak interaction, $R_t$ monotonically grows. Individual regularities of all elements is almost equal (except the first) and they slowly grow with increasing $D$. This is related to the effect of coherence resonance since the noise intensity is lower than the optimal value. The first element demonstrates a high degree of coherence, but it does not contribute much to the averaged $R_t$ along the array. Thus, for weak coupling, cooperative dynamics does not manifest itself.

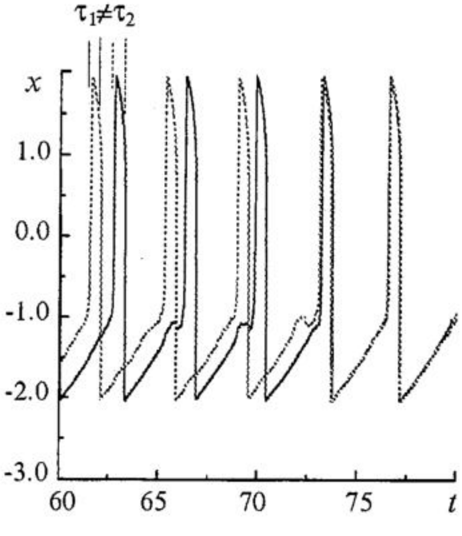

Fig. 3. Causality of firing events

For strong interaction, $R_t$ has a well-defined maximum for $D \approx 0.0004$ that is close to the optimal value for an individual system. In this case, noise-induced excitation waves from the first unit penetrate deeply along the array and causes spatial synchronization of firing events. Note, that individual regularities decrease near the boundaries. This fact shows that both noise-induced waves and the effect of mutual stochastic synchronization (discussed below) play an important role in the self-organizing process.

The coupling strength $g \approx 0.012$ corresponds to some critical behavior where the

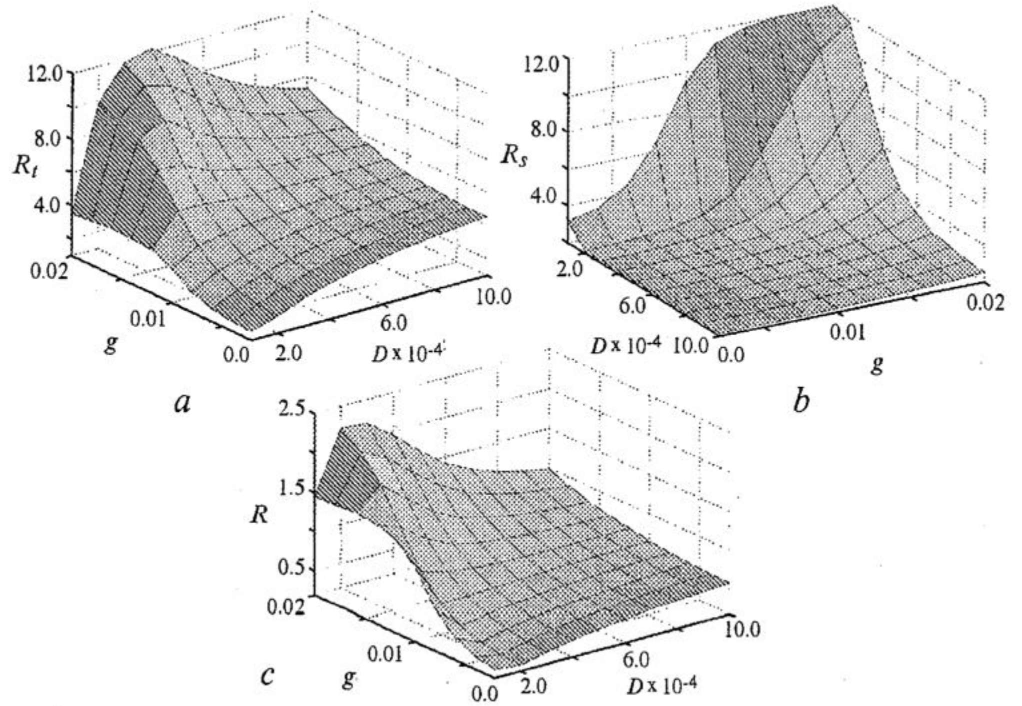

Fig. 4. Integral characteristics for (*a*) the temporal regularity $R_t$, (*b*) the spatial regularity $R_s$, and (*c*) the summarized regularity $R=R_t/7.8+R_s$

above mechanisms contribute in an equal way. Within a wide range of noise intensities, $R_t$ maintains a constant value. The one-dimensional array becomes insensitive to variation of the noise intensity $D$. This is related to the combination of individual coherence resonance effects and the regularization in the form of excitable waves.

The spatial regularity $R_s$ behaves in a simpler way. It grows with increasing coupling and with decreasing noise intensity, approaching a maximal value $R_s$=1 (Fig. 4, *b*). Let us introduce a spatio-temporal regularity as the sum of the spatial component $R_s$ and the temporal component $R_t$ (normalized to its maximal value in the individual system):

$$R = R_t/R_{t\max} + R_s. \tag{4}$$

This index allows us to characterize both the possibility of excitation waves and the temporal degree of coherence. It is interesting to note two peculiarities. First of all, the maximal value is shifted to a smaller value of the noise intensity $D\approx0.00025$. Moreover, there is region of minimal value of $R$ that corresponds to the absence of coherence in the noise-induced firing events along an array. This region is located at the same range of $D$ as a global maximum but shifted to weak couplings.

In this section we investigated the propagation of noise-induced waves and the appearance of spatio-temporal structures in homogeneous media ($g_j$=const., $a_j$=const. for $j$=2,...,100). How will the observed structures transform if the excitable media is disordered, i.e. the excitation thresholds and coupling strengths are randomly distributed along an array?

## 4. Cluster synchronization

The collective dynamics of an ensemble of coupled excitable units of significant interest for many biomedical applications [21]. A population of identical units with the same coupling properties serves as the simplest model. In nature, however, full identity in the properties and operating conditions of the units can only be an idealization. In our work, in contrast to most previous studies, we investigate ordering effects in ensembles of elements that are

(i) nonhomogeneous, i.e. the activation parameters $a_j$ are random numbers distributed uniformly on [1.0; 1.1];

(ii) coupled with the strengths $g_j$ which have a random uniform distribution on some range $\Delta=g_{\max}-g_{\min}$ ($g_{\min}$=0.005, but $g_{\max}$ and, hence, the mean level $(g_{\max}+g_{\min})/2$) are varied).

Thus, our model provides disorder between interacting units in different ways. The question of interest is how such elements adjust their motions in accordance with one another to reach some kind of coherence?

In our experiments with varying distribution intervals for the coupling strength and with a certain level of noise, three basic types of space-time behavior in a one-dimensional array (1) of 100 units was observed. For a vanishing and very narrow $\Delta$, the behavior is totally incoherent that is reflected in the irregular pattern of black (firing state) and white points (Fig. 5, *a*). The firing events in individual units occur at frequences that are randomly spread in the range [0.05;0.27] (Fig. 5, *b*). In this case, no stable frequency- or phase-locked groups can be detected. A qualitatively different behavioral pattern is encountered for a broader range of coupling (Figs 5, *c* and *d*). Here, synchronized groups, i.e., clusters of stochastic elements, appear. Within each cluster the frequency difference between any two oscillators vanishes or is small in comparison with the difference between neighboring clusters. To describe spatiotemporal patterns (Figs 5, *a* and *c*) in terms of the causality principle let us calculate the probability of interruption of firing on the $j$-th element. In the clusterless case, the distribution of probability along

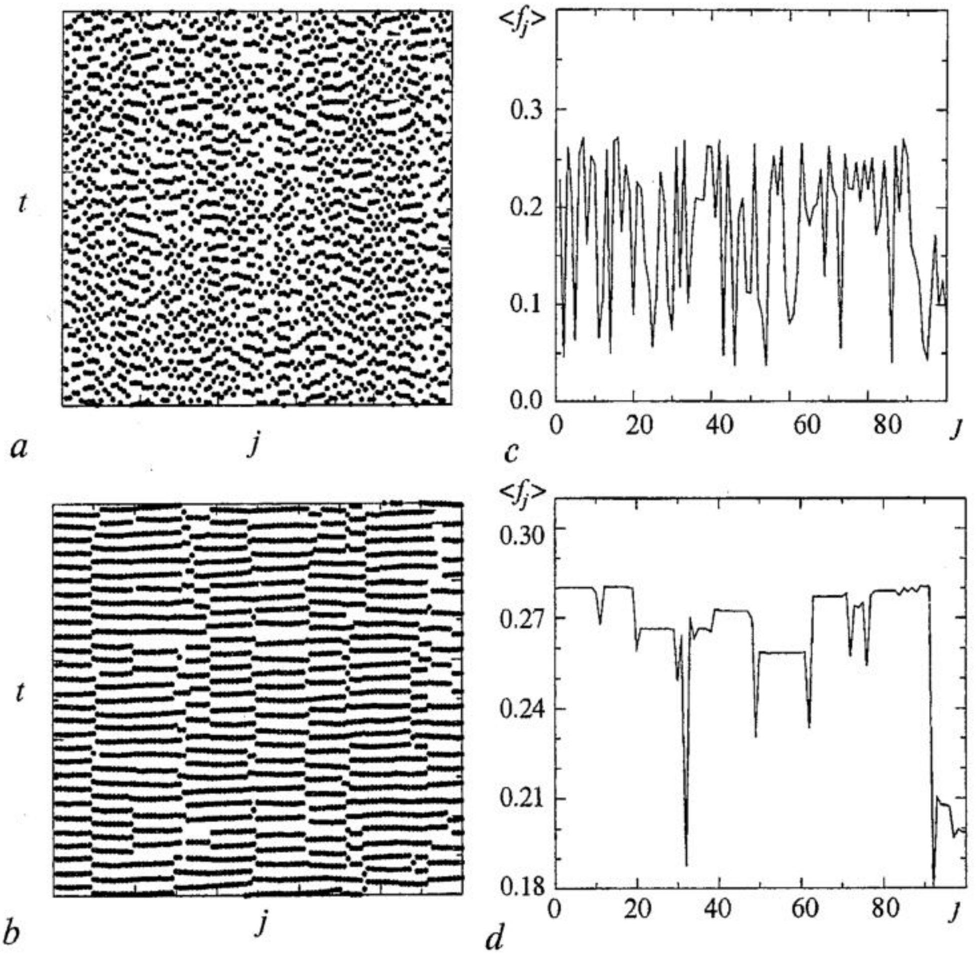

Fig. 5. Spatiotemporal evolution and mean firing frequencies $<f_j>$ of an array of 100 excitable units at $D$=0.025 for different widths of the coupling range for $\Delta$=0.002 (*a*, *b*) and for $\Delta$=0.1 (*c*, *d*). A sequence of clusters are clearly seen in the latter case

an array is random (Fig. 6, *a*). For a cluster structure, the function $P$ contains a number of local maxima whose locations coincide with the boundary of the respective clusters (Fig. 6, *b*). Hence, interruption of mutually-conditioned discharges takes place in excitable

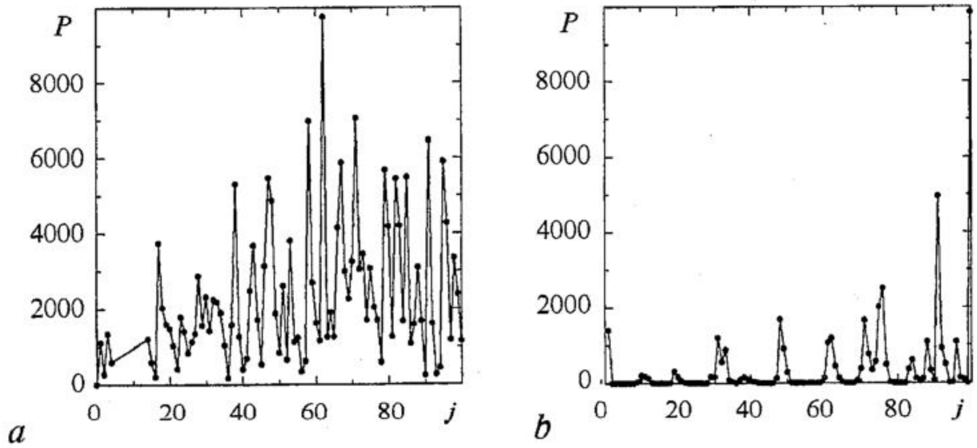

Fig. 6. Probability of firing interruption (*a*) without clustering and (*b*) with a cluster structure

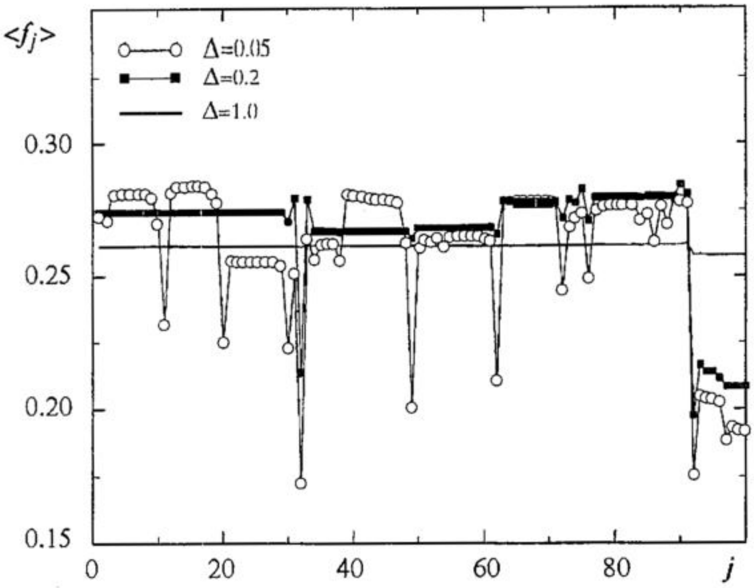

Fig. 7. Reduction of the number of frequency-locked clusters with an increasing width of the coupling range ($D$=0.025)

units at the boundary of a cluster. With a broader coupling interval, the number of clusters decrease (Fig. 7) until finally the global synchronous state (one-cluster state), where all units fire simultaneously, is achieved. Since the incoherent behavior and the totally synchronized behavior are well understood [22, 23], we focus our study on clustering of noise-induced oscillations.

Let us consider now an individual cluster as a spatial meta-unit of an array and describe its main properties. Because of the assumed distribution of system parameters, the elements in a cluster have different randomly scattered frequencies for vanishing coupling, i.e. there is no correlation between the firing events of different cells. With interaction, a frequency locking effect which is responsible for cluster formation takes place (Fig. 8, *a*). In this case, the elements composing the cluster display regular synchronous firings. However, the variance of the pulse duration $\sigma^2_j=\langle\tau^2_j\rangle-\langle\tau_j\rangle^2$ changes within a cluster. It is minimum in the center of cluster and the difference in $\sigma_j$ between neighboring elements increases near the ends of the cluster (Fig. 8, *b*). Thus, with frequency entrainment, oscillators demonstrate different degrees of mutual synchronization.

Frequency-locking entrainment is closely related to the phase conditions. For stochastic systems one has to use the notion of «effective synchronization» [24]. In the presence of Gaussian noise (or another random process with unlimited distribution function) the phase-locked state inevitably has to be broken at some moment. Thus, the system is supposed to be effectively synchronized if the phase locking is observed during a finite but long enough time (determined a priori). A measure of stochastic synchronization is the cross-diffusion coefficient $D_{\mathrm{eff}}^j = {}^1\!/\!{}_2 d/dt[\langle\phi^2_j(t)\rangle-\langle\phi_j(t)\rangle^2]$ [25]. This quantity describes the spreading in time of an initial distribution of the phase difference $\phi_j(t)$* [26] between neighboring elements. In our study, the cross-diffusion coefficient attains a vanishing value within each cluster (Fig. 8, *c*) and assumes different nonzero values for inter-cluster units. This agree with the stronger condition of phase synchronization which provides high degree of collective entrainment within clusters of

---

[*] We use the instantaneous phase introduced as $\Phi_j(t)=2\pi(t-t_k)/(t_{k+1}+t_k)+2\pi k$, where $t_k$ is the time of the $k$ th firing as defined by the threshold crossing of $x_j(t)$ at $x$=1.0.

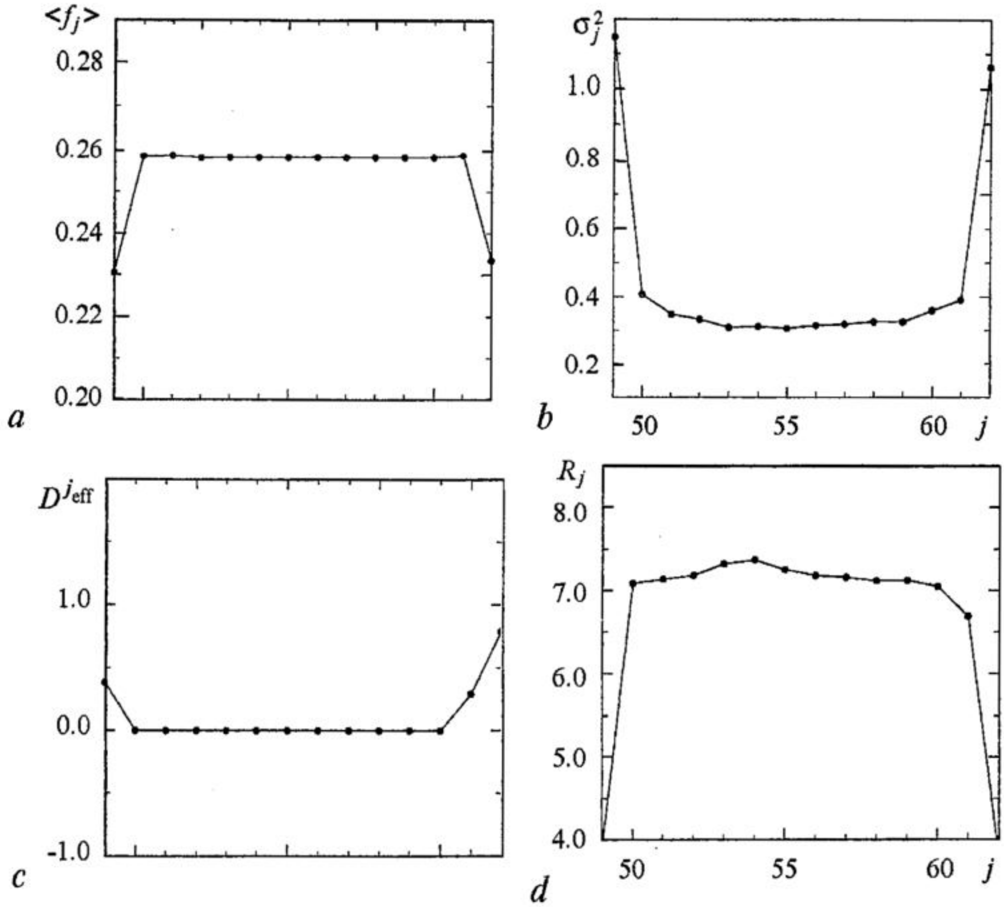

Fig. 8. Mean firing frequency $<f_j>$ (*a*), deviation of pulse duration $\sigma^2_j$ (*b*), effective cross-diffusion coefficient $D_{\mathrm{eff}}^j$ (*c*) and noise-induced regularity $R_j$ (*d*) within a single cluster. The widths of the coupling interval and noise intensity are fixed at 0.1 and 0.025, respectively

stochastic oscillators. Hence, the notion of effective synchronization can be generalized to the spatially extended group of elements. Similar effects have been observed for coupled Van der Pol oscillators with fluctuations [19]. What are the coherence properties of such frequency-locked clusters? It is clearly seen that the regularity exhibits a maximum value inside the synchronized state (Fig. 8, *d*), while the outer-cluster elements demonstrate a lower level of coherence. Comparative analyses of the regularity and pulse deviation functions allow us to assume that high coherence behavior within a cluster is related to synchronization phenomenon.

In general, the collective response of a cluster is characterized by two aspects. The first is a synchronization effect that leads to the frequency and phase entrainment. The second is the regularity of each functional unit due to coherence resonance effects. Remarkably, the regularity averaged over the spatial coordinate can be maximized within each cluster by tuning the noise (Fig. 9). At weak external noise, a cluster considered as a whole functional unit demonstrates weak coherence in spite of the fact that firings in the elements of the cluster tend to occur simultaneously. This is related to the relatively large fluctuations of the pulse duration of each composed elements. With increasing *D*, the coherence of the temporal and spatial structure of the firing process is enhanced and reaches a maximum. At large noise, the frequency and phase fluctuations grow rapidly and this leads to the destruction of the coherence properties for the composed units and, hence, of the spatial coherence structure. Because of the phenomenon of array-enhanced coherence resonance [23], the regularity of the whole cluster is much higher than that of the uncoupled elements (compare the curves *1*, *2* and the dashed curve in Fig. 9).

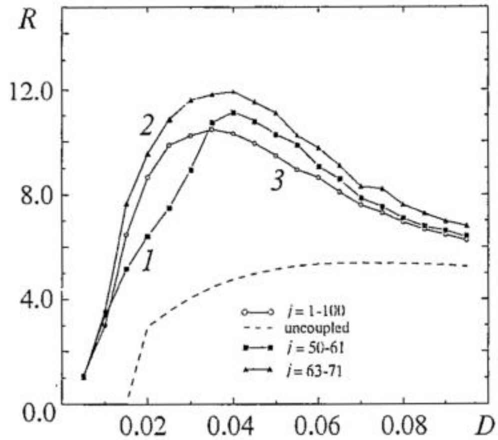

Fig. 9. Illustration of synchronization-enhanced coherence resonance for the system (1) demonstrating cluster structure for $\Delta$=0.1. The regularity averaged over spatial the coordinate $R$ is plotted versus noise intensity for individual clusters (curve*1* and *2*) and for the whole array with a cluster structure (curve *3*). Dashed curve corresponds to the uncoupled array

Let us return to the full system. Now an array composed by excitable elements can be considered in macro level as a sequence of clusters whose size and structure is determined by a random distribution of firing properties and the degree of interaction. Fig. 10 illustrates the ordering effect caused by the stochastic synchronization and the resulting high coherence within each cluster at the optimal level of noise. The coherence of the net output is averaged over a set of clusters. Because of the frequency difference between clusters, the regularity of the array output is lower than the maximum value of each cluster (curve *3* in Fig.9).

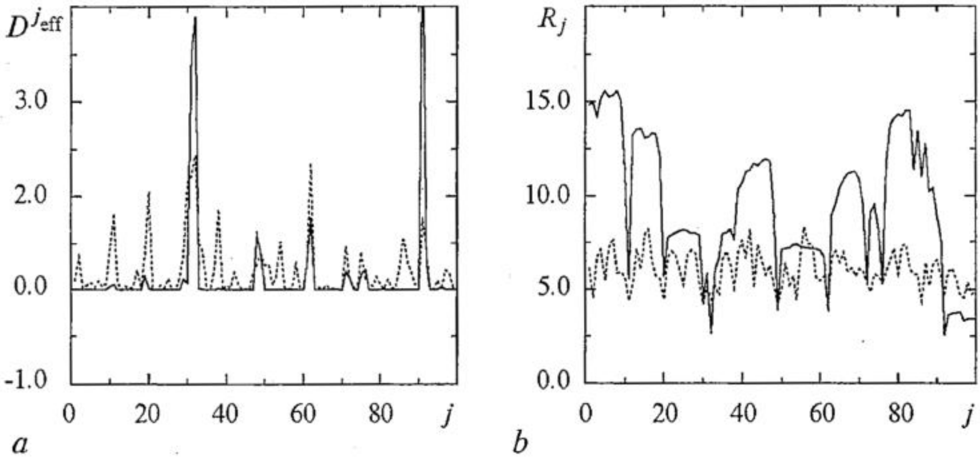

Fig. 10. Synchronous (*a*) and coherence (*b*) properties along the array with cluster structure for varying noise level. The width of the coupling interval is fixed at 0.1

## 5. Conclusions

Our investigations of the coherence properties in an ensemble of diffusively coupled excitable systems showed that self-organization can manifest itself in two ways:

(i) A one-dimensional lattice of excitable units with at least one inhomogeneous element (in our case, a unit with lower excitation threshold) demonstrates excitation waves. The degree of coherence of such a structure can be enhanced by tuning the noise intensity and/or the coupling strength;

(ii) A random distribution of the system parameters responsible for the excitory properties and the strength of interaction leads to cluster formation defined as stochastic phase locking and as a mean frequency entrainment between a group of cells. Composed by a number of elements with different properties, each cluster can be considered as a «spatial» excitable unit exhibiting coherence resonance. Gain of regularity within each cluster is associated with the effect of stochastic synchronization.

We believe that these effects can be of importance for biological applications where the background noise may play a constructive role in ordering phenomena in a large networks of excitable elements through the synchronization mechanisms.

*This work was partly supported by grant CRDF (REC-006), grant RFBR (01-02-16709). O.S. aslo acknowledges INTAS grant (YSF 01/1-0023).*

## References

1. *Shibata M., Bures J.* Optimum topographical conditions for reverberating cortical spreading depression in rats // J. Neurobiol. 1974. Vol. 5. P.107.

2. *Winfree A.T.* Sudden cardiac death: A problem in topology // Sci. Amer. 1983. Vol. 248. P. 144.

3. *Murray D.* Mathematical Biology. Berlin: Springer-Verlag, 1989.

4. *Romanovsky Yu.M., Stepanova N.V., Chernavsky D.S.* Mathematical Models in Biophysics. M: Nauka, 1975 (in Russian).

5. *Keener J., Sneyd J.* Mathematical Physiology. New York: Springer, 1998.

6. *Russel D.E., Wilkens L.A., Moss F* . Use of behavioral stochastic resonance by paddlefish for feeding // Nature 1999. Vol. 402. P. 291.

7. *Neiman A., Pei X., Russell D., Wojtenek W., Wilkens L., Moss F., Braun H.A., Huber M.T., Voigt K.* Synchronization of the noise electrosensitive cells in the paddlefish // Phys. Rev. Lett. 1999. Vol. 82. P. 660.

8. *Gang H., Ditzinger T., Ning C.Z., Haken H.* Stochastic resonance without external periodic force // Phys. Rev. Lett. 1993. Vol. 71. P. 807.

9. *Neiman A., Saparin P.I., Stone L.* Coherence resonance at noisy precursors of bifurcations in nonlinear systems // Phys. Rev. E. 1997. Vol. 56. P. 270.

10. *Pikovsky A.S., Kurths J.* Coherence resonance in a noise driven excitable system // Phys. Rev. Lett. 1997. Vol. 78. P. 775.

11. *Postnov D.E., Han S.K., Yim T., Sosnovtseva O.V* . Experimental observation of coherence resonance in cascaded excitable systems // Phys. Rev. E. 1999. Vol. 59. P. 3791.

12. *Han S.K., Yim T., Postnov D.E., Sosnovtseva O.V.* Interacting coherence resonance oscillators // Phys. Rev. Lett. 1999. Vol. 83. P. 1771.

13. *Postnov D.E., Setsinsky D.V., Sosnovtseva O.V.* Stochastic synchronization and the growth in regularity of the noise-induced oscillations // Tech. Phys. Lett. 2001. Vol. 27. P. 49.

14. *Haken H.* Principles of Brain Functioning. Berlin: Springer-Verlag, 1996.

15. *Ermentrout G.B., Kopell N.* Frequency plateus in a chain of weakly coupled oscillators // SIAM J. Math. Ann. 1984. Vol. 15. P. 215.

16. *Osipov G.V., Sushchik M.M.* Synchronized clusters and multistability in arrays of oscillators with different natural frequencies // Phys. Rev. E. 1998. Vol. 58. P. 7198.

17. *Manrubia S.C., Mikhailov A.S.* Mutual synchronization and clustering in randomly coupled chaotic dynamical networks // Phys. Rev. E. 1999. Vol. 60. P. 1579.

18. *Nekorkin V.I., Makarov V.A., Velarde M.G.* Clustering and phase resetting in a chain of bistable nonisochronous oscillators // Phys. Rev. E. 1998. Vol. 58. P. 5742.

19. *Vadivasova T.E., Strelkova G.I., Anishchenko V.S* . Phase - frequency synchronization in a chain of periodic oscillators in the presence of noise and harmonic forcings // Phys. Rev. E. 2001. Vol. 63. P. 036225(1-8).

20. *FitzHugh R.* Impulses and physiological states in theoretical models of nerve membrane // Biophysical Journal. 1961. Vol. 1. P.445.

21. *Mosekilde E., Maistrenko Yu., Postnov D.* Chaotic Synchronization: Applications to Living Systems - Singapore: World Scientific, 2002.

22. *Neiman A., Schimansky-Geier L., Cornell-Bell A., Moss F.* Noise-enhanced phase synchronization in excitable media // Phys. Rev. Lett. 1999. Vol. 83. P. 4896.

23. *Hu B., Zhou C.* Phase synchronization in coupled nonidentical excitable systems and array-enhanced coherence resonance // Phys. Rev. E. 2000. Vol. 61. P.R1001.

24. *Malakhov A.N.* Fluctuations in Autooscillatory Systems. M.: Nauka, 1968.

25. *Stratonovich R.L.* Topics in the Theory of the Random Noise. New York: Gordon and Breach Science Publisher, 1981.

*Saratov State University*

*Received 13.05.02*

УДК: 537.86 631.373

# ОБРАЗОВАНИЕ ИНДУЦИРОВАННЫХ ШУМОМ ПРОСТРАНСТВЕННЫХ СТРУКТУР В ВОЗБУДИМЫХ СРЕДАХ

*О.В. Сосновцева, Д.Е. Постнов, А.И. Фомин*

Исследуется образование когерентных структур в популяции возбудимых систем, находящихся под воздействием шума. Показано, что однородные одномерные решетки с хотя бы одним «вырожденным» элементом демонстрируют индуцированные шумом волны зажигания, степень упорядоченности которых имеет максимум при некоторой оптимальной интенсивности шума. При случайном разбросе параметров одномерного массива, ответственных за возбуждение и силу взаимодействия элементов, наблюдается эффект кластерной синхронизации индуцированных шумом колебаний.

*Dmitry Postnov* is a professor of the Chair of Radiophysics and Nonlinear Dynamics of Saratov State University, Candidate of Science in Physics and Mathematics since 1990, Doctor of Science in Physics and Mathematics since 2001. He is an author of 50 papers in scientific journals and of book «Chaotic Synchronization. Applications to living systems» (World Scientific, 2002).

*Olga Sosnovtseva* received her PhD degree in 1997. She is an author of more than 30 papers in international journals. Her present research interests are focussed on modelling dynamics of coupled biological oscillators.

E-mail: olga@chaos.ssu.runnet.ru

Applied problems of nonlinear oscillation and wave theory

Izv. VUZ «AND», vol.10, № 3, 2002

# SPECIAL APPROACHES TO GLOBAL RECONSTRUCTION OF EQUATIONS FROM TIME SERIES

*B.P. Bezruchko, Ye.P. Seleznev, V.I. Ponomarenko, M.D. Prokhorov,*
*D.A. Smirnov, T.V. Dikanev, I.V. Sysoev, A.S. Karavaev*

Some problems arising during global reconstruction from time series are illustrated by reconstruction of etalon equations and modeling of real-world radiophysical systems. Efficiency of specialized approaches oriented to modeling of restricted classes of systems is demonstrated and new specific techniques are proposed.

## 1. Introduction

In practice, to obtain a mathematical model from general laws of nature (from «the first principles») by individualizing them with reference to the object of investigation is often impossible. Typically, numerous phenomena of different nature which details are not clear affect the process under investigation or the first principles (similar to Newton's laws in mechanics) for the field of interest are not discovered yet. In such a case, experimental data become the main source of information about an object and the problem of an *empiric* model construction arises. Its simplest example is approximation of a set of points on the plane $(x,y)$ by a functional dependence $y=f(x)$. Since results of observations[1] are presented, as a rule, in the form of time series (sequences of observable values, measured at discrete time instants), then the problem transforms into modeling from time series. It is relevant in physics, meteorology, seismography, medicine and physiology, etc.

Here, we mean modeling of complicated (mainly, chaotic) behavior. Earlier this problem was solved with the help of statistical models [1], since complicated behavior associated only with very large numbers of degrees of freedom. However, in 1960-70s scientific community got to understand that complicated behavior can be exhibited even by simple (low-dimensional) *nonlinear* dynamical systems [2,3]. After that, there appeared a significant interest to construction of dynamical empiric models in the form of

- difference equations $\mathbf{x}(t_i)=\mathbf{F}(\mathbf{x}(t_{i-1}),\mathbf{c})$, where $\mathbf{x}=(x_1,x_2,\ldots,x_D)\in R^D$ is a state vector, $\mathbf{F}$ is a vector-valued function, $\mathbf{c}\in R^M$ is a vector of its parameters, $t_i$ is discrete time [4-6];

---

[1] An experimentally measured quantity is usually called«an experimental observable» or simply «an observable».

- ordinary differential equations (ODEs) $\dot{\mathbf{x}}(t)=\mathbf{F}(\mathbf{x}(t),\mathbf{c})$ [4,7];
- delay differential equations (DDEs) [8,9];
- partial differential equations [10].

A peak of interest to the problem of global[2] reconstruction was observed in 1990s [11-36], which was followed by the appearance of reviews on this subject [37-40]. But then disadvantages of the developed approaches were shown and difficulties of empiric modeling determined to a significant extent by the use of universal structures and polynomial approximation became apparent. All that reduced, in part, attention to this research area. In the latest papers devoted to global reconstruction, one observes certain shift of focus to problems of dynamical variables and model structure selection [41-50], though there are also some works oriented to further development of universal structures and techniques [51-53].

*The purpose of this work* is to illustrate some difficulties arising in global reconstruction from time series and to present approaches and technologic tricks for their overcoming. In section 2 we describe a general scheme for empiric modeling and the standard approach and analyze peculiarities of its application. Our original results concerning different stages of the scheme are presented in the rest of the paper which is organized as follows. In section 3 the problem of dynamical variables selection is considered. In section 4 we demonstrate possibilities of a specialized model structure selection on the example of nonautonomous systems. A specific technique for parameter estimation, based on peculiarities of behavior of systems with delayed feedback and efficient in the case of noisy time series, is shown in section 5. In section 6 we present a special method of model refinement which is based on some properties of transient processes and allows to optimize model structure by excluding superfluous terms from it. We summarize and present generalizing considerations on the problem of global modeling in section 7.

## 2. Typical scheme of empiric modeling and standard approach

Despite the variety of existing approaches and practical situations, it is possible to distinguish the following basic stages in the procedure of modeling from a scalar time series.

1. Organization of an experiment (if there is such a possibility) and obtaining a time series of an observable quantity $\eta$ (a training time series): $\{\eta(t_i)\}_{i=1}^{N_\eta}$, where $t_i=t_0+(i-1)\Delta t$, $\Delta t$ is a sampling interval, $N_\eta$ is the time series length.

2. Choice of the model equations type (stochastic or deterministic, difference or differential, etc).

3. Choice of model variables $x_1,\ldots,x_D$. Here, one specifies the number of variables $D$ and the kind of their relation with the observable $\eta$. As a rule, it is necessary to obtain time realizations of lacking (hidden) variables from the observable series.

4. Selection of the forms of approximating functions $F_k$ (i.e. components of $\mathbf{F}$), $k=1,\ldots,D$, which will enter right-hand sides of model equations. On the stages 2-4, model *structure* is specified, after that only stages of calculation remain.

5. Estimation of model parameters $c_1,\ldots,c_M$ from a time series data.

6. Diagnostic check-up of a model, i.e. investigation of solutions to the obtained equations and their comparison with the observed process, criteria of quality being determined by modeling purposes.

Under statistical modeling, one uses, as a rule, ARMA-models [1] which are linear stochastic difference equations where subsequent values of an observable are model

---

[2] The term «global» means that model equations (written down in a closed form) describe behavior of an object in the entire phase space (globally).

variables. Under nonlinear dynamics approach to modeling, one can imagine (in contrast to linear case) arbitrarily many different forms of equations. They differ from each other by both function kinds and kind of relation between dynamical variables $x_1,\ldots,x_D$ and an observable $\eta$. Therefore, the problems of variables and model structure selection become more difficult. This situation became easier after Takens [54] and Sauer et al [55] had shown that it is possible to obtain from a scalar time realization $\eta(t)$ of a dynamical system such vectors $\mathbf{x}(t)$ that are related to the original state vectors in one-to-one and smooth fashion. So, they «legalized» theoretically the use of sequential values of an observable $[\eta(t_i),\eta(t_i+\tau),\ldots,\eta(t_i+(D-1)\tau)]$ ($\tau$ is a constant delay) or its sequential derivatives $[\eta(t_i),\dot{\eta}(t_i),\ldots,d^{D-1}\eta(t_i)/dt^{D-1}]$ as coordinates of vectors $\mathbf{x}(t_i)$, given $D\geq 2m+1$ (sufficient but not necessary condition), where $m$ is a dimension of the manifold which the phase orbit of an original system belongs to. Even though it does not mean that employment of different variables (e.g., obtained by integration [56]) is necessarily less effective for modeling.

The choice of variables often dictates a model structure. For example, if sequential derivatives are used for reconstruction from a scalar time series, then model equations assume the form

$$\begin{aligned} \dot{x}_1 &= x_2, \\ \dot{x}_2 &= x_3, \\ &\ldots, \\ \dot{x}_D &= F(x_1,x_2,\ldots,x_D), \end{aligned} \tag{1}$$

where $x_1(t)=\eta(t)$, i.e. they involve the only function $F$.

After the equation type and the way of dynamical variables reconstruction are chosen, one should select the forms of functions entering right-hand sides. Under global modeling, a required function $F$ is most commonly looked for in the pseudo-linear form, i.e. linear combination of nonlinear *basis* functions $f_i$:

$$F(\mathbf{x}) = \Sigma_{j=1}^{M} c_j f_j(\mathbf{x}). \tag{2}$$

One widely uses the standard polynomial basis: $1,x_1,\ldots,x_D,x_1^2, x_1x_2,\ldots,x_D^2,\ldots$, i.e. representation of $F$ in the form of the multivariate algebraic polynomial of some order $K$. Coefficients $c_j$ are estimated, as a rule, via the least-squares routine[3], i.e. by minimization of the quantity $\varepsilon^2=1/N\Sigma_{i=1}^{N}(x_D(t_i)-F(\mathbf{x}(t_i)))^2$.

Choice of dynamical variables and model structure is often oriented to construction of models in a universal form. Thus, widely exploited model ODEs (1) with a polynomial in the right-hand side are often called *standard* [17,18]. This term could be referred to all the other cases when no information on specific features of an object is incorporated into the model structure. Their pretensions to universality are theoretically validated [55]. Nonetheless, all the achievements[4] in modeling of real-world objects we are aware of are

---

[3] One could also employ the more general maximum likelihood principle [57]. But it is reasonable only under the high noise levels that is not our case. So, we have used the least-squares approach.

[4] Global model ODEs with polynomials are used for control [11,26], attractor characteristics estimation from short and noisy time series [30], signal classification [23,24], and confidential transmission of information [31]. Under the standard approach, there were obtained models qualitatively reproducing complex dynamics of Belousov - Zhabotinski reaction [21], electrochemical process of copper dissolution in sulphuric acid [19], a certain regime of vortex fluid movement [20].

isolated rare instances. A blunders at any of the stages of modeling scheme can become an obstacle. Choice of variables can be unfortunate. But even suitable variables can not help if the form of functions is inappropriate. Thus, the popular standard structure can not be the best one for the entire multitude of real-world systems and situations. As a rule, it provides very cumbersome equations exhibiting divergent solutions (polynomial fit is especially inefficient in high-dimensional spaces).

Seemingly, a promising way of the further development of global reconstruction methods is rejection of the pretensions to model structure universality and creation of specialized approaches oriented to some classes of objects. It is reasonable to consider sufficiently important classes which specific features are known. But development of specialized techniques for parameter estimation and model refinement seems also quite useful. All these considerations are illustrated in the next sections.

## 3. Dynamical variables selection: preliminary testing for single-valuedness and continuity

As it has been already mentioned, in constructing model equations in the form $\mathbf{y}(t)=\mathbf{F}(\mathbf{x}(t))$ from a time series $\{\eta(t_i)\}$, one forms the series of state vectors $\{\mathbf{x}(t_i)\}$, where $\mathbf{x}=(x_1,x_2,\ldots,x_D)\in R^D$, $x_k$ are dynamical variables, $D$ is a model dimension. Coordinates of vectors $\mathbf{x}$ can be obtained as sequential derivatives, time delays, etc. Then, the series of quantities to enter left-hand sides of model equations $\{\mathbf{y}(t_i)\}$ is obtained from the series $\{\mathbf{x}(t_i)\}$ according to the chosen model type: either by numerical differentiation of $\{\mathbf{x}(t_i)\}$ for ODEs $d\mathbf{x}(t)/dt=\mathbf{F}(\mathbf{x}(t))$, or just by the shift of $\{\mathbf{x}(t_i)\}$ along the time axis for discrete maps $\mathbf{x}(t_{i+1})=\mathbf{F}(\mathbf{x}(t_i))$. Finally, the forms of approximating functions $F_k$ are specified and their parameters are estimated.

An uncontrolled choice of the variables can make approximation of the dependencies $y_k(\mathbf{x})$ with a smooth function extremely problematic [58] or even make these dependencies non-unique. Here, we describe the method of estimating suitability and «convenience» of the chosen variables $x_k$ for constructing a *global* dynamical model. It is based on testing the series $\{\mathbf{x}(t_i)\}$ and $\{\mathbf{y}(t_i)\}$ for single-valuedness and continuity of each dependency $y_k(\mathbf{x})$ in the entire region of an observed motion [46]. Importantly, we use local characteristics rather than averaged ones [35, 59].

Our technique is based on the following consideration. If a dependency $y(\mathbf{x})$ is single-valued and continuous in a domain $V$, then the difference $|y(\mathbf{x})-y(\mathbf{x}_0)|$ tends to zero when $\|\mathbf{x}-\mathbf{x}_0\|\to 0$ for each $\mathrm{x}_0\in V$. In practice, violation of this condition may be viewed as a sign of non-single-valuedness or discontinuity of the dependency $y(\mathbf{x})$. Since the observable time series has a finite length, the above-mentioned limit, strictly speaking, cannot be found. However, it is possible to trace a tendency in variations of the quantity $|y(t_i)-y(t_j)|$ when the vectors $\mathbf{x}(t_i)$ and $\mathbf{x}(t_j)$ are made closer and closer, down to a certain *finite* distance. Given sufficiently large amount of data $N_\eta$, high accuracy of measurements, and low noise level, this distance can be made small enough for each region of the observed motion.

The method of testing consists in the following (Fig. 1, *a*). The domain $V$ is partitioned into identical hypercubic boxes of the size $\delta$, all boxes containing at least two vectors are selected (they are denoted $s_1,s_2,\ldots,s_M$). Difference between maximal and minimal values of $y$ inside a box $s_k$ is called *local variation* $\varepsilon_k=\max_{\mathbf{x}\in s_k}y(\mathbf{x})-\min_{\mathbf{x}\in s_k}y(\mathbf{x})$. Maximal local variation $\varepsilon_{\max}=\max_{1\le k\le M}\varepsilon_k$ and its graph $\varepsilon_{\max}(\delta)$ are used as the main characteristics of the investigated dependency. The suitability of the considered variables $\mathbf{x}$ and $y$ for global modeling is assessed in the following way.

1) If a dependency $y(\mathbf{x})$ is single-valued and continuous, the value of $\varepsilon_{\max}$ is sufficiently small for small $\delta$ and tends to zero when $\delta\to 0$ (Fig. 1, *b*, filled circles). It is not hard to show that a graph $\varepsilon_{\max}(\delta)$ is a straight line for sufficiently small $\delta$.

2) If a single-valued and continuous dependency has a region of very steep slope (a «jump»), then $\varepsilon_{\max}$ remains rather big for sufficiently small $\delta$, since that region is

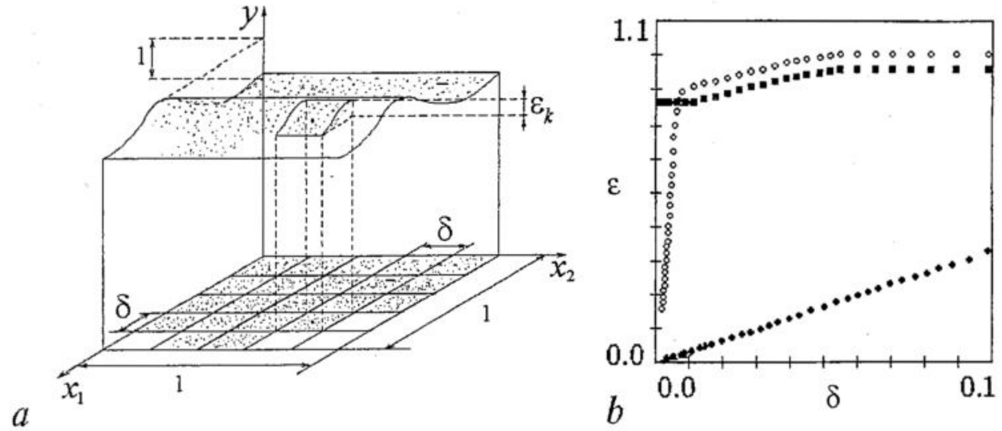

Fig. 1. *a* - Illustration for a technique of testing a dependency $y(\mathbf{x})$ for single-valuedness and continuity in the case $D$=2. *b* - Possible appearance of graphs $\varepsilon_{\max}(\delta)$ for different variants of dynamical variables

situated within one box. However, the further decrease of $\delta$ leads to the decrease of $\varepsilon_{\max}$ because the region of a jump becomes divided into several boxes. The graph $\varepsilon_{\max}(\delta)$ exhibits a «breakpoint» at the value of $\delta$ equal to the size of the region of steep slope (e.g., Fig. 1, *b*, white circles). In such a case, the dependency $y(\mathbf{x})$ is also difficult to approximate with a smooth function.

3) If $\varepsilon_{\max}$ remains rather large and does not decrease at $\delta \to 0$ (Fig. 1, *b*, filled squares), then the considered variables are not appropriate for global modeling. Such a situation can be related both with non-uniqueness of the dependency and high noise level.

So, dynamical variables should be selected so that the graph $\varepsilon_{\max}(\delta)$ tend to the origin gradually, without breakpoints, and with small slope (Fig. 1, *b*, filled circles). The most important feature distinguishing the proposed approach and providing its usefulness for global modeling is employment of local (not averaged) characteristics. Let us illustrate it by modeling a real-world radiophysical system: a nonlinear electric circuit (harmonically driven RLC-circuit with switched capacitors) which scheme is shown in Fig. 2, *a*. The element K is an electronic key, a microscheme comprising dozens of

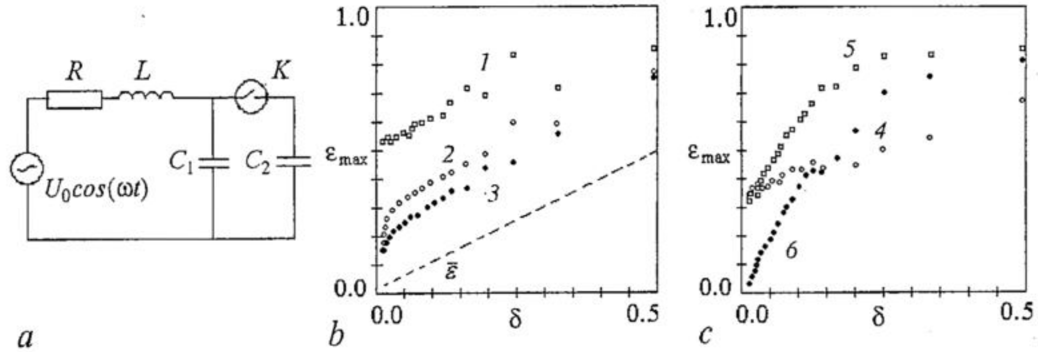

Fig. 2. *a* - The scheme for the circuit with switched capacitors: $C_1$=0.1 μF, $C_2$=4.4 μF, $L$=0.03 H, $R$=10Ω, $U_{thr}$=-0.2 V, $U_0$=2.344 V, driving frequency equals 2.98 kHz, sampling frequency equals 250 kHz. *b* - The graphs $\varepsilon_{\max}(\delta)$ for different variants of the model structure (for the dynamical variable $x_1=I$): *1* - for a dependency $\dot{x}_3(x_1,x_2,x_3)$ of a model (3), white squares; *2* - for a dependency $\dot{x}_3(x_1,x_2,x_3)$ of a model (1), white circles; *3* - for a dependency $\dot{x}_2(x_1,x_2,\varphi)$ of a model (4), filled circles. The graphs $\varepsilon(\delta)$ look similar for all the examples (the graph for the first one is shown with the dashed line). *c* - The graphs $\varepsilon_{\max}(\delta)$ for different variants of the model structure (when the dynamical variable $x_1$ is an integral of the current $I$): *4* - for a dependency $\dot{x}_3(x_1,x_2,x_3)$ of a model (1), white circles; *5* - for a dependency $\dot{x}_1(x_1,x_2,x_3)$ of a model (3), white squares; *6* - for a dependency $\dot{x}_2(x_1,x_2,\varphi)$ of a model (4), filled circles

transistors and other passive elements which is fed from a special source of dc-potential. At small values of voltage $U$ on the capacity $C_1$, the resistance of the key is very large and linear oscillations occur in the circuit $RLC_1$. When the voltage $U$ achieves a threshold value $U_{thr}$, the resistance of the key decreases abruptly and the capacity $C_2$ becomes connected to the circuit. Back switching occurs approximately at the same value of $U$ (in fact, at somewhat smaller value - hysteresis takes place). As a result, the system is nonlinear and exhibits complex dynamics (in particular, chaotic oscillations) at big values of driving amplitude [60,61].

We employ a chaotic time realization of the current $I$ through the resistor $R$ (see Fig. 2, *a*) as an observable time series $\{\eta(t_i)\}$. The data are recorded with the aid of a 12-bit ADC, the sampling interval is $\Delta t$=4 μsec, the driving period is $T=84\Delta t$, the length of the series is $N_\eta=3\cdot 10^4$. Six examples are considered below (three variants of the model ODEs structure for two different observables). The results of the application of the proposed method (Fig. 2, *b*, *c*) and of the model construction are presented. The graphs in Fig. 2 are numbered in agreement with the numbers of the following examples.

*1* - A popular model structure

$$\begin{aligned}\dot{x}_1 &= f_1(x_1,x_2,x_3),\\ \dot{x}_2 &= f_2(x_1,x_2,x_3),\\ \dot{x}_3 &= f_3(x_1,x_2,x_3),\end{aligned} \tag{3}$$

where $x_1(t_i)=\eta(t_i)$, $x_2(t_i)=\eta(t_i+\tau)$, $x_3(t_i)=\eta(t_i+2\tau)$ are time delay coordinates, $\tau=21\Delta t$ is the first zero of the autocorrelation function. A smoothing polynomial is constructed for numerical differentiation. All three dependencies $\dot{x}_k(x_1,x_2,x_3)$, $k$=1,2,3 are analyzed. The value of $\varepsilon_{\max}$ does not tend to zero when $\delta$ decreases for all $k$. All graphs $\varepsilon_{\max}(\delta)$ look similarly, one of them is presented in Fig. 2, *b* with white squares (for $k$=3). It indicates the impossibility of constructing an efficient global model that is confirmed in practice completely.

*2* - A standard model (1,2) with $x_1(t_i)=\eta(t_i)$. The dependency $\dot{x}_3(x_1,x_2,x_3)$ is tested. $\varepsilon_{\max}(\delta)$ decreases when $\delta$ decreases (Fig. 2, *b*, white circles) that points out to the possible single-valuedness. The result of modeling: an efficient model, which right-hand sides are algebraic polynomials, can not be obtained. Obviously, a polynomial is inappropriate to fit the dependency $\dot{x}_3(x_1,x_2,x_3)$. Another form of the approximating function is necessary here. Its choice is a difficult problem which is not a subject of the present paper.

*3* - Following the recommendations on the reconstruction of nonautonomous systems [33,34], we construct a model in the form

$$\begin{aligned}\dot{x}_1 &= x_2,\\ \dot{x}_2 &= F(x_1,x_2,\varphi),\end{aligned} \tag{4}$$

where $x_1(t_i)=\eta(t_i)$ and $\varphi$ is the phase of driving. The dependency $\dot{x}_2(x_1,x_2,\varphi)$ is tested. The time series of the phase $\varphi$ is obtained as $\varphi(t_i)=\omega t_i \pmod{2\pi}$, the angular frequency $\omega$ is assumed to be known. The graph $\varepsilon_{\max}(\delta)$ (Fig. 2, *b*, filled circles) shows that the dependency is, possibly, single-valued. However, an efficient model with harmonic driving and polynomial fit can not be obtained. Again, one needs to select a special form of the function $F$.

*4* - A standard model (1,2) with $x_1(t_i)=\int_{t_1}^{t_i}\eta(t)dt$. This variable makes physical sense, it is the summed charge on the capacities $C_1$ and $C_2$. The time series $\{x_1(t_i)\}$ is obtained via the numerical integration of the measured time series of the current $I$ (using the method of trapeziums). The value of $\varepsilon_{\max}(\delta)$ for the dependency $\dot{x}_3(x_1,x_2,x_3)$ does not decrease when $\delta$ decreases (Fig. 2, *c*, white circles) and remains large. An effective model can not be constructed.

*5* - A model (3) with $x_1(t_i) = \int_{t_1}^{t_i} \eta(t)dt$ and delayed coordinates $x_2(t_i)=x_1(t_i+\tau)$ and $x_3(t_i)=x_1(t_i+2\tau)$, where $\tau$ is again the first zero of the ACF. All three dependencies $\dot{x}_k(x_1,x_2,x_3)$, $k$=1,2,3 are tested. The graphs $\varepsilon_{\max}(\delta)$ do not tend to the origin when $\delta$ decreases in all three cases. One of them (for $k$=1) is shown in Fig. 2, *c* with white squares. An effective model can not be constructed.

*6* - A model (4) with $x_1(t_i) = \int_{t_1}^{t_i} \eta(t)dt$. A graph $\varepsilon_{\max}(\delta)$ shows that the dependency $\dot{x}_2(x_1,x_2,\varphi)$ is single-valued and, moreover, varies «gradually» (Fig. 2, *c*, filled circles). A reconstructed model (4) with additive harmonic driving and bivariate polynomial of the 11th order demonstrates a chaotic attractor qualitatively similar to the experimental one (see also section 4s) and provides an accurate forecast 5*T* ahead.

It is significant that an optimistic estimate according to the criterion $\varepsilon_{\max}(\delta)$ and good results of the global reconstruction are achieved only in the last (the sixth) case. The graphs for averaged over all the boxes local variation $\bar{\varepsilon}(\delta)$ are, however, practically the same for all above-mentioned choices of variables (one of them is shown in Fig. 2, *b* with the dashed line). It means that the average quantity $\bar{\varepsilon}$ does not provide all information necessary for global modeling. Therefore $\bar{\varepsilon}$ can be used in dynamical modeling only as an *additional* characteristic.

## 4. Model structure selection: nonautonomous systems under regular external driving

Here, we consider another cause of the standard approach inefficiency. In fact, its failure is inevitable «payment» for the generality of model structure. Probability to guess optimal model form without using a priori information or special preliminary investigation of the object is quite low. Therefore, we suggest to choose some classes of systems and modify the standard structure with reference to that classes. Here, we propose such a modification for modeling systems under regular external driving. It consists in the use of *nonautonomous* ODEs. That is function explicitly depending on time are incorporated into the model equations. First, we consider the simplest case of harmonic additive driving. Model is suggested to be constructed in the form

$$\begin{aligned} \dot{x}_1 &= x_2, \\ \dot{x}_2 &= x_3, \\ &\cdot\ \cdot\ \cdot, \\ \dot{x}_D &= F(x_1,x_2,\dots,x_D) + a\cos(2\pi t/T) + b\sin(2\pi t/T), \end{aligned} \qquad (5)$$

where $F$ is an algebraic polynomial of some order $K$ (at $D$=2, this is just an equation of harmonically driven oscillator). However, it is insufficient only to incorporate the driving into the last equation (5), a necessary condition for the success of modeling is to estimate driving period $T$ from a time series with high accuracy.

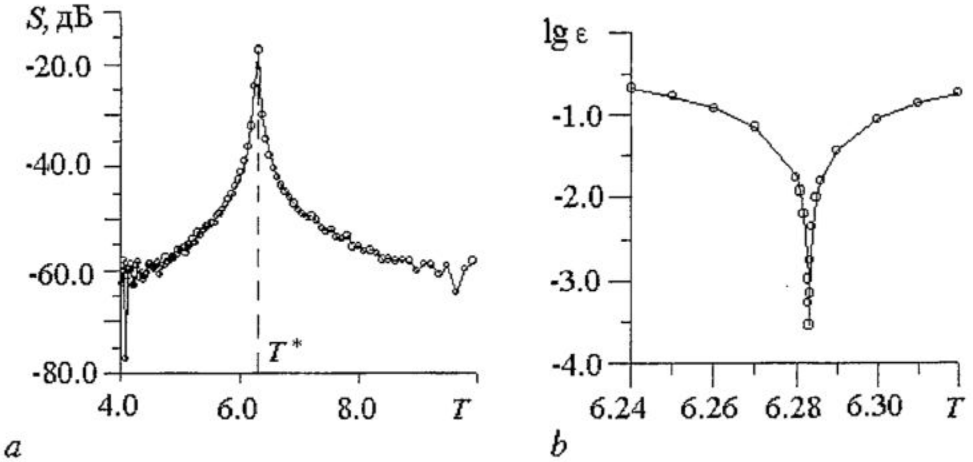

Fig. 3. *a* - Typical appearance of the power spectrum for harmonically driven chaotic systems: there is a pronounced peak. *b* - Approximation error for a model (5) versus trial value of driving period $T$

Prerequisites for construction of model equations in the form (5) can be a priori information or the presence of a discrete peak in the power spectrum of an observed time series (Fig. 3, *a*). Location of the latter can also serve as a rough estimate of driving period. Given a precise value of $T$, parameters $a$ and $b$ and polynomial coefficients are easily estimated via the linear least-squares routine. But to estimate $T$ is not so simple since it enter equation (5) in a *nonlinear* way. Therefore, it is estimated individually using a special procedure [33] (it is illustrated in Fig. 3, *b* where the graph of an approximation error versus trial value of $T$ is shown). Importantly, error in its estimation $\Delta T=T-T_0$ (where $T_0$ is an unknown «truth» value) leads to a significant «phase shift» between the truth driving and its model fit if the training time series is long. The following relationships between relative error of driving approximation $\varepsilon_T$, and quantities $\Delta T/T_0$ and $T_N/T_0$ (where $T_N$ is the duration of the observed time realization) hold

$$\varepsilon_T \approx 2\pi\cdot 3^{-1/2}\cdot(\Delta T/T_0)\cdot(T_N/T_0). \qquad (6)$$

It follows that the driving period should be estimated more accurately for longer training time series, otherwise incorporation of explicit time dependence is useless.

A result of application of the proposed technique to modeling of the above-mentioned (section 3) harmonically driven RLC-circuit with switched capacitors from the integrated time series of current $I$ (i.e. in the case selected as the best for modeling with the help of the testing method of section 3) are presented in Fig. 4. Obtained empiric model (5) with $D$=2 and $K$=11 (and excluded superfluous terms) behaves like the original system and provides sufficiently accurate forecast quite far ahead.

Harmonic force represents an important but sufficiently narrow class of possible ways of driving. The proposed approach to modification of standard structure can be extended to more complex and realistic situations, namely, for

1. arbitrary *way of entry* of harmonic driving;
2. arbitrary *form* of regular (i.e. periodic or quasiperiodic) driving.

For the first situation, significantly bigger than for a model (5) degree of generality can be achieved by using a polynomial $F$ with alternating coefficients [44]:

$$\begin{aligned} \dot{x}_1 &= x_2, \\ \dot{x}_2 &= x_3, \\ &\ldots, \\ \dot{x}_D &= F(x_1, x_2, \ldots, x_D, t), \end{aligned} \qquad (7)$$

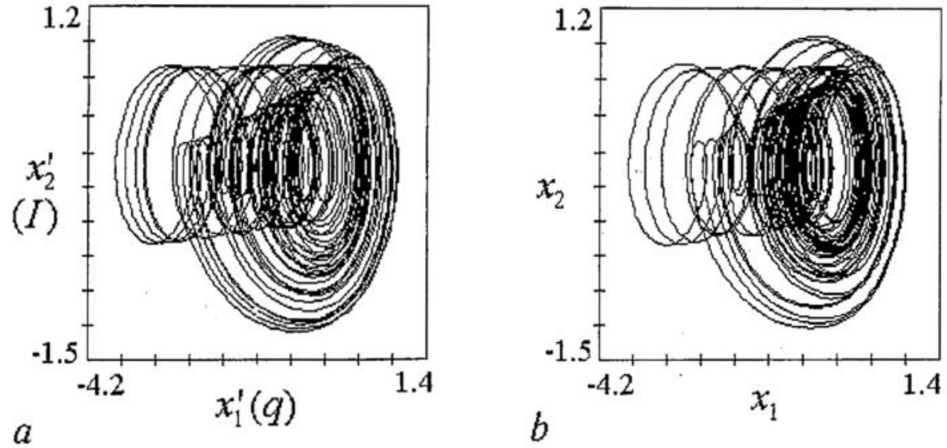

Fig. 4. *a* - Projection of an experimental orbit for the circuit with switched capacitors (shown in Fig. 2,*a*) onto the plane summed charge - current. *b* - A corresponding projection for the best reconstructed model, i.e. a model (5) with $D$=2 and $K$=11

where $x_1=\eta$, and $F$ reads

$$F\,(x_1,x_2,\dots,x_D,t) = \Sigma_{l_1,l_2,\dots,l_D=0}^{K}\,(c_{l_1,l_2,\dots,l_D} + a_{l_1,l_2,\dots,l_D}\cos\omega t + b_{l_1,l_2,\dots,l_D}\sin\omega t)\,\Pi_{j=1}^{D} x_j^{\,l_j}, \qquad (8)$$

$$\Sigma_{j=1}^{D} l_j \le K.$$

To estimate parameters of a model (7, 8), one can exploit an above mentioned procedure where accurate determination of the driving period $T$ is provided.

To illustrate of efficiency and advantages of the structure (7,8), we present a numerical example: reconstruction of equations from chaotic time series of Toda oscillator when driving is not only additive. Original equations read

$$\begin{aligned} \dot{u}_1 &= u_2, \\ \dot{u}_2 &= -0.45u_2 + (5+4\cos t)(e^{-u_1}-1) + 7\sin t. \end{aligned} \qquad (9)$$

Time series is obtained here (and in all numerical examples presented below) by numerical integration of original equations with the help of Runge-Kutta routine. The best model (7, 8) is achieved at $D$=2, $K$=9, it exhibits chaotic attractor practically identical to the original one (Fig. 5, *a*, *b*). Such results can not be achieved with models (5) (Fig. 5, *c*). Standard models (1,2) demonstrate, as a rule, globally unstable orbits (Fig. 5, *d*). Prediction times for the best models (7,8), (5) and (1,2) are equal to $7T$, $1.5T$ and $0.15T$, respectively.

For the second situation (arbitrary regular driving), we propose to use the structure of equations (7) involving time dependence but not necessarily harmonic:

$$F(x_1,x_2,\dots,x_D,t) = f(x_1,x_2,\dots,x_D) + g(t), \qquad (10)$$

where $f$ is an algebraic polynomial, and function $g(t)$ describes the driving and involves also free parameters. Two approaches to the specification of $g(t)$ are possible. The first one is to guess a special formula on the basis of *a priori* information. The second approach is more universal and can be used in the absence of detailed knowledge of the form of driving which is approximated as

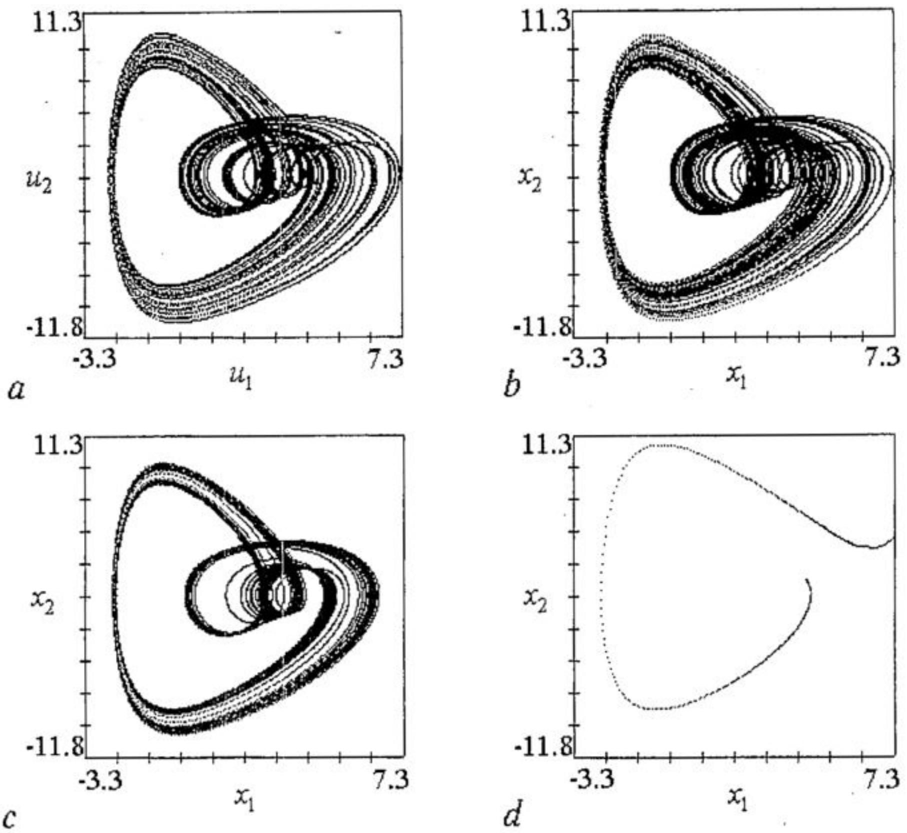

Fig. 5. *a* - Projection of attractor of Toda oscillator (9). *b-d* - Projections of phase orbits for a model (7, 8) ($D$=2, $K$=9), a model (5) ($D$=2, $K$=10) and a standard model ($D$=4, $K$=6), respectively

$$g(t) = a_0 + \Sigma_{j=1}^{K_1} a_{1,j}\cos(2\pi jt/T_1 + \varphi_{1,j}) + \ldots + \Sigma_{j=1}^{K_m} a_{m,j}\cos(2\pi jt/T_m + \varphi_{m,j}). \quad (11)$$

Here, $m$=1 for the periodic case, while quasiperiodic driving is described as the sum of $m$>1 trigonometric polynomials with different periods $T_m$ and different orders $k_m$.

Procedure of estimating parameters of the model (7, 10) also rests on the least-squares technique. But, since here several free parameters can enter the expression for the driving *g in a nonlinear way*, it is reasonable to use one of well-known iterative methods for the solution to the nonlinear least-squares problem (we use a modified Levenberg - Marquardt routine [62]).

Efficiency of the approach was verified in numerical experiments (reconstruction of equations from time series of Toda oscillator under different forms of driving: pulse periodic, periodic with subharmonics, quasiperiodic [63]). We note that efficient models with trigonometric polynomials (11) can be achieved for very large number of harmonics (that is necessary to describe uneven driving signal). This is an important advantage of the proposed approach, since instability of models (1,2) with algebraic polynomials of high orders seems the main reason for the standard approach failures.

The considered stages (dynamical variables and model structure selection) are the key ones in modeling. However, efficient specialized techniques for parameter estimation and model refinement are also useful. Techniques of such a sort are presented in the following two sections.

## 5. Model parameters estimation: quick determination of delay time from noisy time series

Here, we describe a technique of parameter estimation for DDEs. The technique is based on some specific properties of time realizations of delayed feedback systems [47, 48]. We consider one of the most popular first-order DDE as an object of investigation

$$\varepsilon_0\dot{x}(t) = -x(t) + f(x(t - \tau_0)), \tag{12}$$

where $\tau_0$ is the delay time, $f$ is a nonlinear function, and parameter $\varepsilon_0$ characterizes inertial properties of the system. In general case, Eq. (12) is a mathematical model of an oscillating system composed of a ring with three ideal elements: nonlinear, delay, and inertial ones. In a radiophysical version of the ring (Fig. 6), an amplifier with the transfer function $f$ plays the role of nonlinear device, a delay line provides a delay $\tau_0$, and a filter defines the parameter $\varepsilon_0$. We develop a technique for estimating $\tau_0$, $f$, and $\varepsilon_0$ from the time series.

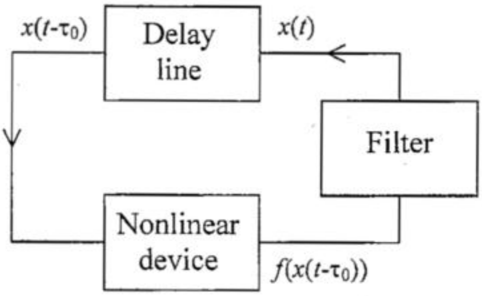

Fig. 6. Radiophysical model of time-delay system

The proposed method of estimating $\varepsilon_0$ exploits the features of extrema shape and location in the temporal realization $x(t)$ of the system (12). The peculiarities of extrema location in time are clearly illustrated by $N(\tau)$ plot in Fig. 7. To construct it one has to define for different $\tau$ values the number $N$ of pairs of extrema in $x(t)$, that are separated in time by $\tau$. If $N$ is normalized to the total number of extrema, then for sufficiently large extrema number, it can be used as an estimation of probability to find a pair of extrema in $x(t)$ separated by the interval $\tau$. Let us explain the qualitative features of $N(\tau)$ for various values of parameter $\varepsilon_0$.

In the absence of inertial properties ($\varepsilon_0$=0) differentiation of Eq. (12) gives

$$\dot{x}(t) = \dot{x}(t-\tau_0)df(x(t-\tau_0))/dx(t-\tau_0). \tag{13}$$

From Eq. (13) it follows that if $\dot{x}(t-\tau_0)=0$, then $\dot{x}(t)=0$. Thus, for $\varepsilon_0=0$ every extremum of $x(t)$ is followed within the time $\tau_0$ by the extremum. As the result, $N(\tau)$ shows a maximum for $\tau=\tau_0$ in Fig. 7, *a*.

In the presence of inertial properties ($\varepsilon_0>0$), which corresponds to real situations, the most probable value of the time interval between extrema in $x(t)$ shifts from $\tau_0$ to larger values. This effect can be explained using the ring system shown in Fig. 6: the filter

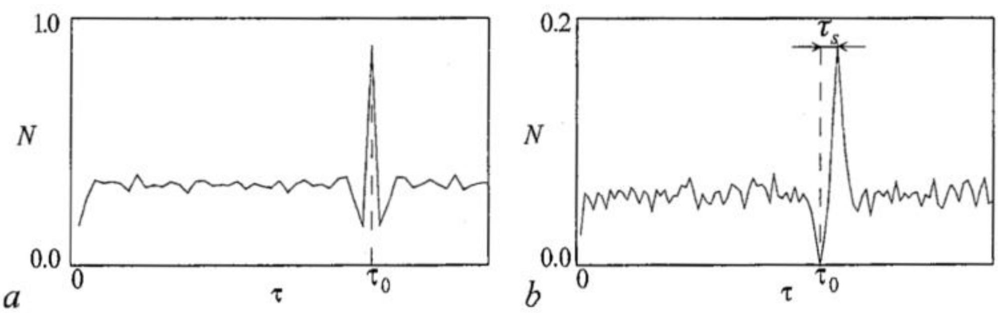

Fig. 7. Number $N$ of pairs of extrema in a realization of Eq. (12) separated in time by $\tau$, as a function of $\tau$. $N(\tau)$ is normalized to the total number of extrema in time series: *a* - $\varepsilon_0$=0, *b* - $\varepsilon_0$>0

introduces a certain additional delay in the system. As the result, the extrema in $x(t)$ can be found most often at the distance $\tau_0+\tau_s$ apart (Fig. 7, *b*). For instance, the computational investigation of Eq. (12) with quadratic nonlinear function $f(x)=\lambda-x^2$ allows us to obtain an estimation $\tau_s\approx\varepsilon_0/2$ for large values of the parameter of nonlinearity $\lambda$.

For $\varepsilon_0>0$ the extrema in $x(t)$ are close to quadratic ones and therefore $\dot{x}(t)=0$ and $\ddot{x}(t)=0$ at the extremal points. It can be shown that in this case there are practically no extrema in $x(t)$ separated in time by $\tau_0$. To prove this, let us differentiate Eq. (12) with respect to $t$:

$$\varepsilon_0\ddot{x}(t) = -\dot{x}(t) + \dot{x}(t-\tau_0)df\,(x(t-\tau_0))/dx(t-\tau_0). \tag{14}$$

If for $\dot{x}(t)=0$ in a typical case $\ddot{x}(t)=0$, then, as it can be seen from Eq. (14), for $\varepsilon\neq0$ the condition $\dot{x}(t-\tau_0)\neq0$ must be fulfilled. Thus, there must be no extremum separated in time by $\tau_0$ from a quadratic extremum and hence $N(\tau_0)\rightarrow0$. For $\tau\neq\tau_0$, the derivatives $\dot{x}(t)$ and $\dot{x}(t-\tau_0)$ can be simultaneously equal to zero, i.e., it is possible to find extrema separated in time by $\tau$. The proposed method of $\tau_0$ determination does not need significant time of computation because only operations of comparing and adding can be used for the extrema definition and $N(\tau)$ construction.

To recover the parameter $\varepsilon_0$ and the nonlinear function $f$ of system (12) from the chaotic time series we plot in a plane a set of points with coordinates $(x(t-\tau_0),\varepsilon_0\dot{x}(t)+x(t))$. According to Eq. (12), which can be written in the form

$$\varepsilon_0\dot{x}(t) + x(t) = f(x(t-\tau_0)), \tag{15}$$

the constructed set of points reproduces the function $f$. Since the parameter $\varepsilon_0$ is a priori unknown, one needs to plot $\varepsilon x(t)+x(t)$ versus $x(t-\tau_0)$ under variation of $\varepsilon$, searching for a single-valued dependence in the plane $(x(t-\tau_0),\ \varepsilon\dot{x}(t)+x(t))$, which is possible only for $\varepsilon=\varepsilon_0$. As a quantitative criterion of single-valuedness in searching for $\varepsilon_0$ we use the minimal length of a line $L(\varepsilon)$, connecting all points ordered with respect to $x(t-\tau_0)$ in the plane $(x(t-\tau_0),\ \varepsilon\dot{x}(t)+x(t))$. The minimum of $L(\varepsilon)$ is observed at $\varepsilon=\varepsilon_0$. The set of points constructed for the defined $\varepsilon_0$ in the plane $(x(t-\tau_0),\ \varepsilon\dot{x}(t)+x(t))$ reproduces the nonlinear function, which can be approximated if necessary. In contrast to methods presented in [8,35] which use only extremal points or points selected according to a certain rule for the nonlinear function recovery, the proposed technique uses all points of the time series. It allows one to estimate the parameter $\varepsilon_0$ and to reconstruct the nonlinear function from short time series even in the regimes of weakly developed chaos.

To test the efficiency of the proposed technique we apply the method to a time series produced by the Mackey-Glass equation

$$\dot{x}(t) = -bx(t) + ax(t-\tau_0)/(1+x^c(t-\tau_0)), \tag{16}$$

which can be converted to Eq. (12) with $\varepsilon_0=1/b$ and the function

$$f(x(t-\tau_0)) = ax(t-\tau_0)/[b(1+x^c(t-\tau_0))]. \tag{17}$$

The parameters of the system (16) are chosen to be $a=0.2$, $b=0.1$, $c=10$, $\tau_0=300$ to produce a dynamics on a high-dimensional chaotic attractor.

Fig. 8 illustrates the reconstruction of the system parameters. To construct the $N(\tau)$ plot we use 10000 points of the time series of $x(t)$. The time series exhibits about 600 extrema and $N(\tau)$ is normalized to their total number. The time derivatives

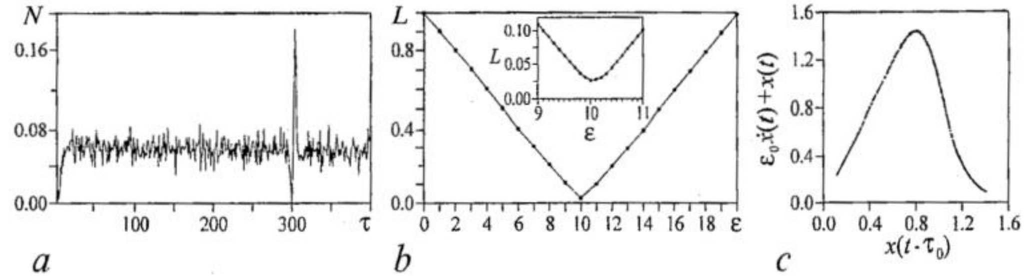

Fig. 8. *a* - Normalized number $N$ of pairs of extrema in the time series of Eq. (16) separated in time by $\tau$ for $\tau=1,\ldots,400$. *b* - Length $L$ of a line connecting points ordered with respect to $x(t-\tau_0)$ in the plane $(x(t-\tau_0),\varepsilon\dot{x}(t)+x(t))$ as a function of $\varepsilon$. The inset shows $L(\varepsilon)$ in the neighborhood of the minimum. *c* - The recovered nonlinear function

$\dot{x}(t)$ are estimated from the time series by applying a local parabolic approximation. The absolute minimum of $N(\tau)$ takes place exactly at $\tau=\tau_0=300$, where $N(300)=0$. $L(\varepsilon)$ is normalized to the most uncorrelated point set. To reduce the computation time one can choose a large initial step of $\varepsilon$ variation and then to reduce it in the neighborhood of minimum $L(\varepsilon)$. Thus, in Fig. 8, *b* the step of $\varepsilon$ variation is 1 and in the inset this step is reduced to 0.1. The minimum of $L(\varepsilon)$ takes place exactly at $\varepsilon=\varepsilon_0=1/b=10$. The recovered nonlinear function (Fig. 8, *c*) coincides practically with the true function (17). Note, that for the construction of the $L(\varepsilon)$ plot and for the recovery of the function $f$ we use only 1000 points of the time series.

To investigate the robustness of the method to perturbations we apply it to the data produced by adding a zero-mean Gaussian white noise to the time series of Eq. (16). We found out that the method is still efficient for a noise level of 10%.

As another example, we consider an experimental time series from an electronic oscillator with delayed feedback. For the case when the filter (see Fig. 6) is a low-frequency first-order RC-filter this oscillator is given by

$$RC\dot{V}(t) = -V(t) + f(V(t-\tau_0)), \tag{18}$$

where $V(t)$ and $V(t-\tau_0)$ are the delay line input and output voltages, respectively; $R$ and $C$ are the resistance and capacitance of the filter elements. Eq. (18) is of form (12) with $\varepsilon_0=RC$. In our experiment the nonlinear device has a quadratic transfer function. The proposed method allows us to define accurately the parameters of the system.

The procedure of the delay time estimation from the $N(\tau)$ plot considered with systems like (12) can be successfully applied to time series gained from a more general class of time-delay systems

$$\dot{x}(t) = F(x(t), x(t-\tau_0)). \tag{19}$$

Time differentiation of Eq. (19) gives

$$\ddot{x}(t) = \frac{\partial F(x(t),x(t-\tau_0))}{\partial x(t)}\dot{x}(t) + \frac{\partial F(x(t),x(t-\tau_0))}{\partial x(t-\tau_0)}\dot{x}(t-\tau_0). \tag{20}$$

Similarly to Eq. (14), Eq. (20) implies that in the case of quadratic extrema derivatives $\dot{x}(t)$ and $\dot{x}(t-\tau_0)$ do not vanish simultaneously, i.e., if $\dot{x}(t)=0$, then $\dot{x}(t-\tau_0)\neq 0$.

In principle, it is possible to extend the proposed method of $\tau_0$ definition from time series to high-dimensional time-delay systems having the following form

$$x^{(n)}(t) + a_1 x^{(n-1)}(t) + \ldots + a_{n-1}\dot{x}(t) = F(x(t),x(t-\tau_0)), \tag{21}$$

where $x^{(n)}(t)$ is the derivative of order $n$ and are $a_1,\ldots,a_{n-1}$ the coefficients. Differentiation of Eq. (21) with respect to t gives

$$\begin{gathered} x^{(n+1)}(t) + a_1 x^{(n)}(t) \ldots + a_{n-1}\ddot{x}(t) = \\ = \frac{\partial F(x(t),x(t-\tau_0))}{\partial x(t)}\dot{x}(t) + \frac{\partial F(x(t),x(t-\tau_0))}{\partial x(t-\tau_0)}\dot{x}(t-\tau_0). \end{gathered} \tag{22}$$

The condition $\dot{x}(t-\tau_0)\neq 0$ for $\dot{x}(t)=0$ will be satisfied if the left-hand side of Eq. (22) does not vanish. In general, a probability to obtain zero in the left-hand side of Eq. (22) is very small and therefore, the $N(\tau)$ plot qualitatively must have a shape similar to that inherent in the case of first-order delay-differential equations like (12) and (19).

The proposed method of estimation of the parameter $\varepsilon_0$ and the nonlinear function can be also applied to a variety of nonscalar time-delay systems. For instance, the dynamics of an electronic oscillator with delayed feedback containing two identical in-series RC-filters is described by the second-order delay-differential equation

$$\varepsilon_0^2\ddot{V}(t) + 2\varepsilon_0\dot{V}(t) = -V(t) + f(V(t-\tau_0)), \tag{23}$$

where $\varepsilon_0=RC$. Plotting $\varepsilon^2\ddot{V}(t)+2\varepsilon\dot{V}(t)+V(t)$ versus $V(t-\tau_0)$ under variation of $\varepsilon$, we can estimate the parameter $\varepsilon_0$ by the location of the minimum of $L(\varepsilon)$ and recover the function $f$. Thus, the proposed technique of parameter estimation can be successfully applied to a wide class of time-delay systems.

## 6. «Technologic trick»: model structure optimization using transients

Usually, global models are constructed from time realizations of established motion corresponding to an attractor in phase space. Such an approach seems reasonable when the problem of predicting future behavior of an object after establishing of oscillations is addressed. However, for modeling object dynamics in wide region of phase space, success is more probable when one uses time realizations of transient processes (when a phase orbit has not yet settled down onto an attractor). In this section we will show how this property of transients (to explore wider region of phase space) can be used to refine a model (to optimize its structure).

To detect a part of a time series which is the optimal for modeling, we compare performance of global models obtained from different parts of a time series (some of them involve a transient while the others do not). Let us use etalon differential equations of Van der Pol - Toda oscillator as an object of modeling:

$$\begin{aligned} \dot{x}_1 &= x_2, \\ \dot{x}_2 &= (1-x_1^2)x_2 - 1 + \exp(-x_1). \end{aligned} \tag{24}$$

Reconstruction is performed form a chaotic scalar time series of the $x_1$-coordinate with a transient (a phase orbit is shown in Fig. 9, *a*). Models of the form (1) with $D$=2 are constructed in two variants differing from each other by the form of a function $F(x_1,x_2)$. In the first case, a bivariate algebraic polynomial of some order $K$ is employed:

$$F(x_1,x_2) = \Sigma_{i,j=0}^{K} c_{ij} x_1{}^i x_2^j, \quad i+j \le K. \tag{25}$$

In the second case, $F$ is given by

$$F(x_1,x_2) = (\lambda - x_1{}^2)x_2 + f_K(x_1), \tag{26}$$

where $f_K(x_1)$ is a univariate algebraic polynomial of the order $K$, which approximates exponential function. To assess a model quality, right-hand side reconstruction error $\sigma$ is calculated. This quantity compare functions entering right-hand sides of an object $F_0$ and a model $F$:

$$\sigma = \textstyle\int\int_S (F(x_1,x_2) - F_0(x_1,x_2))^2 dx_1 dx_2, \tag{27}$$

where $S$ is an integration domain containing the phase orbit (hence, much larger than the domain of an attractor). The lower is $\sigma$, the better is a model.

A procedure of searching for an optimal for modeling part of the time series (*reconstruction window*) consists in following. A certain length of a window ($M$ points) is specified. A reconstruction window can be denoted as $\{\eta(t_i)\}_{i=m}^{m+M-1}$, where $m$ is the number of its initial point. The initial point of the original time series coincides with the initial point of a reconstruction window for $m$=0. When $m$ increases, a reconstruction window moves along a time series into the region of an attractor. Models are constructed for different values of $m$. Optimal location of the reconstruction window corresponds to minimum on the graph $\sigma(m)$.

Graphs $\sigma(m)$ in Fig. 9, *b* show that the best results for a model (1,25) are obtained with the use of the transient (the curve 1, small $m$). For a model (1,26) the results are better by an order of magnitude (the curve 2), but they are almost independent on the location of the reconstruction window. It can be explained as follows. The first model structure (1,25) includes variety of «superfluous» terms, e.g., the terms $x_1 x_2$, $x_1 x_2{}^2$, $x_1{}^2 x_2{}^2$, etc, which are not relevant for the original equation (24). Theoretically, model coefficients corresponding to superfluous terms should vanish. But in practice their estimated values differ from 0 due to truncation errors and impossibility of accurate approximation of exponential function by a finite power series. Superfluous terms can become significant outside of reconstruction window and lead to essential differences between an object and a model. For a model (1,25) involving superfluous terms, $\sigma$ depends essentially on $m$ (Fig. 9, *b*) that is induced by essential dependence of

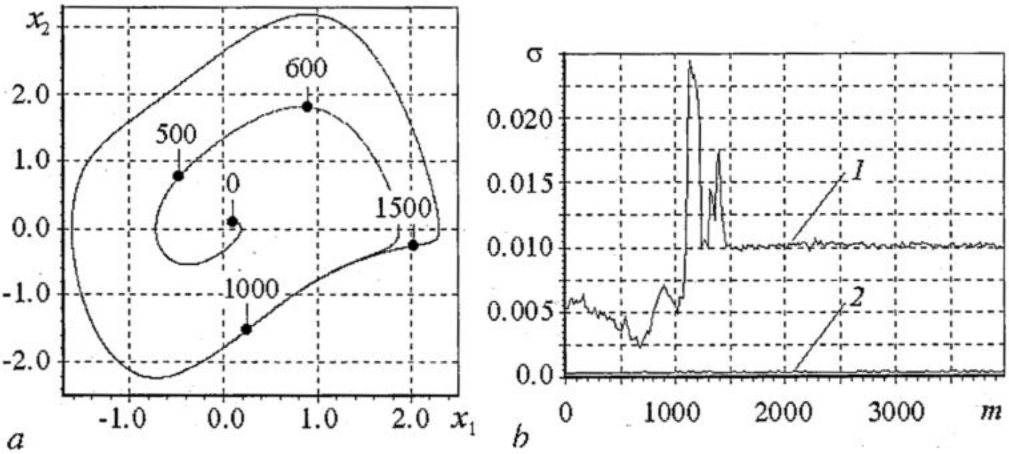

Fig. 9. *a* - A phase orbit of the system (24). *b* - Model error $\sigma$ (27) versus the location m of reconstruction window for a model (1,25) (the curve 1) and a model (1,26) (the curve 2) with polynomials of 7th order

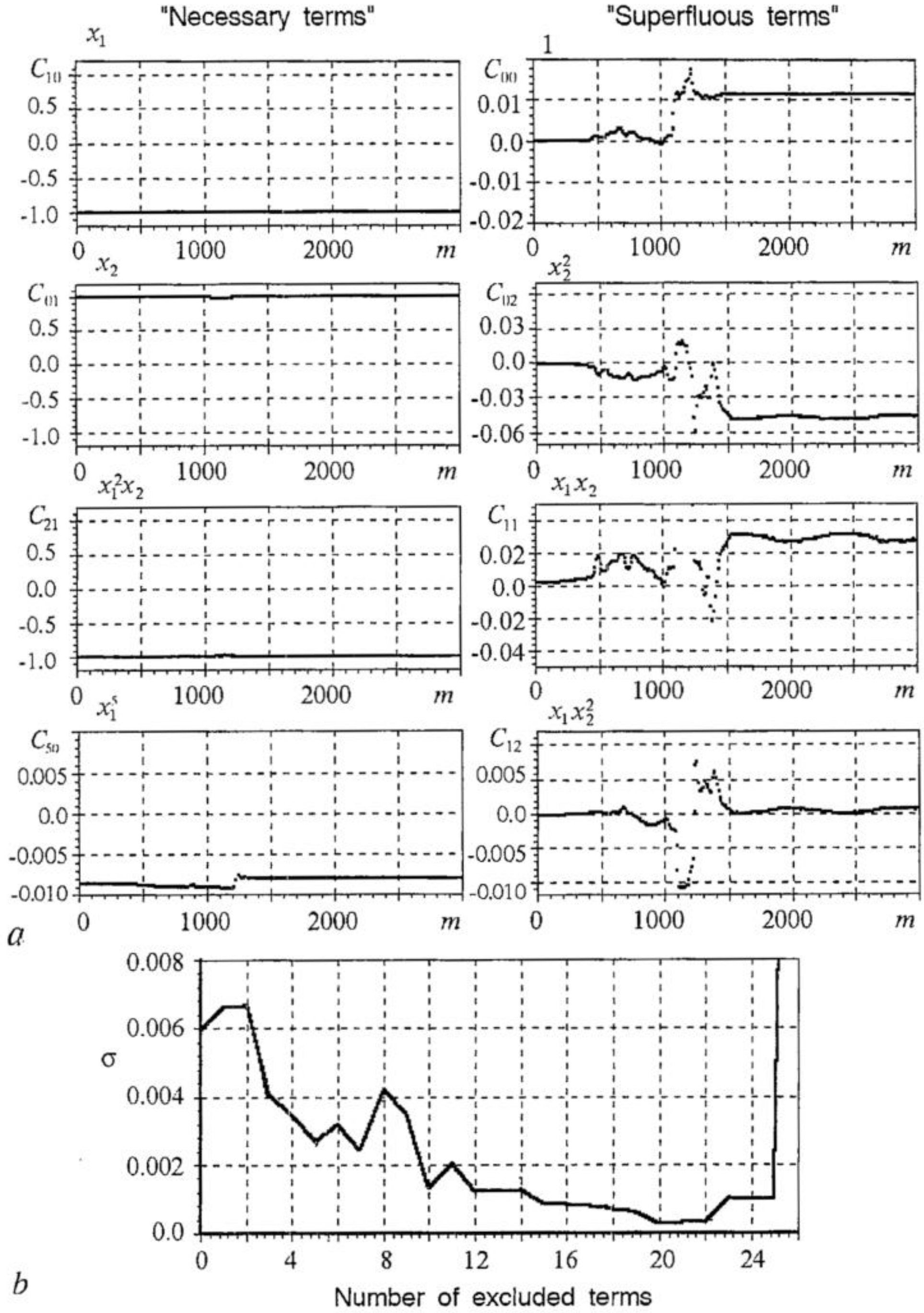

Fig. 10. Results of reconstruction of the system (24) from a scalar time series. *a* - Dependencies of coefficients (corresponding to presented near the graphs polynomial terms) of a model (1,25) on the location $m$ of reconstruction window. *b* - Model error σ versus the number of excluded terms, a «starting» model structure being (1,25)

«superfluous coefficients» on $m$ (Fig. 10). For a model (1,26), the use of a transient does not have advantages because model refinement is due to the absence of superfluous terms rather than extension of the explored region in the phase space.

Let us look again at Fig. 10, *a* where graphs for necessary terms are grouped on the left and for superfluous terms - on the right. The superfluous coefficients are obviously less stable than the necessary ones, the instability appearing close to the beginning of the time series (in the region of a transient). Resting on these considerations, we propose a procedure of model structure refinement based on sequential excluding of terms with the less stable coefficients from the model. The degree of stability (reliability) of some coefficient $a$ can be defined as the ratio of its mean value to its standard deviation $m_1=\langle a\rangle/\langle(a-\langle a\rangle)^2\rangle^{1/2}$, where angle brackets designate average over the ensemble of values of $a$, obtained at different $m$.

Thus, to optimize a model structure, the less stable coefficient (with smallest $m_1$) is found and a corresponding term is excluded from the model, reconstruction procedure is repeated for the simplified structure, and so on until exclusion of a new term leads to model deterioration. In Fig. 10, *b* we show a dependence of the model error $\sigma$ on the number of excluded terms obtained during reconstruction from time series of the system (24) starting from the model structure (1,25). The proposed procedure are shown to allow for essential enhancement of the model quality.

## 7. Conclusions

To construct dynamical models means to follow the path pointed by an optimistic outlook of determinism. There is neither guarantee that the path will lead out to the highway, nor assurance that such a highway always exists. But even if a dynamical model of an object is possible, one needs accuracy and «technological purity» to achieve a success. An error at any stage of the empiric modeling scheme presented in section 2 can make obtaining an efficient dynamical model impossible. Let us remember, by way of an analogy, how at the early stage of microelectronics underestimation of the role of dust particles and foreign microinclusions turned, e.g., production of a diode into art and did not allow to do with confidence such things that nowadays are being done routinely. So, let us hope for the absence of principal and overwhelming obstacles on the way of empiric modeling.

However, we believe that to progress in this field, one needs to develop not only original technical tricks but also (this is, possibly, the main thing) new approaches oriented to sufficiently narrow classes of systems. For the latter, a special preliminary analysis of time series and attraction of a priori information are necessary. Our work shows prospects and necessity of such a «specialization». The main results are following:

1 the proposed technique for preliminary investigation of times series of dynamical variables (section 3) allows to find variants which are the most suitable for modeling. Its advantage is in the use of local characteristics which reveal even small regions of non-uniqueness or discontinuity in dependencies between dynamical variables and quantities to enter left-hand sides of equations. However, even good choice of variables does not guarantee a success: one needs to succeed in the choice of functions form and model parameters estimation;

2 the proposed modifications of the standard structure of model equations (section 4) allow to obtain efficient models of nonautonomous systems in the case of arbitrary regular driving, while the standard approach does not give satisfactory results;

3 a special way of estimating delay time for DDEs reconstruction is proposed (section 5). It is based on peculiarities of time realizations of delayed feedback systems and efficient even when dealing with highly noisy data;

4 employed model structure often turns out very cumbersome. Therefore, it is rather important to delete «superfluous» terms (which carry only distortions) from the model. To detect such terms, we propose a special procedure which uses reconstruction from different parts of a transient process realization.

All the presented approaches are demonstrated by constructing models from numerical solutions of etalon equations and from time realizations of real-world (radiophysical) systems.

*The work was supported by the Russian Foundation for Basic Research (grants № 02-02-17578, 02-02-06502, 02-02-06503), Russian Academy of Sciences (youth grant № 23), American Civilian Research and Development Foundation (award № REC-006), and Federal Special Program «Integration» (Reg. № B0075).*

## References

1. *Box G. and Jenkins G.* Time series analysis: Forecasting and Control, revised ed., Holden-Day, San Francisco, 1976.

2. *Lorenz E.N.* Deterministic nonperiodic flow // J. of the Atmospheric Sciences, 1963. Vol. 20. P. 130-141.

3. *Ruelle D. and Takens F.* On the nature of turbulence // Commun. Math. Phys., 1971. Vol. 20. P. 167-192.

4. *Crutchfield J.P. and McNamara B.S.* Equations of motion from a data series // Complex Systems, 1987. Vol. 1. P. 417-452.

5. *Farmer J.D. and Sidorowich J.J.* Predicting chaotic time series // Phys. Rev. Lett., 1987. Vol. 59. P. 845-848.

6. *Casdagli M.* Nonlinear prediction of chaotic time series // Physica D, 1989. Vol. 35. P. 335-356.

7. *Cremers J. and Hubler A.* Construction of differential equations from experimental data // Z. Naturforschung A, 1987. Vol. 42. P. 797-802.

8. *Bünner M.J., Popp M., Meyer Th., Kittel A., Rau U. and Parisi J.* Recovery of scalar time-delay systems from time series // Phys. Lett. A, 1996. Vol. 211. P. 345-349.

9. *Voss H. and Kurths J.* Reconstruction of non-linear time delay models from data by the use of optimal transformations // Phys. Lett. A, 1997. Vol. 234. P. 336-344.

10. *Bär M., Hegger R. and Kantz H.* Fitting partial differential equations to space-time dynamics // Phys. Rev. E, 1999. Vol. 59. № 1. P. 337-343.

11. *Breeden J.L. and Hubler A.* Reconstructing equations of motion from experimental data with unobserved variables // Phys. Rev. A, 1990. Vol. 42, № 10. P. 5817-5826.

12. *Baake E., Baake M., Bock H.J. and Briggs K.M.* Fitting ordinary differential equations to chaotic data // Phys. Rev. A, 1992. Vol. 45, № 8, P. 5524-5529.

13. *Brown R., Rulkov N.F. and Tracy E.R.* Modeling and synchronizing chaotic systems from time-series data // Phys. Rev. E, 1994. Vol. 49, № 5. P. 3784-3800.

14. *Judd K., Mees A.I.* On selecting models for nonlinear time series // Physica D, 1995, V. 82. P. 426-444.

15. *Small M. and Judd K.* Comparison of new nonlinear modeling techniques with application to infant respiration // Physica D, 1998. Vol. 117. P. 283-298.

16. *Judd K., Mees A.I.* Embedding as a modeling problem // Physica D, 1998, V. 120. P. 273-286.

17. *Gouesbet G. and Maquet J.* Construction of phenomenological models from numerical scalar time series // Physica D, 1992. Vol. 58, P. 202-215.

18. *Gouesbet G., Letellier C.* Global vector-field approximation by using a multivariate polynomial $L_2$ approximation on nets // Phys.Rev. E, 1994. Vol. 49, P. 4955-4972.

19. *Letellier C., Le Sceller L., Dutertre P., Gouesbet G., Fei Z. and Hudson J.L* Topological characterization and global vector field reconstruction of an experimental electrochemical system // J. Phys. Chem., 1995. Vol. 99. P. 7016-7027.

20. *Letellier C., Le Sceller L., Gouesbet G., Lusseyran F., Kemoun A. and Izrar B.* Recovering deterministic behavior from experimental time series in mixing reactor // AIChE Journal, 1997. Vol. 43, № 9. P. 2194-2202.

21. *Letellier C., Maquet J., Labro H., Le Sceller L., Gouesbet G., Argoul F. and Arneodo A.* Analyzing chaotic behavior in a Belousov-Zhabotinskyi reaction by using a global vector field reconstruction // J. Phys. Chem., 1998. Vol. 102. P. 10265-10273.

22. *Timmer J.* Modeling noisy time series: physiological tremor // Chaos, 1998. Vol. 8, № 7. P. 1505-1516.

23. *Kadtke J.* Classification of highly noisy signals using global dynamical models, Phys. Lett. A, 1995. Vol. 203. P. 196-202.

24. *Kadtke J., Kremliovsky M.* Estimating statistics for detecting determinism using global dynamical models, Phys.Lett. A, 1997. Vol. 229. P. 97-106.

25. *Gribkov D.A., Gribkova V.V., Kravtsov Yu.A., Kuznetsov Yu.I. and Rzhanov A.G.* «Reconstruction of dynamical system structure from time series» // Radiotekh. i electron., 1994. Vol. 39, № 2. P. 269-277.

26. *Gribkov D.A., Gribkova V.V., Kravtsov Yu.A., Kuznetsov Yu.I., Rzhanov A.G. and Chepurnov A.S.* «Constructing model of system for stabilization of resonance frequency and temperature of linear electron accelerator section from experimental data» // Vestnik of Moscow State University, 1994, series 3. Vol. 35, №. 1. P. 96-98.

27. *Anosov O.L., Butkovskii O.Ya. and Kravtsov Yu.A.* Nonlinear chaotic systems identification from observed time series // Math.Models and Methods in Appl. Sciences, 1997. Vol. 7, № 1. P. 49.

28. *Anosov O.L., Butkovskii O.Ya. and Kravtsov Yu.A.* «Minimax procedure for identification of chaotic systems from an observable time sequence» // Radiotekh. i electron. 1997. Vol. 42, № 3. P. 313-319.

29. *Pavlov A.N. and Janson N.B.* «Application of technique for mathematical model reconstruction to electrocardiogram» // Izv. Vyssh. Uchebn. Zaved. Priklad. Nelin. Dinam., 1997, V. 5, № 1. P. 93-108.

30. *Pavlov A.N., Janson N.B. and Anishchenko V.S.* «Application of statistical methods for solution to problem of global reconstruction» // Pis'ma v Zh. Tekh. Fiz., 1997. Vol. 23, № 8. P. 7-13.

31. *Anishchenko V.S. and Pavlov A.N.* Global reconstruction in application to multichannel communication // Phys.Rev. E, 1998. Vol. 57, № 2. P. 2455-2457.

32. *Anishchenko V.S., Pavlov A.N. and Janson N.B.* Global reconstruction in the presence of a priori information// Chaos, Solitons & Fractals, 1998. Vol. 8. P. 1267-1278.

33. *Hegger R., Kantz H., Schmuser F., Diestelhorst M., Kapsch R.-P. and Beige H.* Dynamical properties of a ferroelectric capacitors observed through nonlinear time series analysis // Chaos, 1998. Vol. 8, № 3. P. 727-754.

34. *Bezruchko B.P., Seleznev Ye.P. and Smirnov D.A.* «Reconstruction of equations of nonautonomous nonlinear oscillator from a time series: models, experiment» // Izv. Vyssh. Uchebn. Zaved. Priklad. Nelin. Dinam., 1999. Vol. 7, № 1. P. 49-67.

35. *Bünner M.J., Meyer Th., Kittel A. and Parisi J.* Recovery of the time-evolution equation of time-delay systems from time series // Phys. Rev. E, 1997. Vol. 56. P. 5083-5089.

36. *Hegger R., Bünner M.J., Kantz H. and Giaquinta A.* Identifying and modelling delay feedback systems // Phys. Rev. Lett. 1998. Vol. 81. P. 558 -561.

37. *Pavlov A.N., Janson N.B. and Anishchenko V.S.* «Reconstruction of dynamical systems» // Radiotekh. i electron., 1999. Vol. 44, № 9. P. 1075-1092.

38. *Anosov O.L., Butkovskii O.Ya. and Kravtsov Yu.A.* «Reconstruction of dynamical systems from chaotic time series (brief review)» // Izv. Vyssh. Uchebn. Zaved. Priklad. Nelin. Dinam., 2000. Vol. 8, № 1. P. 29-51.

39. *Bünner M.J., Ciofini M., Giaquinta A., Hegger R., Kantz H., Meucci R. and*

*Politi A.* Reconstruction of systems with delayed feedback: (I) Theory // Eur. Phys. J. D, 2000, V. 10. P.165-176. Reconstruction of systems with delayed feedback: (II) Applications // Eur. Phys. J. D, 2000. Vol. 10. P.177-185.

40. *Kantz H. and Schreiber T.* Nonlinear Time Series Analysis, Cambridge University Press, Cambridge, 1997.

41. *Voss H.U., Schwache A., Kurths J. and Mitschke F.* Equations of motion from chaotic data: A driven optical fiber ring resonator // Phys. Lett. A, 1999, V. 256 P. 47-54. *Timmer J., Rust H., Horbelt W. and Voss H.U.* Parametric, nonparametric and parametric modelling of a chaotic circuit time series // Phys. Lett. A, 2000. Vol. 274. P. 123-130.

42. *Horbelt W., Timmer J., Bunner M.J., Meucci R. and Ciofini M.* Identifying physical properties of a $CO_2$-laser by dynamical modeling of measured time series // Phys. Rev. E, 2001. Vol. 64, 016222.

43. *Horbelt W., Timmer J. and Voss H.* Parameter estimation in nonlinear delayed feedback systems from noisy data // Phys. Lett. A, 2002 (to be published).

44. *Bezruchko B. and Smirnov D.* Constructing nonautonomous differential equations from a time series // Physical Review E, 2001. Vol. 63, 016207.

45. *Bezruchko B., Dikanev T. and Smirnov D.* Role of transient processes for reconstruction of model equations from time series // Physical Review E, 2001. Vol. 64, 036210.

46. *Smirnov D., Bezruchko B. and Seleznev Ye.* Choice of dynamical variables for global reconstruction of model equations from time series // Physical Review E, 2002, vol. 65, 026205.

47. *Bezruchko B., Karavaev A., Ponomarenko V. and Prokhorov M.* Reconstruction of time-delay systems from chaotic time series // Phys. Rev. E, 2001. Vol. 64, 056216.

48. *Ponomarenko V. and Prokhorov M.* Extracting information masked by chaotic signal of time-delay system // Phys. Rev. E, 2002 (to be published).

49. *Le Sceller L., Letellier C. and Gouesbet G.* Structure selection for global vector field reconstruction by using the identification of fixed points // Phys. Rev. E, 1999. Vol. 60, № 2. P. 1600-1606.

50. *Aguirre L.A., Freitas U.S., Letellier C., Maquet J.* Structure-selection techniques applied to continuous-time nonlinear models // Physica D, 2001. Vol. 158. P. 1-18.

51. *Menard O., Letellier C., Maquet J., Le Sceller L. and Gouesbet G.* Analysis of a nonsynchronized sinusoidally driven dynamical system // Int. J. Bifurcations and Chaos, 2000. Vol. 10, № 7. P. 1759-1772.

52. *Judd K. and Small M.* «Towards long-term prediction», Physica D, 2000. Vol. 136. P. 31-44.

53. *Small M., Judd K. and. Mees A* «Modeling continuous processes from data», submitted to Phys. Rev. E, 2001.

54. *Takens F.* Detecting strange attractors in turbulence // in Dynamical Systems and Turbulence, Warwick, 1980, eds. *Rang D. and Young L.S.* , Lecture Notes in Mathematics, 1981. Vol. 898. P. 366-381.

55. *Sauer T., Yorke J.A. and Casdagli M.* Embedology // J. Stat. Phys., 1991. Vol. 65, № 3-4. P. 579-616.

56. *Janson N.B., Pavlov A.N. and Anishchenko V.S.* One method for restoring inhomogeneous attractors // Int. J. of Bifurcations and Chaos, 1998. Vol. 8, № 4. P. 825-833.

57. *McSharry P.E. and Smith L.A.* Better Nonlinear Models from Noisy Data: Attractors with Maximum Likelihood // Phys. Rev. Lett., 1999. Vol. 83, № 21. P. 4285-4288.

58. *Letellier C., Macquet J., Le Sceller L., Gouesbet G. and Aguirre L.A.* On the

non-equivalence of observables in phase space reconstructions from recorded time series // J. Phys. A: Math. Gen., 1998. Vol. 31. P. 7913-7927.

59. *Kaplan D.T.* Exceptional events as evidence for determinism // Physica D, 1994. Vol. 73. P. 738-748.

60. *Hasler M.* Electric circuits with chaotic behavior // Proc. IEEE, 1978. Vol. 75, № 2. P. 40-55.

61. *Bezruchko B.P. and Seleznev Ye.P.* «Complex dynamics of driven oscillator with piecewise-linear characteristics» // Pis'ma v Zh. Tekh. Fiz., 1994. Vol. 20, № 19. P. 75-79.

62. *Levenberg K.* A method for the solution of certain problems in least squares // in Quarterly of Applied Mathematics, 1944. Vol. 2. P. 164-168.

63. *Bezruchko B.P., Sysoev I.V. and Smirnov D.A.* Reconstruction of model equations for driven systems under regular driving // Proceeding of the 6th International School Chaos'2001, Saratov. P. 17-18.

*Saratov State University*
*Institute of Radio-Engineering*
*and Electronics of RAS, Saratov Branch*

*Received 5.07.2002*

УДК 530.18

# СПЕЦИАЛЬНЫЕ ПОДХОДЫ ПРИ ГЛОБАЛЬНОЙ РЕКОНСТРУКЦИИ УРАВНЕНИЙ ПО ВРЕМЕННЫМ РЯДАМ

*Б.П. Безручко, Е.П. Селезнев, В.И. Пономаренко, М.Д. Прохоров,*
*Д.А. Смирнов, Т.В. Диканев, И.В. Сысоев, А.С. Караваев*

На примерах реконструкции эталонных уравнений и моделирования реальных радиофизических объектов иллюстрируются некоторые проблемы, возникающие при глобальной реконструкции уравнений по временным рядам наблюдаемой. Демонстрируется продуктивность специализированных подходов, направленных на моделирование выделенных достаточно узких классов объектов, и предлагаются оригинальные технологические приемы.

*Bezruchko Boris Petrovich* was born in 1946, graduated from Department of Physics of Saratov State University (1969). He is a Doctor of Science in Physics and Mathematics and a Professor in the Chair of Electronics, Oscillations and Waves of Saratov State University. His research and teaching interests include experimental investigation of nonlinear phenomena in radiophysical and electronic systems, mathematical modeling from experimental observable time series. He published more than 100 papers in Russian and foreign journals. E-mail:sbire@sgu.ru

*Seleznev Yevgeny Petrovich* was born in Saratov (1960), graduated from Saratov State University (1982). He is a Candidate of Science in Physics and Mathematics since 1989. Now, he is a senior researcher in Saratov Branch of the Institute of Radio-Engineering and Electronics of Russian Academy of Sciences. His research and teaching interests include experimental and numerical investigation of nonlinear dynamical systems. He is an author and co-author of about 70 publications.

*Ponomarenko Vladimir Ivanovich* was born in Saratov (1960), graduated from Saratov State University (1982). He is a Candidate of Science in Physics and Mathematics since 1992. Now, he is a senior researcher in Saratov Branch of the Institute of Radio-Engineering and Electronics of Russian Academy of Sciences. His research and teaching interests include nonlinear dynamics, experimental modeling of complex systems, techniques of parallel information processing. He is an author and co-author of about 50 publications.

*Prokhorov Mikhail Dmitrievich* was born in Saratov (1968). He graduated from Department of Physics, Saratov State University (1992). He is a Candidate of Science in Physics and Mathematics since 1997. Now, he is a senior researcher in Saratov Branch of the Institute of Radio-Engineering and Electronics of Russian Academy of Sciences. His research and teaching interests include experimental investigation of nonlinear phenomena in radiophysical systems and their mathematical modeling. He is an author and co-author of 40 publications.

*Smirnov Dmitry Alekseyevich* was born in Ershov, Saratov region (1977). He graduated from the College of Applied Sciences, Saratov State University (1999). He was selected as Soros Student (1996-1999) and Soros Graduate Student (2000,2001). He is a Candidate of Science in Physics and Mathematics in Saratov State University since 2001. Now, he is a junior member of teaching staff in the Department of Nonlinear Processes, Saratov State University. His scientific interests are connected with the phenomenological mathematical modeling, time series analysis, and dynamical systems theory. He is an author and co-author of 38 publications.

*Dikanev Taras Viktorovich* was born in Saratov (1979). He graduated from Department of Nonlinear Processes, Saratov State University (2002). He was selected as Soros Student in 1997-2001. His scientific interests include nonstationary time series analysis, dynamical modeling from time series. He is an author and co-author of 10 publications.

*Sysoev Ilya Vacheslavovich* was born in 1983 in Saratov. In 1999 he graduated from College of Applied Sciences of Saratov State University with silver medal and entered the University, Faculty of Nonlinear Processes. In 2000 he was certified as a Soros student. He had got a stipend of Government of Russian Federation in 2001/02 studying year. His scientific interests include mathematical modeling of nonautonomous systems and times series processing.

Sysoev was a participant of international school-conference «Chaos - 2001», All-Russian schools-conferences «Nonlinear days in Saratov for young scientists» (1998, 2000, 2001) and inter-university scientific conference «Present-day problems of electronics and radiophysics of ultrahigh (microvave) frequencies». He has 5 scientific publications in Proceedings of these Conferences.

*Karavaev Anatoly Sergeevich* was born in 1981 in Saratov, successfully graduated from Physical-Technical Lyceum (1999) and entered Saratov State University, Faculty of Nonlinear Processes. The field of scientific interests is reconstruction of time-delay systems from time series researching. Has 3 publications in scientific journal. Participated in 7 Russian and foreign conferences. Has 3 publications in collections of scientific conferences.

Izv. VUZ «AND», vol.10, № 3, 2002

# NONLINEAR DYNAMICS OF MICROWAVE AND OPTICAL SEMICONDUCTOR OSCILLATORS

*D.A. Usanov, Al.V. Skripal, An.V. Skripal, A.V. Abramov, A.A. Kletsov*

The results of experimental and theoretical investigations of the nonlinear phenomena in microwave and optical semiconductor oscillators are represented. It is shown that one of the reasons of occurrence of various nonlinear phenomena in semiconductor devices of the microwave range is qualitative change of their voltage-current characteristics, in particular occurrence or disappearance of sections of negative differential resistance under the influence of high-power microwave radiation on semiconductor structures. The external optical feedback forming autodyne operating mode of semiconductor lasers acts as the priority mechanism of realization of their nonlinear operating mode in semiconductor laser structures.

## Introduction

By now on the base of semiconductor devices the systems realizing various radio-engineering functions in the microwave and optical range have been created. One of the features of semiconductor devices is the dependence of their characteristics on the power level of the affecting signal [1,2]. As the result of such influence semiconductor devices can essentially change their operating mode.

In the microwave range the reason for such changes can be qualitative change of the current transport mechanism in the semiconductor structures and therefore the change of the shape of the voltage-current characteristics.

In semiconductor elements, which are the sources of optical radiation, one of the mechanism, which results in a great number of nonlinear phenomena, is the external optical feedback, which, in particular, forms the autodyne operating mode of semiconductor lasers [3]. Thereupon, theoretical and experimental investigations of the nonlinear dynamics of semiconductor devices in microwave and optical range under the influence of an external signal are actual ones.

## Microwave semiconductor oscillators

When describing the properties of semiconductor devices in the microwave region it is often considered possible to use their stationary or small-signal characteristics (voltage-current characteristic, impedance). Such approach allows us to successfully construct microwave systems of various types on the base of semiconductor devices. At

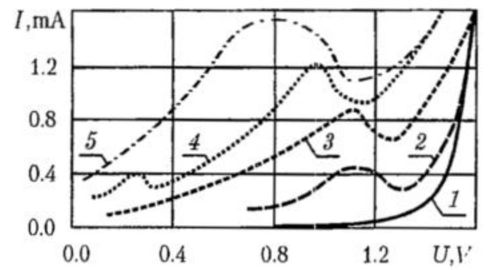

Fig. 1. The voltage-current characteristics of *p-i-n*-diode 2A534A. *P*, mW: *1* - 0; *2* - 40; *3* - 150; *4* - 420; *5* - 680

the same time it is clear that with the increase of the power level of an affecting signal the considerable change of the semiconductor devices properties is possible.

The influence of the strong electromagnetic radiation on the semiconductor devices operating mode has dictated the necessity of creation of the microwave delimiters and in particular on the base of *p-i-n*-diodes. I.e. *p-i-n*-diodes in such devices are under the influence of the high-level microwave power.

As the result of the carried out investigations it was determined that under the certain levels of affecting microwave power the stick-slip change of the rectified current and the stick-slip change of the output spectrum could take place in *p-i-n*-diodes [4, 5], one or more sections with negative differential resistance on the *p-i-n*-diodes voltage-current characteristics could appear. The voltage-current characteristics of *p-i-n*-diode 2A534A under the different levels of input power are shown in Fig. 1. So in the quasiactive delimiter on the base of *p-i-n*-diodes 2A522A and 2A534A with the increase of the input power up to 300 mW the decrease by 5-6 dB of the spectrum component $f_0$, which is the frequency of the input signal (800 MHz), and the rising of the subharmonic at the 400 MHz were observed (Fig. 2, *a*).

At the input power of the 700 mW the spectrum component $f_0/4$ arose (Fig. 2, *b*), at the 1000 mW the noise spectrum was observed, at the 1100 mW the spectrum component $f_0/3$ arose (Fig. 2, *c*), at the 1800 the spectrum component $f_0/6$ arose (Fig. 2, *d*). The initiation of those spectrum components was accompanied by the stick-slip change of power with hysteresis character. The influence of additional signal with the frequency differing from the basic signal frequency on the *p-i-n*-diode can result in the considerable decrease of the basic signal power at which subharmonics appear. The presentation of the equivalent scheme of *p-i-n*-diode as the oscillatory circuit allows us to describe the subharmonics initiation and hysteresis, but not in so complicated sequence as it was observed in the experiment. It was found that the influence of microwave radiation on *p-i-n*-diodes can result in arising on their voltage-current characteristics of one or more sections with negative differential resistance (NDR) of *N*-type and consequently in initiation of generation of high-frequency oscillations and modulation of output microwave signal by the relatively low-frequency oscillations which frequency and form in turn depend on the input power level. The theoretical description of that effect is

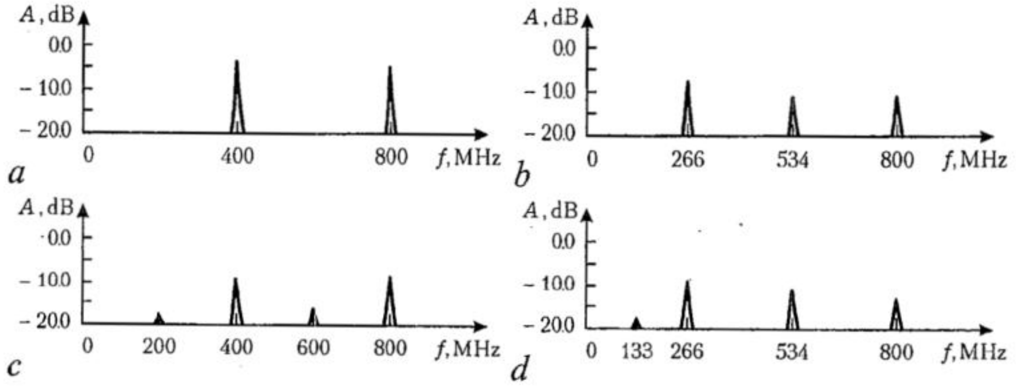

Fig. 2. The spectrograms of the output signal of the microwave delimiter on the base of *p-i-n*-diodes

possible with taking the dependence of diode impedance on the input power level, the charge carriers heating and detection effect into consideration in the physical model [6].

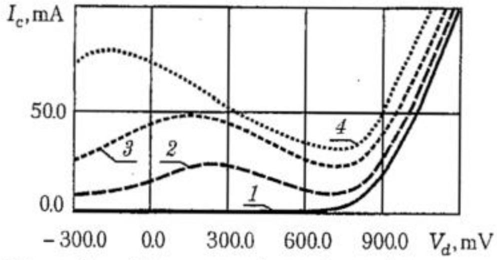

Fig. 3. The experimental voltage-current characteristics of a microwave diode. *P*, mW: *1* - 0; *2* -100; 3 - 300; *4* - 600

The phenomenon of harmonics initiation under the influence of the microwave signal on the semiconductor element was investigated thoroughly. To prevent the influence of the higher harmonics on the characteristics of microwave delimiters on the base of *p-i-n*-diodes the low-pass filters were used. At the same time the arising subharmonics in the wide-band waveguide systems can propagate and therefore influence on the output parameters of a device, in particular, they can increase the power level which leaks through the power delimiter. Carried out experimental investigations show, that introduction into the delimiter scheme of the high-pass filter, which cuts off subharmonics, allows us to reduce essentially the level of microwave power leak [7].

Experimental investigations and theoretical description show, that the influence of high-power microwave field effects dramatically on the current transport mechanism in the structures on the base of *p-n*-junction which results in the qualitative change of the shape of the voltage-current characteristics.

The experimental voltage-current characteristics of the microwave diode for the different power levels of input signal are shown in Fig. 3. As it follows from the experimental results with the increase of the input power up to 150 mW the section of NDR of *N*-type appears on the diodes voltage-current characteristics. The magnitude of the NDR increases with the growth of the input power in the range from 150 to 500 mW. At the input power of 500 mW NDR reaches -20 Ω, and in the feed circuit the low-frequency oscillations of ~200 kHz are initiated [8, 9].

Thus the essential result is: the structures with *p-n*-junction, which are incapable of generating or gaining oscillations without external electromagnetic radiation, under the influence of electromagnetic radiation become capable of that. At that the frequency and the amplitude of the generated signal depend on the affecting signal parameters.

The degree of generality of the obtained results is of interest. Do the similar phenomena appear in semiconductor structures of different types?

Another example when the structure with *p-n*-junction is under the influence of powerful external signal is microwave multipliers. The desire to obtain at the output of the multiplied signal of maximum power results in the increase of the input signal power. Carried out theoretical and experimental investigations have shown, that in multipliers the shape of the voltage-current characteristic qualitatively changes and the section with NDR appears. The change of the voltage-current characteristic shape under the influence of powerful microwave signal allows us to explain the maximum of the multiplying efficiency [10].

One of the best-investigated semiconductor microwave devices is the tunnel diode. There are theoretical investigations of nonlinear dynamics of devices based on tunnel diodes. One of the approximation assumed when modeling the operation of devices on the base of tunnel diodes is that tunnel diode voltage-current characteristic have the section of NDR of *N*-type which remains unchanged with the increase of the affected microwave power.

As the result of carried out experimental investigations it was determined that on the contrary to the situation described above and typical for *p-i-n*-diodes and diodes with non-degenerate *p-n*-junction such influence on the tunnel diode can result in the change of its voltage-current characteristic from *N*-type to exponential one which is typical for non-degenerate *p-n*-junction. The experimental voltage-current characteristics of a tunnel diode at the different values of microwave power are shown in Fig. 4 [11].

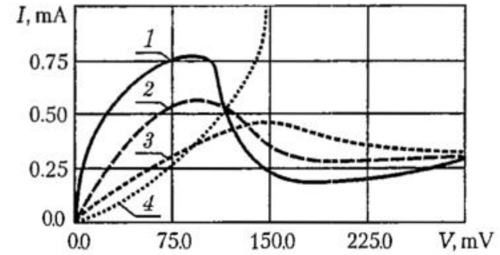

Fig. 4. The experimental voltage-current characteristics of a tunnel diode. *P*, mW: *1* - 0; *2* - 0.05; *3* - 0.2; *4* - 2.2

In the case of using of the tunnel diode as the active element of a microwave oscillator the consequence of the increase of the external signal power is the decreasing of the generating power and subsequent oscillations failure. At that the restoration of the oscillation mode is observed at essentially smaller external microwave power, i.e. the dependence of the power generated by the tunnel diode on the power of the external microwave signal has the hysteresis character [12].

As well known *N*-shape of the tunnel diode voltage-current characteristic is related to the fact that *p*-*n*-junction is formed as a result of a contact of two degenerated semiconductors. Therefore, the disappearance of the section of NDR, which is observed under the influence of microwave radiation, can mean the removal of degeneration in *p*- and *n*-regions of *p*-*n*-junction. The theoretical description of the phenomenon of changing the shape of the tunnel diode voltage-current characteristics under the influence of high-power microwave signal [13] has shown that the disappearance of the section of NDR is related to the decrease of the tunnel component and to the abrupt increase of the diffusion component of the full current because of the free charge carriers heating and appearing the detected signal. The description of the model of the oscillator on the tunnel diode under the influence of an external microwave signal because of the free charge carriers heating and appearing the detected signal is given in [14].

In [15] the experimentally found mode of initiation of NDR and switching in tunnel diode under the influence of an external microwave signal [16] in the case when the bias without microwave signal is essentially less than the peak value is described.

At present to obtain the maximum radiation power in the short-wave part of the microwave range one uses IMPATT-diodes as the active elements of oscillators [17]. In the large-signal mode the effects related to the nonlinear dependence of the IMPATT-diode parameters on the amplitude of an affecting signal are arose. One of them is the effect of changing the IMPATT-diode direct current rating because of the detection process on the diode nonlinear resistance [1].

The results of experimental investigations of the character of changes in voltage-current characteristics of IMPATT-diodes as the dependence on affecting microwave power level were presented in [18]. With the increase of the power level of the microwave signal of frequency 2500 MHz the gradual deformation of the IMPATT-diode voltage-current characteristic which is characterized by the increase of current both at the forward and reversed bias was observed. Further (up to 5.0 W) increase of the external microwave power resulted in the initiation of the section of the abrupt current growth on the voltage-current characteristic (see the arrow in Fig. 5) at the negative bias far away from the avalanche breakdown voltage in the region of thermal current. The steepness of that section and the current surge increased with the growth of the external microwave power. On the left and the right sides from that section the regions of *N*-type NDR appeared (curve 2 in Fig. 5). When the microwave exposure was switched off, the diode voltage-current characteristic took the initial form, which is typical for IMPATT-diodes without the external microwave signal (curve 1 in Fig. 5).

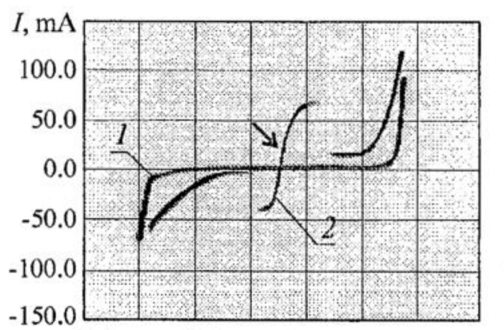

Fig. 5. The experimental voltage-current characteristic of an IMPATT-diode. P, W: *1* - 0; *2* - 5.0

It was experimentally determined that the location of these sections of current surge and NDR on the IMPATT-diode voltage-current characteristic depends essentially on the IMPATT-diode microwave circuit parameters. When the input load of the IMPATT-diode changed as the result of the short-circuiting plug shift on ~0.2 λ (λ is the wavelength of the microwave signal) at the constant power of the input signal of 5.0 W the monotonous shift of the additional section of the abrupt current growth was observed. If with such shift the impedance matching of the coaxial line and the IMPATT-diode takes place then the power of the external microwave signal accepted by the semiconductor structure increases and the sections of NDR of $N$-type appear.

At present the *GaAs* MESFETs are widely used for gain of microwave oscillations. Therefore to discover the specificity of practically used devices with *GaAs* MESFETs under the influence of high-power microwave signal is of interest when the nonlinear properties of transistor become essential ones.

The mode of subharmonic oscillations is the intermediate state before the chaos state, for subharmonics to appear the presence of nonlinear capacity, parallel to nonlinear resistivity, is essential. Since the nonlinear capacities and diodes model the area under the transistor gate, one may suppose that when the microwave signal of rather high power is applied to the transistor input, the subharmonics can arise in its output spectrum.

To find the subharmonics in output spectrum experimentally the amplifier of medium power on the base of *GaAs* MESFET was investigated. The length and the width of the gate and the thickness of the channel, when the charge carrier concentration equals to $(1 \div 2)\cdot 10^{17}$ cm$^{-3}$, is 1 μm, 300 μm and 0.3 μm correspondingly. The transistor was mounted in the microstrip scheme. The signal of frequency of $f_0$=14 GHz from the microwave oscillator G4-111 through the variable attenuator, power amplifier, low-pass filter with the cutoff frequency $f_c < f_0$ was applied to the wattmeter M3-54 and to the spectrum analyzer S4-60.

As the result of the experimental investigations it was determined that with the increasing the power of the input signal up to 140 mW the spectrum components with frequencies divisible to $f_0/9$ appeared. The spectrogram of the output signal is shown in Fig. 6.

The theoretical description of the conditions of subharmonics arising in the output spectrum of the medium-power *GaAs* MESFET with the gate of 1×300 μm, which operated in the amplifier mode, was carried out by means of numerical simulation with the use of equivalent scheme, the nonlinear elements parameters of which depended both on bias magnitude and on input microwave power level [19-21].

As the result of numerical solution of the system of differential equations, describing the equivalent scheme, the dependence of instantaneous values of the current in the load on time was determined. The phase-plane portrait of this system in the mode with stable subharmonic oscillations of current in the load and the spectrogram of the output signal at the input signal of 190 mW are represented in Fig. 7. and 6.

During the experimental researches it was determined that decrease of inductance values of input and load circuits leads to the disappearance of subharmonic oscillations of frequencies divisible to the $f_0/9$ and the occurrence of subharmonic with frequency equal to $f_0/2$ in the analyzed dynamical system [19].

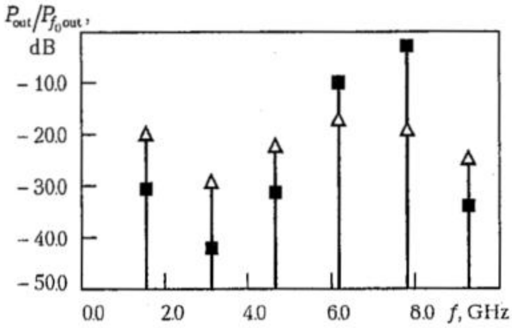

Fig. 6. The spectrogram of the output signal of the *GaAs* MESFET amplifier

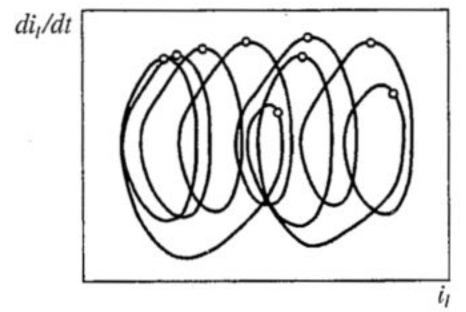

Fig. 7. The phase-plane portrait of the *GaAs* MESFET amplifier

Thus as a result of researches it was experimentally determined and theoretically proved the possibility of subharmonic existence in the output signal spectrum of medium-power microwave amplifier on GaAs MESFET. The intervals of feed voltage and input signal power at which the arising of subharmonics is possible were determined. These subharmonics are characterized by large whole number equal to the ratio of input signal frequency and subharmonic frequency. It is shown that on the going out of these intervals, including the case when power exceeds the certain value, subharmonics in the spectrum disappear. The latter indicates that with change of external signal level and, as a consequence, direct current rating, the nonlinear characteristics of transistor stipulating for bifurcation peculiarities change.

## Optical semiconductor autodynes

At present semiconductor laser diodes are an integral part of data-measuring fibre-optical systems. One of the nonlinear effects widely used in practice in such systems is the effect of autodyne detection in active area of the semiconductor laser structure, arising due to influence of the optical signal formed by an external optical feedback on the laser diode. The reflected wave leads to the change of the charge carrier concentration in the active medium and to the change of the optical generation frequency [3]. Significant interest to effect of autodyne detection in semiconductor lasers is caused by an opportunity of creation on their basis of simple measuring gauges with high sensitivity to the reflected signal [21-28].

The semiconductor laser with external optical feedback can be described by the composite resonator model [29]. Theoretical analysis is based on the solving of the field equation for a complex electric field and the rate equation for density of charge carriers [30, 31].

The system consisting of the semiconductor laser and an external reflector combines functions of the oscillator and the electromagnetic wave phase detector in one device. For researched objects with small reflectance (not more than 1%) the functions of the oscillator and of the detector are realized practically independent from each other. With growth of a feedback level their mutual influence grows, in particular, the form of autodyne signal begins to differ from the form of interference signal formed by the same movement of a reflector in interference system with decoupling from a source of radiation. At the same time the level of a feedback, stationary phase, character of movement of an external reflector influence essentially the form of autodyne signal [32-34].

In approximation of a stationary field the expression for linearized normed power of electric field $P/P_0$ can be represented as [35]:

$$P/P_0 = \cos(\omega\tau),$$

and the phase equation for stationary wave phase in the external resonator for the laser with a feedback can be represented as

$$\varphi = \varphi_0 - C\sin(\varphi+\mathrm{arctg}(\alpha)),$$

where $\varphi_0=\omega_0\tau$ is stationary wave phase for the laser without feedback, $C=\tau z(1+\alpha^2)^{1/2}$ is the parameter of an external optical feedback, $\omega_0$ is the resonance frequency of the natural resonator of the laser diode without a feedback on a threshold of generation, $\alpha$ is the factor of widening of generation line, $\tau$ is the roundtrip time of the external resonator, $z$ is the factor of external optical feedback.

For object vibrating under the sine wave law the function of stationary wave phase in the external resonator for the laser with a feedback $\varphi(t)=\omega(t)\tau(t)$ was set as:

$$\varphi(t) = \varphi_{0F} + \varphi_{0A}\sin(\Omega t),$$

where $\varphi_{0F}$ is the value of stationary phase at the fixed distance $L$ to reflector, $\varphi_{0A}$ is the amplitude of change of phase, $\Omega$ is the frequency of vibrations of the reflector.

In Fig. 8 the dependences of average normed power $P/P_0$ on time $t$ are represented. They describe movement of external reflector with frequency of mechanical oscillations $\Omega = 1/T$ ($T$ is the period of oscillations of the reflector) and amplitude $\xi = 1$ μm for the laser with wave length of $\lambda = 1.3$ μm where the specified parameters are related to amplitude of change of phase as:

$$\varphi_{0A} = 4\pi\xi/\lambda.$$

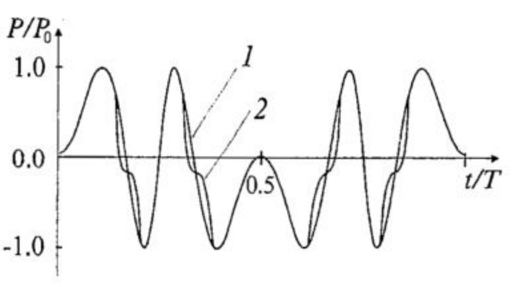

Fig. 8. Dependences of the average normed power $P/P_0$ on time $t$ at the vibrations of an external reflector described by parameters $\varphi_{0F} = \pi/2$, $\varphi_{0A} = 2\pi$, $L = 1.5$ sm, for two values of feedback parameter: *1* - $C = 0.09$, *2* - $C = 0.2$

As follows from Fig. 8, with growth of feedback parameter $C$ the deviation from the initial form of autodyne signal appears to be different on various sections of dependence $P(t)$. At the same time it is possible to single out sections with abrupt changes of inclination angle of autodyne signal which as calculations have shown correspond to occurrence of a mode of continuous relaxational oscillations [3].

In Fig. 9 the results of calculation of dependence of autodyne signal on time $t$ normed on the period $T$ and phase-plane portraits of autodyne system signal are represented. Hear $C = 0.8$, $\alpha = 5$, the amplitude of vibration $\xi = 0.2\lambda$, stationary phase $\omega_0\tau_0 = 1.6\pi$ (Fig. 9, *a*), $\omega_0\tau_0 = 0.6\pi$ (Fig. 9, *b*). As follows from Fig. 9, *a*, *b* the degree of the deviation of the form of autodyne signal from harmonic law at the fixed values of

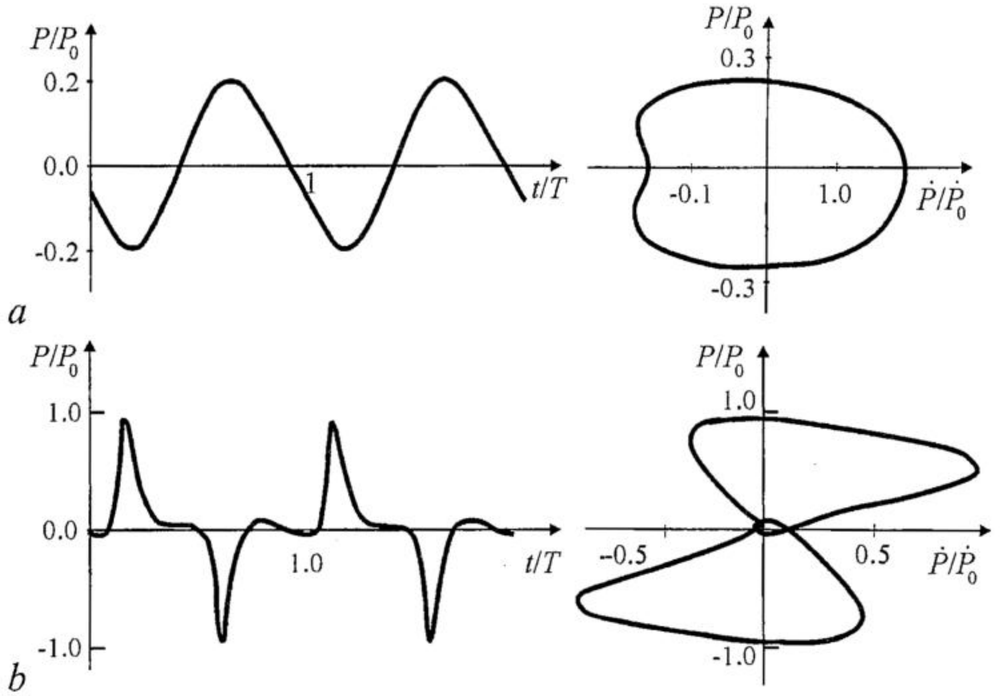

Fig. 9. Dependences on time and phase-plane portraits of power of autodyne signal of system with parameters: $C = 0.8$, $\alpha = 5$, $\xi = 0.2\lambda$, $\varphi_0$: *a* - $1.6\pi$, *b* - $0.6\pi$. Here $P_0$, $\dot{P}_0$ - the maximal values of output power and it's derivative in a range of values of $\varphi_0$ from 0 up to $2\pi$

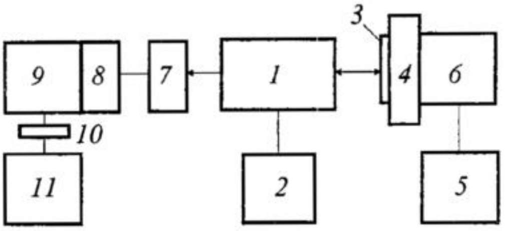

Fig. 10. The scheme of experimental setup: *1* - the semiconductor laser, *2* - the source of current, *3* - the reflector, *4* - the piezoceramics, *5* - the generator of sound oscillations, *6* - the micrometric mechanism, *7* - the photodetector, *8* - the filter of alternative signal, *9* - the amplifier, *10* - the analog-digital converter, *11* - the computer

feedback parameters and values of vibration amplitudes is defined by the magnitude of stationary phase $\omega_0\tau_0$.

Experimental researches of structure of the phase-plane portrait of autodyne signal were carried out with the help of setup the scheme of which is represented in Fig. 10.

Radiation of the semiconductor laser 1 (ILNP-206), fed by the DC source 2, was directed on the reflector 3 fixed on piezoceramics 4, vibrations of which were stimulated by the generator of sound oscillations 5. The opportunity of moving of vibrating reflector was provided with the micrometric mechanism 6. The part of the reflected radiation returned to the resonator of the semiconductor laser, output power change of which was registered by the photodetector 7. The signal from the photodetector went through the amplifier 9 containing the filter of an alternative signal 8, to an input of the analog-digital converter 10 of computer 11.

In Fig. 11 the measurement results of the signal of autodyne system are represented at various values of stationary phase. As follows from Fig. 9 to Fig. 11, theoretical and experimental curves of autodyne signal and the phase-plane portraits are in good correspondence. However at the certain distances up to the external reflector on the phase-plane portraits represented in Fig. 11, obtained experimentally, the occurrence of noise component of autodyne signal was observed. At the same time a degree of noise blurring of phase trajectory is various for its various sections. It is related to the fact that at the certain values of stationary phase the mode of generation of the semiconductor laser can change qualitatively starting from certain value of amplitudes of vibrations of reflector [35].

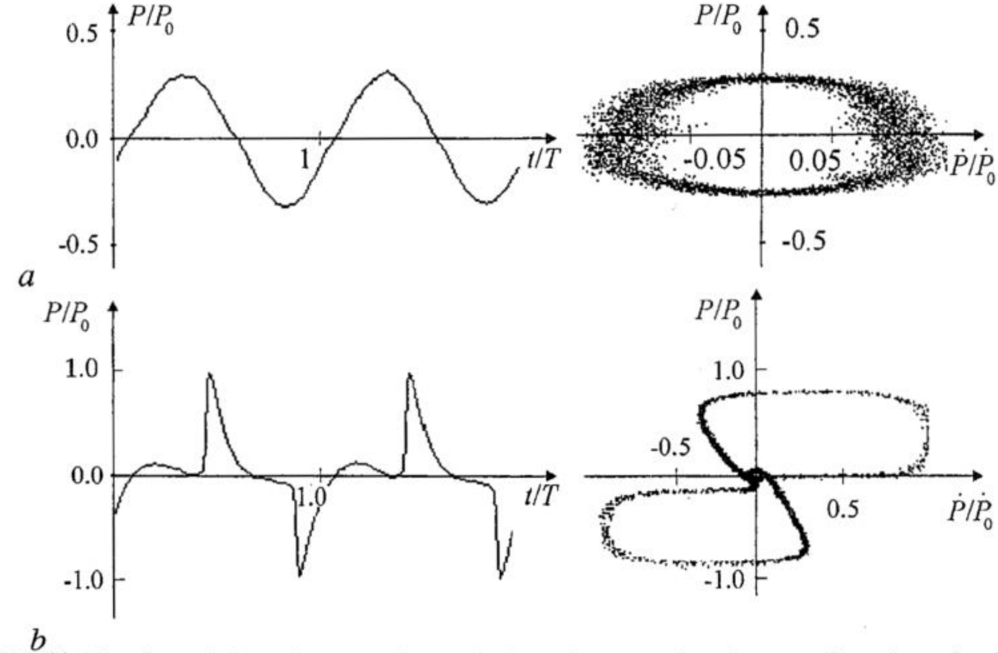

Fig. 11. Experimental dependences on time and phase-plane portraits of power of autodyne signal at various values of stationary phase $\varphi_0$: *a* - $1.5\pi$, *b* - $0.5\pi$

It is proved by the phase-plane portraits of output power $P$ at movement of reflector of laser radiation for various values of a current through the laser diode that are shown in Fig. 12.

As follows from Fig. 12, increase of a current through the laser diode results in consecutive change of the phase trajectories describing the transition of the laser from the mode of spontaneous radiation (Fig. 12, *a*) in the laser mode (Fig. 12, *b*), then in the mode of unstable generation (Fig. 12, *c*, *d*) and later in the mode with a high degree of nonlinearity of autodyne system signal. Distinctive feature of unstable generation mode of the semiconductor laser is not the blurring of trajectories on the whole phase-plane portrait, but only their blurring on its separate sections (Fig. 12, *c*, *d*). Such behavior of

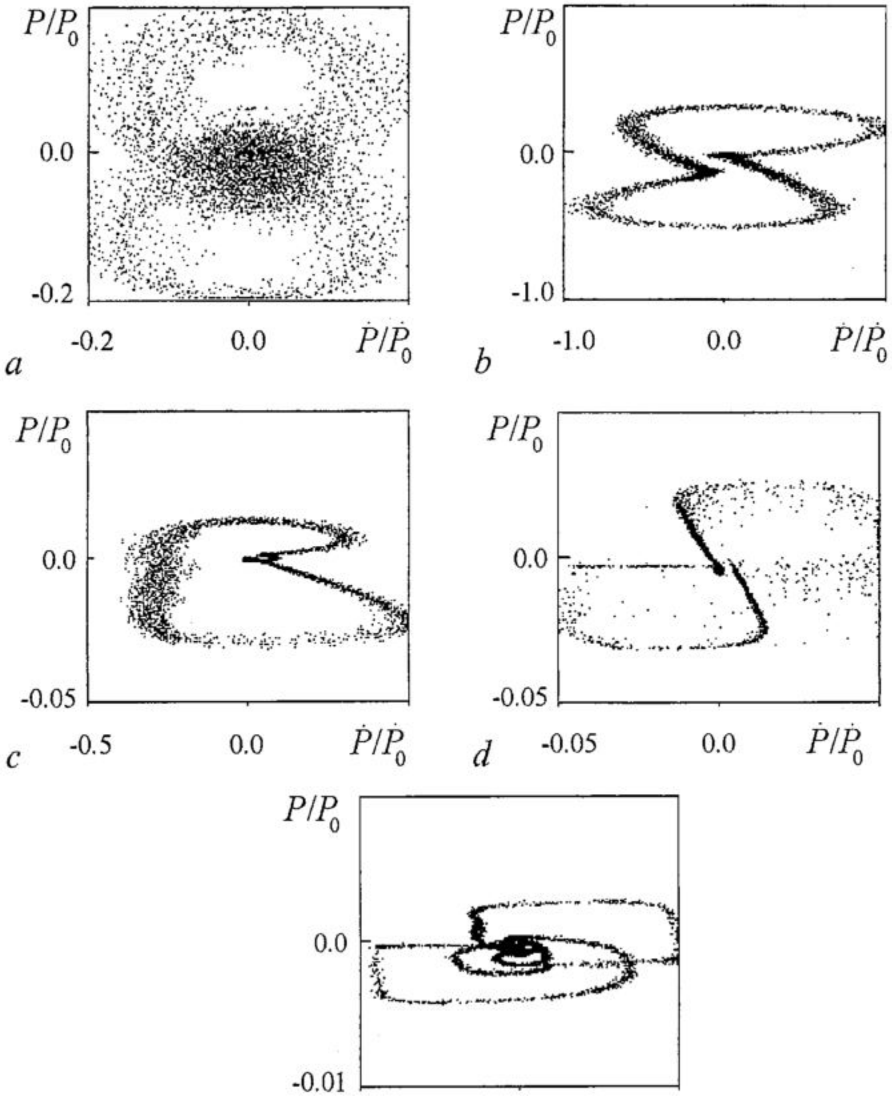

Fig. 12. Phase-plane portraits of output power of the semiconductor laser at movement of a reflector of laser radiation for various values direct currents of the laser diode: *a* - 58 mA, *b* - 63 mA, *c* - 68 mA, *d* - 70 mA, *e* - 78 mA

phase trajectories is related to strong dependence of operating mode of the semiconductor laser on position of the external reflector.

## Conclusion

Thus, the results of experimental and theoretical researches given in the present work show that one of the reasons of occurrence of a various nonlinear phenomena in semiconductor devices of the microwave range is qualitative change of their voltage-current characteristics, in particular occurrence or disappearance of sections of negative differential resistance under the influence of high-power microwave radiation on semiconductor structures.

It is shown that in semiconductor laser structures the external optical feedback forming autodyne mode of operation of semiconductor lasers acts as the priority mechanism of realization of their nonlinear operating mode.

*The work was supported by the Program on Educational Ministry of Russian Federation.*

## References

1. *Usanov D.A., Skripal A.V.* Physics of semiconductor devices operation in microwave circuits. Saratov: Saratov University Publish., 1999. 376 pp.
2. *Petermann K.* Laser Diode Modulation and Noise. Kluwer Academic Press, Dordrecht, The Netherlands. 1988. 390 p.
3. *Kalinkin M.Yu., Usanov D.A., Skripal A.V.* Autodyne detection in semiconductor-laser-generated relaxation oscillation// Proc. SPIE. 2000. Vol. 4002 P. 176-179.
4. *Vinenko V.G., Krasovskij S.V., Usanov D.A.* Modulation of a target signal in microwave power limiters on p-i-n-diodes// Elektronnaja tekhnika. Ser. 1. 1987. Vol. 4. pp. 38-39.
5. *Dzehtser G.B., Nikolaev J.I., Orlov O.S.* To a question on interaction of the plane semiconductor diode with an electronic microwave field// Voprosi radioelektroniki. Ser. 6. Radioelektronnja tehknika. 1971. Part 3. P. 3-12.
6. *Usanov D.A., Skripal A.V., Ugrjumova N.V.* Occurrence of negative differential resistance in p-i-n-diode structures at influence of microwave radiation// Izvestija Vuzov. Electronica. 1997. № 3-4. P. 48-52.
7. *Usanov D.A.* The possible lines of investigation for the semiconductor microwave electronics device parameters improvement // Radiotekhnika. 1999. № 4. P.96-99.
8. *Usanov D.A., Skripal A.V., Ugrjumova N.V.* Occurrence of negative resistance in structures on a basis of p-n-junction in the microwave field// Fizika i Tekhnika Poluprovodnikov. 1998. V.32, № 11. pp. 1399-1402.
9. *Usanov D.A., Skripal A.V., Ugrjumova N.V.* Occurrence of negative differential resistance on volt-current characteristics of diode structures on a basis of p-n-junction at influence of microwave radiation of a high level of power// Radiotehknika i elektronica. 2000. V. 45, № 12. P. 1509-1513.
10. *Usanov D.A., Skripal A.V., Posadskij V.N., Ugrjumova N.V.* Efficiency of frequency multiplication with the help of semiconductor diodes in a strong microwave field// Thes. of VI International sience-tech. conf. «Electrodynamics and engineering of the microwave and short-wave radiation» Samara, 1999. Vol. VII. Part.2 (23). P. 148-149.

11. *Usanov D.A., Korotin B.N., Orlov V.E., Skripal A.V.* Removal of degeneration in p-and n-areas of p-n-junction with external microwave signal// Pis'ma v Zhurnal Tekhnicheskoi Fiziki. 1990. Vol. 16, Part. 8. P. 50-51.

12. *Usanov D.A., Orlov V.E., Korotin B.N., Skripal A.V.* Influence of an external microwave signal on the work of the microwave oscillator on the tunnel diode// Izvestija VUZOV. Radiophysics. 1991. Vol. 34, № 1. P. 81-85.

13. *Usanov D.A., Skripal A.V., Korotin B.N., Orlov V.E.* Influence of heating microwave field on a type of volt - current characteristic of the tunnel diode// Pis'ma v Zhurnal Tekhnicheskoi Fiziki. 1993. Vol.19, Part.7. P. 81-85.

14. *Skripal A.V., Usanov D.A., Abramov A.V.* Nonlinear dynamics of the oscillator on the tunnel diode at influence of an external microwave signal// Izvestija VUZOV. Prikladnaja nelineinaja dinamika. 2000. Vol.8, № 4. P. 66-73.

15. *Usanov D.A., Skripal A.V., Ugrjumova N.V., Venig S.B., Orlov V.E.* Occurence of a mode of negative differential resistance and switching in the tunnel diode under the influence of an external microwave signal// Fizika i Tekhnika Poluprovodnikov. 2000. Vol. 34, Part. 5. P. 567-571.

16. *Usanov D.A., Venig S.B., Orlov V.E.* The negative differential resistance of the tunnel diode induced by an external microwave signal// Pis'ma v Zhurnal Tekhnicheskoi Fiziki. 1999. Vol. 25, № 2. P. 39-42.

17. *Tager A.S., Vald-Perlov V.M.* IMPATT diodes and their application in the microwave engineering. M.: Sovetskoe Radio, 1968. 480 p.

18. *Usanov D.A., Skripal A.V., Kletsov A.A.* Effect of occurrence of N-type negative differential resistance areas on volt-current characteristics of IMPATT diodes in a strong microwave field// Materials of 11-th International conference «Microwave engineering and telecommunication technologies» Crimico, 2001. 10-14 September 2001. Sevastopol. P. 170-171.

19. *Skripal A.V., Usanov D.A., Tyajlov V.S., Vasilieva A.V.* Subharmonic Generation in GaAs FET Amplifier// Proc. 11 International Microwave Conf. MIKON-96. Poland. Warsaw. May 27-30.1996, Vol. 2. P. 450-453.

20. *Usanov D.A., Skripal A.V., Tjazhlov V.S., Vasileva A.V.* Occurrence of subharmonic components in a spectrum of output signal of GaAs MESFET// Works of 3rd All-Russia scientific and technical conferences with the international participation «Actual problems of solid-state electronics and microelectronics». Divnomorskoe 1996. 8-13 Sept. Taganrog RTU. P. 80-82.

21. *Skripal A.V., Usanov D.A., Vasileva A.V., Tjazhlov V.S.* Modelling of the microwave amplifiers on GaAs MESFET, operating in a nonlinear mode// Fizika volnovih processov i radiotehknicheskie sistemi. 1998. Vol.1. № 2-3. P. 30-32.

22. *Mocker H.W., Bjork P.E.* High accuracy laser Doppler velocimeter using stable long wavelength semiconductor lasers// Appl. Opt. 1989. Vol. 28. P. 4914-4919.

23. *Shinohara S., Mochizuki A., Yoshida H., Sumi M.* Laser Doppler velocimeter using the self-mixing effect of a semiconductor laser diode// Appl. Opt. 1986. Vol. 25. P. 1417-1419.

24. *Shimizu E.T.* Directional discrimination in the self-mixing type laser Doppler velocimeter// Appl. Opt. 1987. Vol. 26. P. 4541-4544.

25. *Jentik H.W., F.F. de Mul, Suichies H.E., Aarnoudse J.G., Greve J.* Small laser Doppler velocimeter based on the self-mixing effect in a diode laser// Appl. Opt. 1988. Vol. 27. P. 379-385.

26. *Koelink M.H., Weijers A.L., Greve J., Aarnoudse J.G., Graaf R., Dassel A.C.M.* Self-mixing laser Doppler velocimetry of liquid flow and of blood perfusion in tissue// Appl. Opt. 1992. Vol. 31. P. 5844-5851.

27. *Koelink M.H., Slot M., de Mul F.F.* Laser Doppler velocimeter based on the

self-mixing effect in a fiber-coupled semiconductor laser: theory// Appl. Opt. 1992. Vol. 31. P. 3401-3408.

28. *Margin A.V.* Doppler gauge of velocity based on injected laser// Technical Physics. 1994. Vol. 64, № 1. P. 184-189.

29. *Tromborg B., Osmundsen J.H., Olesen H.* Stability analysis for a semiconductor laser in an external cavity// IEEE J.Quantum Electron. 1984. Vol.20. P. 1023-1032.

30. *Olesen H., Osmundsen J.H., Tromborg B.* Nonlinear dynamics and spectral behavior for an external cavity laser// IEEE J. Quantum Electron. 1986. Vol. 22. P. 762-773.

31. *Osinski M., Buus J.* Linewidth broadening factor in semiconductor lasers (an overview)// IEEE.J. Quant. Electron. 1987. Vol. 23. P. 9-24.

32. *Kalinkin M.Yu., Usanov D.A., Skripal A.V.* Determination of mechanical vibration form of external reflector by response of autodyne interference system based on a semiconductor laser// Proc. SPIE. 1999. Vol. 3726. P. 49-51.

33. *Skripal A.V., Usanov D.A., Kalinkin M.Yu.* Determination of comlicated movment form of the object by the signal of autodyne detection of semiconductor laser// Technical Physics. 2000. Vol. 70. P. 125-129.

34. *Skripal A.V., Usanov D.A., Vagarin V.A. and Kalinkin M.Yu.* Autodyne detection in a semiconductor laser as the external reflector is moved// Technical Physics. 1999. Vol. 44. P. 66-68.

35. *Usanov D.A., Skripal A.V., Kalinkin M.Yu.* Formation of autodyne signal in the semiconductor laser at the movement of an external reflector// Izvestija VUZOV. Prikladnaja nelineinaja dinamika. 1998. Vol. 6, № 1. P. 3-9.

*Saratov State University*

*Received 4.07.2002*

УДК 621.382

# НЕЛИНЕЙНАЯ ДИНАМИКА ПОЛУПРОВОДНИКОВЫХ СВЧ И ОПТИЧЕСКИХ ГЕНЕРАТОРОВ

*Д.А. Усанов, Ал.В. Скрипаль,*
*Ан.В. Скрипаль, А.В. Абрамов, А.А. Клецов*

Приведены результаты экспериментальных и теоретических исследований нелинейных явлений в полупроводниковых СВЧ и оптических генераторах. Показано, что одной из причин появления разнообразного спектра нелинейных явлений в полупроводниковых устройствах СВЧ-диапазона является качественное изменение вида их вольтамперных характеристик, в частности, появление или исчезновение участков отрицательного дифференциального сопротивления при воздействии мощного микроволнового излучения на полупроводниковые структуры. В полупроводниковых лазерных структурах в качестве приоритетного механизма реализации нелинейного режима их работы выступает внешняя оптическая обратная связь, формирующая автодинный режим работы полупроводниковых лазеров.

*Usanov Dmitry* graduated from the Faculty of Physics of Saratov State University in 1965. Doctor of Science in Physics and Mathematics since 1989, Professor of Chair of Solid State Physics since 1990. Head of Chair of Solid State Physics of Saratov State University. He is the author of monographs, textbooks, more than 300 articles in the sphere of solid state electronics, physics of semiconductors and radiophysics. He is the author of more than 90 inventions and patents, the member of the IEEE, Honored Man of Science of Russian Federation (1998).

*Skripal Alexander* graduated from the Faculty of Physics of Saratov State University in 1976. Doctor of Science in Physics and Mathematics since 1998, Professor of Chair of Solid State Physics of Saratov State University since 1998. He is the author of more than 100 scientific publications, textbooks and inventions in the sphere of solid state electronics, semiconductor physics and radiowave control.

*Skripal Anatoli* graduated from the Faculty of Physics of Saratov State University in 1982. Doctor of Science in Physics and Mathematics since 1998, Professor of Chair of Solid State Physics of Saratov State University. He is the author of more than 100 scientific publications in the field of coherent optics, laser physics, physics of magnetic liquids, biophysics.

*Abramov Anton* graduated from the Faculty of Physics of Saratov State University in 2002. He is the post-graduate student of Chair of Solid State Physics of Saratov State University since 2002. He is the author of 15 scientific publications. His scientific interests include semiconductor physics, solid state electronics.

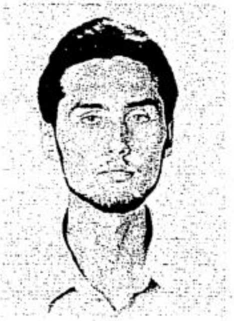

*Kletsov Alexei* graduated from the Faculty of Physics of Saratov State University in 1999. He is the post-graduate student of Chair of Solid State Physics of Saratov State University since 1999. He is the author of 5 scientific publications. His scientific interests include semiconductor physics, microwave electronics.

Innovations in applied physics

Izv. VUZ «AND», vol.10, № 3, 2002

# OPTICAL PROPERTIES OF COLLOIDAL-GOLD BIOCONJUGATES

*N. G.Khlebtsov, V.A. Bogatyrev, L.A. Dykman,*
*Ya.M. Krasnov, A.G. Melnikov*

We discuss optical properties of single or aggregated colloidal-gold conjugates that can be fabricated by adsorption of a biopolymer onto the surface of nanoparticles. To simulate extinction and scattering of light by such structures, we apply the generalized multisphere Mie solution and the discrete dipole approximation along with a computer model of cluster-cluster aggregation. Our consideration includes the following topics: statistical and orientational averaging of optical observables; optical effects related to the chain-like structures; effects of polymer coating and interparticle spacing; simulation of kinetic changes in the optical properties of aggregated sols formed during biospecific binding; modification of the exact multipole approach for the case of two-layered monomers. In the rest of this paper, we give a short review of our experimental work on the topic (including biomedical applications) and provide experimental examples concerning the optical monitoring of biospecific interactions on a nanometer scale.

## 1. Introduction

Colloidal-gold (CG) nanoparticles have been widely used during the past years as effective optical transducers of biospecific interactions [1]. In particular, the resonance optical properties of nanometer-sized CG particles have been employed to design biochips and biosensors [1-3] used as analytical tools in biology (determination of DNA, RNA, proteins, and metabolites), medicine (drugs screening, antigen and antibody determination, virus and bacterial diagnostics), and chemistry (on-line environmental monitoring, quantitative analysis of solutions and disperse media). As a special and important example one should note polynucleotide detection, based on the formation of 3-D ordered structures that result from hybridizing conjugate linkers with complementary oligonucleotides [4, 5]. These systems can potentially detect femtomolar concentrations of oligonucleotides [1].

It is well known [6, 7] that the surface plasmon resonance (SPR) of gold nanoparticles near 520 nm controls the characteristic spectral properties of colloidal-gold sols. The formation of aggregated structures results in substantial changes in the value and spectral position of SPR because of the strong electrodynamic interaction of cluster gold particles when their average spacing is comparable to or less than the particle size [8, 9]. This strategy (analogous to the sol-particle immunoassay, SPIA [10]) can be applied to protein detection at nanogram level [11] as well as to sensitive clinical diagnostics [12, 13]. It is clear that optimization of the nano-gold-markers methodology demands a deep insight into the optical properties of conjugates and aggregates built from these monomers. However, noticeable progress in the field has been achieved only very recently because of the strong electrodynamic many-particle interaction of cluster nanoparticles when its spacing is less than their size [14].

This paper gives an overview of our recent work (including the work supported by CRDF grant REC-006) [14-23] related to theoretical and experimental studies of extinction and light scattering properties of colloidal gold bioconjugates and to some biomedical applications of the markers developed [24-29]. Besides we present here some new data that have not been published anywhere before.

## 2. Theoretical study

***2.1. Computer model for cluster aggregation.*** A three-dimensional lattice model with Brownian or linear trajectories of single particles and intermediate clusters was employed to simulate the aggregation process. At the initial time moment, $N_0$ particles are generated at randomly selected points of a cubic lattice with size $L$. When a particle moves to a lattice point adjacent to another particle or intermediate cluster, a combined cluster is formed. This model produces diffusion-limited (Brownian trajectories) or ballistic (linear trajectories) clusters with fractal dimension $d_f \approx 1.8$ and $d_f \approx 2.0$, respectively. A more detailed description of the model can be found elsewhere [30].

### *2.2. Light scattering and extinction by a single aggregate.*

***2.2.1. Discrete dipole approximation (DDA).*** Consider the scattering of a plane electromagnetic wave propagating in a dielectric surrounding medium with the refractive index $n_0$

$$\mathbf{E}_0 = \mathbf{e}_0 \exp(\hat{\imath}\mathbf{kr}), \quad |\mathbf{e}_0| = 1, \quad |\mathbf{k}| = k = 2\pi n_0/\lambda, \quad \hat{\imath} = (-1)^{1/2}, \tag{1}$$

by a single cluster built from $N$ small spherical nanoparticles with radius $a$ and complex refractive index $n(\lambda)$. In the DDA method [31], a real aggregate is replaced by a set of point dipoles $\mathbf{d}_i = \mathbf{d}(\mathbf{r}_i)$, $i$=1-$N$. The linear equations for the interacting dipoles can be written in the form [16]

$$\Sigma_{jm=1}^{3N} A_{il,jm} d_{jm} = \alpha_i e_{0l} \exp(\hat{\imath}\mathbf{kr}_i), \quad il = 1 - 3N, \tag{2}$$

where $\alpha_i$ is the polarizability of the $i$th dipole, the combined indices are $il=3(i-1)+l$, $jm=3(j-1)+m$; $i,j$=1-$N$; and indices $l,m$=1,2,3 ($x,y,z$) correspond to the Cartesian components of vectors or tensors. The explicit form of the dipole interaction matrix $A_{il,jm}$ can be found in Ref. [16]. The solution of the linear systems of Eqs. (2) allows one to calculate all the basic optical characteristics of the aggregate. For instance, the extinction cross section, determining the spectrum of optical density of a dilute suspension, can be calculated from the optical theorem [6, 14]

$$C_e = 4\pi k \mathrm{Im} \Sigma_i \, (\mathbf{e}_0 \mathbf{d}_i) \exp(-\hat{\imath}\mathbf{kr}_i). \tag{3}$$

In the above sketch description we omitted some important questions related to the choice of optical polarizability and renormalization of interdipole spacing. The readers are referred to the corresponding discussion in review [14] and to the references therein. In short, we used the interparticle spacing parameter $\gamma = d_L/a$ as a fitting parameter of a theory providing for the best agreement between theoretical predictions and experimental observations [32].

In practical applications, one usually needs average results for random orientations of clusters rather than calculations for a particular structure with a fixed orientation. In principle, such averaging can be carried out by numerical integration over Euler angles that define the orientation of a scatterer with respect to the incident wave. However, an analytical solution of such a problem turns to be much more effective as compared with the straightforward numerical approach. Examples of such analytical solutions are well known in the T-matrix method including its application to the cluster light scattering [14]. In works [18, 20], we derived an exact analytical solution for integral extinction, scattering, and absorption DDA cross sections averaged over random orientations of scatterers. Application of the solutions was illustrated by practical computations of averaged extinction cross sections for several examples of fractal clusters (soot in air and colloidal aggregates built from polystyrene, gold, or silver nanoparticles).

The interaction matrix in Eq. (2) does not depend on the incident wave orientation, so it is convenient to perform orientational averaging in the cluster coordinate frame. Using the inverse matrix $B=A^{-1}$ to solve Eq. (2), we obtain the following general equation for the extinction cross section

$$\langle C_e\rangle = 4\pi k \mathrm{Im}\{\Sigma_{i,j=1}^{N} \Sigma_{p,q=1}^{3} \alpha B_{ip,jq} E_{pq}^{ij}\}, \quad E_{pq}^{ij} = \langle \tilde{V}_{pq} \exp(-\hat{\imath}\mathbf{k}\mathbf{r}_{ij})\rangle, \tag{4}$$

where the angle brackets mean integration over Euler angles that define the orientation of the incident wave in the cluster frame, $\tilde{V}_{pq}=e_p e_q$ is the second-rank tensor, and $e_p$ are the Cartesian components of the polarization vector in the cluster frame. The general scheme for calculation of average cross sections according to Eq. (4) consists in the following: First, we represent the tensor $\tilde{V}_{pq}$ as a linear combination of irreducible spherical tensors in the incident wave coordinate frame. Such a transformation can be performed using Clebsh-Gordan coefficients and Wigner rotation functions [14]. Then, we expand the plane incident wave in a series over vector spherical harmonics (VSH) and perform orientational averaging by using the orthogonality properties of VSH and Wigner functions. Omitting the technical details of calculations, we give the final result:

$$\langle C_e\rangle = 4\pi k \mathrm{Im}\{\mathrm{Spur}(T)\}, \quad \langle C_a\rangle = 4\pi k \mathrm{Spur}(W), \tag{5}$$

where the matrices $T$ and $W$ are defined by equations

$$\hat{A}\hat{T} = \alpha\hat{E}, \qquad W = \eta|\alpha|^2\hat{B}\hat{E}\hat{B}^{+}, \tag{6}$$

and the explicit form of parameter $\eta$ and an auxiliary matrix $E$ can be found in Refs. [18,20].

***2.2.2. Generalized multiparticle Mie solution (GMM).*** For large dielectric monomers or metal nanoparticles, the DDA model fails because of the multipole nature of electrodynamic particle coupling. An exact solution of the cluster-light-scattering problem can be formulated rather simply, using a generalized Mie theory for multisphere configurations [33, 34]. An incident electromagnetic field $\mathbf{E}_{inc}^{\,i}$ for the $i$th particle can be expanded over VSH $\mathbf{Y}_{mn1}^{(\tau)}=N_{mn}^{(\tau)}(k\mathbf{r}_i)$; $\mathbf{Y}_{mn2}^{(\tau)}=\mathbf{M}_{mn}^{(\tau)}(k\mathbf{r}_i)$ of the first kind ($\tau$=1; spherical Bessel generating functions are used)

$$\mathbf{E}_{inc}^{\,i} = \Sigma_{n=1}^{\infty} \Sigma_{m=-n}^{n} \Sigma_{p=1}^{2} \hat{\imath} E_{mn} p_{mnp}^{\,i}\, \mathbf{Y}_{mnp}^{(1)}(k\mathbf{r}_i), \tag{7}$$

where $E_{mn}$ are normalization coefficients. For a plane wave (see Eq. (1)) with the incidence direction defined by Euler angles ($\varphi=\alpha$, $\vartheta=\beta$, $\psi=\gamma$) in the $i$th coordinate frame, the expansion coefficients are

$$\bar{p}_{mnp}^{\,i} = \exp(\hat{\imath}\,\mathbf{k}\mathbf{r}_i) \exp(-\hat{\imath}m\varphi) 1/n(n+1)[\tau_{mnp}(\vartheta) \cos\psi - \hat{\imath}\tau_{mn3-p}(\vartheta) \sin\psi], \tag{8}$$

$$\mathbf{kr}_i = k[x_i \sin\vartheta \cos\varphi + y_i \sin\vartheta \sin\varphi + z_i \cos\vartheta], \tag{9}$$

where the functions $\tau_{mnp}(\vartheta)$ ($p$=1, 2) correspond to the well-known light scattering functions $\tau_{mn}(\cos\vartheta)$, $\pi_{mn}(\cos\vartheta)$ [6].

The scattered field from the $i$-th particle can be expanded over VSH of the third kind (Hankel generating functions are used) in the same manner as in Eq.(6)

$$\mathbf{E}_s{}^i = \Sigma_{n=1}^{\infty} \Sigma_{m=-n}^{n} \Sigma_{p=1}^{2} \, iE_{mn} a_{mnp}{}^i \, \mathbf{Y}_{mnp}{}^{(3)}(k\mathbf{r}_i). \tag{10}$$

The application of the usual boundary conditions leads to the following simple relations between the expansion coefficients

$$a_{mnp}{}^i = \bar{a}_{np}{}^i \, p_{mnp}{}^i, \tag{11}$$

where $\bar{a}_{n1}{}^i = \bar{a}_n{}^i$ , $\bar{a}_{n2}{}^i = b_n{}^i$ are the usual Mie coefficients for an isolated homogeneous sphere [6]. Solution (11) is a crucial one in the GMM as it gives a simple and exact relation between $p_{mnp}{}^i$ (exciting field) and $a_{mnp}{}^i$ (scattered field). The unknown expansion coefficients of the exciting field can be found from the superposition principle that leads to the set of linear equations

$$\Sigma_{j=1}^{N} \Sigma_{\nu=1}^{\infty} \Sigma_{\mu=-\nu}^{\nu} \Sigma_{q=1}^{2} H_{mnp,\mu\nu q}{}^{ij} \, p_{\mu\nu q}{}^j = \bar{p}_{mnp}{}^i, \tag{12}$$

where $\bar{p}_{mnp}{}^i$ are the known expansion coefficients of the incident field in the $i$th coordinate frame. The interaction matrix $H$ is determined by the «coefficients of translation» of VSH based on spherical Hankel functions of the first kind (see explicit relations in Ref. [14]).

Once Eqs (12) are solved and coefficients $a_{mnp}{}^i$ are found, one can calculate all characteristics of light scattered by a cluster. For example, the extinction cross section is given by equation

$$C_e = 4\pi/k^2 \, \Sigma_{i=1}^{N} \Sigma_{n=1}^{M} \Sigma_{m=-n}^{n} \Sigma_{p=1}^{2} C_{mn} \mathrm{Re}[a_{mnp}{}^i \, (p_{mnp}{}^i)^*], \tag{13}$$

where coefficients $C_{mn}$ depend on VSH normalization. The light scattering observables can be averaged over random cluster orientations by using T-matrix cluster formulation and the corresponding theorems for orientational averaging [34, 35].

***2.3. Calculation of extinction and light scattering spectra for ensembles of clusters.*** A model for the dynamic simulation of extinction spectra during the aggregation process was developed in our work [16]. We assume that a cluster suspension is dilute so that the single scattering approximation is valid. This means that the extinction (optical density or absorption) $A(\lambda)$ is directly proportional to the sum of extinction cross sections of clusters per unit volume. It is convenient to normalize the extinction spectra to the monomer optical density $A_m(a, \lambda_{\max})$ at the maximum of extinction of monomers $C_{em}(\lambda_{\max})$

$$A_m(\lambda) \equiv A(a, \lambda)/A_m(a, \lambda_{\max}) = C_e(a, \lambda)/C_{em}(a, \lambda_{\max}). \tag{14}$$

The cluster-size distribution at an arbitrary stage of aggregation can be described by a set of number pairs $(p, N_p)$, where $p$ is the number of particles per aggregate from a given monodisperse ensemble $(p, N_p)$, and $N_p$ is the number of such aggregates. Light extinction by the $(p, N_p)$ ensemble is given by the normalized extinction cross section

$$\overline{\langle Q_p \rangle} = \overline{\langle C_{ep}(R_m, \lambda) \rangle} / pC_{em}(R_m, \lambda), \tag{15}$$

where the angle brackets denote the averaging over random cluster orientations in a monodisperse ensemble of clusters, and the horizontal bar designates statistical averaging over cluster configurations of ensemble $(p,N_p)$. The optical density of the suspension is given by the relationship

$$E(\lambda) = E_m(R_m,\lambda)\Sigma_p \nu_p \langle Q_p \rangle, \qquad (16)$$

where $\nu_p$ is the fraction of $p$-cluster particles of the total number of initial monomers $N_0$

$$\nu_p = pN_p / \Sigma_p pN_p = pN_p / N_0. \qquad (17)$$

For calculation of the absolute values of extinction and scattering intensity, we used a gold concentration of gold 57 μg/ml (cuvette thickness 1 cm).

***2.4. Statistical and orientational averaging of light scattering observables: some important simplifications.*** It is clear that calculation of $\overline{\langle C_{ep} \rangle}$ quantities is a challenging step of the simulations. In both methods (DDA and GMM), the analytical procedures of orientational averaging imply that the cluster T-matrix (i.e., actually, the corresponding inverse interaction matrix) has to be found. At moderate numbers of cluster particles (say, $N \le 3000$), the DDA analytical method can be implemented in a usual PC without any problem. However, the GMM analytical solution needs a huge RAM volume even for small ($N \sim 100$) metal clusters because of the multipole nature of the electrodynamic interaction (see discussion in Refs. [14, 34]). Having in mind that actually we need both orientational and statistical averaging over cluster configurations, we encounter a serious calculation problem.

However, these difficulties suggest that statistical averaging over a *large number of random configurations* is perhaps all we need. In other words, we can hazard a conjecture that statistical averaging actually includes the orientational one. Symbolically, our hypothesis can be written as follows:

$$\overline{\langle C_{ep} \rangle} \approx \overline{C_{ep}}. \qquad (18)$$

To verify this hypothesis, we generated monodisperse statistical ensembles of clusters with $N$=const. and then calculated two sets of the averaged parameters, for example $\overline{\langle C_e \rangle}$ and $\overline{C_e}$. Two quantities were computed: the extinction cross section $C_e$, or the corresponding absorption $A_e$, and the normalized scattered intensity $S_{90}=S(\theta=90)$[1] (for simplicity, we will subsequently omit the subscript 90). Some data obtained are listed in Table. We drew two important conclusions from these results: First, to simulate the extinction of light by an aggregated suspension, it is sufficient to account only for random cluster configurations, i.e., without orientational randomization. Second, the scattered intensity is more sensitive to cluster orientations than extinction is. Therefore, one has to use a big statistical monodisperse ensemble in order to eliminate fluctuations in the calculated scattered intensity. The first conclusion leads to great simplifications, as we can use effective and fast codes for clusters with fixed orientations instead of huge RAM consuming codes for analytical T-matrix averaging.

***2.5. Effects of aggregate form and interparticle spacing.*** Looking at the internal structure of real or simulated clusters, one can note numerous chain-like fragments. Therefore, it would be desirable to understand possible optical effects related to the formation of such chain-like nanoparticle structures. We can make a rough-cast evaluation by using a homogeneous spheroidal model that can be easily treated by the T-matrix method [14]. Fig. 1 shows the spectral dependence of extinction calculated for randomly oriented spheroids with equivolume radius 30 nm and axis ratio $e=a/b$=1, 1.3,

---

[1] Along with our own routines, we used numerical codes gmm01s and scsmtm1, kindly provided by Yu-lin Xu (Univ. of Florida, USA) and Daniel Mackowski (Auburn Univ., USA). Thanks to both colleagues.

Table

Comparison of extinction $A_1 \equiv \overline{A_{ext}}$, scattered intensity $S_1 \equiv \overline{S_{90}}$ (statistical averaging only) and $A_2 \equiv \overline{\langle A_{ext} \rangle}$, $S_2 \equiv \overline{\langle S_{90} \rangle}$ (both orientational and statistical averaging). Calculations for clusters built from $N$=10 or 100 gold particles with diameters 15 and 30 nm coated by 2.5 nm polymer shell with $n_2$=1.4. All data are averaged over 100 independent cluster configurations.

| $d$, nm | $N$ | λ=400 nm | | | | λ=500 nm | | | | λ=600 nm | | | |
|---|---|---|---|---|---|---|---|---|---|---|---|---|---|
| | | $A_1$ | $A_{2c}$ | $S_1$ | $S_{2c}$ | $A_1$ | $A_{2c}$ | $S_1$ | $S_{2c}$ | $A_1$ | $A_{2c}$ | $S_1$ | $S_{2c}$ |
| 15nm | 10 | .665 | .664 | .189 | .185 | .955 | .954 | .176 | .174 | .213 | .213 | .163 | .161 |
| | 100 | .674 | .672 | .275 | .278 | .922 | .921 | .364 | .368 | .296 | .298 | .589 | .603 |
| 30nm | 10 | .711 | .708 | .763 | .744 | .894 | .893 | .779 | .766 | .551 | .545 | .201 | .195 |
| | 100 | .671 | .667 | .448 | .470 | .777 | .775 | .487 | .513 | .904 | .897 | .256 | .251 |

1.5, and 2. The optical constants of gold and the surrounding medium (water) were calculated according to Ref. [36]. With an increase in the axis ratio, one can observe the red shift of the extinction maximum and the appearance of a short wavelength mode (peak splitting [6]). Fig. 2 shows extinction spectra calculated for a randomly oriented linear chain of 13-nm gold spheres with interparticle spacing 1.1 nm. Again, one can observe a noticeable red shift of peaks and its splitting. Note that our results essentially differ from the data published recently by Lazarides and Schatz [37]. Perhaps, their Fig. 8 from [37] was calculated with an insufficiently large multipole expansion order.

The interparticle distance $\Delta d$ is a key parameter that determines the electrodynamic coupling of gold monomers. We have shown [16] that for clusters built from contacting silver or gold nanospheres, the convergence of the GMM method is too slow due to the multipole nature of the interparticle interaction. However, if the cluster particles are separated by a small distance, the number of multipole terms in a series is decreased down to a tractable level. This effect is illustrated in Fig. 3, where the

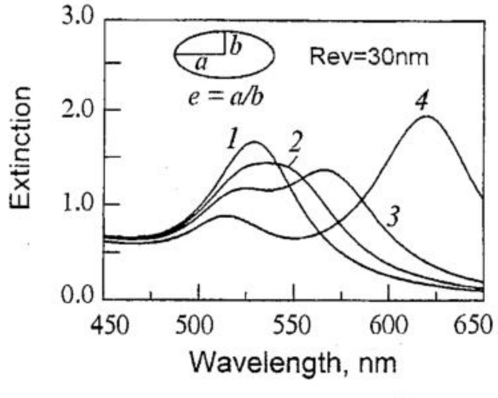

Fig. 1. Extinction spectra of randomly oriented gold nanospheroids in water. The equivolume diameter $d_v$=30 nm and axis ratio $e=a/b$=1(sphere *1*), 1.3 (*2*), 1.5 (*3*), and 2 (*4*)

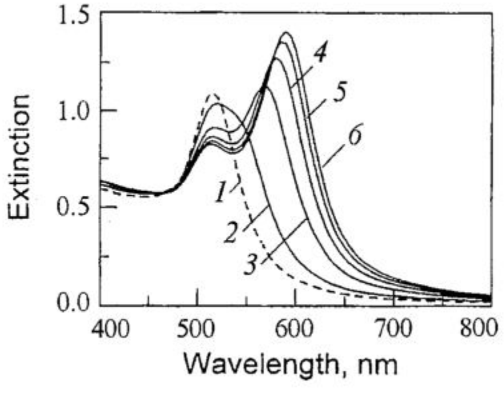

Fig. 2. Extinction spectra of randomly oriented chains built from 13 nm gold particles separated by 1 nm distance in water. The number of spheres equals to 1 (*1*), 2 (*2*), 4 (*3*), 6 (*4*), 8 (*5*), and 10 (*6*)

normalized extinction cross section $Q_{ev}=C_e/\pi a_v^2$ ($a_v$ is the equivolume cluster radius) is plotted as a function of multipole order at different distances between particles. The parameters of the model ($a$=6.2 nm, $\lambda$=520 nm) correspond to the surface plasmon resonance of monomers. Generally, our data concerning this point are in agreement with the data of Ref. [38].

***2.6. Optical properties of two-layered gold conjugates.*** Adsorption of a biopolymer onto gold nanoparticles results in the formation of a complex structure that can be approximated by a simplest two-layered model: gold core + homogeneous polymer shell, as it was introduced in our work [36]. Recently, the importance of this model was emphasized in relation to the optimization of a colorimetric gold nanoparticle sensor [39] and to the studies of adsorption phenomena [40]. We have studied the optical properties of a two-layered model for gold bioconjugates in detail. Here, we present only illustrative examples of the simulations.

In our calculations, the polymer shell was treated as homogeneous nonabsorbing dielectric with refractive index $n_2$=1.4 or 1.5. The shell thickness $s$ was equal to 5 or 10 nm and was close to the sizes of globular proteins. The refractive index of bulk gold $n_1=n_1(\lambda)$ was used for the conjugate core. Fig. 4 shows changes in extinction spectra caused by polymer adsorption ($s$=5 nm, $n_2$=1.5 at $c_g$=const=57 μg/ml). Increasing the shell thickness and their refractive index leads to a corresponding increase in optical effects. The maximal extinction and scattering are observed for particle diameters 60 nm; however, the maximal *relative* change in extinction and scattering

$$\delta A = [A(\lambda_{ext}^{\max}, s=5) - A(\lambda_{ext}^{\max}, s=0)] / A(\lambda_{\text{ext}}^{\max}, s=0), \tag{19}$$

$$\delta S = [S(\lambda_{sca}^{\max}, s=5) - S(\lambda_{sca}^{\max}, s=0)] / S(\lambda_{sca}^{\max}, s=0), \tag{20}$$

is observed for the smallest (10-nm) particles (Fig. 5, dashed curves). The red shift of extinction and scattering is also maximal for the smallest particles and then decreases with an increase in the particle diameter (up to 80 nm). On the other hand, the finest particles have a higher polymer adsorption capacity. Therefore, to estimate the efficiency

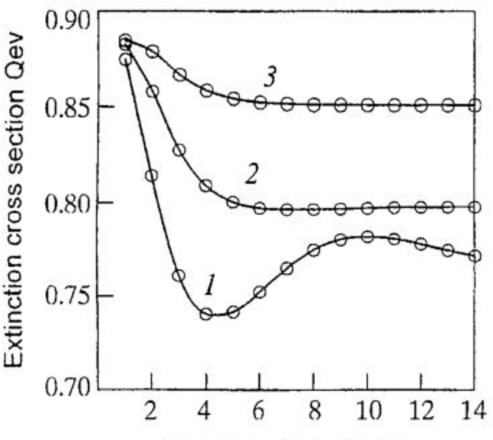

Fig. 3. Dependence of the normalized extinction cross section $Q_{ev}=C_e/\pi a_v^2$ on the number of multipoles included in VSH expansions of the GMM method. Calculations for randomly oriented bispheres ($d=2a$=12.4 nm, $\lambda$=520 nm) in contact $\Delta d$=0.0 (*1*) and separated by distances $\Delta d$=0.05$d$ (*2*) and $\Delta d$=0.1$d$ (*3*) in water

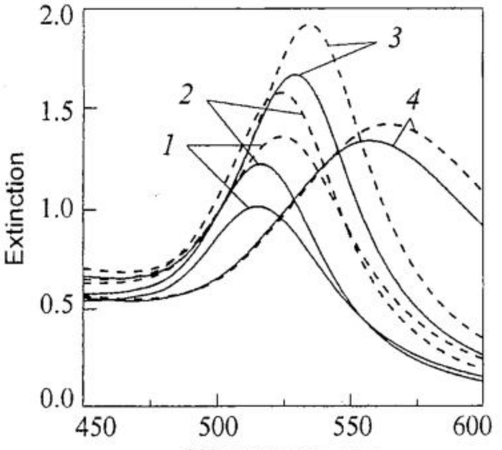

Fig. 4. Extinction spectra of gold particles in water (diameters $d$=10 (*1*), 20 (*2*), 60 (*3*), and 100 (*4*) nm, solid lines) and the same particles coated by a 5-nm polymer shell with the absolute refractive index $n_2$=1.5 (dashed lines)

of optical response per adsorbed polymer molecule, we introduce the SPIA efficiency parameter[2]

$$E = (\text{optical effect})/(\text{polymer adsorption}) \sim (\text{optical effect})/\delta V, \qquad (21)$$

where $\delta V=(a+s)^3/a^3-1$ is the relative change in the volume of a conjugate. For example, for the relative changes in light absorption and scattered intensity $\delta S$, we have

$$E_A=\delta A/\delta V, \quad E_S=\delta S/\delta V. \qquad (22)$$

The solid lines in Fig. 5 show the dependencies of the efficiency parameters $E_A$ and $E_S$ calculated for $s$=5 nm and 10 nm, $n_2$=1.4, $c_g$=const=57 μg/ml. It is clear that 60-nm gold particles are the best optical transducers of biospecific interactions that result in adsorption of biopolymers onto the particle surface. We also studied another situation when the polymer and gold concentrations were fixed whereas the particle diameter was considered as an optimization parameter. Again, we concluded that 60-nm particles gave the highest optical response. A more detailed consideration will be published separately.

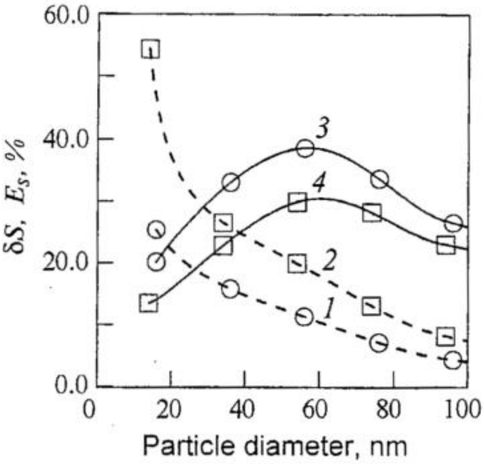

Fig. 5. Dependences of the relative change in scattering $\delta S$(dashed lines) and the SPIA efficiency parameter $E_S$ (solid lines) on the diameter of gold particles (in water) coated by a 5-nm (curves 1 and 3) and a 10-nm (curves 2 and 4) polymer shell with the absolute refractive index $n_2$=1.4

***2.7. Dynamic simulation of optical effects caused by particle aggregation.*** To simulate the temporal dynamics of extinction and scattering spectra during the aggregation process, we introduced the following model [15]: The time corresponding to the formation of 10 new clusters in a system was used as a sample time interval. After each interval, the cluster-size distribution function was determined and the corresponding spectra were calculated according to the procedure described in Section 2.3. The simulations were performed by the DDA method with intersection parameter $\gamma=(4\pi/3)^{1/3}=$ $=1.612$ on a lattice with size $L$=46 and the number of initial monomers $N_0$=500 (the monomer density $\rho=N_0/L^3\approx0.005$). Almost identical data were obtained during larger-scale simulations with $L$=58, $N_0$=1000. The dynamic simulation was terminated after the cluster with size $N$=200 had been generated. To smooth the statistical fluctuations, we repeated all calculations by using independent cluster generations and then averaged the theoretical spectra. Fig. 6 shows an example calculated for 15-nm monomers, the curves in the figure correspond to 100 newly formed aggregates. The appearance of the secondary absorption peak in the red region and the complex dynamics of the spectra resemble to a large extent, our experimental observations. For a deeper consideration, the readers are referred to Ref. [15].

***2.8. Exact multipole model for clusters built from two-layered conjugates.*** To simulate the aggregation of colloidal-gold biomarkers, we introduce an exact multipole model based on a combination of the GMM method and the two-layered model for a single bioconjugate. The above consideration of GMM in Section 2.2.2 shows that all

---

[2] One of variants SPIA technique is based on measurements of small changes in extinction caused by adsorption of biopolymers onto surface of gold nanoparticles [12, 13].

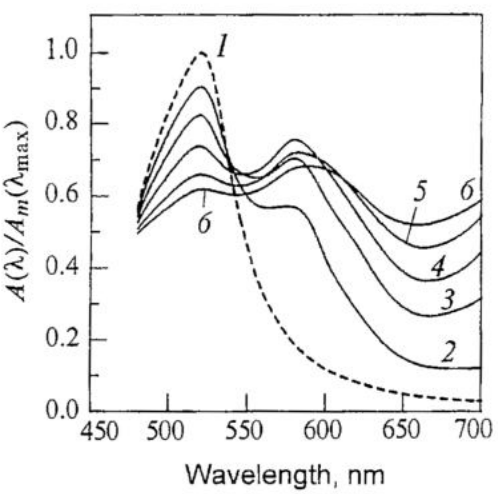

Fig. 6. Theoretical extinction spectra calculated for 15-nm gold sol at different stage of aggregation (dynamic simulation). Dashed curves correspond to single particles, curves 2-6 were calculated by using DLCA aggregation model and the modified DDA method with renormalization lattice parameter $\gamma$=1.62. The number near curves designate sequential time moments corresponding to the formation of 100 new clusters

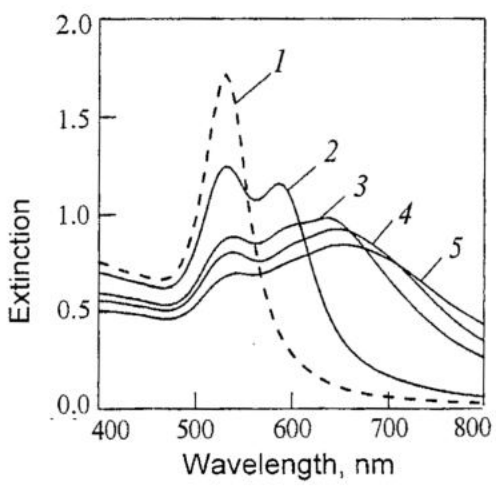

Fig. 7. Theoretical extinction spectra calculated by the exact GMM method for aggregates built from *1* (dashed line), 2 (*2*), 10 (*3*), 20 (*4*) and 50 (*5*) two-layered monomers (core-mantle model of a bioconjugate: 60 nm gold core and 2.5 nm polymer shell, $n_2$=1.4). All spectra were averaged over random orientations of clusters and over 10 statistical configurations of monomers

optical properties of an *i*th monomer are included in the single-particle coefficients $\bar{a}_{np}^{\,i}$. It is clear that the GGM solution can be applied to an arbitrary monomers that possess spherical symmetry. Therefore, one can generalize the standard GMM solution by replacing the well-known Mie coefficients for a homogeneous sphere with its two-layered analogs [6]. We have made the corresponding modifications of our GMM codes and the codes received from Yu-lin Xu and D. Mackowski. These modified codes were tested by benchmark computations performed independently in our laboratory and in the University of Florida, by Yu-lin Xu. At present, the exact two-layered multipole model is extensively used in simulation of the optical properties of aggregated conjugates. An illustrative example is shown in Fig.7. The extinction spectra were calculated for aggregates built from 1, 2, 10, 20, and 50 gold conjugates. The core diameter was 60 nm and the shell thickness was 2.5 nm, $n_2$=1.4, so that the interparticle distance was 5 nm. The spectra of individual clusters were averaged over random orientations and additionally averaged over 10 cluster configurations. As in Fig.6, the aggregation results in the appearance of additional red-shifted peak of extinction. This effect is observed at a rather small number of monomers, because the average cluster size is large enough due to the large diameter of monomers.

## 3. Experimental

***3.1. Materials and methods.*** In this Section, we give a short review of our experimental results related to the optics of colloidal-gold conjugates. Colloidal-gold particles were synthesized according to procedures described in Refs. [16, 36], by reducing tetrachloroauric acid with sodium citrate. The protocol for preparing conjugates of CG to biospecific macromolecules, which involves preparing and purifying an aqueous probe solution, determining the «gold number», coupling the probe to the label, adding a secondary stabilizer, concentrating the marker, and optimizing the end product, has been described elsewhere [41].

***3.2. Optical properties of clusters formed during slow and fast aggregation.*** Our first experimental study [16] was related to the optical properties of colloidal gold aggregates formed during aggregation initiated by addition of the NaCl salt. The extinction spectra (400-800 nm) of aggregates of colloidal-gold particles (diameters 5, 15 and 30 nm) and silver particles (diameter 20 nm) were studied experimentally and theoretically. We have found that during fast aggregation corresponding to the formation of the diffusion-limited (DLCA) clusters, the spectra were dependent on the size of the primary particles. For aggregates of 15- and 30-nm gold particles and for 20-nm silver particles, we recorded spectra with an additional red extinction maximum, whereas the extinction spectra for aggregates of 5-nm particles had a single red-shifted extinction maximum. The slow aggregation resulted in a decrease in the plasmon extinction peak (without an essential red shift) and in the broadening of the long-wavelength extinction wing. According to the TEM data, the fast aggregation gave typical ramified DLCA aggregates, whereas the slow aggregation led to small compact structures along with an appreciable number of single (not aggregated) particles. To explain these findings, we used a computer diffusion-limited cluster-cluster aggregation model. The optical properties of the aggregates were computed by the coupled dipole method (CDM or DDA) and by a rigorous multipole method (GMM). The bulk optical constants of metals were modified by the size-limiting effect of nanoparticles. It was shown that a modified version of DDA [32] allows one to explain the shape of the experimental spectra for DLCA aggregates and the dependence of the spectra on the particle size.

***3.3. Optical properties of clusters formed by biospecific aggregation. Correlation between the extinction spectra and cluster structure.*** In paper [22], we reported on the optical properties of aggregates formed by biospecific interactions like antigen/antibody, with one or both reaction components immobilized on gold particles. In the case of biospecific aggregation, the temporal changes in the absorption spectra differed from those recorded during rapid and slow salt aggregations. As in the case of rapid salt aggregation, the absorption peak decreased and shifted to the red part of the spectrum with simultaneous broadening. However, we did not observe the second red peak of the optical density. According to the transmission electron microscopy data, the slow, rapid, and biospecific aggregations resulted in small clusters with compact structures, branching aggregates of the fractal type, and aggregates without direct conductive contacts of the primary particles, respectively. It is supposed that the recorded differences in the absorption spectra can be explained by the corresponding differences in aggregate structures. We have found a direct correlation between the amount of the second added protein initiating aggregation on the one hand, and the rate of spectral changes on the other. Using these spectral changes, we have plotted a calibration curve for a sufficiently rapid and technically simple quantitative test like sol-particle immunoassay (SPIA).

Using TEM and spectrophotometry, we recorded three types of structures realized during the aggregation of colloidal-gold particles or bioconjugates, and also three types of the corresponding absorption-spectrum changes. In the slow salt aggregation, relatively small, compact aggregates form that have fractal dimension $d_f>2$. Such a type of aggregation is accompanied by small decreases in the main absorption-peak and by non-uniform widening of the long-wave wing. The rapid salt aggregation leads to the formation of fairly loose aggregates with the characteristic branching DLCA [22] structure and a fractal dimension of about 1.8. Contrary to the data of Ref. [42], we recorded in this case the presence of a second long-wave absorption peak for gold particles with direct ohmic contact. Finally, a characteristic of biospecific aggregates is the presence of a biopolymer interlayer among the aggregate's gold particles, which prevents a direct conductive contact. The absorption-spectrum peak of such aggregates is reduced substantially and is shifted toward the red region, with the value of the peak decrease correlating with the concentration of the component initiating the aggregation of the conjugate.

***3.4. A method for the differential spectroscopy of scattered light.*** Adsorption of a polymer onto the gold-particle surface results in relatively small changes in the optical density. The same is true for the initial stages of aggregation. Simple speculations [21] suggest that light scattering spectra can be more informative for adsorption of a polymer onto the particle surface, as well as for the initial stages of aggregation as compared to the absorption technique. Recently, we proposed a new method [43] to study biospecific interactions in systems of conjugates of colloidal gold nanoparticles. The method is based on measuring the differential spectra of light scattered at 90° within the wavelength range 350-800 nm. Addition of complementary components to the bioconjugate probe results in aggregation of nanoparticles that can be monitored by light scattering and extinction spectra. To this end, we have developed a special attachment to the Specord M-40 spectrophotometer and a corresponding measurement procedure called by us *differential light scattering spectroscopy.* The method has been compared with the usual spectrophotometry as applied to colloidal gold conjugated to various polymers including proteins and oligonucleotides. Our experiments with the gold particles of different sizes showed a higher potential sensitivity of the suggested method as compared with spectrophotometry. It is expected that the differential light scattering spectroscopy can be used to develop an analytical biospecific test for various biopolymers.

By contrast to known studies, in paper [43] we presented for the first time the experimental data about kinetic changes in extinction and scattering spectra caused by non-specific or biospecific aggregation of colloidal-gold conjugates. In both cases, already at 1-2 minutes after mixing the reagents we observed an essential increase in the resonance scattering maximum (up to 20 and even 400 times). Simultaneously, we recorded weaker changes in the extinction spectra. This observation allows one to assume that the developed light scattering technique can be used as a sensitive analytical test.

Fig. 8 shows an example of kinetic measurements of extinction and scattering spectra during biospecific aggregation. As a model system (designated as CG-15+PrA) conjugates of 15-nm particles to Protein A (Sigma, USA) were used. Aggregation was initiated by addition of the human IgG solution (Serva, Germany). The PrA molecule has two or more sites for biospecific binding of IgG molecules. Data in Fig. 8 correspond to an equimolar amount of reagent binding sites. Note how strongly the resonance scattering peak is increased in comparison with extinction spectral changes.

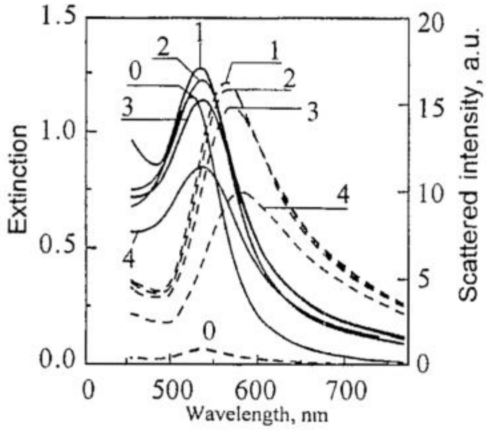

Fig. 8. Kinetics changes in extinction (solid lines) and right angle scattering (dashed lines) spectra of conjugates CG-15nm + Protein A (sample volume 4 ml; the gold number is 5 μg/ml). The numbers near curves correspond to the initial conjugate sol (0), and to the time intervals at 2 (1), 7 (2), 30 (3), and 90 (4) minutes after addition of 150 μl IgG at a concentration 1 mg/ml

***3.5. Biological and medical applications of colloidal-gold markers.*** A pioneering biomedical application of colloidal gold was published by Maclagan in 1944 [44]. Since 1971, colloidal gold conjugates have been used traditionally in immunocyto- and histochemical studies as markers for electron microscopy [45]. Gradually, the scope of use of gold markers was broadened. Currently, they are used in light microscopy methods and in various versions of force microscopy [46]. In addition, colloidal-gold conjugates are used in solid-phase-assay systems, such as dot-blot analysis [47], immunochroma-tographic test strips [48], and amplification of the immune response of experimental animals [49].

In our group, the fabricated colloidal-gold conjugates were used in studying the surface of nitrogen-fixing soil bacteria [24, 25] by TEM and dot-blot analysis [41] (perhaps, the first application of gold markers to dot-blot analysis of soil bacteria was described in 1989 [50]). Additionally, our markers and experimental procedures were used to develop an assay for a rapid diagnosis of acute enteric infections [26], as well as in studies of a proliferative antigen of the initial cells of a wheat stem meristem [27]. Recently, we recorded for the first time changes in the infrared spectra of Protein A-colloidal-gold conjugate after its interaction with immunoglobulin [51]. This result may serve as a basis for the development of new assay systems to detect biospecific interactions of the antigen-antibody type at *the single-molecule level.* Finally, one of the promising field, is the application of colloidal gold markers to preparation of antibodies both *in vitro* (by combinatorial phage display approach [28]), and *in vivo* (for amplification of the immune response [29]). Note that this intriguing amplification effect or, in other words, the adjuvant properties of gold sols have yet to be explained.

*This work was partially supported by CRDF Grant № REC-006, and by RFBR Grants № 01-03-33130 and № 01-04-48736. We thank D.N. Tychinin (IBPPM RAS) for help in preparation of the manuscript, Yu-lin Xu (Univ. of Florida, USA) and Daniel Mackowski (Auburn Univ., USA) for the GMM computer codes.*

## References

1. *Schalkhammer Th.* Metal nano clusters as transducers for bioaffinity interactions // Chem. Monthly. 1998. V. 129. P. 1067.

2. *Lyon L.A., Musick M.D., Natan M.J.* Colloidal Au-enhanced surface plasmon resonance immunosensing // Anal. Chem. 1998. V. 70. P. 5177.

3. *Mulett W.M., Lai E.P.C., Yeung J.M.* Surface plasmon resonance-based immunoassays // Methods. 2000. V. 22. P. 77.

4. *Mirkin C.A., Letsinger R.L., Mucic R.C., Storhoff J.J.* DNA-based method for rationally assembling nanoparticles into macroscopic materials // Nature. 1996. V. 382. P. 607.

5. *Boal A.K., Ilhan F., DeRoucher J.E., Thurn-Albrecht Th., Rotello V.M.* Self-assembly of nanoparticles into structured spherical and network aggregates // Nature. 2000. V. 404. P. 746.

6. *Bohren C.F., Huffman D.R.* Absorption and Scattering of Light by Small Particles. -New York: Wiley, 1983.

7. *Khlebtsov N.G., Bogatyrev V.A., Dykman L.A., Melnikov A.G.* Optical properties of colloidal gold and its biospecific conjugates // Colloid J. 1995. V. 57. P. 384.

8. *Storhoff J.J., Lazarides A.A., Mucic R.C., Mirkin C.A., Letsinger R.L., Schatz G.C.* What controls the optical properties of DNA-linked gold nanoparticle assemblies? // J. Am. Chem. Soc. 2000. V. 122. P. 4640.

9. *Schatz G.S.* Electrodynamics of nonspherical nobel nanoparticles and nanoparticle aggregates // Theochem. 2001. V. 573. P. 73.

10. *Leuvering J.H., Thal P.J., van der Waart M., Schuurs A.H.* Sol particle immunoassay (SPIA) // J. Immunoassay. 1980. V. 1. P. 77.

11. *Ciesiolka T., Gabius H.-J.* An 8 to 10 fold enhancement in sensitivity for quantitation of proteins by modified application of colloidal gold // Anal. Biochem. 1988. V. 168. P. 280.

12. *Englebienne P., Van Hoonacker A., Valsamis J.* Rapid homogeneous immunoassay for human ferritin in the Cobas Mira using colloidal gold as the reporter reagent // Clin. Chem. 2000. V. 46. P. 2000.

13. *Englebienne P., Van Hoonacker A., Verhas M.* High-throughput using the surface plasmon resonance effect of colloidal gold nanoparticles // Analyst. 2001. V. 126. P. 1645.

14. *Khlebtsov N.G., Maksimova I.L., Tuchin V.V., Wang L.* Introduction to light scattering by biological objects // In: Handbook of Optical Biomedical Diagnostics / Tuchin V.V. (Ed.), -Bellingham, Washington: SPIE, 2002. P. 31.

15. *Khlebtsov N.G., Dykman L.A., Krasnov Ya.M., Melnikov A.G.* Extinction of light by aggregated gold particles and aggregated conjugates of gold particles to biospecific macromolecules // In: Electromagnetic and Light Scattering by Nonspherical Particles: Theory and Applications / Obelleiro F., Rodriguez J. L., Wriedt T. (Eds), - Vigo, Spain. 1999. P. 43.

16. *Khlebtsov N.G., Dykman L.A., Krasnov Ya.M., Melnikov A.G.* Light absorption by the clusters of colloidal gold and silver particles formed during slow and fast aggregation // Colloid J. 2000, V. 62. P. 765.

17. *Khlebtsov N.G.* An approximate method for calculating scattering and absorption of light by fractal aggregates // Opt. Spectrosc. 2000. V. 88. P. 594.

18. *Khlebtsov N.G.* Orientational averaging of the integral cross sections in the discrete dipole method // In: Light Scattering by Nonspherical Particles: Halifax Contributions / Videen G., Fu Q., Chylek P. (Eds), -Adelphy, Marylend: Army Research Laboratory, 2000. P. 123.

19. *Khlebtsov N.G., Dykman L.A., Bogatyrev V.A., Krasnov Ya.M., Medvedev B.A.* Extinction and scattering of light by gold nanoparticle clusters resulting from salt and biospecific aggregation // Ibid. P. 245.

20. *Khlebtsov N.G.* Orientational averaging of integrated cross sections in the discrete dipole method // Opt. Spectrosc. 2001. V. 90. P. 408.

21. *Bogatyrev V.A., Medvedev B.A., Dykman L.A., Khlebtsov N.G.* Light scattering spectra of colloidal gold aggregates: experimental measurements and theoretical simulations // In: Saratov Fall Meeting 2000: Optical Technologies in Biophysics and Medicine II / Tuchin V.V. (Ed.), Proc. SPIE, V. 4241. -Bellingham, Washington: SPIE, 2001. P. 42.

22. *Dykman L.A., Krasnov Ya.M., Bogatyrev V.A., Khlebtsov N.G.* Quantitative immunoassay method based on extinction spectra of colloidal gold bioconjugates // Ibid. P. 37.

23. *Bogatyrev V.A., Dykman L.A., Krasnov Ya.M., Plotnikov V.K., Khlebtsov N.G.* Biospecific assembling of gold nanoparticles with protein or oligonucleotide linkers as studied by light scattering and extinction spectra // In: Saratov Fall Meeting 2001: Optical Technologies in Biophysics and Medicine III / Tuchin V.V. (Ed.), Proc. SPIE, V. 4707. -Bellingham, Washington: SPIE, 2002 (in press).

24. *Egorenkova E.V., Konnova S.A., Fedonenko Yu.P., Dykman L.A., Ignatov V.V.* Role of the polysaccharide components of Azospirillum brasilense capsules in bacterial adsorption on wheat seedling roots // Microbiology. 2001. V. 70. P. 36.

25. *Chumakov M.I., Dykman L.A., Bogatyrev V.A., Kurbanova I.V.* Investigation of the cell surface structures of Agrobacteria involved in bacterial and plant interactions // Microbiology. 2001. V. 70. P. 232-238.

26. *Dykman L.A., Bogatyrev V.A.* Use of the dot-immunogold assay for the rapid

diagnosis of acute enteric infections // FEMS Immunol. Med. Microbiol. 2000. V. 27. P. 135-137.

27. *Sumaroka M.V., Dykman L.A., Bogatyrev V.A., Evseeva N.V., Zaitseva I.S., Shchyogolev S.Yu., Volodarsky A.D.* Use of the dot-blot immunogold assay to identify a proliferative antigen in the initial cells of a wheat stem meristem // J. Immunoassay. 2000. V. 21. P. 401-410.

28. *Sumaroka M.V., Dykman L.A., Bogatyrev V.A., Zaitseva I.S., Sokolov O.I., Shchyogolev S.Yu., Harris W.J.* Preparation, selection and immunodetection of antibodies to low-molecular-weight compounds by using hapten-colloidal gold conjugates and combinatorial phage libraries // Allergology and immunology. 2000. V. 1. P. 134-135.

29. *Dykman L.A., Sumaroka M.V., Staroverov S.A., Zaitseva I.S., Bogatyrev V.A.* The immunogenicity of colloidal gold // Biol. Bull. 2002 (in press).

30. *Khlebtsov N.G., Melnikov A.G.* Structural anisotropy of fractal clusters and orientational optic effects in transmitted light // Colloid J. 1998. V. 60. P. 781.

31. *Draine B.T.* Electromagnetic scattering by compounded spherical particles // In: Light scattering by Nonspherical Particles / Mishchenko M.I., Hovenier J.W., Travis L.D. (Eds), San Diego: Academic Press, 2000. P. 131.

32. *Markel V.A., Shalaev V.M., Stechel E.B., Kim W., Armstrong R.L.* Small-particle composites. I. Linear optical properties // Phys. Rev. B. 1996. V. 53. P. 2425.

33. *Yu-lin Xu.* Electromagnetic scattering by an aggregate of spheres. // Appl. Opt.1995. V. 34. P. 4573.

34. *Fuller K.A., Mackowski D.W.* Electromagnetic scattering by compounded spherical particles // In: Light Scattering by Nonspherical Particles: Theory, Measurements, and Applications / Mishchenko M.I., Hovenier J.W., Travis L.D. (Eds), - San Diego: Academic Press, 2000. P. 225.

35. *Khlebtsov N.G.* Orientational averaging of light scattering observables in the T-matrix approach // Appl. Opt. 1992. V. 31. P. 5359.

36. *Khlebtsov N.G., Bogatyrev V.A., Dykman L.A., Melnikov A.G.* Spectral extinction of colloidal gold and its biospecific conjugates // J. Colloid Interface Sci. 1996. V. 180. P. 436.

37. *Lazarides A.A., Schatz G.C.* DNA-linked metal nanosphere materials: Structural basis for the optical properties // J. Phys. Chem. B. 2000. V. 104. P. 460.

38. *Lazarides A.A., Schatz G.C.* DNA-linked metal nanosphere materials: Fourier-transform solutions for the optical response // J. Chem. Phys. 2000. V. 112. P. 2967.

39. *Nath N., Chilkoti A.* A colorimetric gold nanoparticle sensor to interrogate biomolecular interactions in real time on a surface // Anal. Chem. 2002. V. 74. P. 504.

40. *Eck D., Helm Ch.A., Wagner N.J., Vaynberg K.A.* Plasmon resonance measurements of the absorption and adsorption kinetics of a biopolymer onto gold nanocolloids // Langmuir. 2001. V. 17. P.957.

41. *Dykman L.A., Bogatyrev V.A.* Colloidal gold in solid-phase analysis. A review // Biochemistry (Moscow). 1997. V. 62. P. 350.

42. *Danilova Yu.E.* Localization of Optical Excitations in Colloidal Silver Aggregates. PhD Thesis, Inst. Automatics and Electrometry RAS, Novosibirsk, 1999.

43. *Bogatyrev V.A., Dykman L.A., Krasnov Ya.M., Plotnikov V.K., Khlebtsov N.G.* A method of differential spectroscopy of scattered light for studies of biospecific assembling of gold nanoparticles with protein or oligonucleotide probes // Colloid J. 2002 V. 64. № 6.

44. *Maclagan N.F.* The serum colloidal gold reaction as a liver function test // Brit. J. Exp. Pathol. 1944. V. 25. P. 15.

45. *Faulk W., Taylor G.* An immunocolloid method for the electron microscope // Immunochemistry. 1971. V. 8. P. 1081.

46. *Neagu C., van der Werf K.O., Putman C.A.J., Kraan YM., de Grooth B.G., van Hulst N.F., Greve J.* Analysis of immunolabeled cells by atomic force microscopy, optical microscopy, flow cytometry // J. Struct. Biol. 1994. V. 112. P. 32.

47. *Moeremans M., Daneels G., van Dijck A., Langanger G., De Mey J.* Sensitive visualization of antigen-antibody reactions in dot and blot immune overlay assays with immunogold and immunogold/silver staining // J. Immunol. Methods. 1984. V. 74. P. 353.

48. *Shyu R.H., Shyu H.F., Liu H.W., Tang S.S.* Colloidal gold-based immunochromatographic assay for detection of ricin // Toxicon. 2002. V. 40. P. 255.

49. *Shiosaka S., Kiyama H., Wanaka A., Tohyama M.* A new method for producing a specific and high titre antibody against glutamate using colloidal gold as a carrier // Brain Research. 1986. V. 382. P. 399-403.

50. *Bogatyrev V.A., Ivanova L.Yu., Schwartsburd B.I., Khlebtsov N.G.* Use of colloidal gold in immunodot technique // 19th Meeting FEBS, Rome, July 2-7, 1989. Abstr. Book, P. 30.

51. *Kamnev A.A., Dykman L.A., Tarantilis P.A., Polissiou M.G.* Surface-enhanced Fourier transform infrared spectroscopy of protein A conjugated with colloidal gold // In: Metal Ions in Biology and Medicine, V. 7 / Khassanova L., Collery Ph., Maymard I., Khassanova Z., Etienne J.-C. (Eds), -Paris: John Libbey Eurotext, 2002. P. 104.

*Institute of Biochemistry and Physiology*
*of Plants and Microorganisms*
*Saratov State University*

*Received 21.05.2002*

УДК 535.36

# ОПТИЧЕСКИЕ СВОЙСТВА БИОКОНЪЮГАТОВ КОЛЛОИДНОГО ЗОЛОТА

*Н.Г. Хлебцов, В.А. Богатырев, Л.А. Дыкман, Я.М. Краснов, А.Г. Мельников*

Обсуждаются оптические свойства единичных и агрегированных конъюгатов коллоидного золота, которые синтезируются при адсорбции биополимеров на поверхности золотых наночастиц. Для моделирования ослабления и рассеяния света подобными структурами использована обобщенная теория Ми для произвольной мультисферной конфигурации рассеивателей и метод дискретных диполей вместе с компьютерной моделью кластер-кластерной агрегации. В первой части статьи обсуждаются следующие вопросы: • статистическое и ориентационное усреднение оптических наблюдаемых параметров; • оптические эффекты, связанные с линейными цепочками наночастиц; • влияние полимерного покрытия и межчастичного расстояния на оптические свойства агрегатов; • моделирование кинетических изменений оптических свойств агрегированных золей, формируемых в процессе биоспецифического связывания конъюгатов; • модификация мультипольного подхода для случая двухслойных мономеров. Во второй части статьи дается краткий обзор наших экспериментальных исследований по синтезу, теоретическому моделиро-ванию и практическому применению биомаркеров на основе коллоидного золота (включая биомедицинские приложения), и приводятся экспериментальные примеры оптического мониторинга биоспецифических взаимодействий на нанометровом масштабе.

*Khlebtsov Nikolai Grigor'evich* (1949, Astrakhan), Head of Biophysics Group at the Institute of Biochemistry and Physiology of Plants and Microorganisms, Russian Academy of Sciences, Saratov, Russia; also Professor at the Department of Optics, Saratov State University. Graduated from the Saratov State University in 1972. Doctor of Physical and Mathematical Sciences (1996), PhD (1982). Field of research: Optics of Disperse Systems, Fractal Clusters, Electro-optical Effects in Suspensions and High Polymer Solutions, Radiative Transfer and Light Scattering, Remote Sensing of Atmosphere and Ocean, Biophysics of Microbial Populations. He has about 120 scientific publications.

E-mail: khlebtsov@ibppm.saratov.su

*Bogatyrev Vladimir Alexandrovich* (1958, Monchegorsk), Senior researcher of Biophysics Group at the Institute of Biochemistry and Physiology of Plants and Microorganisms, Russian Academy of Sciences. Graduated from the Saratov State University in 1980, PhD (candidate of biological sciences, 1995). Field of research: Electro-optical effects in microbial suspensions, synthesis and application of colloidal-gold biomarkers. He has about 90 scientific publications.

*Dykman Lev Abramovich* (1962, Saratov), Head of Immunotechnology Group at the Institute of Biochemistry and Physiology of Plants and Microorganisms, Russian Academy of Sciences. Graduated from the Saratov Medical Institute in 1985. PhD of Biology (1996). Field of research: immunology; immunochemistry; microbiology; colloidal chemistry and optics of gold sols. He has about 70 scientific publications.

*Krasnov Yaroslav Mikhailovich* (1971, Kamyshin), Graduate student of Biophysics Group at the Institute of Biochemistry and Physiology of Plants and Microorganisms. Graduated from the Saratov State University in 1985. Field of research: Synthesis and biomedical application of colloidal-gold conjugates, experimental studies of optical properties of aggregated gold nanoparticles. He has 10 scientific publications.

*Melnikov Andrei Gennadievich* (1963, Saratov), Senior researcher of Biophysics Group at the Institute of Biochemistry and Physiology of Plants and Microorganisms. Graduated from the Saratov State University in 1985, PhD from Saratov State University (candidate of physic and mathematical sciences, 1982). Field of research: computer simulation of light absorption and scattering by small particles and aggregates. He has about 40 scientific publications.

Izv. VUZ «AND», vol.10, № 3, 2002

# SPECKLE DIAGNOSTICS OF RELAXATION PROCESSES IN NON-STATIONARY SCATTERING SYSTEMS

*D.A. Zimnyakov, A.P. Sviridov, A.I. Omel'chenko, V.A. Trifonov,*
*D.N. Agafonov, P.V. Zakharov, L.V. Kuznetsova*

Coherent optical method of the study of non-stationary mass transfer in scattering systems on the basis of statistical analysis of spatial-temporal fluctuations of speckle intensity is considered. Non-stationary mass transfer in the case of saturating liquid phase evaporation from a disordered porous layer and structure modification of IR-laser-mediated cartilage tissue are discussed as the possible applications of the developed speckle-diagnostical technique. For liquid phase evaporation from a porous layer, the specific feature such as the anomalous broadening of spectra of speckle intensity fluctuations with decrease of the liquid phase evaporation rate was found out. This feature is caused by peculiarities of development of the fractal-like interface between liquid and gaseous phases in a porous layer. In the case of the thermally induced structure modification of a cartilage tissue, the hysteresis-like form of dependence of the time-averaged contrast of speckle-modulated tissue image on the tissue temperature inside the treatment zone is characteristical. The effect of cartilage thermal modification is presumably caused by the «bound-to-free water» transition in the proteoglycane aggregates as one of the basic components of the tissue structure.

## 1. Introduction

Statistical analysis of random interference patterns, or *speckle patterns*, that appear as a result of the coherent light propagation in scattering media is the one of universally adopted techniques for probing the structural and dynamic properties of weakly ordered condensed matter. The possibility to study the dynamic behavior of ensembles of moving particles at length scales of the order of the wavelength of probe light by means of the correlation analysis of scattered light intensity fluctuations stimulated a great number of experimental and theoretical works dedicated to various aspects of the quasi-elastic light scattering by non-stationary random media. Such well-known speckle technology as the *diffusing-light spectroscopy* (DWS) [1] is now widely used for material testing in various areas of science and technology; there are many classical examples of successful applications of the DWS method and related technologies in studying such complicated processes as a Brownian dynamics of particles in suspensions, a granular flow, a foam formation, a growth of colloidal aggregates and crystallization, etc. (see e.g. Refs 2-6).

In biomedical optics, the statistical and correlation analysis of dynamic speckle patterns induced due to laser light scattering by living tissues is the physical basis for various techniques widely applied for the blood microcirculation monitoring, the burned tissue diagnostics, the cerebral blood flow visualization, etc. [7-14].

Also, the significant research activity in this field was stimulated by existence of fundamental phenomena appearing in the case of scattering of classical waves by disordered systems (such as, e.g., the long-range spatial and temporal correlations of multiply scattered field, the «memory» effect, the effect of coherent backscattering) and demonstrating certain analogies with such quantum-mechanical effect as the electron localization in disordered conductors (the so-called Anderson localization) [15-20].

The goal of this work is to review some novel techniques and results in the field of speckle diagnostics of structural and dynamic properties of weakly ordered multiple scattering media. These techniques are:

1) the study of a non-stationary mass transfer in disordered and ordered porous media on the basis of spectral analysis of dynamic speckle patterns induced by coherent light scattering in porous media;

2) the speckle contrast monitoring of structural changes in collagenous tissues induced by thermal denaturation or modification under laser heating.

On the one hand, the development of these speckle techniques gives the new opportunities in studying the complicated dynamic behavior of real systems with stochastic structure such as, e.g., the structural relaxation forced by thermal processes or non-stationary mass transfer. On the other hand, these methods are based on certain fundamental effects related to light propagation in random media at mesoscopic length scales such as the correlation transfer [21], the evolution of a polarization state of propagating light [22-25], the manifestation of the coherence phenomena in multiple-beam stochastic interference, etc. Thus, we can hope that further development of the above mentioned speckle-based methods leads us to better understanding of processes accompanying the light-matter interaction at microscopic and mesoscopic levels.

## 2. Speckle correlometry as applied to study the interface growth in porous media

One of the possible applications of the speckle-correlation technologies in studying a dynamic behavior of stochastic systems is the analysis of growing phenomena in porous media (e.g. in the course of the evaporation of saturating liquid phase [26] or the development of liquid-gaseous interfaces driven by capillary forces). The specific property of these growth processes is formation of the fractal-like interfaces which fractal nature is mainly caused by a structural randomness of «matrix» media. In such system, the random connections between single pores form a «stochastic network» of channels for propagation of the local boundaries between liquid and gaseous phases. The mobility of an arbitrary local boundary depends on physical properties of a liquid phase and porous medium, as well as on the characteristic size and geometry of pores. A significant variance in sizes and orientations of pores causes stochastic fractal character of the «global» interface between phases in disordered porous media. Thus, the direct observation of the time-dependent dynamics of the local boundaries that form the growing fractal-like interface is an object of great interest.

In our case, we studied such time-dependent dynamics for the case of evaporation of liquid phase from layers of wet porous media. Experimental technique was based on the spectral and correlation analysis of speckle intensity fluctuations induced by laser light scattering in layer of dried porous medium. In this case, the dynamic speckle pattern is caused by a multiple scattering of coherent light by moving local boundaries in single pores located in the vicinity of growing interface. The experimental set-up is shown in Fig. 1.

Single-mode He-Ne laser (the wavelength is 633 nm, the output power is 0.5 mW) was used as illumination source. The laser beam was focused on the surface of the wet porous layer using a lens with the focal length of 200 mm. Scattered light was detected in the paraxial region by CCD camera (EDC-1000L, Electrim, USA) without imaging lens. The distance between the layer and CCD camera was 600 mm. Time delay and integration (TDI) mode of camera was used to get images of dynamic speckle patterns at different stages of the liquid evaporation. For this mode, the acquired image is composed as the set of 1D images of the same line in the detection plane, which are sequentially recorded with given time delay. Brightness distributions along the rows of this image correspond to temporal dynamics of the fluctuating intensity in the points of the chosen line.

Paper layers of different nature, such as copy paper and filter paper of different thickness and porosity, were used in our experiments as the layers of the disordered porous media. Before image recording, the studied samples were wetted by quickly evaporating liquid, such as ethanol or acetone. For each paper sample, the thickness and average porosity were measured. Also, such parameter as the relaxation time $t_{rel}$ was used to characterize the studied systems «porous layer-wetting liquid». It was measured as the time lapse corresponding to *e*-times decay of the liquid mass in the course of evaporation from the saturated layer. For comparison with disordered porous media, the ordered porous layers with cylindrical pores were studied in our experiment. These layers are the glass plates with hexagonally packed cylindrical channels used for fabrication of

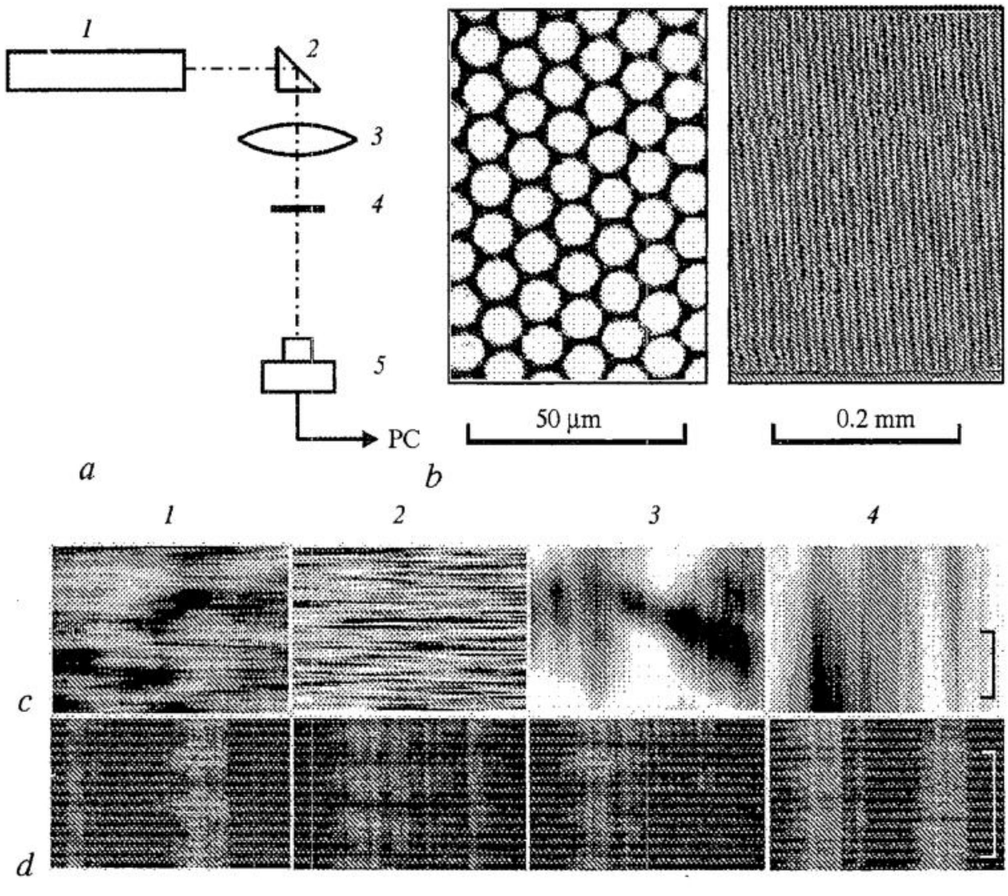

Fig. 1. *a* - scheme of the experimental setup; *1* - laser; *2* - prism; *3* - focusing lens; *4* - sample; *5* - CCD camera; *b* - photos of ordered porous sample. *c*, *d* - TDI images of dynamic speckles at different stages of wetting phase evaporation. *c* - paper layer (thickness 88 μm, porosity 0.56) wetted by acetone; *1* - $t_{dr}$=10 s; *2* - $t_{dr}$=35 s; *3* - $t_{dr}$=240 s; *4* - $t_{dr}$=320 s; bar - 10 s. *d* - sample as in Fig. 1*b*, wetted by ethanol; *1* - $t_{dr}$=30 s; *2* - $t_{dr}$=100 s; *3* - $t_{dr}$=400 s; *4* - $t_{dr}$=580 s; bar - 10 s

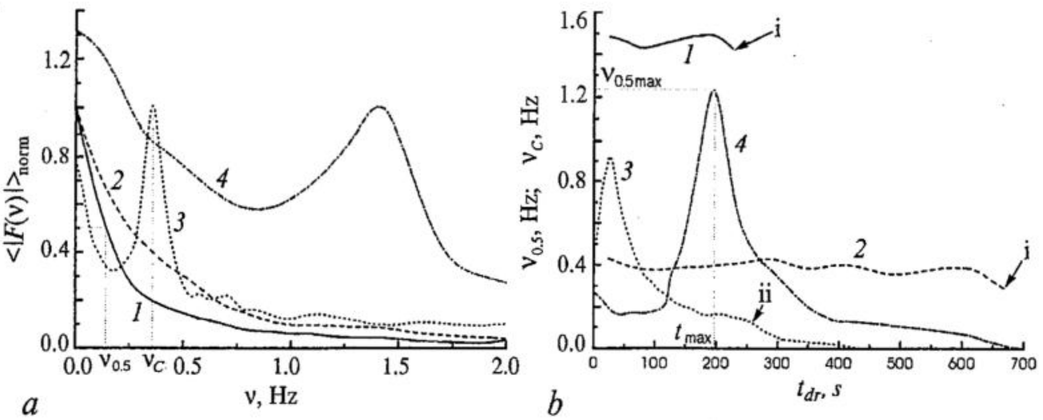

Fig. 2. *a* - typical forms of the normalized Fourier spectrum module of intensity fluctuations for paper layer (thickness 71 μm, porosity 0.68, ethanol) (*1*, *2*) and for ordered sample (Fig. 1,*b*) (*3*, *4*) wetted by ethanol (*3*) and acetone (*4*). *1* - $t_{dr}$=23 s; *2* - $t_{dr}$=150 s; *b* - the dependencies of $\nu_c$ (*1*, *2*; sample as in Fig. 1, *b*) and $\nu_{0.5}$ (*3*, *4*; paper sample, thickness 88 μm, porosity 0.56) on $t_{dr}$. Wetting liquid - acetone (*1*, *3*) and ethanol (*2*, *4*); i - final stage of evaporation; ii - presumable stage of clusterization

the micro-channel plates (MCP) (Fig. 1, *b*). The fragments of typical speckle images for different stages of the liquid evaporation are shown in Fig. 1, *c*, *d*.

For each frame of a sequence of acquired TDI images, the averaged module of the Fourier spectrum of speckle intensity fluctuations was calculated for pixel brightness distributions along each row, using the averaging of values of the spectrum module over the set of rows. The typical forms of the normalized spectrum module are shown in Fig. 2 for disordered and ordered porous media. In the first case, motions of the local boundaries in the porous layer cause the speckle intensity fluctuations in the form of band-limited random process with spectrum half-width $\nu_{0.5}$ depending on the average boundary mobility.

For ordered porous layer, the observed speckle dynamics has quasi-periodic character (Fig. 1, *c*) with center frequency $\nu_C$ depending on the average velocity of local boundaries propagation.

The typical dependencies of $\nu_{0.5}$ for disordered layer and $\nu_C$ for ordered layer on evaporation time $t_{dr}$ are shown in Fig. 2, *b*.

Non-monotonic behavior of $\nu_{0.5}$ with increase of $t_{dr}$ and appearance of its maximum value at certain stage of evaporation characterized by $t_{\max}$, can be mentioned as specific property of the observed speckle dynamics in case of disordered layers. It was found for all studied paper samples, that $t_{\max}$ and $t_{rel}$ are related as $t_{\max} \sim t_{rel}^{1.08\pm0.10}$. Another feature is that despite the higher mobility of the local boundaries in the case of acetone as evaporating liquid, the speckle dynamics for disordered porous structure is characterized by less values of $\nu_{0.5\max}$ than for ethanol (for comparison, see dependencies of $\nu_C$ on $t_{dr}$ for ordered porous layer).

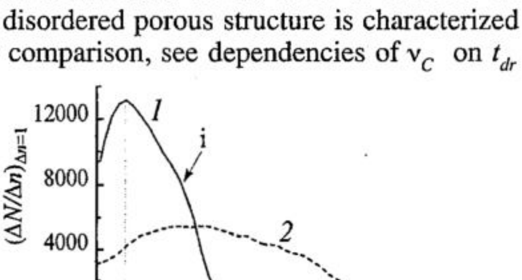

Fig. 3. The dependence of node release rate on *n*. $N_1$=$N_2$=100; $N_3$=30; Ω=6. *1* - *P*=0.3; *2* - *P*=0.1; i - stage of clusterization

These peculiarities can be interpreted in terms of multiple light scattering by a non-stationary ensemble of local boundaries in disordered porous layer. Non-monotonically changing $\nu_{0.5}$ with the increasing time lapse $t_{dr}$ of liquid evaporation is caused by variation of concentration of dynamic scatters (i.e. local boundaries) in the scattering volume. This is due to the effect of multiplication of a random Doppler shift for each scattering event by an effective number of scattering events. This number for multiply scattering system depends on the parameter $(L/l^*)^2$, where $L$ is the characteristic size of the scattering system and $l^*$ is the effective value of the transport mean free path depending on the scatter concentration [1,19,27]. For drying disordered porous layer, the growth of fractal interface [28] between phases causes simultaneous changes in $L$ (which is related to the interface «height») and in $l^*$ (which is proportional to the inverse of concentration of moving local boundaries in the zone of interface growth). In the case of a slab scattering geometry, the decay of temporal correlation of fluctuating scattered field depends on the dimensionless parameter $k^2\langle\Delta\bar{r}^{\,2}(\tau)\rangle(L/l^*)^2$ [19,27], where $k$ is the wave-number of light in the scattering medium, $\langle\Delta\bar{r}^{\,2}(\tau)\rangle$ is the variance of the scatter displacements for the time lapse $\tau$ and $L$ is the slab thickness. The value of $\langle\Delta\bar{r}^{\,2}(\tau)\rangle$ can be considered as corresponding to the generalized Brownian motion of the scattering sites: $\langle\Delta\bar{r}^{\,2}(\tau)\rangle=K\tau^{\theta}$, where $K$ is determined by scatter mobility and $\vartheta$ depends on dynamic properties of the scattering system.

The rigorous analytical form of the temporal correlation function of field fluctuations is determined by scattering conditions and optical properties of the scattering medium, such as the diffuse reflectivity and can be found only for a limited number of the diffuse-scattering systems [27]. However, from the principle of similarity it follows that the correlation time $\tau_c$ of field fluctuations varies as $\tau_c\sim(l^{*2}/k^2KL^2)^{1/\vartheta}$ in the dependence on the parameters of scattering system. Considering the porous layer initially wetted by liquids with approximately equal values of refractive index and assuming the same dynamical properties of the ensemble of local boundaries ($\vartheta_1=\vartheta_2=\vartheta$) but different mobility parameters ($K_1\neq K_2$), the ratio of $\nu_{0.5\max}$ can be expressed as:

$$(\nu_{0.5\max})_1/(\nu_{0.5\max})_2=(\tau_{\max})_2/(\tau_{\max})_1= \\ =\{K_{1\max}L_{1\max}{}^2l_{2\max}{}^{*2}/K_{2\max}L_{2\max}{}^2l_{1\max}{}^{*2}\}^{1/\vartheta}. \tag{1}$$

The ratio $l_2^*/l_1^*$ can be modified using the relation for the transport mean free path: $l^*=\{c\sigma(1-g)\}^{-1}$, where $c$, $\sigma$ and $g$ are the effective values of the concentration, scattering cross-section and anisotropy parameter of moving scattering sites (local boundaries). We can assume that for wetting liquids with close values of the refractive index ($n_1\approx1.354$ at 633 nm for acetone and $n_2\approx1.358$ for ethanol) the effective values of $\sigma$ and $g$ are approximately equal and the ratio $l_2^*/l_1^*$ can therefore be reduced to $c_1/c_2$.

Hence, we obtain:

$$(\nu_{0.5\max})_1/(\nu_{0.5\max})_2=\{K_{1\max}\gamma_{1\max}{}^2/K_{2\max}\gamma_{2\max}{}^2\}^{1/\vartheta}, \tag{2}$$

where the parameter $\gamma=\tilde{L}c$ characterizes the effective surface density of dynamic scattering sites, or the number of stochastically moving local boundaries per unit area of porous layer.

Computer simulation of stochastic irreversible growth of interfaces in 3D lattices with different number of connections $\Omega$ between nodes was used to analyze the behavior of the ratio $\gamma_1/\gamma_2$ in the course of interface growth. The simulation model was similar to the Eden model [29]. At the initial moment, the $N_1\times N_2\times N_3$ lattice ($N_1=N_2>>N_3$) was assumed consisting of occupied nodes. Interface growth is related to sequential release of the occupied nodes beginning from the lattice boundaries. Each occupied node can be released with given probability $P$ at the current simulation step if it has at least one connection with free neighboring nodes released at previous steps. The number of connections $\Omega$ per lattice cell as the model parameter was varied from 6 (the simple cubic lattice) to 14 (the cubic lattice with «diagonal» connections between layers). The growth process for each set of simulation parameters was characterized by the relaxation parameter $n_{rel}$ evaluated as the number of steps corresponding to $e$-times decay of the amount of occupied nodes.

The extreme case of $P=1$ leads to appearance of the «conventional» non-fractal interface propagating in the lattice with constant velocity. Decreasing probability of the node release causes the fractal-like growing interfaces with the increasing height of the growth zone for a given position of interface. Despite the simplicity of this model, it has allowed us to interpret the general features of the interface growth in porous layers that are manifested in the observed spectra of scattered light fluctuations. Typical behavior of the amount of nodes $(\Delta N_f/\Delta n)_{\Delta n=1}$ released at each step is illustrated by Fig. 3 as depending on the number of steps.

The maximal value $(\Delta N_f/\Delta n)_{\Delta n=1}$ obtained at $n=n_{\max}$ corresponds to maximally developed interface between the regions of occupied and free nodes. Analysis of the relation between $n_{\max}$ and $n_{rel.}$ leads to the approximately linear dependence $n_{\max}\sim Gn_{rel}^{1.05\pm0.10}$ for $0.001\leq P\leq 0.5$ and $6\leq\Omega\leq 14$, where $G$ depends on the model parameters $P$, $\Omega$, $N_1=N_2$, $N_3$. Such tendency is very similar to the above mentioned relation between the measured values of $t_{\max}$ and $t_{rel}$. Evaluations of effective surface density of occupied nodes for the zone of growth made at $n=n_{\max}$, show it as monotonically decaying to the value close to 1 with increasing $P$ (Fig. 4). In contrast, values of $\gamma_{\max}$ estimated for small values of $P$, are close to 3 as a manifestation of the growing interface fractality. In the case of relatively high growth rates ($P\geq 0.20$-$0.25$), the dependencies of $(\Delta N_f/\Delta n)_{\Delta n=1}$ on $n$ show the appearance of the sharp decay in this parameter at final stage of release of nodes, which corresponds to the division of the region of occupied nodes into separate clusters at the final stage of growth (Fig. 3, marked by arrow). This peculiarity appears «smoothed» at low growth rates. Similar tendencies can be mentioned for experimentally obtained curves $\nu_{0.5}(t_{dr})$ (Fig. 2, *b*), where the noticeable sharp decay in $\nu_{0.5}$ takes place at the final stage of acetone evaporation (marked by arrow). In contrast, similar curve for ethanol is characterized by the significantly less peculiarity of this type.

The ratio of $K_1/K_2$ was estimated using a consideration of the mass transfer of evaporating phase for the zone of interface growth. The following relation can be written for the mass flux from the growth zone: $|J|\approx C\rho\langle a\rangle^2 c\tilde{L}\langle S\rangle_{\tau=1}$, where $C$ is the dimensionless parameter related to the pore geometry, $\rho$ is the liquid density, $\langle a\rangle$ is the characteristic size of the pore cross-section and $\langle S\rangle_{\tau=1}$ is the average path travelled by moving local boundaries per unit time. With used assumptions, the traces of moving local boundaries can be considered as the fragments of 3D fractal curves characterized by the fractal dimension equal to $2/\vartheta$ [30]. Estimation of the average length of trace $\langle S\rangle_{\tau=1}$ by use of the average boundary displacement per unit time $\langle\Delta\bar{r}^2(\tau=1)\rangle^{1/2}=K^{1/2}$ as the scale gives the following relation: $\langle S\rangle_{\tau=1}\sim K^{1/\vartheta}$ and, correspondingly, $|J|\sim K^{1/\vartheta}\gamma$. Thus, for the same

Table

The estimated values of $\vartheta$; subscript «1» corresponds to acetone as wetting liquid; «2» - to ethanol

| Sample | $t_{\max1}$, $s$ | $t_{\max2}$, $s$ | $(\nu_{0.5\max})_1$, Hz | $(\nu_{0.5\max})_2$, Hz | $\vartheta$ |
|---|---|---|---|---|---|
| 1[a] | ≈46 | ≈286 | ≈0.59 | ≈0.65 | ≈1.05 |
| 2[b] | ≈31 | ≈195 | ≈0.92 | ≈1.21 | ≈0.96 |
| 3[c] | ≈54 | ≈207 | ≈0.78 | ≈1.42 | ≈1.04 |

[a] Filter paper; thickness 135 μm, porosity 0.84;

[b] Copy paper; thickness 88 μm, porosity 0.56;

[c] Copy paper; low quality; thickness 71 μm, porosity 0.68.

porous system saturated by liquids with $\rho_1 \approx \rho_2$ and different values of $K$, the ratio $K_1/K_2$ can be expressed as $\{(J_1/\gamma_1)/(J_2/\gamma_2)\}^{\vartheta}$. The parameter $J/\gamma$ at $t_{dr}=t_{\max}$ is related to the value of $t_{\max}$. For the simulation model, the following relation between $(\Delta\tilde{N}_f/\Delta n)_{\max}/\gamma_{\max}$ and $n_{\max}$ was obtained for $0.001 \leq P \leq 0.5$: $(\Delta\tilde{N}_f/\Delta n)_{\max}/\gamma_{\max} \sim n_{\max}^{-\beta}$, where the value $(\Delta\tilde{N}_f/\Delta n)_{\max}/\gamma_{\max}$ was estimated for unit area of the zone of growth and $\beta$ is of the order of 1 ($\beta=1.00 \pm 0.05$). Assuming the similar relation between $J_{\max}/\gamma_{\max}$ and $t_{\max}$ for studied porous samples, we obtain the approximating relation:

$$(\nu_{0.5\max})_1/(\nu_{0.5\max})_2 = (t_{\max 2}/t_{\max 1})\{\gamma_{\max 1}{}^2/\gamma_{\max 2}{}^2\}^{1/\vartheta}. \tag{3}$$

For paper layers saturated by acetone and ethanol, the measured ratios $t_{\max 2}/t_{\max 1}$ vary from 4 to 6.5, depending on paper porosity and density. The ratios $(\nu_{0.5\max})_1/(\nu_{0.5\max})_2$ vary between 0.4 and 1.0. The measured typical values of these parameters for three paper samples are presented in the Table. The results of simulation of irreversible growth (Fig. 4) allow us to estimate $\gamma_{\max 1}/\gamma_{\max 2}$ for two porous systems with $K_1 >> K_2$ as the values of the order of 2.5 - 3.0; this leads to the value of $\vartheta$ close to 1 (estimations of $\vartheta$ made for the value of $\gamma_{\max 1}/\gamma_{\max 2}$ equal to 2.75, are presented in the Table).

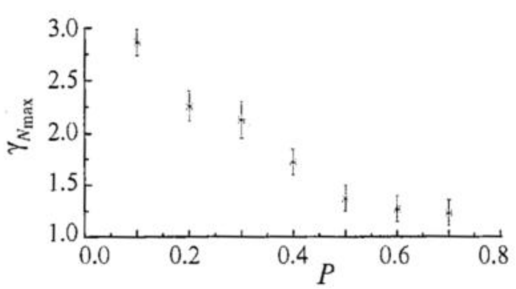

Fig. 4. The effective surface density of released nodes vs node release probability at $n=n_{\max}$ (results of simulation); $N_1=N_2=100$; $N_3=30$; $\Omega=6$

Hence, the typical magnitudes of $\vartheta$ obtained from experimental results allow us to suppose that the dynamics of local boundaries, which causes the interface growth in the course of liquid phase evaporation from stochastic porous layers such as paper, is in general similar to the «classical» Brownian dynamics.

## 3. Speckle-contrast-based monitoring of the tissue structure modification

Analysis of spatial-temporal fluctuations of scattered coherent light is a modern approach in the study of non-stationary scattered systems, such as living tissues. We can enumerate many examples of applying quasi-elastic scattering methods for tissue diagnostics. These involve above mentioned modifications of laser Doppler flowmetry (see, e.g., Refs [7, 8]) and DWS technique as applied to blood microcirculation monitoring and burned tissue diagnostics [9], laser speckle contrast analysis (LASCA) for similar applications [10-12, 14], and speckle contrast measurements in study of mechanical properties of tissues [13].

One of possible approaches in the study of spatially heterogeneous non-stationary media by the use of the speckle technologies is the contrast analysis of time-averaged dynamic speckle patterns in the image plane. In this case the image of object surface, which is illuminated by coherent light, is recorded with the exposure time $T$ comparable with the correlation time $\tau_c$ of intensity fluctuations of image-modulating dynamic speckles. This causes the blurred speckle pattern on the recorded image, which is characterized by the reduced value of contrast decaying with increase of $T/\tau_c$ ratio. For tissue images captured with $T$=const, the presence of dynamic macro-inhomogeneities in the scattering volume (such as, e.g., large vessels or local variations of the blood perfusion level) will induce the spatial variations of the locally estimated contrast for blurred image-modulating speckles. This effect can be applied to functional imaging of living tissues by the use of local estimates of the speckle contrast as the visualization parameter; in particular, such imaging technique was discussed in Refs [10, 11]. More recent example of speckle imaging of living tissues is application of the LASCA technique for visualization of cerebral blood flow reported in Ref. 14.

Here we present the results of the contrast analysis of time-averaged dynamic speckle patterns to monitor the structure modification of thermally treated collagenous tissue, such as cartilage. Laser-induced thermal reshaping of cartilage is a modern approach in laser medicine [31]. One of the probable mechanisms of this reshaping is presumably related to «bounded-to-free» water transition induced in macro-molecular structure of proteoglycan aggregates (PGA), one of the components of cartilage tissue [32, 33]. Another thermally activated mechanism of tissue reshaping is the partial thermal denaturation of the collagen matrix as the second basic component of cartilage tissue. In particular, the changes in mechanical properties of thermally treated collagen were studied in Ref. [34], where the empirical relations between mechanical properties of the thermally modified tissue, its shrinkage as a result of thermal modification, treatment temperature and time duration of a treatment procedure were established. It was found that mechanical properties decreased with increasing shrinkage, and that the maximal allowable shrinkage before significant material property changes occurred was between 15% to 20%. At larger values of tissue shrinkage, the progressive increase of the proportion of collagen fibrils undergoing denaturation was observed by means of the transmission electron microscopy. The abrupt increase in the tissue shrinkage rate was observed at the temperatures above 60 ° C.

Recent studies also revealed the existence of noticeable changes in physical and mechanical characteristics of the heated cartilage in the narrow temperature region near 70° C [31-33]. In particular, changes in tissue scattering properties were observed for this temperature range in the course of thermal treatment of cartilage. This effect was interpreted in terms of water release from heated zone and subsequent decrease of scattering centers sizes [35].

Also, the alterations of mechanical properties of the cartilage during the tissue treatment that are, for instance, revealed as the relaxation of the internal stress, are related to the time-dependent inhomogeneous deformation of tissue. In its turn, the process of thermal treatment of cartilage tissue illuminated by coherent light must be accompanied by expressed speckle dynamics of scattered optical field due to the time-dependent mutual local displacements of scattering sites such as collagen fibrils that form the tissue matrix. This is why statistical analysis of speckle intensity fluctuations can be used for monitoring of modification processes. The importance of such monitoring for laser reshaping of the native cartilage is caused by the necessity to provide conditions for proper tissue modification and to avoid the dramatic changes in cartilage structure caused by collagen denaturation in the treatment zone.

In experiments, the transmittance mode of probe He-Ne laser light propagation through a layer of thermally modified cartilage tissue was chosen to study the temperature-dependent dynamics of image-modulating speckles. Fig. 5, *a* shows the scheme of experimental setup. Single-mode He-Ne laser (1) (633 nm, linear polarization, output power 5 mW) was used as a light source. Laser beam was expanded by $50^{\times}$ telescopic system (2) and put on the front surface of ex-vivo sample (3) of porcine cartilage. Samples were prepared as 15 mm×25 mm pieces of 1.5 mm thickness. Speckle-modulated images of the sample back surface were captured by CCD-camera (5) (EDC-1000L, Electrim, USA) with zoom lens (4) (LMZ13A5M, 12.5-75 mm). Such detection geometry causes relatively high level of the detected light intensity and relatively low-frequency intensity fluctuations for image-modulating speckles, or their slow dynamics, in comparison with detection of the backward scattered light due to typically small values of the scattering angle. This had allowed us to choose the appropriate parameters of the image acquisition procedure for the range of exposure times and frame recording rates

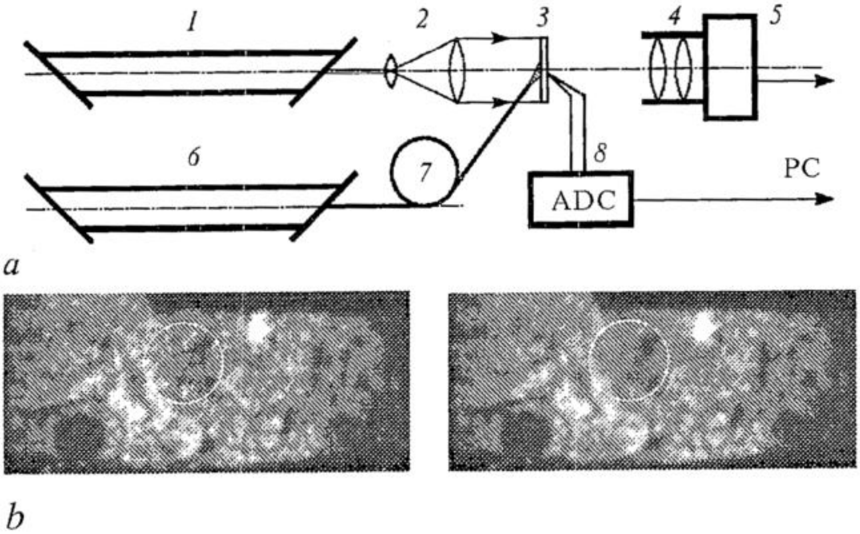

Fig. 5. *a* - scheme of the experimental setup; *b* - time-averaged images of the treated tissue; left panel - before treatment; right panel - during the treatment; treatment zone is marked by white circle

typical for used video capture system and, in its turn, to provide the detailed analysis of slow speckle dynamics for the treatment zone. Besides, image analysis with use of the transmitted light allows us to exclude an influence of the tissue surface reflection on speckle pattern formation that in this case is caused only by the bulk scattering into the probed volume.

Optimal conditions for speckle-modulated image recording are determined by two concurring factors that depend on the aperture of imaging lens: the appropriate mean size of speckles in the image plane and the appropriate brightness of speckle-modulated image captured with exposure time that is comparable with the correlation time of speckle intensity fluctuations. The larger average size of image-modulating speckles in the case of smaller imaging lens aperture leads to minimization of distortions of speckle statistics caused by the finite photosensitive area of each CCD pixel. But the decrease of imaging lens aperture causes a decrease of average brightness of image captured with given exposure time and, as a result, a decrease in the dynamic range of detected speckle intensity and the signal-to-noise ratio. For used experimental conditions and typical values of the correlation time of speckle intensity fluctuations, the optimal value of imaging lens aperture was found to be of the order of $f/12$, where $f$ is the focal length of the imaging lens. In this case, the estimated average speckle size in the image plane was 10 - 12 μm; this value is comparable with the pixel size for used CCD camera and thus the integration of spatial intensity fluctuations over each local detection zone (CCD pixel photosensitive area) takes place. On the basis of the sampling theorem (see, e.g., Ref. [36]), these detection conditions will cause the certain diminishing of the estimated contrast values due to the low-frequency spatial filtering properties of the detector in comparison with the ideal detection conditions, when the speckle size is much larger than the CCD pixel size, and a great number of image-modulating speckles is covered by the whole CCD photosensitive area.

Thermal treatment of the sample was provided by Erbium fiber laser (6) ($\lambda$=1.56 μm, output power up to 3.5W) with multimode quartz fiber (7) (0.6 mm diameter) as a light-delivering system (LS-1,5, IRE-Polus, Russia). The wavelength of 1.56 μm provides the bulk absorption of laser radiation by tissue and corresponds to the edge of one of the water absorption bands in the near infrared region [36]. For tissue, the penetration depth of treating laser radiation is of the order of 1 mm. The fiber tip was placed at 15 mm from the sample surface and the diameter of treatment zone was about 4 mm. Thin wire thermocouple (30 μm in diameter, (8)) was used to control the current tissue temperature $T$ in the central part of the zone. It was embedded into the sample so that the distance from the nonirradiated back surface of the sample was about 0.5 mm. The use of such thin thermocouple provides locality and fast response of dynamic measurements of the sample temperature. Notice that direct laser heating of thermocouple tip may cause some error. Our rough theoretical estimates of a maximal difference between the temperature of the laser-heated thermocouple and that of surrounding medium were made using the comparison of the heat transfer from thermocouple body to medium and heat deposition due to laser irradiation. These estimates give the difference about 3° C for typical values of the used beam intensity. In practice, this difference should be much less due to simultaneous heating by laser as thermocouple and tissue. Indeed, at high absorption coefficient of tissue the temperature of thermocouple may be less than the tissue temperature despite its being heated by laser. As to our experiments, the validity of the thermocouple use is obliquely confirmed from cooling dynamics measured immediately after the laser was switched off. In the case of a noticeable difference between temperatures of the thermocouple body and surrounding medium, this should cause the noticeable jump-like changes in measured temperature values because of the fast equalization of the body temperature and that of surrounding medium. Any distortions of this form at the initial stage of sample cooling were not observed in our case. Notice finally that the tissue subsurface temperature near the back surface should be slightly less than the temperature near the irradiated surface.

Sequential recording of speckle-modulated images of sample surface was carried during the laser treatment and after the laser was switched off. After the capture of frame sequences, the time series averaging of speckle intensity fluctuations was carried out for each pixel in the image plane using a sampling window of given width $2K+1$:

$$\tilde{I}_{i,j}^{\,k} = \Sigma_{m=-K}^{K} I_{i,j}^{\,k+m} \,/\, (2K+1), \tag{4}$$

where $k$ is the number of image in the frame sequence, and $i$, $j$ are the pixel coordinates in the image plane. The window width determined by the number of averaged frames was chosen in correspondence to the correlation time of intensity fluctuations in the center of treatment zone. The number of averaged frames corresponding to the window width varied from 3 to 7 for typical image capture parameters (exposure is 10 ms, sampling interval $\Delta t$ is 400 ms). This scheme of speckle-modulated image processing is based on the fundamental relations between statistical properties of the spatial-temporal fluctuations of dynamic speckles. Such relations allow the evaluation of the correlation time of speckle intensity fluctuations by the use of analysis of exposure-dependent speckle contrast as applied to time-averaged images of dynamic speckle patterns. Our scheme of speckle-modulated image processing reproduces in general the basic steps typical for laser speckle contrast analysis (LASCA), namely:

1) recording of time-averaged dynamic speckle pattern with given exposure time (in our case this procedure is similar to construction of image by averaging over the number of sequential frames sampled by the window of given width; the advantage of this approach is related to possibility to obtain values of the time-averaged speckle intensity with high temporal resolution determined by the frame sampling interval used for the frame sequence recording; on the contrary, in the case of using traditional LASCA technique the temporal resolution is determined by the used exposure time comparable with the window width for our case);

2) statistical analysis of spatial fluctuations of the time-averaged speckle intensity; digital image processing procedure in our case is the same as for LASCA technique.

The example of time-averaged image of tissue before and during the treatment is presented in Fig. 5, *b*. Treatment zone with expressed speckle dynamics is characterized by smaller level of pixel brightness fluctuations. Averaged images were processed to obtain the local estimates of the contrast $V_{i,j}^{\ k} = \sigma_{Ii,j}^{\ k}/\langle \tilde{I} \rangle_{i,j}^{\ k}$ for different regions of each frame obtained with the window width of $2K+1$. The time-dependent mean square root value $\sigma_{Ii,j}^{\ k}$ and the mean value $\langle \tilde{I} \rangle_{i,j}^{\ k}$ of 8-bit pixel brightness were calculated for a set of pixels inside the circular sampling area:

$$\langle \tilde{I} \rangle_{i,j}^{\ k} = (1/M)\Sigma_{m,n}\, \tilde{I}^{\ k}_{i+m,j+n} \Big|_{m^2+n^2\leq r^2},$$
$$\sigma_{Ii,j}^{\ k} = [(1/M)\Sigma_{m,n}\, (\tilde{I}^{\ k}_{i+m,j+n} - \langle \tilde{I} \rangle^{k}_{i,j})^2 \Big|_{m^2+n^2\leq r^2}]^{1/2}, \tag{5}$$

where $r$ is the radius of sampling area and $M$ is the number of pixels inside the area. The area radius was chosen at least 3 times wider than the average speckle size, but less than the treatment zone radius.

To characterize the relative changes in $V_{i,j}^{\ k}$ in the course of «thermal treatment-thermal relaxation» cycle, the normalized contrast value $\tilde{V}_{i,j}(t)=V_{i,j}(t)/V_{i,j}(0)$ was used, where $t=k\Delta t$ is the time lapse and $V_{i,j}(0)$ is the initial contrast. This normalization procedure allows us to compare the behavior of the time-averaged contrast for various treatment conditions independently on the initial contrast value that significantly varies across the imaged tissue surface. Typical behavior of $\tilde{V}_{i,j}(t)$ for central part of treatment zone is shown in Fig. 6; the dependence of current temperature $T$ measured with use of the termocouple in the vicinity of the back surface on the time lapse is also presented. At the first stage of treatment (time lapse interval from 0 to ≈20 s), the increase of $T$ is accompanied by the decay in $\tilde{V}_{i,j}(t)$. The second stage ($20\text{s}\leq t\leq 60\text{s}$) corresponds to thermally induced modification of cartilage and, being examined by the statistical properties of image-modulating speckles, is characterized by suppression of speckle dynamics that results in the increase of $\tilde{V}_{i,j}(t)$. The increasing heat loss rate at temperatures above 60° C becomes comparable with the rate of the heat deposition due to tissue irradiation by IR laser light for used treatment conditions and so causes a significant fall of the tissue temperature rate; as a result, a plateau-like region appears on the $T(t)$ dependence. The final stage, or thermal relaxation of the treated tissue, is accompanied by non-monotonic changes of the normalized contrast value with common tendency to increase.

This behavior leads to a specific, «loop-like» form of dependencies of $\tilde{V}_{i,j}(t)$ on $T$ (Fig. 7) in the treated zone related to the irreversible thermal modification of tissue structure due to partial relieving of heterogeneously stressed collagen matrix. Thus, the evolution of dynamic scattering system such as modified cartilage tissue depending on treatment conditions can be described by a set of similar trajectories in $(T,\tilde{V})$ plane. For arbitrary trajectory the following typical stages of system evolution can be singled out and a corresponding scenario of system behavior can be considered:

1) the stage of $\tilde{V}$ decay caused by increasing thermal deformations of heterogeneously stressed scattering structure consisting of 3D network of collagen fibres (collagen matrix) fixed by macro-mole-

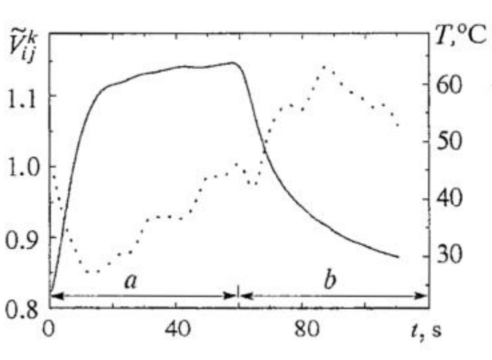

Fig. 6. The dependencies of $\tilde{V}_{i,j}(t)$ (dotted curve) and $T$ (full curve) on $t$ during and after the laser treatment ($a$ and $b$, respectively). Er laser output $P$ is 1.2 W

cular ensemble of water-coated proteoglycane aggregates;

2) the stage of partial stress relaxation, characterized by the rapid increase in $\tilde{V}$ with slightly increasing tissue temperature; the width of loop, $\Delta\tilde{V}$, depends on the duration of the plateau-like region of $T(t)$ dependence;

3) the stage of formation of a new, partially relieved stable spatial configuration of the scattering system accompanied by decrease in $\tilde{V}$;

4) the final stage of thermal relaxation of modified cartilage structure. The behavior of the scattering system at this stage is generally similar to that described for the first stage (in particular, both fragments of $\tilde{V}(T)$ are characterized by close values of the trend line slope).

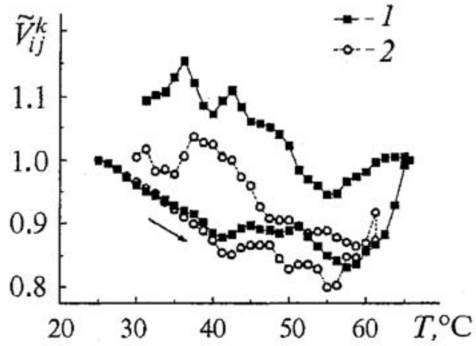

Fig. 7. The dependencies of $\tilde{V}_{i,j}(t)$ on $T$ for treatment-relaxation cycle. Squares (1), $P$=1.2 W, near the center of treatment zone; circles (2),$P$=0.8 W, near the center of zone. Black arrow indicates the heating stage; gray arrows indicate the thermal relaxation stage

Following from experimentally observed non-monotonic behavior of the time-averaged speckle contrast with increase of the tissue temperature, we can conclude that the specific feature of cartilage thermal modification is the appearance of the additional factor changing sufficiently the thermally activated dynamic behavior of tissue scattering structure for measured values of tissue temperature above 60° C. These changes are manifested not only in variations of the speckle contrast, but also in behavior of the tissue diffuse transmittance as well as the internal stress [37]. At the initial stage of thermal treatment, the decay in $\tilde{V}$ with increasing temperature can be interpreted in terms of thermally activated irreversible local deformations of tissue collagen matrix revealed at macroscopic level as the tissue shrinkage [34]. Another well-known manifestation of thermal modification of the collagen structure due to partial denaturation are the temperature-induced changes in tissue optical properties, say, the birefringence [38]. On the basis of empirical relation between the relative value of tissue shrinkage, the temperature and the duration of thermal treatment given in Ref. 34, the instantaneous rate of thermally induced irreversible deformation of collagen fibrils can be approximately estimated as:

$$\dot{\varepsilon}(t,T) \approx -K_1(T)t^{K_2(T)-1}/(1+K_3(T)t^{K_2(T)})^2, \tag{6}$$

where $K_1(T)$, $K_2(T)$, $K_3(T)$ are the empirically evaluated temperature-dependent coefficients. This expression gives the abrupt increase of the deformation rate with increasing temperature and its slow decay at the final stage of collagen thermal modification, when the tissue deformation exceeds 25% and collagen native structure is almost totally denaturated [34]. Mutual displacements of the structure-forming elements such as collagen fibrils in the course of tissue deformation will induce intensity fluctuations of coherent light scattered by the modified tissue structure. These intensity fluctuations are characterized by the correlation time depending on characteristic time interval required for displacement of scattering sites such as collagen fibrils at the distance of the order of the wavelength $\lambda_0$ of illuminating light and, correspondingly, are related to the scattering structure deformation rate:

$$\tau_c \sim \Lambda\lambda_0/l\,\dot{\varepsilon}n, \tag{7}$$

where $l$ is the characteristic distance between scattering sites for a probed medium, $n$ is the medium refractive index and the factor $\Lambda$ depends on the average number of scattering events, illumination and detection conditions. With the use of such simple phenomenological model, it is possible to give qualitative interpretation of the decay in the correlation time of speckle intensity fluctuations and, correspondingly, in the time-averaged speckle contrast with increasing tissue temperature that is observed at the initial stage of the cartilage thermal treatment. In turn, the increase of $\tilde{V}$ observed at the second stage of modification process, cannot be completely interpreted in terms of further progress in thermal modification of collagen matrix due to partial denaturation of the collagenous component of cartilage tissue. With the tissue shrinkage progress, the appearance and accumulation of new scattering centers due to thermal denaturation of collagen fibrils is rather accompanied by further decrease in correlation time of speckle intensity fluctuations or tissue transmittance. In particular, the additional study of dynamic light scattering by soft collagenous tissue such as porcine sclera in the course of its thermal denaturation at fixed temperatures in the range from 60° C to 90° C showed the monotonic decrease in the correlation time of scattered light intensity fluctuations with the increasing tissue temperature. Also, the additional oblique argument against the mechanism of the time-averaged speckle contrast increase for the temperatures slightly above 60° C that can be directly related to thermally activated denaturation of the collagen matrix, is that the thermally induced dramatic changes in collagen structure should appear for sufficiently larger values of laser beam intensity and exposure time than that used for laser-mediated cartilage reshaping. Typically, the thermally induced deformations of cartilage tissue accumulated to the final phase of the initial stage of thermal treatment, are significantly less than critical values of 15-20% given in Ref. 34. Thus, in our case we should not expect the decay in the tissue deformation rate and, correspondingly, increase of the time-averaged speckle contrast due to degradation of the collagen matrix. In particular, the examination of the cartilage after the laser treatment with an optical microscope [39,40] did not show any evidence of dramatic changes in matrix structure for appropriately chosen reshaping conditions.

Thus, the change in behavior of $\tilde{V}$ in the narrow interval of the measured tissue temperature slightly above 60 °C can be presumably related with the manifestation of one or several adequately effective thermally activated mechanisms of relaxation of the matrix deformation rate. At present time, the total physical picture of this effect is not yet fully understood but the mechanism of bounded to free water transition in the proteoglycan aggregates (PGA) structure due to dissociation of PGA macromolecules was discussed as the probable candidate for the role of such stress relaxation controlling mechanism [33]. The argument supporting this hypothesis is that the mechanical properties of cartilage tissue are strongly influenced by the interactions between subsystems of collagen matrix and PGA as the tissue basic components. Therefore, the alterations in hydrodynamic properties of PGA ensemble as the ground substance will cause the change in deformability of a whole tissue. In particular, it was found by means of a dynamic light scattering [41] that the thermal dissociation of proteoglycan macromolecules at temperatures above 60° C is accompanied by the significant increase in the translational diffusion coefficient of PGA.

In further study of tissue modification process, analysis of «loop-like» curves plotted in $(T,\tilde{V})$ coordinates (in particular, the relation between loop height $\Delta\tilde{V}$ and duration of plateau-like region on $T(t)$ curve) can be applied for evaluation of kinetic parameters of the internal stress relaxation, in addition to recently described approaches, such as the study of thermal and mechanical effects, tissue diffuse transmittance and/or reflectance measurements, FTIR spectroscopy, and examination by the use of optical and atomic force microscopy.

## 4. Conclusion

Presented results illustrate the potentialities of various modifications of the speckle correlometric techniques in studying the dynamic properties of local scatters that form weakly ordered multiple scattering systems of various nature. Further development of speckle-based coherent optical technologies can be related to the application of polarization discrimination of multiple scattered speckle patterns as well as the use of partially coherent probe light with the controllable coherence length. These approaches open the way for precise analysis of the light transfer processes in disordered scattering systems due to possibility of selection of partial components of multiple scattered optical fields with given pathlength distributions.

*This work was supported in part by CRDF grant REC-006 and by RFBR grant № 01-02-17493.*

## References

1.*Pine D.J., Weitz D.A., Chaikin P.M., and Herbolzheimer E.* Diffusing-light spectroscopy. Phys. Rev. Lett. 60, 1134-1137 (1988).

2. *Maret G. and Maret G.* Multiple light scattering from disordered media. The effect of Brownian motion of scatterers. Z. Phys. B 65, 409-413 (1987).

3. *Menon N and Durian D.J.* Diffusing-wave spectroscopy of dynamic in a three-dimensional granular flow. Science 275, 1920-1922 (1997).

4. *Kao M.H., Yodh A.G., and Pine D.J.* Observation of Brownian motion on the time scale of hydrodynamic interactions. Phys. Rev. Lett. 70, 242-245 (1993).

5. *Yodh A.G., Georgiades N., and Pine D.J.* Diffusing-wave interferometry. Optics Communications 83, 56-59 (1991).

6. *Boas D.A., Bizheva K.K., and Siegel A.M.* Using dynamic low-coherence interferometry to image Brownian motion within highly scattering media. Optics Letters 23, 1087-1089 (1998).

7. *Stern M.D.* In vivo evaluation of microcirculation by coherent light scattering. Nature (London) 254, 56-58 (1975).

8. *Essex T.J.H. and Byrne P.O.* A laser Doppler scanner for imaging blood flow in skin. J. Biomed. Eng. 13, 189-194 (1991).

9. *Boas D.A. and Yodh A.G.* Spatially varying dynamical properties of turbid media probed with diffusing temporal light correlation. J. Opt. Soc. Am. A 14, 192-215 (1997).

10. *Fercher A.F. and Briers J.D.* Flow visualization by means of single-exposure speckle photography. Optics Communications 37, 326-330 (1981).

11. *Briers J.D. and Webster S.* Laser speckle contrast analysis (LASCA): a non-scanning, full-field technique for monitoring capillary blood flow. J. Biomed. Opt. 1, 174-179 (1996).

12. *Sadhwani A., Schomacker K.T., Tearney G.J., and Nishioka N.S.* Determination of Teflon thickness with laser speckle. I. Potential for burn depth diagnostics. Appl. Opt. 35, 5727-5735 (1996).

13. *Jacques S.L. and Kirkpatrick S.J.* Acoustically modulated speckle imaging of biological tissues. Opt. Lett. 23, 879-881 (1998).

14. *Dunn A.K., Bolay H., Moskowitz M.A. and Boas D.A.* Dynamic imaging of cerebral blood flow using laser speckle. Journal of Cerebral Blood Flow and Metabolizm 21, 195-201 (2001).

15. *M.P. van Albada and Lagendijk A.* Observation of weak localization of light in arandom medium. Phys. Rev. Lett. 55, 2692-2695 (1985).

16. *Wolf P. and Maret G.* Weak localization and coherent backscattering of photons in disordered media. Phys. Rev. Lett. 55, 2696-2699 (1985).

17. *Akkermans E., Wolf P.E., Maynard R., and Maret G.* Theoretical study of the coherent backscattering of light by disordered media. J. Phys. France 49, 77-98 (1998).

18. *Stephen M.J.* Temporal fluctuations in wave propagation in random media. Phys. Rev. B 37, 1-5 (1988).

19. *MacKintosh F.C. and John S.* Diffusing-wave spectroscopy and multiple scattering of light in correlated random media. Phys. Rev. B 40, 2382-2406 (1989).

20. *John S. and Stephen M.* Wave propagation and localization in a long-range correlated random potential. Phys. Rev. B 28, 6358-6369 (1983).

21. *Ackerson B.J., Dougherty R.L., Reguigui N.M. and Nobbman U.* Correlation transfer: application of radiative transfer solution methods to photon correlation problems. J. Thermophys. And Heat Trans. 6, 577-588 (1992).

22. *MacKintosh F.C., Zhu J.X., Pine D.J. and Weitz D.A.* Polarization memory of multiply scattered light. Phys. Rev. B 40, 9342-9345 (1989).

23. *Bicout D., Brosseau C., Martinez A.S. and Schmitt J.M.* Depolarization of multiply scattering waves by spherical diffusers: influence of size parameter. Phys. Rev. E 49, 1767-1770 (1994).

24. *Zimnyakov D.A. and Tuchin V.V.* About interrelations of distinctive scales of depolarization and decorrelation of optical fields in multiple scattering. JETP Letters 67, 455-460 (1998).

25. *Zimnyakov D.A.* On some manifestations of similarity in multiple scattering of coherent light. Waves in Random Media 10, 417-434 (2000).

26. *Zimnyakov D.A., Zakharov P.V., Trifonov V.A. and Chanilov O.I.* Study of interface evolution in porous media with the use of dynamic light scattering. JETP Letters 74, 237-243 (2001).

27. *Lemieux P.-A., Vera M.U. and Durian D.J.* Diffusing-light spectroscopies beyond the diffusion limit: The role of ballistic transport and anisotropic scattering. Phys. Rev. E 57, 4498-4515 (1998).

28. *Shaw T.M.* Drying as an immiscible displacement process with fluid counterflow. Phys. Rev. Lett. 59, 1671-1674 (1987).

29. *Pietronero L., Tosatti E.* Eds. Fractals in Physics, North-Holland, Amsterdam (1986).

30. *Feder J.* Fractals, Plenum Press, New York (1988).

31. *Sobol E., Sviridov A.,Omel'chenko A., Bagratashvili V., Kitai M., Harding E., Jones N., Jumel K., Mertig M., Pompe W., Ovchinnikov Y., Shekhter A. and Svistuchkin V.* Laser reshaping of cartilage. Biotech Genetic Eng Rev. 17, 553-577 (2000).

32. *Wong J.F., Milner T.E., Kim H.H., Nelson J.S. and Sobol E.N.* Stress relaxation of porcine septal cartilage during Nd:YAG (1.32(m) laser irradiation: mechanical, optical, and thermal responses. Journal of Biomedical Optics 3, 409-414, (1998).

33. *Sobol E., Sviridov A., Omel'chenko A., Bagratashvili V., Bagratashvili N. and Popov V.* Mechanism of laser-induced stress relaxation in cartilage. Proc. SPIE 2975, 310-315 (1997).

34. *Wall M.S., Deng X.-H., Torzilli P.A., Doly S.B., O'Brien S.J. and Warren R.F.* Thermal modification of collagen. J. Shoulder Elbow Surg., 8, 339-344 (1999).

35. *Bagratashvili V., Bagratashvili N., Sviridov A., Sobol E., Omel'chenko A., Tsypina S., Gapontsev V., Samartsev I., Feldchtein F. and Kurano R.* Kinetics of water transfer and stress relaxation in cartilage heated with 1.56 μm fiber laser. Proc.SPIE 3914, 102-107 (2000).

36. *Hale G.M. and Querry M.R.* Optical constants of water in the 200 nm to 200 μm wavelength region. Applied Optics 12, 555-563 (1973).

37. *Wong B.J., Milner T.E., Harrington A., Ro J., Dao X., Sobol E.N. and Nelson J.S.* Feedback-controlled laser-mediated cartilage reshaping. Arch. Facial Plast. Surg., 1, 282-287 (1999).

38. *Maitland D.J. and Walsh J.T.* Quantitative measurements of linear

birefringence during heating of native collagen. Lasers in Surgery and Medicine, 20, 310-318 (1997).

39. *Sobol E.N., Bagratashvili V.N., Sviridov A.P., Omel'chenko A.I., Ovchinnikov Yu.M., Shekhter A.B. and Helidonis E* . Cartilage shaping under laser radiation. Proc. SPIE, 2128, 43-47 (1994).

40. *Sviridov A.P., Sobol E.N., Jones N. and Lowe J.* Effect of Holmium laser radiation on stress, temperature and structure in cartilage. Lasers in Medical Science, 13, 73-77 (1998).

41. *Jamieson A.M., Blackwell J., Reihanian H., Ohno H., Gupta R., Carrino D.A., Caplan A.I., Tang L.H. and Rosenberg L.C.* Thermal and solvent stability of proteoglycan aggregates by quasielastic laser light-scattering. Carbohydrate Research, 160, 329-341 (1987).

*Saratov State University*
*Institute of Laser and Information*
*Technologies of Russian Academy*
*of Sciences, Almus Ltd*

*Received 25.06.2002*

УДК 535.361

# СПЕКЛ-ДИАГНОСТИКА РЕЛАКСАЦИОННЫХ ПРОЦЕССОВ В НЕСТАЦИОНАРНЫХ РАССЕИВАЮЩИХ СИСТЕМАХ

*Д.А. Зимняков, А.П. Свиридов, А.И. Омельченко, В.А. Трифонов,*
*Д.Н. Агафонов, П.В. Захаров, Л.В. Кузнецова*

Рассмотрен когерентно-оптический метод исследования процессов нестационарного массопереноса в рассеивающих средах на основе статистического анализа пространственно-временных флуктуаций интенсивности спекл-модулированных оптических полей, рассеянных объектами. В качестве примеров рассмотрены: анализ нестационарного массопереноса при испарении насыщающей жидкости из неупорядоченного пористого слоя и анализ структурной модификации хрящевой ткани в процессе ее нагрева ИК лазерным излучением. В случае испарения жидкости из пористого слоя обнаружен эффект аномального уширения спектра флуктуаций интенсивности спекл-модулированного рассеянного излучения при уменьшении скорости испарения жидкой фазы, обусловленный особенностями развития фрактального фронта испарения. Характерной особенностью термической модификации структуры хрящевой ткани является существование гистерезиса зависимости контраста спеклов, модулирующих изображение исследуемой ткани в когерентном свете, от температуры ткани в зоне модификации. Механизм структурной модификации хрящевой ткани предположительно связан с термически активированным переходом «связанная вода - свободная вода» в структуре протеогликановых агрегатов как одной из базовых составляющих хрящевой ткани.

*Dmitry A. Zimnyakov* was born in 1956 in Saratov. He received his degree of Doctor of Science in Physics and Mathematics at from Saratov State University. He is a Professor of the Optics Department of Saratov State University. He is an author of more than 120 scientific papers, textbooks and book chapters, editor and co-editor of 4 SPIE Proceedings books. His scientific interests include the statistical optics, biomedical optics and biophysics.

*Alexander P. Sviridov* was born in 1952 in Zhitomir (Ukraine). He is PhD, Senior Scientist of Institute of Information and Laser Technologies of Russian Academy of Sciences. Author of about 90 articles in the fields of laser interaction with materials, spectroscopy. He specialized mostly in the studies of optical properties, non-invasive diagnostics of biological tissues and development of hyperthermal laser technologies for medical applications.

*Alexander I. Omel'chenko* was born in 1954 in Berdsk, Novosibirsk reg. He received his degree of Candidate of Science in Phys. and Math. at the Institute of Nuclear Physics in Tashkent. He is a Senior Research Scientist of the Biophotonics laboratory at the Institute of Laser and Information Technologies. He is an author of more than 60 scientific papers and contributions in scientific journals. His research interests are connected with biomedical optics and biomechanics.

*Valery V. Trifonov* was born in 1952 in Saratov. He is a Vice-Director of Precision Mechanics and Control Institute of Russian Academy of Sciences and a President of «Almus» Company. He is a co-author of 10 scientific papers. His scientific interests include the laser metrology and optical methods of material testing.

*Dmitry N. Agafonov* was born in 1976 in Saratov. He graduated from Saratov State University in 1999. He is a PhD student of the Optics Department of Saratov State University. He is a co-author of 11 scientific papers. His scientific interests include the statistical optics and biomedical optics. He is a SPIE student member.

*Pavel Zakharov* graduated from Saratov State University in 2000 with specialty of Biomedical Optics and Laser Biophysics. Now he is a PhD student in the Optics Department and his research is focused on speckle correlometry of non-stationary mass transfer in porous media. His scientific interests cover the fields of coherent optics, novel techniques of digital signal processing, data acquisition systems. He is a SPIE student member.

*Liana V. Kuznetsova* was born in 1979 in Tbilisi. She graduated from Saratov State University in 2002. She is a PhD student of the Optics Department of Saratov State University. She is a co-author of 8 scientific papers. Her scientific interests are connected with biomedical optics and biophysics. She is a SPIE student member.

Methodical papers on nonlinear dynamics

Izv. VUZ «AND», vol.10, № 3, 2002

# PHYSICAL EXPERIMENT IN UNIVERSITY EDUCATION

*B.S. Dmitriev, Yu.I. Levin, Yu.P. Sharaevsky*

The role of physical experiment in modern university education is discussed. The principles of organization of a training and research physical practical work for the lower years students at faculty of nonlinear processes of the Saratov university are stated. The concrete examples of experimental researches are cited.

## Introduction

Exactly 40 years ago the academician P.L. Kapitsa spoke at the General meeting of the Academy of Sciences of the USSR with a report, which gave the title to a famous book «Experiment. Theory. Practice» [1]. The work is well known to physicists - its main idea is comparison of theoretical and practical physics development in the USSR. As the editor of «The Journal of Theoretical and Practical Physics» P.L. Kapitsa estimated relation of articles on experimental physics to articles on theoretical physics as 1:4 or 1:3. Work of great scientists - naturalists, who made a large contribution to development of modern natural science, was making invariably in an intimate connection with theory and experiment. Harmonious development of theory and experiment «is absolutely necessary in all fields of natural science». Still the famous lord Kelvin compared theory with millstones, and data of experiment with grain. Much as millstones whirled by themselves - it would be nothing useful. But quality of flour is determined by quality of grain that is why «high quality of experiment is a necessary condition not only for forming an advanced theory, but also for getting practical results». It is hard to determine the mentioned relation of theoretical and experimental works today, and the idea of high quality of physical experiment, its role nowadays and teaching to this art, is urgent today.

In our opinion, preservation and development of the experiment on location is an important element of the correct formation of a modern natural picture of the world in the mind of the student. For a first year student (a physicist) experiment begins with a physical practical work and connected with a course of general physics. It should be noted, that organization of physical education at the University begins with its base - the course of physics, being understood in a broad sense: a course of lectures, seminars, laboratories, demonstrational experiments, manuals and so on.

Unfortunately it should be noted, that the role of physical experiment does not often get due attention in modern manuals. Courses of general physics undergo an excessive «theorization» - statement of fundamental classical experiments «disappears» from the pages of training aids, and some of them changed radically established conceptions in physics. For science the most valuable experiments were those ones, results of which contradicted theoretical expectations, though many experiments were organized «under the direction» of one or another, sometimes hypothetical, but always theoretical scheme, in the context of which they wanted to understand experimental facts. Just such experiments played a decisive role in the picture of the modern natural science. Side by side with simplicity and clearness of an idea (sometimes just «witty») these experiments were notable for striking, even for today, resolution. Estimations on the Mickelson - Morley experiment are usually traditionally given as an example from a chrestomathy [2]. And some years before the very «sensitive» experiment, results of the skilful experimentalist Rowland (1878) on direct verification of the Maxwell's idea about magnetic field of a moving charge (paragraph 770 of «The Treatise about electricity» [3]) were published. The idea of the experiment is simple - the magnetic field of a rotating charged ebonite disk should be determined. What can be surprising for a modern student here? Of course, experimental art - the value of the found magnetic field was equal to $10^5$ (!) of the earth magnetic field value. This is an extremely hard experiment even for today, but it is difficult to find a description of the measuring method. There are some other similar examples. We can observe the same situation with modern experiments. But when explaining some effects, their enclosure was rather convincing. (For example, when studying resonance - the application of the Mössbaur effect for measuring of fantastically little effects of changing frequency when studying «gravitational violet shift» of the photon in experiments of Paund and Rebka). It seems to us, that the student of nowadays should know about such unique investigations. An educated specialist should get even «a grain» of art and culture of organization of great experiments in the university lecture-room. The usage of the adjective «great» is quite justified - many of the experiments have a «Nobel» character.

Leading university centers pay serious attention to a new approach in creation of training laboratories, corresponding to «the spirit of modern physical investigations» [4-8]. They should provide interest for the student in researches in the physical laboratory, but it is not so easy, as he is «charmed» by the computer technology, which is fascinating and seems all-powerful to him. The practical work is only «ideologically» connected with the course of lectures; its principal task is not verification of «correct» laws, and mainly mastering of measuring techniques, analysis of reasons of experimental results difference, correcting of experiments. All this is directed to overcome «intellectual sterility» of the student. Organization of an effective process of studies in the physical laboratory demands changing technology of the accepted method: creation of multifunctional module facilities with elements of automation of measuring, autonomous composition of elements on such facility to extend the number of being executed exercises, that provides a «storing» system of collection of experimental data. The essential moment is the intensification process of organization of the work at the sacrifice of time saving on usual «routine» procedures (replacement of the facility and mastering of a new one, exception of ineffective measurements, unjustified prolonged «theoretical» test). At the same time it is necessary to take into consideration the natural law of «distribution of students over energies» in depending on their creative abilities, desire and ability to work with the equipment. Equally with a modern «arrangement» of organization of works it is expedient to use «out-of-date» tasks (warmth, sound and so on): the student would not possess some scientific erudition without fundamental studying «the classics». After having carried out experimental investigations by the student, the crucial stage is analysis and processing, showing sufficient erudition, of the received data, usage of a computer to model and demonstrate visually the results.

## Training and research physical practical work for the lower years students

The presented «ideology» was established when creating an integrated training and research practical work «Methods, Technology and Informational Provision of the Physical Experiment» at the faculty of nonlinear processes of the Saratov State University (SSU). The main aim of such laboratory is a detailed analysis of the received experimental results, estimation of influencing factors and reliability of the data, that is the training to the foundations of the physical experiment, showing sufficient erudition.

In the practical work there are 15 multifunctional facilities with electronic measuring systems, 110 students of 2 faculties of the SSU: the faculty of nonlinear processes and the faculty of computer sciences and information technologies, take the course during the academic year, 5 training aids have been published [9-13]. The main directions of researches are carried out in the following fields: physical foundations of mechanics (the conservation law, dynamics of the rotary motion, friction forces of different nature, elastic deformations, mechanical oscillations and resonance); oscillations and waves in different mediums, molecular phenomena, thermodynamics and phase transitions, and electromagnetic phenomena.

Taking into account the strategy of education at the faculty of nonlinear processes, based on the ideas of nonlinear dynamics, let us note only some tasks on oscillations and waves, being solved in the physical laboratory. This is, first of all, a vast class of mechanical pendulums with analysis of their characteristic peculiarities, experimental investigation of nonlinear effects and their comparison with different theoretical models [9]. A series of tasks on investigations of waves in different mediums demonstrates the «international» language of the theory of oscillations: waves in bars and strings, sound waves in free space and an acoustical resonator, capillary-gravity waves on the water surface, the study of which already requires a certain experimental skill. Both velocity of sound and velocity of the electromagnetic wave are measured by a widespread standing wave method. To complete the picture let us adduce some results of experimental investigations.

## Resonance in mechanical systems

A great role and beauty of the phenomenon of resonance in nature are well known. In the training laboratories this phenomenon is usually studied in a oscillatory contour of the radio range or in systems of microwave frequencies and the optical range. In our practical work resonance is studied on torsional oscillations of the disk of the rotary table, carrying out oscillations in the horizontal plane under the action of two elastic springs, creating a torque moment throughout a thread, enveloping the axis of the pulley of the rotary table [10]. Elastic properties of the springs and the moment of inertia of the rotating system determine the oscillation period of such pendulum. The electronic measuring system allows determining the oscillation period with resolution 0.1ms. To excite forced oscillations in such system and to investigate resonance the pulley of the rotary table is connected with an electric motor, allowing changing the frequency of the forced signal and its amplitude. Dependence of amplitude and, what is more interesting, phase of rotary forced oscillations of the system on frequency of external oscillations are investigated in the work. It is interesting to pay attention, that resonance effects for realized mechanical systems are observed with frequencies about 1 Hertz (!). Results of measurements are presented in Fig. 1. Resonance amplitude characteristics ($\alpha$ - the angle of deflection of the system from the equilibrium position) of the free platform and the platform loaded by a ring are shown in Fig. 1, *a*. Dependences of the amplitude of oscillations $\alpha$ and the phase shift $\Delta\phi$ on the period of external oscillations for one of the systems are shown in Fig. 1, *b*.

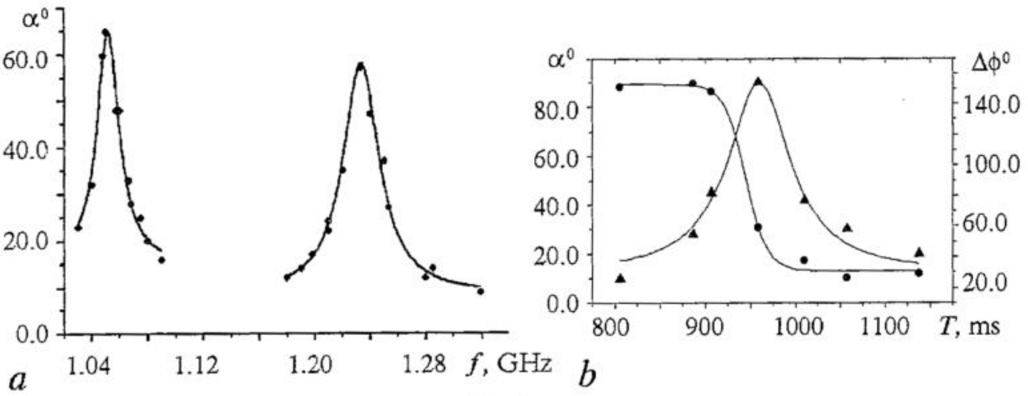

Fig. 1

From received data one can make conclusions about good quality of being investigated mechanical oscillating systems.

At the same time let us note, that such simple oscillating system is a simple and rather precise device to determine moments of inertia of different bodies. It is enough to measure the period of natural oscillations of the free table $T_0$ and its moment of inertia $J_0$, the period of oscillations of the loaded table $T$, the moment of inertia of the table with any figure, placed in an arbitrary way on the disk of the platform, is computed of the relation $J=J_0(T/T_0)^2$. In the table 1 there are found in the experiment and computed moments of inertia of different figures (the moment of the loaded table is $J_0$=0.0026 kg/m$^2$ , moments of inertia of figures are presented in the same units).

Table 1

**Moments of inertia of different figures**

| Figure | a Parallelepiped | | | a Disk | | a Ring |
|---|---|---|---|---|---|---|
| Position | Flat-ways | On the «long» side | On the «short» side | In the center of the platform | On the edge | In the center |
| Experiment | $4.9\cdot10^{-3}$ | $4.18\cdot10^{-3}$ | $9.65\cdot10^{-4}$ | $7\cdot10^{-4}$ | $2.1\cdot10^{-3}$ | $2.48\cdot10^{-4}$ |
| Calculation | $4.92\cdot10^{-3}$ | $4.19\cdot10^{-3}$ | $9.65\cdot10^{-4}$ | $7.1\cdot10^{-4}$ | $2.13\cdot10^{-3}$ | $2.5\cdot10^{-4}$ |

An excellent coincidence attracts attention.

## Measurement of velocity of light

We have already spoken above about the «international» language of the theory of waves. It shows itself in methods of investigating waves of different nature. A wide spread measuring technique of the velocity of sound is the standing wave method, as a rule, here conditions of wave reflection are invariable, they are given by the facility construction. By the same method one can investigate, naturally, electromagnetic waves: to determine the velocity of a electromagnetic wave in the free space. Perhaps, first time in his life a first year student has an opportunity to measure «with his own hands» one of the principal «mysterious» physical constants - «velocity of light».

The facility is very simple; its scheme is given in fig. 2.

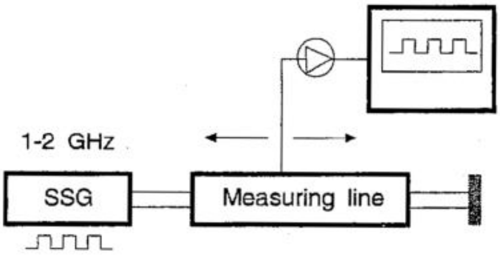

Fig. 2

The source of electromagnetic oscillations is a microwave oscillator in the range of frequencies 1000-2000 MHz. The signal, modulated by a low frequency, went from the signal oscillator to a flat coaxial line, along of which a needle-shaped radio-frequency indicator probe was moving. The signal of the probe was brought to the detector chamber, after which the low-frequency signal was amplified and observed on the screen of the oscillograph. The position of the indicator probe along the shift axis was fixed with the aid of noniuses with resolution to 0.5 mm. The standing wave character was changed easily by the kind of charging of the line: a broken line, a short-circuited or matched line. Length of the measuring line allowed fixing, when the probe moving, some length of waves, in measuring of which one should be especial careful. The signal frequency was determined to tenth parts of a Megahertz on the generator. The result («velocity of light) was determined by these two parameters - signal frequency and wavelength. As we can see, measuring technique is very simple and the art of an experimentalist was in analysis and in provision of conditions of certain measuring of standing wave minimums. In table 2 there are values of velocity of the electromagnetic wave in the air, measured for different conditions of the standing wave.

Table 2

**A broken line**

| *f*, MHz | 1140.7 | 1217.7 | 1259.9 | 1414.1 | 1689 | 1807.7 |
|---|---|---|---|---|---|---|
| λ, mm | 263.23 | 247.46 | 238.82 | 212.25 | 177.58 | 165.55 |
| *c*, $10^8$ m/s | 3.0027 | 3.0134 | 3.009 | 3.0014 | 2.9994 | 2.9927 |

**A circuited line**

| *f*, MHz | 1200.6 | 1276.5 | 1439.4 | 1518.2 | 1557.9 | 1716.7 | 1796.7 |
|---|---|---|---|---|---|---|---|
| λ, mm | 251.30 | 235.42 | 209.15 | 198.57 | 193.02 | 175.25 | 167.35 |
| *c*, $10^8$ m/s | 3.0171 | 3.0052 | 3.01 | 3.0148 | 3.0071 | 3.0085 | 3.0068 |

*c* - velocity of an electromagnetic wave, *f* - signal frequency, λ - wavelength.

The method of a cavity microwave resonator for measuring «*c*» is methodically very close to the one, stated above, and it is one of modern for determining velocity of light (even the depth of the skin-layer of electromagnetic radiation penetration inside of metal is taken into account in the method). That is why organization of the described work, because of its simplicity and clearness, is very useful for a yesterday's schoolboy, especially as it allows a large creative analysis of mistakes of the experiment. On the facility one could demonstrate and value in quantity the effect of «decelerating» the phase velocity of the electromagnetic wave by a dielectric, placed along the wave propagation channel, and even value dependence of dielectric constant on the signal frequency.

# Waves on the water surface

It is interesting to investigate one more type of waves, which, of course, everyone observed more than once - these are waves on the water surface. They are beautiful and usual for us, but these are «especial» waves, as they are similar neither to sound nor to light. As Feiman R. noticed «all difficulties, which only can be in waves, gathered here»[14]. This is one of the most «beautiful» tasks in the theory of waves [15,16]. We can indicate main physical factors, determining existence of the waves, of all variety of waves on water - these are gravity and surface tension. These two effects are compared in a certain field of parameters and these waves are called capillary-gravity. Their characteristic peculiarity is dispersing waves, for which the phase velocity of waves changes with the wavelength. This is a serious research for a student of the first year both in an experimental and theoretical aspects of the phenomenon and, first of all, because of getting to know phase and group velocities. The liquid being investigated is placed in a special container (of organic glass), reminding an irrigation canal. A diaphragm, exciting waves with a certain frequency from a generator, is joined to an edge of the canal. To excite running waves in such canal, the opposite wall is made in the shape of a sloping «bank». A thin probe, submerged a little to the liquid, moves along the canal. Current through the probe depends on depth of its submerging to water, that gives opportunity to observe the wave shape when the probe moves, that is to measure the wavelength. In the measuring scheme we used a dual-beam oscilloscope, on which a reference sine signal, exciting the diaphragm, is observed on a ray and a signal from the probe on another ray. A picture of these two signals, convenient for measuring, can be chosen by means of regulation of parameters of the electrical scheme. Moving the probe along longitudinal coordinates, one gets cophasing or antiphasing position of the signals and determines the wavelength, as a distance between points in a certain phase. Knowing the frequency of the oscilloscope, a phase velocity can be determined easily. Dependence of phase velocity on wavelength for water with temperature 25° C is presented in Fig. 3.

The rated dependence on the relation

$$V_{ph} = (g/k + \sigma k/\rho)^{1/2}$$

is presented by an entire line, here $g$ - gravitational acceleration, $\sigma$ - coefficient of water surface tension, $\rho$ - density of water, $k=2\pi/\lambda$ - wave number, $\lambda$ - wavelength. Values of material constants are chosen for the operating temperature. Data of the experiment are given in form of points. Range of operating frequencies is 6-70 Hz when taking down the dependence, the experiment is rather «punctilious», taking into account, that measuring on low frequencies (~10Hz) on usual oscilloscopes is rather difficult. The experiment depends on many «ruses», that is why the present work can be carried out in the form of a course work with large opportunities for independent researches. The received experimental data reflect principal natural properties of capillary-gravity waves in the range of typical wavelength about 1.7 cm, where minimum value of the phase velocity is about 23 cm/s. As for analysis of quantitative coincidence - this is another theme of the research.

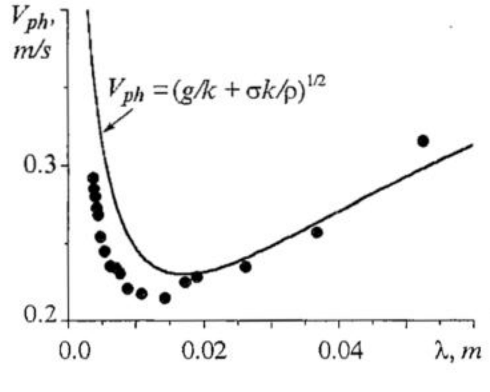

Fig. 3

## Conclusion

In the same work some important moments about a role of physical experiment in training of the modern specialist - physics are shown. By the way of illustration stated principles the results of organization of a new training and research physical practical work for the lower years students at faculty of nonlinear processes SSU are given. Different themes of investigations, which the student gets to know in the physical laboratory, show convincingly wealth and breadth of the experiment on location in the surrounding physical world to a young researcher. The knowledge received at this stage, will allow him creatively and with confidence to participate in the program of researches of scientific laboratories of faculty.

## References

1. *Капица П.Л. Эксперимент.*Теория. Практика. М.: Наука, 1977.

2. *Матвеев А.Н.* Механика и теория относительности. М.: Высшая школа, 1986.

3. *Максвелл Д.К.* Избранные сочинения по теории электромагнитного поля. М.: Государственное издательство технико-теоретической литературы, 1954.

4. *Алешкевич В.А.* Курс общей физики как основа физического образования // Физическое образование в вузах. 2001. Т. 7, №3. С.21.

5. *Портис А.*Физическая лаборатория. М.: Наука, 1972.

6. *Агальцов А.М., Афонин А.П., Горелик В.С. и др.* Научно-исследовательская физическая лаборатория технического исследовательского университета XXI века // Физическое образование в вузах. 2001. Т. 7, № 3. С. 23.

7. *Аржанников А.В., Меледин Г.В., Оришич А.М.* Особенности физического образования в Новосибирском государственном университете // Съезд российских физиков-преподавателей «Физическое образование в XXI веке». Тезисы докладов. Москва, 2000. С. 85.

8. *Бегинин Е.Н., Дмитриев Б.С., Лёвин Ю.И., Шараевский Ю.П.* Роль физического эксперимента в университетском образовании // Современный физический практикум. Сборник тезисов докладов VII учебно-методической конференции стран Содружества. Москва, 2002. С.40.

9. *Бегинин Е.Н., Дмитриев Б.С., Лёвин Ю.И., Шараевский Ю.П.* Маятники. Динамика поступательного и вращательного движений. Саратов: Изд-во ГосУНЦ «Колледж», 2001. 64 с.

10. *Бегинин Е.Н., Дмитриев Б.С., Лёвин Ю.И., Шараевский Ю.П.* Динамика вращательного движения. Колебания и резонанс в механических системах. Саратов: Изд-во ГосУНЦ «Колледж», 2001. 64 с.

11. *Ковылов Н.Б., ЛёвинЮ.И., ШараевскийЮ.П.* Диэлектрические и емкостные методы в физическом эксперименте (обработка измерительной информации). Саратов: Изд-во ГосУНЦ «Колледж», 2000. 32 с.

12. *Бегинин Е.Н., ШараевскийЮ.П.* Электромагнитная индукция. Саратов: Изд-во ГосУНЦ «Колледж», 2000. 24 с.

13. *Ковылов Н.Б., Левин Ю.И., Шараевский Ю.П.* Исследование нелинейных эффектов взаимодействия магнитных полей с различными средами. Саратов: Изд-во ГосУНЦ «Колледж», 2000. 32 с.

14. *Фейнман Р., Лейтон Р., Сэндс М.*Фейнмановские лекции по физике. М.: Мир, 1965. Вып. 4.

15. *Крауфорд Ф.* Волны. М.: Наука, 1974.

16. *Трубецков Д.И., Рожнёв А.Г.* Линейные колебания и волны. М.: Физматлит. 2001. 416 с.

*Saratov State University* *Received 15.07.2002*

УДК 53.001.891.5:378.4

# ФИЗИЧЕСКИЙ ЭКСПЕРИМЕНТ В УНИВЕРСИТЕТСКОМ ОБРАЗОВАНИИ

*Б.С. Дмитриев, Ю.И. Левин, Ю.П. Шараевский*

Обсуждается роль физического эксперимента в современном университетском образовании. Излагаются принципы организации учебно-исследовательского физического практикума для студентов младших курсов на факультете нелинейных процессов Саратовского университета. Приводятся конкретные примеры экспериментальных исследований.

*Dmitriev Boris Savelevich* was born in Saratov in 1937, graduated from the physical faculty of SSU in 1959, defended the dissertation for the degree of Ph.D. (1967). Now he is the professor of the department of nonlinear physics of SSU, gives courses of general physics (mechanics, molecular physics and thermodynamics, electrodynamics). The field of scientific interests is electronics and microwave radiophysics. He has published more than 120 scientific and scientific-methodical works and manuals.

*Levin Yury Ivanovich* was born in Saratov in 1942, graduated from the physical faculty of SSU in 1965, defended the dissertation for the degree of Ph.D. (1974). Now he is the professor of the department of nonlinear physics of SSU, the head of the faculty of nonlinear processes of SSU, gives lecture courses of «Mathematical methods of natural science», «Linear waves». He has published more than 100 scientific and scientific-methodical works and manuals.

*Sharaevsky Yury Pavlovich* was born in Nikolaevsk-na-Amure of Khabarovsk region in 1942. He is the Doctor of Physico-mathematical Sciences, professor, the head of the department of nonlinear physics of SSU. He gives courses of general physics (mechanics, molecular physics and thermodynamics, electrodynamics) and lecture courses «Concepts of modern natural sciences» in humanities faculties. The field of scientific interests is microwave radiophysics and wave phenomena in magnetic films. He has published more than 120 scientific and scientific-methodical works and manuals.

Зав. редакцией *Н.Н. Левина*
Редакторы *Л.А. Сидорова, Н.Н. Левина,*
*Ж.А. Иванова, А.Ю. Бирюкова*
Обложка художника *Д.В. Соколова, Г.А. Суминой*
Оригинал-макет подготовлен *Г.А. Суминой, О.Н. Афанасьевой*
на компьютерной системе Apple Macintosh

Распространение журнала по подписке и предварительным заявкам
осуществляется Государственным учебно-научным центром «Колледж»
при Саратовском государственном университете. ИНН 6452006136
Банковские реквизиты
р/с № 40603810900000000378 в ЗАО АКБРиР «Экономбанк» г. Саратова,
БИК 046311722, кор.счет банка 30101810100000000722

**Правила подписки за рубежом** на сайте: http://www.periodicals.ru

Сдано в набор 01.07.02. Подписано к печати 16.09.02. Формат 70x108/16
Бумага «Снегурочка». Печать трафаретная. Гарнитура Латинская
Усл. печ. л. 18,55(13,25). Уч.-изд. л. 18,0. Тираж 200. Заказ 271

Издательство ГосУНЦ «Колледж». Лицензия ЛР №020773 от 15.05.98
410012, Саратов, ул. Астраханская, 83
Тел. (845-2)523864, факс (845-2) 523864
E-mail:and@cas.ssu.runnet.ru
http://cas.ssu.runnet.ru

Отпечатано на ризографе GR 3750 издательства ГосУНЦ «Колледж»

EDITOR-IN-CHIEF
*Yu.V.* *Gulyaev*, Member of the Russian Academy of Sciences, Institute of Radioengineering and Electronics of RAS, Moscow

EDITORS
*D.I.* *Trubetskov*, Corresponding Member of the Russian Academy of Sciences, Saratov University
*D.A.* *Usanov*, Member of the International Academy of Sciences of High School, Saratov University

SECRETARY-IN-CHIEF
*B.P.* *Bezruchko*, Professor, Institute of Radioengineering and Electronics of RAS, Saratov University

EDITORIAL BOARD
*V.S.* *Anishchenko*, Professor, Saratov University
*Yu.A.* *Danilov*, Professor, Kurchatov Scientific Centre, Moscow
*A.S.* *Dmitriev*, Professor, Institute of Radioengineering and Electronics of RAS, Moscow
*S.P.* *Kuznetsov*, Professor, Institute of Radioengineering and Electronics of RAS, Saratov
*P. S.* *Landa*, Professor, Moscow University
*G.G.* *Malinetskii*, Professor, Institute of Applied Mathematics of RAS, Moscow
*O.V.* *Rudenko*, Professor, Moscow University
*Yu.M.* *Romanovsky*, Professor, Moscow University
*E.E.* *Son*, Professor, Institute of Physics and Technics, Dolgoprudny
*V.D.* *Shalfeev*, Corresponding Member of the Russian Academy of Engineer Sciences, Nizhny Novgorod University
*V.V.* *Tuchin*, Professor, Saratov University
*V.K.* *Yulpatov*, PhD, Institute of Applied Physics of RAS, Nizhny Novgorod
*V.G.* *Yakhno*, Professor, Institute of Applied Physics of RAS, Nizhny Novgorod